THE UNIVERSITY OF CHICAGO

THE PHOSPHORYLATION-DEPENDENT REGULATION OF THE RNA N^6-METHYLADENOSINE METHYLTRANSFERASE COMPLEX

A DISSERTATION SUBMITTED TO

THE FACULTY OF THE DIVISION OF THE BIOLOGICAL SCIENCES

AND THE PRITZKER SCHOOL OF MEDICINE

IN CANDIDACY FOR THE DEGREE OF

DOCTOR OF PHILOSOPHY

INTERDISCIPLINARY SCIENTIST TRAINING PROGRAM: CANCER BIOLOGY

BY

ALLEN CHENGZHI ZHU

CHICAGO, ILLINOIS

DECEMBER 2021

This dissertation is dedicated to my parents, Yun Yang and Da-Ming Zhu.

Table of Contents

List of Figures

Acknowledgements

As I reflect on my time in graduate school, I am thankful for many who made this journey possible. The work I present in this dissertation would not have been possible without the individuals who have taken time to guide and support me. Thanks to them, I have grown as a scientist and as a person.

First, I would like to express my deep gratitude to my doctorate advisor, Professor Chuan He. When I first rotated in Dr. He's lab, I was struck by his inspirational enthusiasm for new research project ideas. Chuan has always been a source of encouragement, honest and constructive feedback, and continual support. He has taught me how to ask fundamental scientific questions, design experiments to study them, and communicate results. He has also given me plenty of support in collaborations with other labs, conferences, and grant applications. My research and education to date would not have been possible without his guidance.

I would also like to thank my past scientific mentors and advisors: my father Da-Ming Zhu and Jeffrey Price at the University of Missouri, Kansas City; Takuya Akiyama and Matthew Gibson at the Stowers Institute for Medical Research; and Hui Li, Benoit Roux, and Marvin Makinen at the University of Chicago. I would not be where I am today without them.

I would also like to deeply thank my fellow members in the He lab with whom I have worked over the years. As fellow lab mates and friends that I have seen often daily, they have been like family who I have admired and cherished working and living life together. Chuan has assembled a group of talented scientists from various backgrounds, and it has been a pleasure to work with and learn from all of them. The He lab is not only full of brilliant minds, but also kind hearts. Even though it may be the menial tasks of the day, I will look back fondly on

collaborating on experiments, borrowing or lending reagents, teaching or learning lab techniques, or chatting at random times of day throughout lab.

I would like to thank many individuals in the He lab. Scott Zijie Zhang and Ian Roundtree took me under their wing and taught me essential lab techniques when I rotated in the lab. During the summer, Scott also practiced some soccer drills with me. When I officially joined the lab, Bryan Harada served as my very first mentor and endowed me with skills on how to think carefully as a scientist, giving me foundational skills as a researcher. I am also extremely grateful for Dr. Hui-Lung Sun. Dr. Yawei Gao taught me mouse embryonic stem cell skills. My repertoire of skills and ability to generate hypotheses expanded dramatically by watching and learning from him. I am glad we were able to co-author a paper together.

Hailing Shi was one of the first senior graduate students I befriended in lab. I am grateful for her guidance and our friendship even after she has left the lab. Phil Hsu taught me lab techniques, but more importantly, has been a great and faithful friend and role model for how to attain my goals. Dr. Tong Wu has been a kind listener and supporting friend. I thank Drs. Ruitu Lü, Shun Liu, Xiao-Long Cui, Xiaoyang Dou, Xianbin Yu, and Professor Mengjie Chen for their assistance in learning bioinformatics.

I want to thank Caraline and Greg Sepich-Poore for being close friends and for the long, spontaneous conversations about life in lab. Many thanks to Cody He, Linda Zhang, Chang Liu, Diana West-Szymanski, Kinga Padjzik, Siggy Nachtergaele, Alana Beadell, Iryna Irkliyenko, Matthew Ross, Saara-Anne Azizi, and Jeffrey Dewey for their support as well. I also thank Yuru Wang, Yu Xiao, Tong Wu, Lei Yang, Pingluan Wang, and Boyang Gao for the companionship, laughter, and practicing my Mandarin Chinese in lab. Finally, I thank Jordi Tauler for his lab

administration and for making our lives easier. I am grateful for all lab members, both past and present, and I will sincerely miss working with you.

I would also like to thank my research collaborators. I thank Chao Shen and Jianjun Chen for the wonderful collaboration investigating the role of ALKBH5 in acute myeloid leukemia, and for Dr. Fang Yu and Professor Zhijian Qian for their care in working on the RBM33 and ALKBH5 project. I also appreciate working with Professor Marc Bissonnette and Frank Zifeng Deng on colon cancer studies.

I also thank my thesis committee—Professor Chuan He, Professor Kay MacLeod, Professor Yu-Ying He, and Professor Bryan Dickinson—for taking the time to meet with me and for providing recommendations during thesis committee meetings. They have all provided insight or guidance during individual meetings and have shown me different perspectives on approaching scientific questions.

I am deeply grateful for the University of Chicago Medical Scientist Training Program (MSTP) administrative leadership, both past and present, who have been solid pillars of support and to allow me to pursue medicine and research to an interdisciplinary end. Marcus Clark, Shay McAllister, Alison Anastasio, Sarah Laloggia, Hafsah Mohammed, Marisa Davis, and Kristin McCann have been instrumental in making the MSTP a unique and wonderful experience. I thank Mat Schnorenberg and Michael Clark for their mentorship on grant applications, and Reem Elorbany for her mentorship and support. I want to thank my MSTP cohort for journeying with me together.

Of course, my life during graduate school extends beyond the walls of the laboratory as well. There are many communities of wonderful people whom I also want to thank for their

friendship. I want to thank the Pritzker School of Medicine's Bridgeport Free Clinic team for the opportunity to serve our community together. Through this clinic, I have enjoyed learning from role models in leadership such as Saara-Anne Azizi, Jennifer Deng, and Anthony Hung. With Anthony, I shared the pleasure of teaching my first course as. Thank you to Hyde Park UBF for their source of wisdom and care, in particular the Hong family (Pastor Joshua, Missionary Grace, Faith, Pauline, and Joshua) and the Yoon family (Dr. Daniel John, Missionary Mary, and their many children).

I have the best of friends who remained in Chicago with me after college and with whom I have continued to bond with since. I consider myself extremely fortunate and blessed for their support, and I want to thank them and their partners for everything: Enoch Chan, Linda Fu, Caywin Zhuang and Natalie Ramsy, Grace Koh and Joey Rhee, and Sibo Cai and David Ding. I am also thankful for the support I have received from those in other cities: Sean Wang-Lu, Michael Wang-Lu, Bharat Chandar, Erika Zheng, Elizabeth Woo, Gloria Wang, Richard Lee, Yi-Rui Lye, and Young Liu. Phil Hsu, Andy Nian, Emily Woo, Angela Tsang, Cindy Ouyang, Mario Shammas, Saieesh Rao, Jeremiah Kim, and Daniel Dongju Lee—thank you for all the joyful moments in Chicago during graduate school. I have many more I wish to acknowledge who have helped me live a full life thus far but doing so would take require extensive space. To my friends, I am always in awe and amazed by what you do, and I look forward to seeing where your lives take you.

Lastly, and most importantly, I give all my thanks to my family—to my parents Yun Yang and Da-Ming Zhu, and to my sisters Emily and Elaine. I am forever grateful your many selfless sacrifices in raising a family. Thank you for bearing and raising me, for loving me patiently and unconditionally, for showing me a Christlike love, for pushing me to work hard,

and for helping me become who I am now. Thank you for always wanting the best for me, and for hoping and believing in me in times of trial. Thank you for bestowing upon me faith, love, and wisdom. This thesis is dedicated to you.

Abstract

Fundamentally, biological life depends on precise regulation of the expression of genetic information. Post-transcriptional RNA modifications are a major component of regulating gene expression, and N^6-methyladenosine (m^6A) is the most abundant internal mRNA and long non-coding RNA modification. Through its effects on RNA stability, structure, export, splicing, and translation, m^6A influences many biological processes, including embryonic development, immune response, memory, viral infection, and cancer. m^6A is selectively installed on certain mRNA transcripts by the methyltransferase-like 3 (METTL3), which acts as the catalytic subunit of the mammalian m^6A methyltransferase "writer" complex and must be precisely regulated for proper biological function. Meanwhile, m^6A "erasers" ALKBH5 and FTO remove said modification. This dissertation will span three main subjects, all of which are concerned with examining biological roles of mRNA m^6A methylation proteins. First, the characterization and function of METTL3 phosphorylation by the ERK2 kinase reveals its role on m^6A methylation in embryonic stem cells and cancer. Next, this thesis will discuss the effects of m^6A methylation by METTL3 on RIG-I immune signaling and double-stranded RNA formation. Finally, we will report on the effects of the m^6A demethylase ALKBH5 in cancer—in particular, how ALKBH5 promote leukemogenesis and how it forms a complex with RBM33. Together, these perspectives show how the regulation of the m^6A modification has a widespread impact on development, immunity, and cancer.

Chapter I: Introduction

Introduction

The diversity of life requires that every gene, no matter what type of cell or organism, control its expression to meet fluctuating biological demands. Therefore, understanding the mechanisms that govern gene expression is an essential facet of biology research. Understanding the genetic architecture of the cell also explains how physiological or pathological phenotypes occur. Multiple mechanisms control various stages of genetic information flow: transcriptional, post-transcriptional, translational, and post-translational. Yet these regulatory mechanisms are all interconnected.

One class of post-transcriptional regulation is the chemical modification of ribonucleic acid (RNA). In this dissertation, I will discuss work that shows how these RNA modifications are regulated and how they control multiple biological processes. Within this introductory chapter, I will provide an overview of the central dogma of molecular biology and epigenetics, as well as its history. Then we will shift our focus to RNA modifications, with emphasis on N^6-methyladenosine and its biological importance.

The Central Dogma of Molecular Biology

The biological basis for life starts at the genome, which contains all information stored in discrete units known as genes. Genetic information exists in the form of deoxyribonucleic acid (DNA). The central dogma is a framework that explains how genetic information flows from gene to protein. DNA is transcribed into RNA, which often acts as an intermediate carrier of

information but may have other functions as well. Messenger RNA (mRNA) can then be translated and synthesized into protein (Figure 1-1).

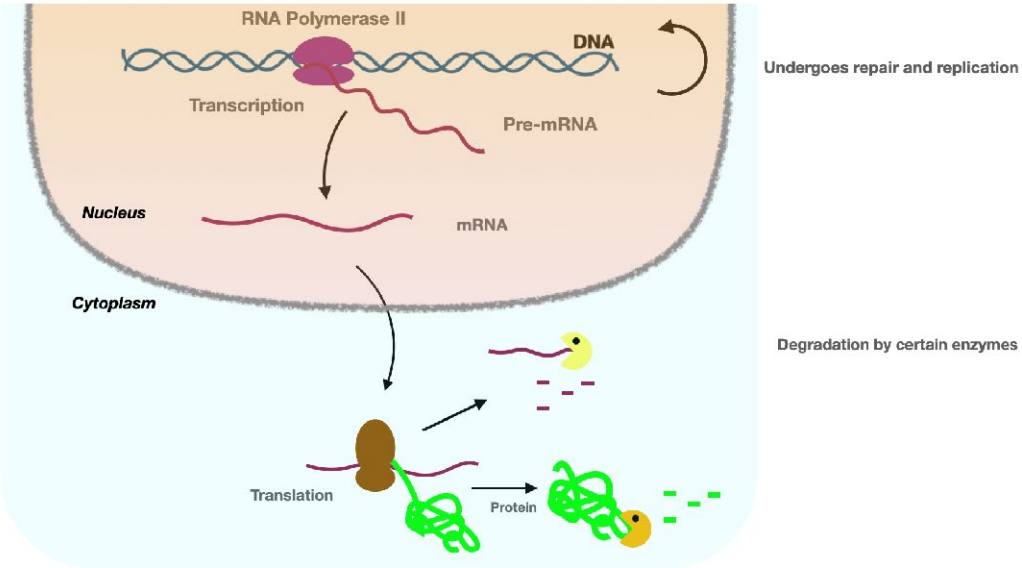

Figure 1-1. The central dogma of molecular biology within the cell.

All genetic information is stored inside the genome, comprised of DNA wrapped around histones to form chromatin. DNA is transcribed by RNA polymerase II into multiple types of RNA. Messenger RNA is protein-coding and is subsequently translated into amino acids that are then folded into protein. Most RNA and protein are temporary and are catabolized into their original monomeric constituents through degradation machinery. These components are then recycled, and the process repeats itself.

Biochemically, the DNA that comprises the genome is a double-stranded biopolymer of individual nucleic acid base pairs; each base is one of four nucleotides: adenine (A), guanine (G), cytosine (C), and thymine (T). RNA polymerase can then copy DNA and form single-stranded ribonucleic acids, although thymine is replaced by uracil (U). mRNA is then translated into a string of amino acids via ribosomal machinery that fold into proteins that execute a whole assortment of functions within the cell.

Alongside this information flow is a series of mechanisms that modulate gene activity and final product level and function. Although every cell in a multicellular organism contains the

same genome, this complex network of mechanisms accounts for cell- and tissue-specific gene expression and enables adaptation to environmental stimuli. In fact, out of three billion base pairs in the genome, approximately one percent codes for protein. Aside from protein-coding genes, DNA also contains many noncoding elements that serve various purposes for controlling the expression of genes. These elements work in concert with other genomic regulatory regions, such as enhancers, silencers, insulators, and boundary elements that can tune the level of transcription of a given gene[1].

A Brief Historical Overview of Epigenetics

After a paradigm-shifting post-Enlightenment era, Gregor Mendel found that physical traits were heritable based on certain principles of inheritance, and Thomas Hunt Morgan showed that the chromosome was the key unit in heredity[2]. In the mid-20th century, Avery, MacLeod, and McCarty isolated DNA as the carrier of genetic information, ushering in an era of molecular biology[3].

The field of biology underwent a paradigm shift upon the rise of "epigenetics." Although the term rapidly came to the forefront in the early 2000's, the word was introduced into modern biology in the mid-20th century by Conrad Hal Waddington[4]. He derived this term from "epigenesis", which contrasted with preformation, the other prevalent paradigm at the time. Waddington originally defined "epigenetics" as the "whole complex of developmental processes" that lie between genotype and phenotype." Ahead of his time, he theorized the "epigenotype" as a biological system in which "concatenations of processes [are] linked together in a network, so that a disturbance at an early stage may gradually cause more and more far-reaching abnormalities in many different organs and tissues"[5]. Genetic systems provide

templates for replication of DNA sequences, whereas epigenetic systems encompass all auxiliary mechanisms involved in determining gene expression.

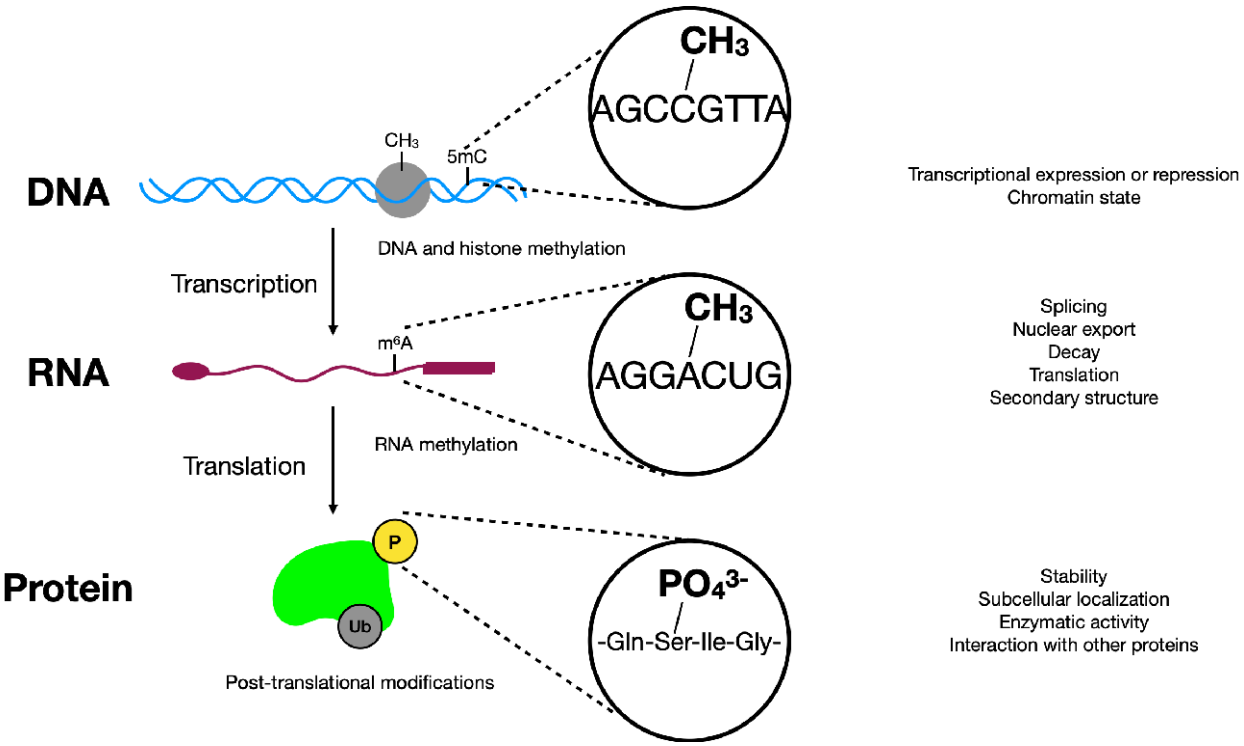

Figure 1-2. Chemical modifications have widespread, substantial effects.

At each level of the genetic information flow, small chemical modifications can play large roles in the metabolism, processing, or activity of the biomolecules. For example, DNA and histone methylation affect gene silencing. RNA methylation affects all parts of the RNA life cycle. Protein phosphorylation or ubiquitination can modify the protein's structure or function.

Epigenetic Mechanisms: Modifications of Histones and DNA

We now discuss a chemical and biochemical understanding of epigenetics, which has come to the fore in the 21st century. Epigenetic phenomena, since the 1990s, usually refer to chemical or structural modifications of chromatin or chemical modifications of the DNA nucleotides themselves (Figure 1-2).

DNA resides within the nucleus and is packaged in a complex with basic proteins, primarily histones. Chemical modification, such as methylation or acetylation can have an

impact on the transcription of genes wrapped around the histone core[6]. The effect on transcription, whether activation or inhibition, depends on which histone tail and amino acid residue is modified. From a chromatin standpoint, the depletion or enrichment of certain characteristic histone modifications also results in relatively open or compact structures of chromatin, referred to as euchromatin or heterochromatin, respectively. Histone modifications play an important role in transcription mechanisms, and interference may have deleterious effects on phenotype.

Another essential component of epigenetics is the methylation of DNA. Robin Holliday first suggested in 1975 a hypothesis that DNA methylation could regulate gene expression[7]. This proposition gained further traction when it was found that patterns of DNA methylation could be inherited and maintained between successive generations of cells. In high eukaryotes, methylation of DNA on carbon-5 of cytosine residues, known as 5-methylcytosine (5mC), occurs on ~3 to 6% of all cytosines and is typically a repressor of transcription and mark of heterochromatic regions of the genome, which includes centromeres, transposons, telomeres, and repetitive DNA elements[8]. In mammals, DNA cytosine methylation is typically mediated through DNA methyltransferases and demethylase enzymes [9]. Despite not being a canonical base, DNA methylation plays an essential role in many biological processes, such as X-chromosome inactivation or epigenetic inheritance from parents to offspring[10]. Other chemical derivatives of DNA, such as 5-hydroxymethylcytosine (5hmC) or N^6-methyladenine (6mA) have begun to emerge as naturally occurring epigenetic marks that could control genetic expression[11, 12].

Epitranscriptomics: Chemical Modifications of RNA

Although epigenetic modifications of DNA and chromatin control transcription, there are other processes that occur post-transcriptionally. Multiple processes—including transcription, messenger RNA (mRNA) processing, export of mRNA from the nucleus, mRNA decay, and protein translation—must be dynamically regulated for proper cellular homeostasis[13].

Like DNA, RNA also contains several naturally occurring chemical modifications. In fact, over 170 distinct chemical derivatives of RNA nucleotides have been discovered, some of which have been known for decades[14]. For instance, the first known modified base, pseudouridine, was discovered in the 1950s. Up until 1995, 93 modifications were known, and they had been identified in molecules that were stable and abundant in the cell—namely, transfer RNAs (tRNAs), ribosomal RNAs (rRNAs), and small nuclear RNAs (snRNAs)[15].

tRNAs are the most heavily modified. In fact, about 80% of the identified RNA modifications thus far have been from tRNAs[16]. Between 10 and 20% of tRNA residues are modified, and up to 39 types have been detected in human cytoplasmic tRNAs[17]. After tRNAs, rRNAs are the most highly modified class of RNAs, with approximately 2% of rRNA nucleotides being modified. In eukaryotes, the most abundant rRNA modification is 2'O-methylation (2'O-Me) of the ribose sugar and the isomerization of uridine to pseudouridylation. Finally, spliceosomal, or small nuclear RNAs (snRNAs), are also extensively modified with 2'O-Me and pseudouridine. These modifications are crucial for the biogenesis, structure, and function of these RNAs.

Even though most RNA modifications are found in noncoding RNAs, eukaryotic mRNAs also contain various modifications. At the 5' end, a cap is added to the transcript during transcription and contains a modified guanine nucleotide, N^7-methylguanosine, that stabilizes the transcript and allows the ribosome to initiate translation[18]. In higher eukaryotes, this cap can

also undergo 2'-O-methylation, which can help distinguish between self and non-self RNAs[19-21].

After the discovery of modifications at the ends of mRNA, internal modifications were also identified. Due to lower abundance, the study of internal mRNA modifications was more difficult. Eventually, though, enhanced methods of detection, such as mass spectrometry and high-throughput sequencing, allowed researchers to characterize more internal mRNA modifications, and they include the following: N^6-methyladenosine (m^6A) as previously mentioned, N^1-methyladenosine (m^1A)[22-25], pseudouridine (Ψ)[26, 27], N^6,2'-O-dimethyladenosine (m^6A_m)[28], 5-methylcytosine (m^5C)[29], N^4-acetylcytosine (ac^4C)[30], and N^7-methylguanosine (m^7G)[31, 32] (Figure 1-3). Quantitative measurements of some these modifications reveal their relative proportions as: 0.2 to 0.6% for m^6A/A, 0.015 to 0.05% for m^1A/A, 0.025 to 0.1% for m^5C/C, 0.001–0.004% for hm^5C/C, 0.2–0.6% for Ψ/U, and 0.003% for m^6Am/all nucleosides[33].

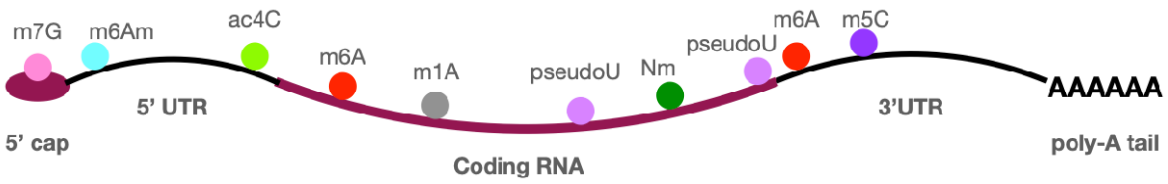

Figure 1-3. Distributions of major mRNA modifications.

An illustration of the distribution pattern of each type of modification along an mRNA, which includes a 5' cap, 5' UTR, coding sequence, 3' UTR, and polyadenylation tail.

Researchers wondered if modifications of mRNA could also play regulatory roles, like that of DNA methylation or histone tail modifications. Could mRNA modifications influence processes that occur during lifetime of mRNA? The most abundant internal mRNA modification, identified in the 1970s, is N^6-methyladenosine (m^6A)[34], and it was found to be essential by accelerating mRNA processing and export in mammalian cells. Although the identification of

m^6A and its function suggested a possible epigenetic role for RNA modifications, the biological significance of messenger RNA modifications had remained relatively elusive and unexplored until the last decade. Given that these modifications were found to be able to influence the metabolism and function of mRNA, the terms “RNA epigenetics” and “epitranscriptomics” were first proposed and coined in 2010 to describe this additional post-transcriptional layer of gene expression regulation analogous to epigenetic regulation by histone and DNA modifications[35].

Despite the identification of RNA modifications, methods for mapping and functional studies have lagged behind those of the epigenome. One reason for this is that detection methods for surveying modifications were still not adequately sensitive for detecting these low-abundance modifications. To study how RNA modifications contribute to cellular function and gene expression, transcriptome-wide detection of these sites is crucial. It was only about a decade ago that substantial regulatory functions of some of the RNA modifications were realized, which drove rapid development of the field in the past decade[35-37]. In addition, major improvements in high-throughput sequencing and more sensitive methods for detection of low-abundance modifications have allowed researchers to study their locations and functions[38, 39]. Most researchers have relied on the development of antibodies that target RNA modifications to enrich methylated RNAs for sequencing. However, other enzyme-assisted and chemical methods have been developed to reduce sample quantity requirements and to improve detection of more sparse modifications[40-45].

Functional characterization of some of these less abundant modifications is still in its infancy, and their low abundance proves to make detection and mapping technically challenging. Furthermore, some studies contest the specificity of some antibody-dependent mapping methods[46]. Even so, technological progress has enabled identification of the writers and

erasers of more internal mRNA modifications, revealing their dynamic nature and biological significance[47, 48] (Figure 1-4). The plethora of mRNA modifications suggests possible crosstalk and additional layers of complexity to the regulation of mRNA that has yet to be discovered.

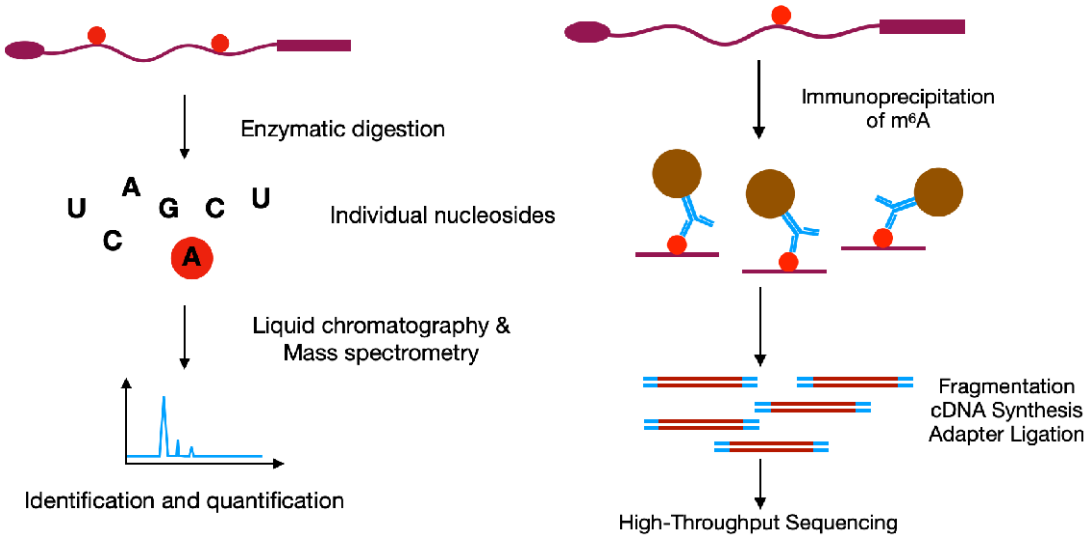

Figure 1-4. Technological advancements have enabled deeper study of mRNA modifications.

High-pressure liquid chromatography and mass spectrometry (left panel) has enabled identification and quantification of nucleosides. To map the modification over the entire transcriptome, high-throughput sequencing (right panel), in tandem with either an antibody-assisted enrichment or enzyme-based method, allows sequencing the modification over the entire transcriptome.

Regulators and Effectors of the m^{6}A Epitranscriptome

Among eukaryotic messenger RNA, *N*^{6}-methyladenosine (m^{6}A), is the most abundant, internal modification and will be the focus of this dissertation. m^{6}A comprises the addition of a methyl group at the nitrogen-6 position of adenosine. Although it was discovered in the 1970s, not much was known about its biological function until the past decade. Only with the discovery that m^{6}A methylation is dynamically regulated and reversible, along with the advent of high-

throughput m^6A sequencing and more sensitive detection methods, did we begin to uncover the major roles m^6A plays in regulating RNA metabolism.

The first m^6A mapping studies report that about ~25% of mRNAs carry m^6A. To be more specific, about 12,000 m^6A sites are distributed across about 7,000 mRNA transcripts. They also report that m^6A is mostly enriched around the 3'UTR near the stop codon, as well as in long internal exons. Typically, these sites are enriched with the DR-m^6A-CH consensus sequence motif (D = G/A/U; R = G/A; H = C/A/U). It also is most often located at the coding regions and 3' untranslated regions (UTR), with enrichment around the stop codon[37, 49].

As m^6A is present on 0.2%-0.6% of all adenosines, this means on average it is present on 1-3 sites per transcript. However, this varies across cellular and tissue context. Moreover, consistent with its dynamic and reversible nature, its modification fraction can vary in response to changes in cellular conditions, such as upon heat shock or activation of signaling pathways.

The dynamic regulation of m^6A methylation requires protein machinery to site-specifically and reversibly install the modification on mRNA. m^6A writers install the modifications, while m^6A erasers remove it (Figure 1-5A). m^6A mediates its effects on the processing or fate of methylated RNAs when bound by one of various m^6A readers (Figure 1-5B).

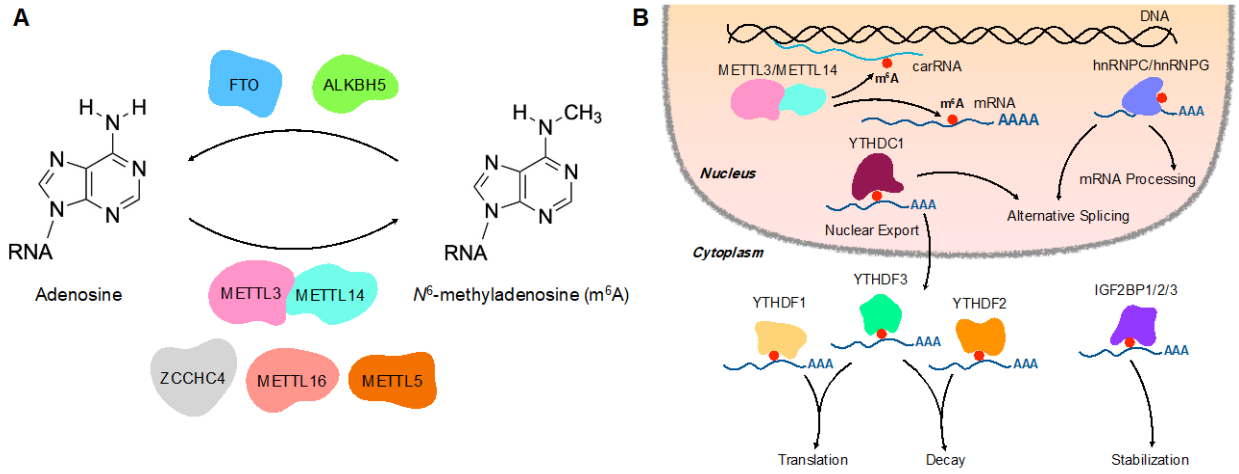

Figure 1-5. Dynamic regulation and effects of m^{6}A methylation.

(A) m^{6}A is installed and removed by methyltransferases ("writers") and demethylases ("erasers"), respectively. Different methyltransferases install m^{6}A on different RNA substrates, although METTL3/METTL14 is the primary m^{6}A writer for mRNA. FTO and ALKBH5 are both m^{6}A erasers, but they have different mechanisms for demethylation. (B) m^{6}A readers recognize and bind to m^{6}A-methylated RNA. Each m^{6}A reader exacts a different function, which includes export, splicing, translation, stabilization, and decay.

m^{6}A writers

Installation of m^{6}A is catalyzed by the methyltransferase "writer" heterodimer protein complex METTL3/METTL14, with other accessory proteins that constitute the complex[49, 50]. Methyltransferase-like 3 (METTL3) is the catalytic subunit, and it uses S-adenosyl-L-methionine (SAM) as a cofactor and methyl group donor for an S_N2-like nucleophilic attack[51]. Meanwhile, its binding partner METTL14 contains a SAM-binding domain and acts as a scaffold that binds to RNA for substrate recognition, as structural studies suggest that METTL3 and METTL14 form a positively charged binding pocket groove to bind negatively charged nucleic acid[52, 53]. METTL3/METTL14 typically recognizes a DRACH motif, with GGACU being the most enriched motif for m^{6}A deposition[50].

Even though METTL3/METTL14 is the heterodimeric core that catalyzes m^6A methylation, several other components also constitute the m^6A methyltransferase complex as well. Wilms' Tumor 1-Associating Protein (WTAP) is a splicing factor and acts as a third crucial component of the writer complex[54, 55]. Although WTAP does not alter METTL3/METTL14 methyltransferase activity in vitro, its loss affects cellular m^6A, which suggests it may direct the m^6A writer complex onto certain targets by enhancing RNA binding activity.

Aside from WTAP, at least thirteen other proteins have been identified as interacting with METTL3. WTAP is known to form a complex with other m^6A writer components ZC3H13, VIRMA, HAKAI, and RBM15[56]. Downregulation of any of these components can lead to aberrant biological activity in multiple species. For instance, ZC3H13 has been found to modulate m^6A methylation in the nucleus, and its knockdown in mouse embryonic stem cells (mESCs) decreases global m^6A levels. Moreover, loss of ZC3H13 or any of the m^6A writer complex components impairs mESC self-renewal and triggers differentiation[57]. It also bridges the catalytic core with other accessory complex components[58]. VIRMA mediates specificity of m^6A methylation in the 3' UTR[59], and its depletion leads to a substantial loss of m^6A[60]. Interestingly, RBM15 and its paralog RBM15B interact with WTAP, and also mediate m^6A deposition, particularly in uridine-rich areas[61-63].

Although METTL3/METTL14 is the primary mRNA m^6A writer, other m^6A writers have also been discovered, although they may recognize different species of RNA. For instance, METTL16 installs m^6A on U6 small nuclear RNA (snRNA) and the *MAT2A* gene[64], which encodes the SAM synthetase expressed in most cells. In low-SAM conditions, METTL16 occupancy on the 3'UTR of *MAT2A* induces splicing that promotes translation, thereby regulating

SAM homeostasis. In contrast to METTL3, METTL16 uses structured RNA in a bulge to deposit m^6A methylation, although it is also important for embryonic development.

Meanwhile, METTL5 and ZCCHC4 install m^6A on specific sites on 18S and 28S of ribosomal RNA (rRNA), respectively[65, 66]. METTL5 forms a heterodimer with TRMT112 to methylate m^6A1832 on 18S rRNA. Depletion of METTL5 compromises translation and pluripotency, showing its importance in mESC differentiation potential[67]. ZCCHC4 primarily methylates human 28S rRNA at the m^6A4220 site containing a stem-loop structure and interacts with a subset of mRNAs; its knockout disrupts codon-specific translation dynamics and stymies cell proliferation[66, 68, 69]. Due to its role in promoting translation, it may also affect several cancers, such as hepatocellular carcinoma[66].

m^6A erasers

The dynamic nature of m^6A occurs in part due to active demethylation by "eraser" proteins. The two known "eraser" enzymes are Fat Mass and Obesity-associated protein (FTO) and AlkB Homologue 5 (ALKBH5)[36, 70]. Both demethylase proteins are part of the non-heme Fe^{2+}- and α-ketoglutarate (KG)-dependent dioxygenase AlkB family of proteins that can oxidatively demethylate N-methylated nucleic acids.

The reversibility of m^6A methylation came to light when the first m^6A demethylase Fat Mass and Obesity-Associated Protein (FTO) was identified. Prior to 2011, FTO was only known to be linked with obesity in population studies and, later, an a-KG-dependent nucleic acid demethylase[71], until Jia et al. found that it reversed m^6A methylation on mRNA[36], by converting it sequentially to two other modifications, N^6-hydroxymethyladenosine (hm^6A) and then N^6-formyladenosine (f^6A) before complete demethylation[72]. Then, it was shown that FTO

regulates poly(A) sites and 3' UTR length, which affects splicing, and that FTO can also demethylate m^6A and N^6,2'-O-dimethyladenosine (m^6A_m) on snRNAs, cap (m^6A_m) on cytoplasmic mRNA, and m^1A on tRNA in both the cytoplasm and nucleus[73].

ALKBH5 was discovered soon after FTO as another m^6A eraser[70]. Although the two m^6A erasers are in the same AlkB family, ALKBH5 is smaller in size and has different structural properties, with a much smaller active site cavity which may explain its more potent binding preference to smaller-sized molecule inhibitors[70]. In its initial publication, ALKBH5 was shown to demethylate m^6A, and ALKBH5 deficiency in mice impaired spermatogenesis and fertility[70]. Interestingly, ALKBH5 activity also affects multiple aspects of mRNA metabolism, such as mRNA export and processing within nuclear speckles. Another study found that removal of m^6A by ALKBH5 in germ cells ensures proper splicing and degradation of the 3' UTR during spermiogenesis[74]. Unlike the mechanism of m^6A writers, which recognize target transcripts by conserved consensus sequences, m^6A serves as a conformational marker to promote substrate recognition by m^6A erasers.

m^6A readers

m^6A can affect the metabolism of mRNAs in multifaceted ways and is involved in almost every aspect of the mRNA life cycle, due to the diverse array of "reader" proteins that recognize and bind preferentially to m^6A-modified RNA (Figure 1B). Of the known m^6A readers, the first to be discovered were members of the YT521-B Homology (YTH) domain family, which has five members: YTHDF1, YTHDF2, YTHDF3, YTHDF1, and YTHDC2. Crystal structures of the YTH domain bound to m^6A-containing RNA have revealed a conserved structural basis for selectively binding m^6A at a DR-m^6A-CH consensus sequence[75-77]. The YTHDF proteins are similar to

each other; they are predominantly cytoplasmic, and they contain a C-terminal YTH domain, with the remaining majority of the protein a large, disordered, low-complexity domain. YTHDF2 regulates stability of RNA by promoting degradation of m^6A-methylated RNA[78]. Specifically, YTHDF2 is able to recognize m^6A-methylated mRNA through its C-terminal YTH domain, whereas its N-terminal region localizes the YTHDF2-mRNA complex to sites of degradation, such as processing bodies (P-bodies). This decay can occur when YTHDF2 recruits the CCR4-NOT deadenylase complex or through an RNase P/MRP-mediated endoribonucleolytic pathway.

In contrast, YTHDF1 can promote translation by interacting with translation initiating factors, thereby facilitating ribosome assembly[79]. In its original publication, YTHDF1 was found to promote translation efficiency and ribosome loading of its target mRNA transcripts. With depletion of METTL3, YTHDF1 had virtually no effect on translation, indicating its dependency on m^6A. Although YTHDF1 may promote translation, its exact mechanism is not clear, although it may rely on eukaryotic initiation factor 3 (eIF3) and factor 4G (eIF4G)-mediated loop formation.

Meanwhile, YTHDF3 has been found to promote both translation and degradation[80]. It also plays a unique role in recognizing m^6A-methylated circular RNAs[81]. YTHDF1/2/3 are cytoplasmic m^6A readers, whereas YTHDC1 is a nuclear m^6A reader that promotes nuclear export, regulates splicing, and affects nuclear decay of methylated transcripts[82-84]. Finally, YTHDC2 is an RNA helicase-containing m^6A reader that promotes translation and regulates meiosis and plays a crucial role in the mammalian germline[85, 86]. The role of YTHDC2 was further dissected when it was shown that it positively regulates translation at sites of m^6A methylation in coding sequence regions on structured mRNAs[87].

Aside from readers containing the YTH domain, the family of Insulin-like Growth Factor 2 mRNA-Binding Proteins (IGF2BP1/2/3) are also found to enhance RNA stability and

translation[88]. For instance, they are known to stabilize *MYC* transcript and, thus, have been found to play oncogenic roles in cancer. Other readers in the heterogeneous nuclear ribonucleoprotein (hnRNP) family, which recognizes methylated transcripts in a structural switch-based mechanism, can modulate RNA splicing[89-92]. Another reader includes Fragile X Mental Retardation Protein (FMRP), which contains three KH domains and one RGG domain. It can impact both RNA export, translation, and stability[93].

Crosstalk and synergy between YTHDF proteins

Despite the unique biological roles that YTHDF1, YTHDF2, and YTHDF3 each play, it has been proposed that YTHDF proteins have synergistic effects with one another. This possibility arose when the function of YTHDF3 was first reported. Shi et al. found that YTHDF3 recognized nascent m^6A methylated mRNA and enabled binding specificity of YTHDF1 or YTHDF2 to their respective targets, so they hypothesized a model in which YTHDF3 recognizes and then shuttles m^6A-modified RNA to YTHDF1 or YTHDF2[80]. These results provided the first hint that coordinated functional interaction occurs among the three YTHDF proteins. Another report showed that YTHDF2 and YTHDF3 each recruit different deadenylase complexes to degrade somatic mRNAs, resulting in a synergistic somatic cell reprogramming[94].

Later, it was proposed that the YTHDF paralogs may have redundant functions by binding to all m^6A sites to primarily promote mRNA degradation[95]. This was further shown by structural and in vivo studies of mouse gametogenesis[96, 97]. YTHDF2 is necessary for proper differentiation, but knockout of all three readers is required to prevent functional compensation by other YTHDF readers. All three YTHDF proteins coordinate in facilitating RNA decay; however,

YTHDF1 and YTHDF2 appear to play distinct roles in different cellular contexts based on published data.

How does m^6A methylation affect development and differentiation of cells?

Given the fundamental regulatory roles and prevalence of m^6A, it may come as no surprise that METTL3 is critical and necessary for proper biological function, and its removal substantially affects many biological processes. One of these processes is stem cell differentiation[98-100]. Genetic knockout of *Mettl3* in mouse embryonic stem cells (mESCs) was found to be lethal. The loss of METTL3 in mESCs depletes m^6A and increases stability of transcripts that maintain pluripotency, such as *Nanog* or *Sox2*. Less m^6A methylation of these transcripts reduces turnover rate, which impedes removal of pluripotency factors[98, 101]. The result is a delay in proper lineage commitment and fate transition, leading to early embryonic lethality. The m^6A writer complex can also bind to SMAD2/3 to destabilize pluripotency transcripts like *NANOG* in human pluripotent stem cells[99]. Furthermore, METTL3 is required for proper differentiation of adult hematopoietic stem cells to upregulate MYC expression often found in differentiated cells[102, 103].

METTL3/METTL14 is also essential for neurogenesis[104, 105]. Depletion of either protein prolongs cell cycle progression in murine neural progenitor cells. Adult neural stem cells lacking METTL3 showed inhibited neuronal development and proliferation, as well as a skewed differentiation towards the glial lineage, due to decreased *Ezh2* transcript m^6A methylation[12].

YTHDF2 plays an important contribution to the balancing self-renewal and differentiation within hematopoietic stem cells. Li et al. found that, upon knockout of *YTHDF2* in human umbilical cord HSCs, the number of functional HSCs expanded, due to reduced degradation of

m^{6}A methylated mRNAs of transcription factors critical to maintain a stem cell state[106]. Another study similarly utilized *Ythdf2* knockout mice to find that YTDHF2 also facilitates decay of WNT signaling transcripts to reduce stemness[107].

Depletion of m^{6}A skews the stem cells towards a more naïve state, which also severely shapes proper development of immunity. Deletion of *Mettl3* from murine T cells attenuates their homeostatic expansion due to the lack of m^{6}A on the mRNAs of the STAT signaling pathway, which inhibits differentiation[108]. METTL3 is also involved in differentiation of T follicular helper cells that are critical for humoral immunity[109]. Depletion of METTL3 in dendritic cells impaired their functional maturation[110], and in early-stage B cells, the METTL3/METTL14 complex is critical for maturation at multiple points through IL7-induced proliferation and YTHDF2-mediated decay of key transcripts[111]. Germinal center B cell proliferation also relies on METTL3 for proper *Myc* mRNA stabilization[112].

How does m^{6}A methylation affect the immune system?

Knockout of *Ythdf1* in mice slows tumor growth and enhances the cross-priming capacity of dendritic cells (DCs)[113]. This phenomenon occurs because YTHDF1 promotes translation of m^{6}A-modified cathepsins, lysosomal proteases that can degrade tumor neoantigens, thereby repressing CD8$^+$ T cell cross-priming. Therefore, targeting YTHDF1 control of DC cross-priming could provide a new avenue of therapy in tandem with checkpoint blockades or other treatments[114].

m^{6}A can also affect cancer immunotherapy. It was found that FTO inhibition in tumor cells resulted in greater m^{6}A methylation and YTHDF2-mediated decay of mRNAs that drive glycolysis[115]. Dampening glycolysis in tumor cells permits greater metabolic activity and an

enhanced anti-tumor response by surrounding cytotoxic T cells. Thus, FTO inhibition is a potential immunogenic therapeutic strategy.

m^6A also affects the tumor microenvironment, which is often immunosuppressive and thwarts immunotherapies[116]. Dong et al. recently found that, upon macrophage-specific *Mettl14* knockout in mice, *Ebi3* exhibits decreased m^6A methylation and upregulated expression in tumor-associated macrophages, resulting in more dysfunctional CD8+ T cells and a compromised anti-tumor response. [117]. These results suggest METTL14 inhibitors could play a key role in immunotherapy.

How does m^6A methylation affect cancer?

Because m^6A methylation affects gene expression, its dysregulation in cancer can promote tumorigenesis. Due to the vast number of studies, we will only highlight a few examples. Acute myeloid leukemia (AML), a hematopoietic malignancy in which hematopoietic stem and progenitor cells retain unlimited self-renewal capacity, has been found to have elevated METTL3 expression. Vu et al. report that depletion of METTL3 in AML enhances myeloid differentiation and inhibits leukemogenesis[118], as METTL3 deposits m^6A on mRNA transcripts that regulate differentiation and apoptosis, including *MYC*, *PTEN*, and *BCL2*. Similarly, Barbieri et al. found that METTL3 maintains AML by recruitment to chromatin at transcription start sites to install m^6A and promote translation of *SP1* and *SP2* mRNA[119].

Another example of the role of m^6A in cancer is shown by Liu et al. in endometrial cancer, albeit in a tumor-suppressive role[120]. Most endometrial tumors exhibit reduced m^6A methylation or METTL3 expression, and an R298P hotspot mutation in METTL14 is quite

prevalent among patients[121]. Endometrial cancer cells show reduced m^{6}A methylation, with many affected transcripts enriched in the AKT signaling pathway. Mechanistically, reduced m^{6}A methylation on the *PHLPP2* transcript reduces YTHDF1-mediated translation of PHLPP2, a negative regulator of AKT signaling. Furthermore, mTORC2 complex components, which phosphorylates and activates AKT—*PRR5*, *PRR5L*, and *mTOR*—also exhibited reduced m^{6}A methylation, resulting in less decay by YTHDF2. The result is greater abundance of the mTORC2 complex and, in turn, AKT phosphorylation (Figure 1-6).

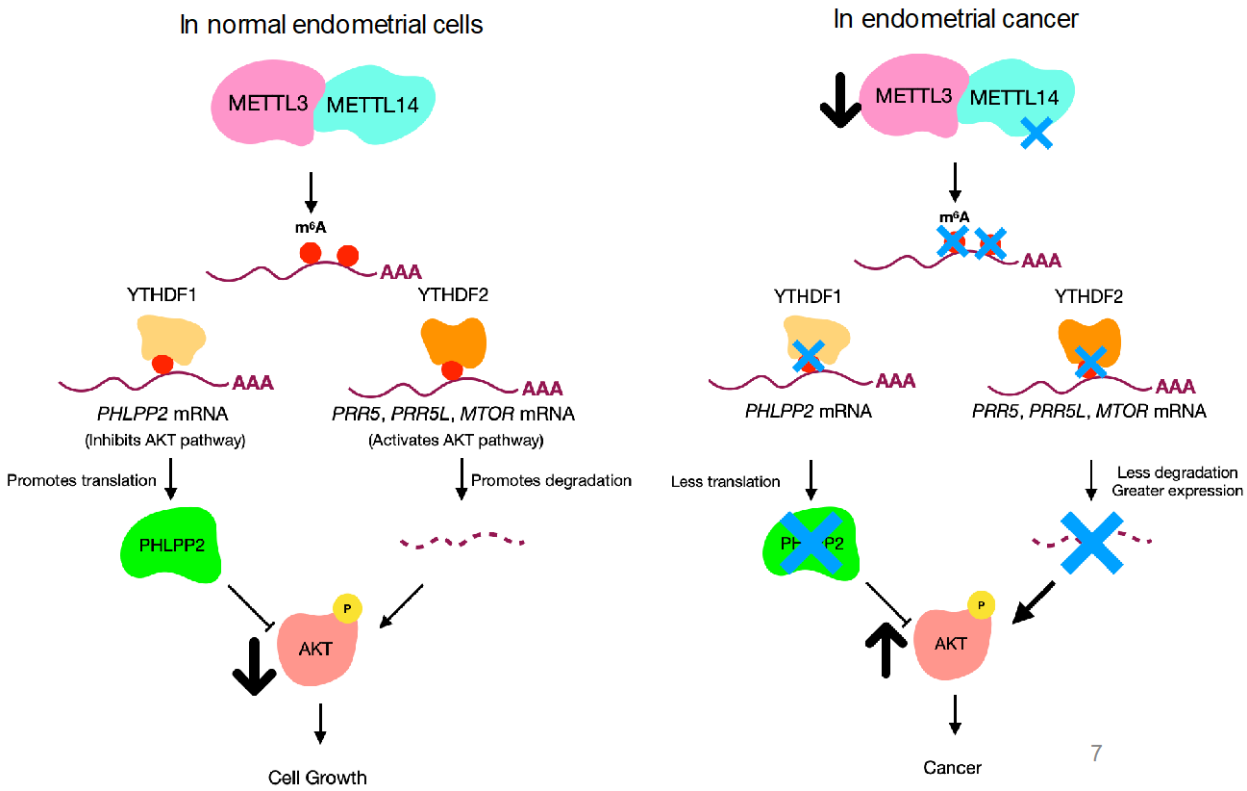

Figure 1-6. Aberrant METTL3/METTL14 activity promotes endometrial cancer growth.

Low expression of METTL3 or an R298P METTL14 mutation is often found in endometrial cancer. This reduced m6A methylation results in altered metabolism of key transcripts. PHLPP2 is recognized by YTHDF1, and a few others are recognized and bound by YTHDF2. Reduced methylation results in dysregulated AKT pathway activation.

In acute myeloid leukemia, FTO promotes leukemic transformation through demethylation of target genes such as *ASB2* and *RARA*, which promote all-*trans*-retinoic acid (ATRA)-induced differentiation in normal hematopoietic stem cells[122]. Intriguingly, some AML cells naturally inhibit FTO through production of R-2-hydroxyglutarate (R-2HG), thereby elevating global m^6A levels[123]. R-2HG is produced by a mutant form of isocitrate dehydrogenase 1/2 (IDH1/2) often found in AML. Because R-2HG is structurally very similar to α-KG, it acts as a natural small molecule inhibitor of Fe^{2+}/α-KG-dependent dioxygenases[124] (Figure 3A). In R-2HG-sensitive leukemia cells, R-2HG enzymatically inhibits FTO, resulting in accumulation of m^6A on transcripts, leading to YTHDF2-mediated destabilization of targets such as *MYC* and *CEBPA*[123] (Figure 3B).

Much like FTO, Zhang et al. found that ALKBH5 expression is heightened in GSCs and predicts poorer prognosis[125]. Knocking down *ALKBH5* hindered GSC self-renewal, proliferation, and tumorigenesis because ALKBH5 demethylates and reduces expression of *FOXM1*. In breast cancer cells, hypoxia induces expression of ALKBH5, which then demethylates *NANOG* mRNA, resulting in enrichment of cancer stem cells[126].

In hepatocellular carcinoma (HCC), m^6A methylation on *SOCS2* mRNA, a tumor suppressor gene, allows for YTHDF2-mediated degradation, enabling proliferation and migration[127].

The role of YTHDF3 in a pathological context has not been studied as extensively. Nevertheless, it was recently found that YTHDF3 can promote breast cancer metastases to the brain[128]. YTHDF3 was found elevated in metastases relative to primary tumors, and promoted extravasation, invasion, and angiogenesis, all of which are necessary steps for metastasis. This could occur because YTHDF3 binds to m^6A-methylated brain metastatic transcripts—including *ST6GALNAC5*, *GJA1*, *EGFR*, and *VEGFA*—and promotes their translation. Elsewhere, YTHDF3

was shown to suppress antiviral Type I interferon signaling by promoting the translation of *FOXO3* mRNA[129]. In CRC, YTHDF3 binds and degrades m^6A-modified lncRNA *GAS5*, which stabilizes YAP, thereby permitting CRC tumor progression.

m^6A methylation on chromatin-associated regulatory RNAs (carRNAs) affects transcriptional regulation

In addition to post-transcriptional regulation of mRNA fate, m^6A has also regulates transcription through chromatin-associated regulatory RNAs (carRNAs), A study in 2020 by Liu et al. reported that, in mESCs, METTL3 installs m^6A onto carRNAs, which include promoter-associated, enhancer, and repeat RNAs (Figure 4A). m^6A methylation of these carRNAs dramatically alters the state of chromatin, with loss of carRNA m^6A methylation leading to a more active local and global chromatin state, as well as transcriptional activation[84, 130].

YTHDC1 promotes the decay of a portion of m^6A methylated carRNAs—LINE1 repeat element RNAs, in particular—by recruiting the nuclear exosome targeting complex (NEXT)[84]. Mechanistically, this occurs because these carRNAs can recruit CBP/EP300 and YY1, which promote a euchromatic state, and because stabilization of carRNAs may promote active chromatin H3K4me3 and H3K27ac histone methylation (Figure 4B).

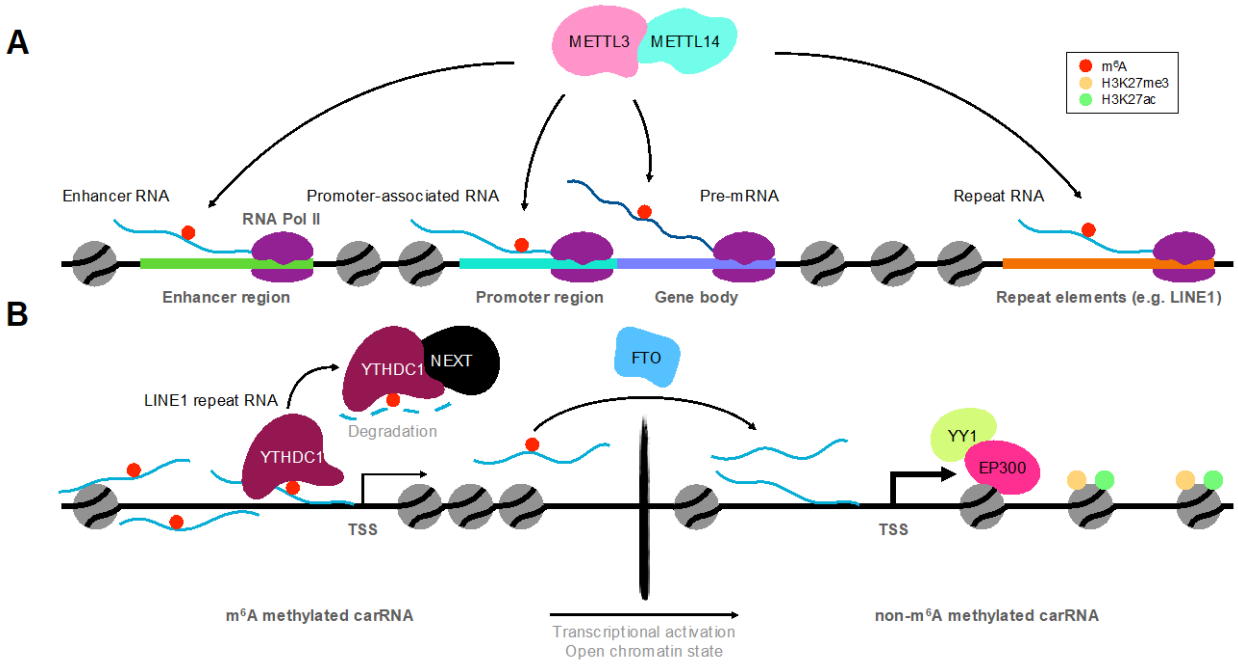

Figure 1-7. m^{6}A methylation on carRNAs regulates transcription and chromatin.

(A) m^{6}A methylation also occurs on enhancer, promoter-associated, and repeat noncoding RNAs, in addition to messenger RNAs. (B) YTHDC1 degrades a portion of m^{6}A-methylated carRNAs, resulting in less transcription and active histone marks.

Since then, additional studies have further elucidated the regulatory functions of carRNA m^{6}A[131-134]. One study found m^{6}A methylation on intracisternal A particle (IAP) elements, a subfamily of endogenous retroviruses[131]. They suggest m^{6}A methylation suppresses IAPs through a YTHDF reader-mediated degradation. Two other studies find METTL3-dependent m^{6}A methylation on IAP repeat RNAs or LINE1 RNAs promotes recruitment of H3K9 methyltransferase SETDB1/TRIM28 to promote heterochromatin formation and downregulate transcription[132, 133]. Mechanistically, YTHDC1 binds to m^{6}A-marked repeat RNAs to recruit SETDB1[132] and to recruit METTL3 in a positive feedback loop[133]. Overall, YTHDC1 is emerging as a major m^{6}A reader of carRNA and regulator of chromatin. In addition to methylation-

dependent decay of carRNA, other mechanisms involving recruitment of histone modifiers by m^6A to install repressive histone marks have also been proposed and should be examined as well.

How do post-translational modifications of protein affect gene expression?

The third and final stage of the general central dogma of molecular biology is protein. Proteins carry out a wide variety of functions in living systems, including, but not limited to, catalytic, regulatory, signaling, and structural functions, thus contributing to virtually every life process within and between cells. We have discussed modification events at the DNA and RNA levels, but similar phenomena also occur at the protein level to regulate their functions. A post-translational modification (PTM) is a biochemical mechanism in which an amino acid is covalently modified through an enzymatic reaction to change its structure and/or function[135]. Generally, a PTM can be reversible or irreversible; the reversible reactions are often covalent modifications, whereas the irreversible ones are proteolytic. Like nucleic acid modifications, PTMs can occur on a developmental or physiological time scale at multiple sites on a protein[136]. This complexity creates a combinatorial explosion in the number of potential molecular states for a protein, thereby allowing for a rapid response to changes in environmental stimuli or stress[137, 138].

Out of over 400 known PTMs, the most prevalent include phosphorylation, acetylation, ubiquitination, methylation, SUMOylation, and glycosylation[139]. For the purposes of this dissertation, we will only review the PTMs pertinent to our experimental results.

Phosphorylation

Protein phosphorylation was first identified 1906 by Phoebus Levene through the discovery of phosphate in the protein vitellin[140]. 20 years later, the first enzymatic phosphorylation of protein was demonstrated[141]. Phosphorylation is a crucial, reversible regulatory mechanism that plays a key role in the activities of enzymes, membrane channels, and many other proteins. Many enzymes are activated and deactivated by phosphorylation and dephosphorylation events, respectively, by means of kinases and phosphatases. Since many kinases themselves are activated by phosphorylation, this can lead to a cascade of kinase activation. This activation of kinases transduces signal to form highly interactive networks that, when integrated, allow the cell to function.

One example of kinase signaling is the family of mitogen-activated protein kinases (MAPKs). These MAPKs are essential regulators of the cell, as they are major components of pathways that control embryogenesis, cell differentiation, cell proliferation, and apoptosis. MAPKs are regulated by phosphorylation cascades that usually begin with auto-phosphorylation and dimerization of a tyrosine kinase receptor[142]. For example, Epidermal Growth Factor Receptor (EGFR) is activated upon binding to an Epidermal Growth Factor (EGF) extracellular ligand. This leads to phosphorylation and activation of MAP/ERK (MEK) kinase, which then activates the MAPKs ERK1/2. Activation of ERK1/2 can then activate multiple transcription factors that then modulate gene expression (Figure 1-8). This cascade, in concert with several other signaling pathways, results in changes in biological output.

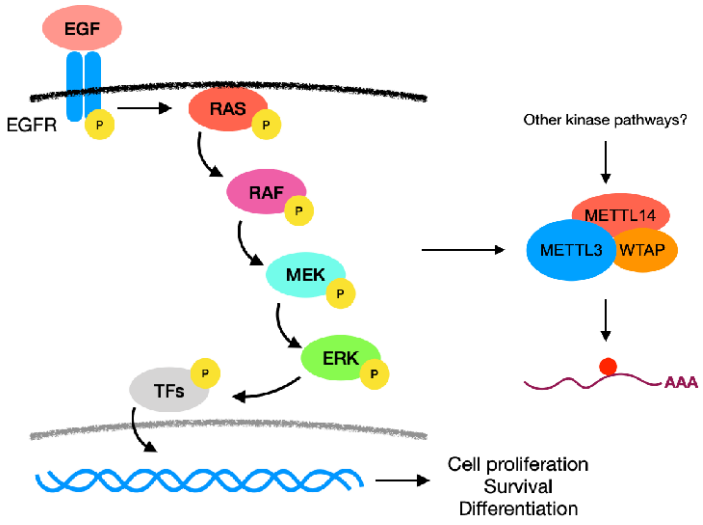

Figure 1-8. Cell signaling pathways.

Activation of cell signaling pathways is necessary for activation or repression of certain genes. In the case of the ERK pathway, phosphorylation activates a signaling cascade that results in activation of many transcription factors.

Ubiquitination

Ubiquitination is one of the most important PTMs and was first studied in 1975. Unlike phosphorylation, ubiquitination involves conjugation of ubiquitin, a polypeptide of 76 residues, to any of the 20 amino acids, although it tends to most often occur on lysine. It is installed onto a protein by an E1-E2-E3 thioester cascade that activates, conjugates, and ligates the ubiquitin onto its target protein[143]. Conversely, ubiquitin is removed by deubiquitinating (DUB) enzymes. A key feature of ubiquitin is its seven lysine residues, all of which can also be ubiquitinated to give rise to isopeptide-linked ubiquitin chains. Lys48-linked chains are the predominant type, existing in greater than half of all linkages, and their main role is to target the ubiquitinated protein for degradation by the proteasome[144]. The second most abundant is Lys63, which performs other nonproteolytic roles[145]. Ongoing research continues to

characterize the more “atypical” ubiquitin linkages (Lys6, Lys11, Lys27, Lys29, Lys33), some of which have been linked to control of the cell cycle and intracellular trafficking[146].

SUMOylation

Some ubiquitin polypeptides also undergo further post-translational modification of their own, in addition to ubiquitination. This includes the small ubiquitin-like (Ubl) modifier (SUMO) family, which constitute the most well studied Ubl modification system. SUMO proteins are 10-kDa polypeptides that also function as reversible PTMs by forming isopeptide bonds with epsilon-amino groups of acceptor lysine residues. Like ubiquitination, SUMO proteins are installed by an enzymatic cascade[147]. SUMOylation has multiple molecular consequences that depend on the substrate protein. It can block protein interactions, recruit SUMO-binding proteins, or change the conformation of the substrate protein. SUMOylation occurs in almost every compartment of the cell and affects essential biological functions such as cell growth, migration, stress response, and tumorigenesis[148].

Outlook

From this overview of gene expression, we can see that information required for synthesis of biomolecules is encapsulated within the genome of a cell. This information is discretely encoded in nucleotides and amino acids, so it can be said to assume a “digital” form to effect cellular function. However, the cell is very sensitive to different amounts of signaling, so it cannot tolerate aberrant genetic activity. The cell is able to fine-tune its expression epigenetically, epitranscriptomically, and post-translationally through various chemical modifications and interactions. These slight adjustments in gene expression can be said to be

"analog" in nature. It is the precise, interwoven control and repair of both digital and analog elements that almost miraculously enables the cell to survive and divide, and for the higher organism to thrive and reproduce.

Outline of this dissertation

One crucial mechanism is the post-transcriptional regulation of gene expression through the chemical modification of RNA. After the identification of m^6A regulatory proteins, their pivotal role in development and disease processes has also been established, providing avenues for therapeutic treatment in disease. Even so, questions about the regulation and effects of m^6A remain. In this dissertation, I aim to first study the phosphorylation of METTL3 (Chapter 2), how METTL3 affects RIG-I innate immunity activation (Chapter 3), and how ALKBH5 affects cancer cells as an m^6A eraser (Chapter 4).

Although it is known that the m^6A methyltransferase complex installs m^6A onto mRNA transcripts, it is not well understood how cells may dynamically regulate m^6A deposition in response to various stimuli within the cell. This is especially important for cells that undergo rapid changes in cell signaling. In Chapter 2, we describe how METTL3 and the rest of the m^6A writer complex are phosphorylated. We biochemically characterize how METTL3 and WTAP phosphorylation by the ERK2 kinase affects the m^6A complex and the impact this has on m^6A methylation of the transcriptome. We examine the contributions of METTL3 and WTAP phosphorylation to maintaining pluripotency in mouse embryonic stem cells and to cancer growth. ERK-phosphorylated METTL3 prevents decay of the m^6A writer complex by recruitment of the deubiquitinase USP5, thereby upregulating m^6A methylation and promoting stem cell differentiation.

m^6A is also known to affect the shape and structure of RNA. Because pattern recognition receptors sensors of foreign genetic material detect double-stranded RNA or DNA for downstream activation of a type I interferon response, we wondered whether m^6A upon cellular RNAs could affect the activation of the RIG-I sensor. In Chapter 3, we investigate how METTL3 affects formation of double-stranded RNAs, and whether m^6A methylation affects RIG-I activation. We find that loss of METTL3 significantly enhances the Type I interferon response upon stimulation of RIG-I. Sequencing of double-stranded RNAs and RIG-I-bound RNAs reveals enrichment of those species in METTL3-depleted HeLa cells. This work suggests that m^6A methylation suppresses antiviral innate sensing pathways by reshaping double-stranded RNAs.

ALKBH5, as one of the two known m^6A erasers, affects many biological processes, including spermatogenesis in mice and host response to viral infection through changes in mRNA metabolism. Like FTO, it also plays a role in multiple cancers. In Chapter 4, we investigate the role of ALKBH5 in leukemia, given that its high expression spells poorer prognosis for AML patients. Specifically, we examine how ALKBH5 affects leukemia proliferation, leukemogenesis, leukemic stem cell self-renewal, and find that ALKBH5 promotes all those processes. Mechanistically, this is due in large part to m^6A demethylation of *TACC3* mRNA, leading to reduced post-transcriptional degradation. Subsequently, this leads to increased MYC and reduced P21 expression, thereby promoting cancer growth. In the second part of Chapter 4, we investigate another facet of ALKBH5—namely, its interaction with RBM33, which acts as an RNA binding scaffold. We find that ALKBH5 and RBM33 are both necessary for m^6A eraser activity and promote head and neck cancer.

Finally, in Chapter 5, we conclude by summarizing more recent findings in the field of m^6A methylation and RNA epigenetic regulation. We discuss broader impacts, important yet unanswered questions, and unexplored frontiers in the field.

In the Appendix at the end of this dissertation, I include excerpts from a review I wrote with my advisor on the topic of the therapeutic applications of RNA m^6A methylation, particularly in cancer treatment.

Chapter II: Phosphorylation of METTL3 by the ERK2 Kinase Stabilizes METTL3 Through USP5 and Increases m^6A Methylation

Note:

The following section (*Chapter II*) is reproduced verbatim with minor adjustments to the text and figures from my co-first authored reference "Stabilization of ERK-Phosphorylated METTL3 by USP5 Increases m^6A Methylation." There are also alterations in the chapter title, figure numbering, and reference labeling. This project was performed in collaboration with Hui-Lung Sun and published in *Molecular Cell* on November 19, 2020.[1] H.S. and I carried out most of the experiments, assembled the figures, and wrote the manuscript. I analyzed CRISPR screen, RNA-seq, and m^6A-seq data. I also performed most of the mass spectrometry experiments and a portion of the ubiquitination and protein stability experiments.

Authors:

Hui-Lung Sun*, Allen C Zhu*, Yawei Gao, Hideki Terajima, Qili Fei, Shun Liu, Linda Zhang, Zijie Zhang, Bryan T Harada, Yu-Ying He, Marc B Bissonnette, Mien-Chie Hung, Chuan He.

*These authors contributed equally to this work.

[1] Sun, H. L., Zhu, A. C., Gao, Y., Terajima, H., Fei, Q., Liu, S., Zhang, L., Zhang, Z., Harada, B. T., He, Y. Y., Bissonnette, M. B., Hung, M. C., & He, C. (2020). Stabilization of ERK-Phosphorylated METTL3 by USP5 Increases m^6A Methylation. *Molecular Cell*, *80*(4), 633–647.e7. Used with permission from Elsevier.

Abstract

N^6-methyladenosine (m^{6}A) is the most abundant mRNA modification and is installed by the METTL3-METTL14-WTAP methyltransferase complex. Although the importance of m^{6}A methylation in mRNA metabolism has been well documented recently, regulation of the m^{6}A machinery remains obscure. Through a genome-wide CRISPR screen, we identify the ERK pathway and USP5 as positive regulators of the m^{6}A deposition. We find that ERK phosphorylates METTL3 at S43/S50/S525 and WTAP at S306/S341, followed by deubiquitination by USP5, resulting in stabilization of the m^{6}A methyltransferase complex. Lack of METTL3/WTAP phosphorylation reduces decay of m^{6}A-labeled pluripotent factor transcripts and traps mouse embryonic stem cells in the pluripotent state. The same phosphorylation can also be found in ERK-activated human cancer cells and contribute to tumorigenesis. Our study reveals an unrecognized function of ERK in regulating m^{6}A methylation.

Introduction

Recent studies have shown that messenger RNA (mRNA) modifications play a critical role in regulating biological and pathological processes [37]. Among over 150 known RNA modifications, *N*^{6}-methyladenosine (m^{6}A) is an evolutionarily conserved and the most abundant internal mRNA modification in eukaryotic mRNA. m^{6}A is reversibly, site-selectively installed on mRNA transcripts by "writers," with a portion that can be removed by "erasers". The m^{6}A methylation is mediated by a core complex of three components: METTL3, METL14, and WTAP [50]. The crystal structure of the METTL3 and METTL14 complex suggests that METTL3 is the catalytic component while METTL14 contributes to substrate RNA binding. WTAP, on the other hand, recruits METTL3 and METTL14 to nuclear speckles [54, 100]. Meanwhile, "eraser" proteins FTO and ALKBH5 remove m^{6}A modification [36, 70].

Increasing evidence suggests that the m^6A modification is involved in the regulation of RNA splicing, localization, stability, and translation [78-80, 82, 89]. It has been found that m^6A affects numerous physiological and pathological processes. For example, loss of METTL3 in mouse embryonic cells (mESCs) depletes m^6A and increases stability of certain transcripts such as *Nanog* [98, 100]. This impedes decay of pluripotency factors, thereby delaying proper lineage priming and fate transition, leading to early embryo lethality [101]. Furthermore, METTL3 knockdown is known to induce apoptosis [38] and METTL3 overexpression can promote tumorigenesis in multiple cancer types [118, 119, 127, 149-157].

The importance of m^6A methylation has been well described, yet gaps in our understanding of how this process is regulated remain. We therefore used a genome-wide CRISPR screen to identify regulators of m^6A methylation. The biological importance of these regulations was further studied in mESCs and relevant cancer cells.

Results

ERK Activation Promotes mRNA m^6A Methylation

To identify regulators of m^6A RNA methylation, we employed a circular RNA GFP reporter containing a consensus GGACU motif in HeLa cells. The GFP pre-mRNA transcript is assembled by back-splicing to generate a circular RNA that joins two exon fragments of GFP, as depicted in Figure 2-1A. m^6A methylation of the GGACU motifs on the circular RNA can drive translation initiation of the GFP transcript, producing GFP fluorescence signal. Consequently, the GFP signal from this circular RNA reporter can be used as a readout of m^6A methylation. Indeed, consistent with a previous report [158], circRNA containing GGACT was translated into GFP, whereas mutation to GGTCT reduced GFP levels. Co-expression of METTL3 increased GFP expression from the GGACT reporter but not the GGTCT control (Figure 2-1B).

Furthermore, signal from the GGACT reporter was decreased by catalytic mutant D395A METTL3, as well as siMETTL3, siMETTL14, and siWTAP, but was increased by siFTO and siALKBH5 (Figure 2-1B).

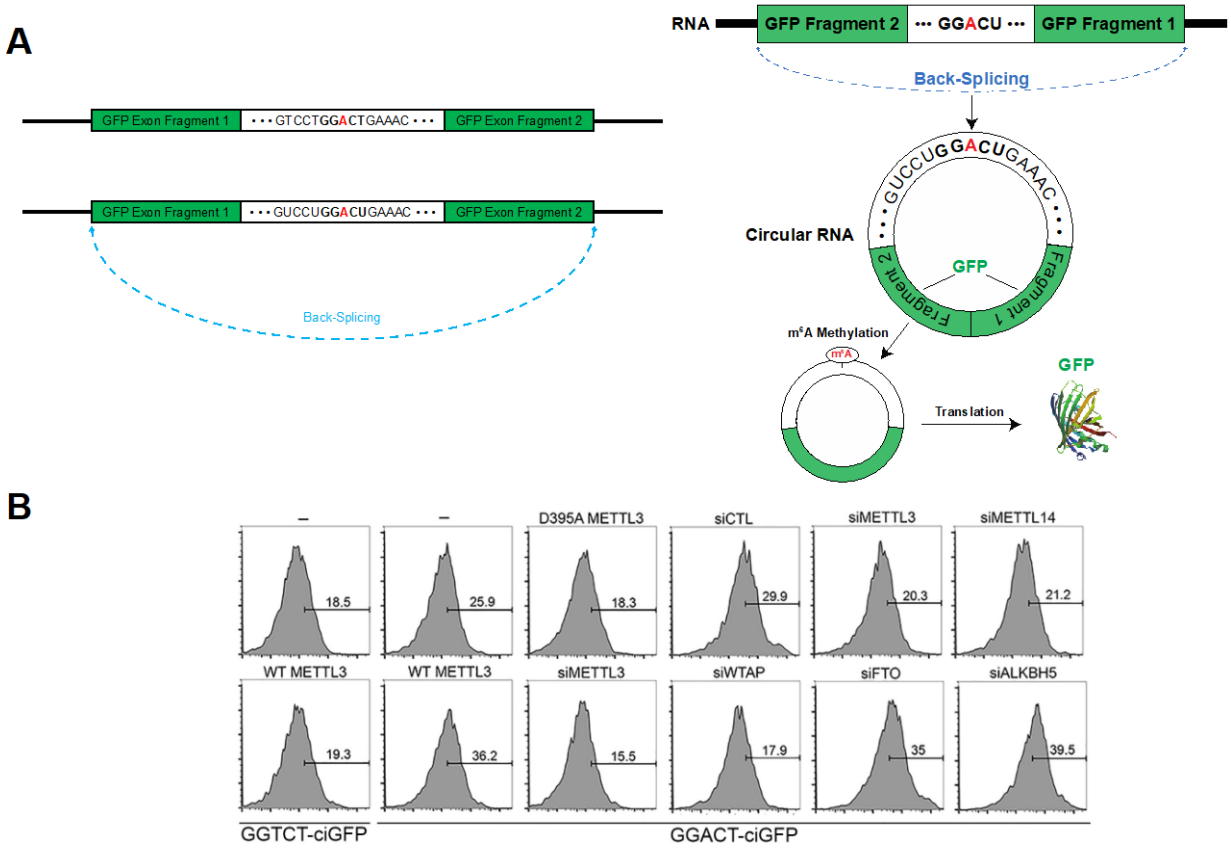

Figure 2-1. A circular RNA translation reporter may reveal regulators of m^{6}A methylation.

(A) Schematic diagram of a circular RNA (circRNA) translation reporter consisting of a single exon and two introns with complementary sequences. The exon containing GGACU can be back-spliced to generate circRNAs that drive GFP translation. (B) Representative flow cytometry analyses of HeLa circular-GFP GGACT or control GGTCT reporter cells transfected as indicated for 48 hr.

Next, we performed a CRISPR knockout-based genomic screen targeting 19,050 genes and 1,864 miRNA [159]. Combining a CRISPR knockout library with a circular RNA m^{6}A-GFP reporter allowed us to screen for possible regulators of m^{6}A methylation (Figure 2-2).

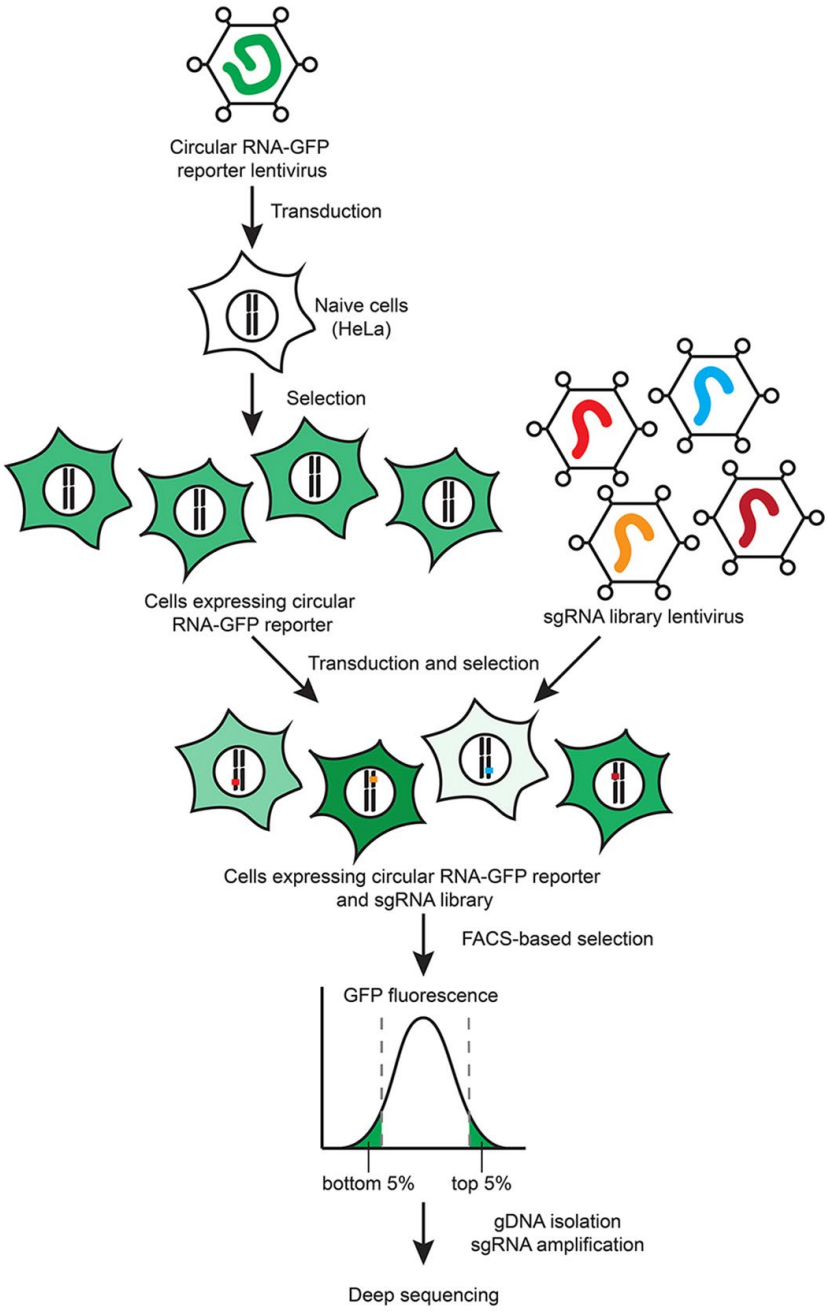

Figure 2-2. Overview of the CRISPR screen.

Cas9 knockout libraries are packaged into lentivirus and then transduced into HeLa cells contain circRNA GFP reporters. Cells with the top and bottom 5% GFP expression are collected by flow cytometry. The sgRNA are amplified from genomic DNA and then analyzed by next-generation sequencing followed by statistical analyses to identify candidate genes.

Knockout of genes that promote or suppress m^{6}A methylation would decrease or increase translation of the GFP transcript, respectively. Cells with the top and bottom 5% of GFP expression were therefore collected, followed by high-throughput sequencing in order to identify negative and positive regulators of m^{6}A methylation, respectively. We compared the genes that were enriched in the low-GFP-expressing and the high-GFP-expression populations (Table S1). As expected, knockout of METTL3 led to low GFP signal in the screen (Figure 2-3A). Interestingly, pathway enrichment analysis of the gRNAs in low-GFP-expressing cells identified genes involved in the RAS and MAPK signaling pathways (Figure 2-3A, B and Table S2).

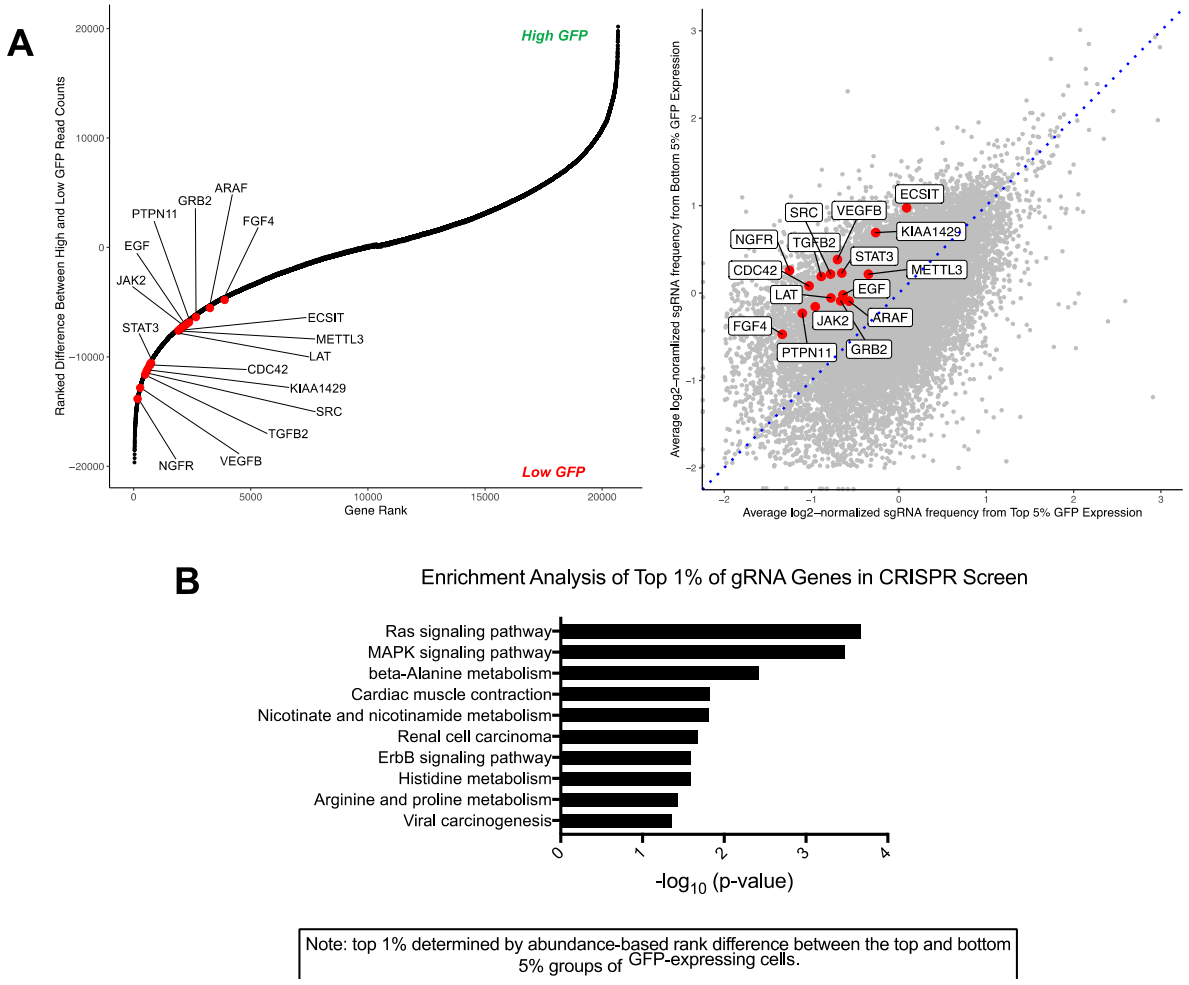

Figure 2-3. ERK Activation Promotes mRNA m^{6}A Methylation.

Figure 2-3, continued. ERK Activation Promotes mRNA m^{6}A Methylation.
(A) Positive regulators for the m^{6}A pathway identified in the CRISPR screening using circular GGACU-GFP reporters. (B) Pathway analysis of sgRNA enriched in the bottom 5% GFP cells with circRNA GFP reporters.

Several hits which are known to activate ERK, including SHC1, CDC42, MAP3K1, PTPN11, and GRB2, decreased GFP signal from the GGACT reporter significantly more than the control GGTCT reporter (Figure 2-4).

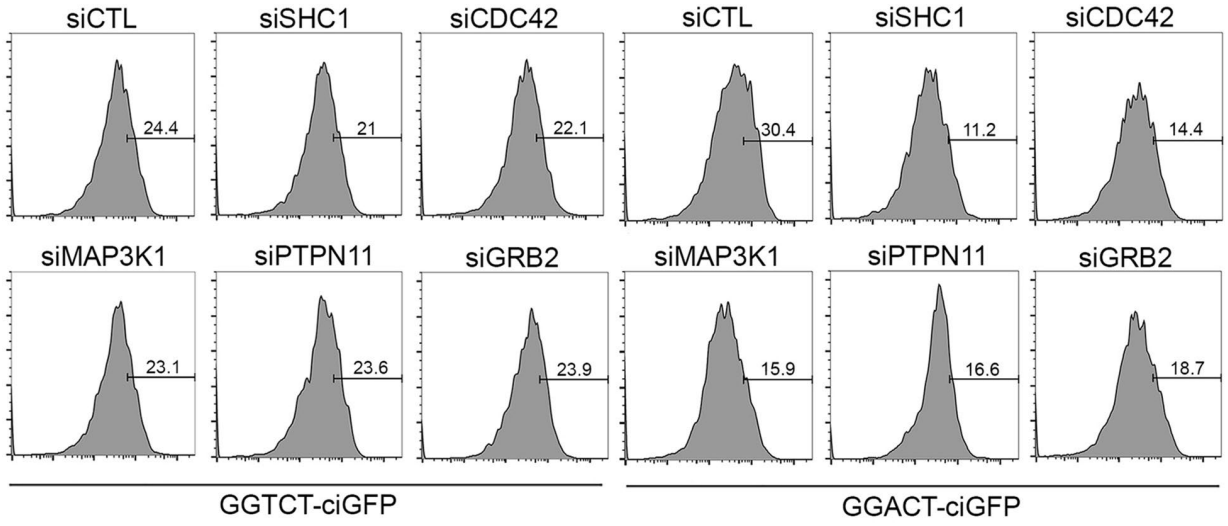

Figure 2-4. Flow cytometry analysis of circular RNA GGACU GFP reporter.

Representative flow cytometry analyses of HeLa circular-GFP GGACT or control GGTCT reporter cells with ERK activator knocked down for 48 hr.

To determine how the RAS/MAPK pathway affects m^{6}A methylation, we investigated the status of the m^{6}A methyltransferase complex during MAPK pathway activation. A phos-tag gel [160] revealed that constitutively active MEK S218D/S222D, BRAF V600E, or HER2 V659E, increased the phosphorylation-dependent mobility shift of METTL3 and WTAP, but not METTL14 (Figure 2-4A). We further co-transfected a panel of 13 oncogenic kinases, including ATM, ATR, IKK-α, IKK-β, IKK-ε, AKT, GSK-3β, mTOR, MEK, CDC2, FAK, EGFR, and HER2 with METTL3 in 293T cells. As shown in Figure 2-4B, MEK and HER2, which activate

ERK, induced the most significant phosphorylation-dependent mobility shift of METTL3. We also employed *NANOG* 3' UTR, which contains three m^{6}A consensus RRACT motif sites that mediate the methylation-dependent decay of *NANOG* [126], as a readout of the cellular m^{6}A methylation activity. Mutation of the adenosine residue (AAACT to AATCT, and GGACT to GGTCT) resulted in increased luciferase activity, suggesting that the mutation prevented methylation and thereby increased the stability of the luciferase-*NANOG* 3'-UTR fusion mRNA. We noticed that overexpression of the m^{6}A methyltransferase complex (METTL3-METTL14-WTAP) decreased wild type RRACT but not mutant RRTCT reporter expression. Overexpression of the ERK activators alone decreased WT *NANOG* 3'UTR reporter expression, and the effect was enhanced with the m^{6}A methyltransferase complex (Figure 2-4C). Together, our results show that the activation of MAPK pathway promotes mRNA m^{6}A methylation.

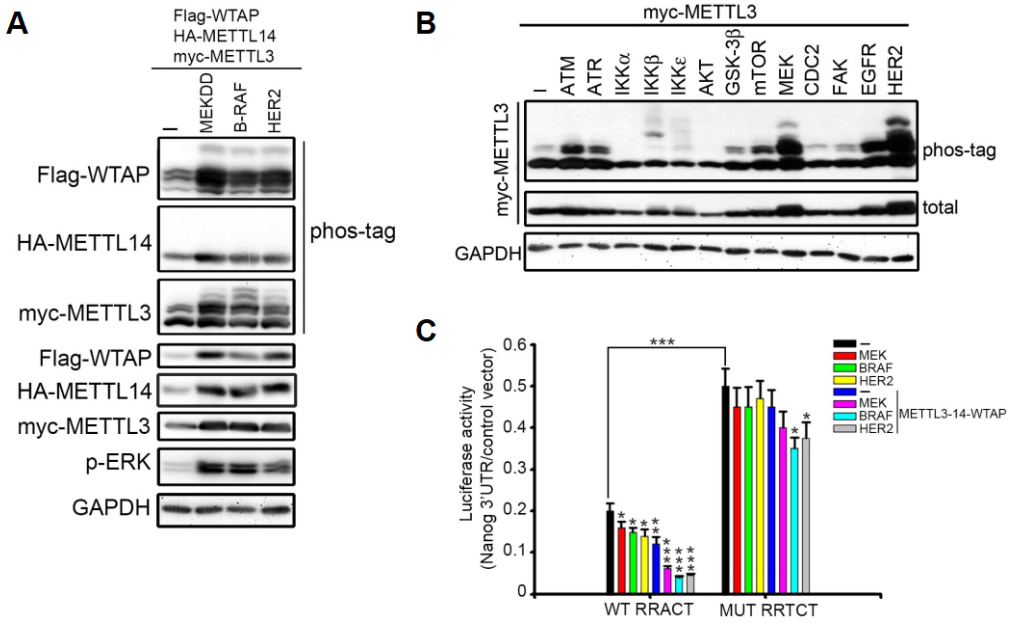

Figure 2-5. The MAPK pathway promotes phosphorylation of METTL3.

(A) Lysates of 293T cells transfected with the m^{6}A writer complex and ERK-activated kinase were analyzed by SDS-PAGE or phos-tag SDS-PAGE. (B) Lysates of 293T cells transfected with METTL3 and 13 different oncogenic kinases were analyzed by SDS-PAGE or phos-tag SDS-PAGE. (C) 293T cells were transfected with a luciferase reporter containing wild type, mutant *NANOG* 3'UTR or random negative control, m^{6}A writer complex, and ERK-activated kinase for 48 hr before luciferase assay. The ratio of luciferase activity in cells transfected with *NANOG*-3'UTR relative to control vector was determined. (n = 3 per group, data represent mean ± SEM, p values were calculated by Student's t test). *p < 0.05, **p < 0.01, ***p < 0.001.

ERK Phosphorylates METTL3 and WTAP

To determine how ERK activates m^{6}A methylation, we first tested whether ERK interacts with the mRNA m^{6}A methyltransferase complex. Co-immunoprecipitation showed that METTL3 associates with ERK1 and ERK2 upon BRAF transfection (Figure 2-6A). Considering that ERK1 and ERK2 are highly similar and possess identical substrate specificity *in vitro*, we focused on ERK2 hereafter because ERK2 expression exceeds ERK1 in most cells. The interaction between ERK2 and WTAP was also observed after RAF activation (Figure 2-6B). The interaction of endogenous ERK2 with METTL3 and WTAP was observed in A375 cells, a

human melanoma cell line with constitutively active ERK due to a BRAF V600E mutation (Figure 2-6C). After MEK stimulation, activated ERK translocates into the cell nucleus to activate nuclear substrates, or forms a dimer to activate cytoplasmic substrates [161]. As shown in Figure 2-6D, ERK activated by BRAF co-localizes with METTL3 and WTAP in the nucleus, suggesting that METTL3 complex could be a nuclear substrate of ERK.

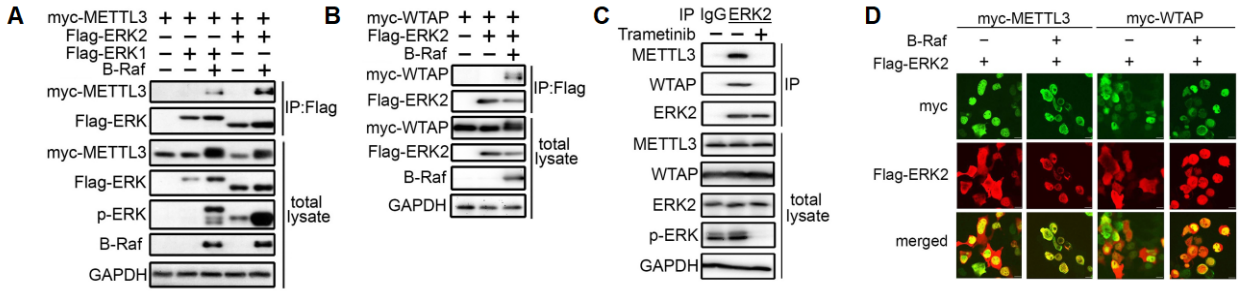

Figure 2-6. ERK phosphorylates METTL3 and WTAP.

(A) Lysates of 293T cells transfected as indicated were subjected to IP with anti-Flag antibody followed by IB. (B) Lysates of 293T cells transfected as indicated were subjected to IP with anti-Flag antibody followed by IB. (C) A375 cells were treated with or without 0.1 μM trametinib for 1 hr. Cell lysates were analyzed by IP and IB as indicated. (D) Immunofluorescence analysis of 293T cells co-transfected with myc-METTL3 or myc-WTAP (green), Flag-USP5 with or without constitutively active BRAF. Scale bars, 10 mm.

ERK displays a specificity for phosphorylation at the serine/threonine-proline (S/T-P) motif. Since the S/T-P motif is found in many proteins, ERK either uses a common docking domain [162] to bind to a D domain (K/R$_{0-2}$-X_{1-6}-φ-X-φ) or uses the F-site recruitment site (FRS) to bind to the F-site (FX-F/Y-P) [163]. Analysis using the Eukaryotic Linear Motif database (http://elm.eu.org) revealed residues 415-421 in METTL3 and residues 71-77 in WTAP as potentially conserved D domains (Figure 2-7A). We found that a CD mutant (321N) form of ERK2, but not an FRS mutant (263A) form, abolished its interaction with METTL3 and WTAP (Figure 2-7B). Mutational analysis of the putative D domain residues of METTL3 and WTAP

abolished the interaction. Co-IP showed that ERK2 only binds to the myc-tagged domain where the D-domain is located (Figure 2-7C). These results support the interaction of ERK with METTL3 and WTAP.

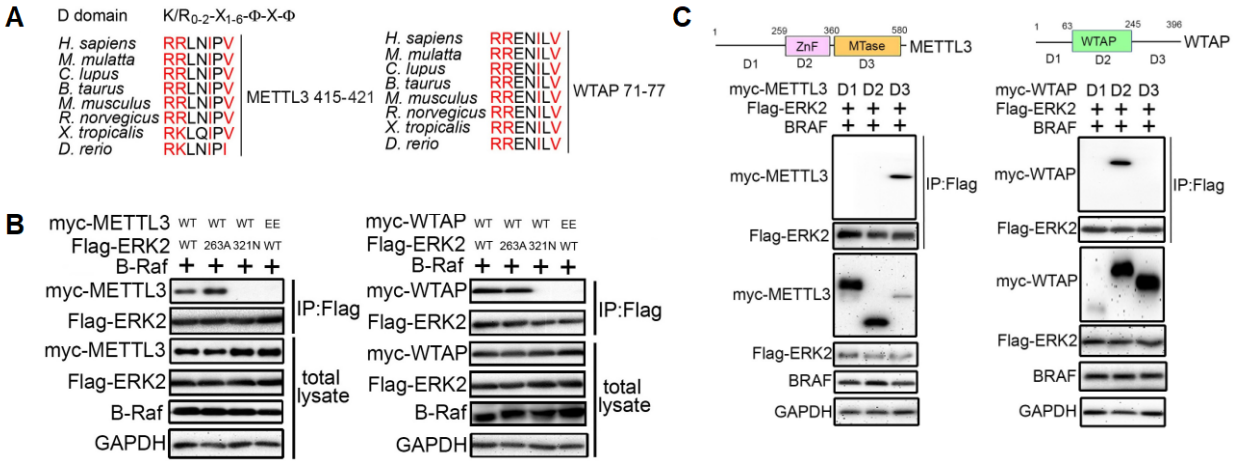

Figure 2-7. ERK interacts with METTL3 and WTAP through a common docking interaction.

(A) Sequence alignment of the conserved D-domain on METTL3 and WTAP predicted by the eukaryotic linear motif website. The D domain possesses a consensus binding sequence of (Lys/Arg)0-2-(X)1-6-Φ-X-Φ; where Φ is a hydrophobic residue such as Leu, Ile, Val, Phe, and X is any amino acid. (B) Interaction between wild-type (WT) or mutant METTL3, WTAP, and ERK2 in lysates from BRAF-expressing 293T cells transfected as indicated was examined by co-immunoprecipitation. EE, R415E/R416E METTL3 or R71E/R72E WTAP. (C) Flag-ERK2 and myc-METTL3 or myc-WTAP domains were co-transfected into 293T cells for 48 hr, followed by IP with anti-Flag antibody and IB as indicated. Schematic representation of the different truncation constructs of myc-METTL3 and Flag-ERK2 used to narrow down the binding sites were indicated above the blot.

Given the physical interaction between ERK and METTL3, and that calf intestinal alkaline phosphatase can eliminate the mobility shift induced by ERK (Figure 2-9A), we examined whether METTL3 is a physiological substrate of ERK. *In vitro* kinase assay suggests that ERK directly phosphorylates METTL3 (Figure 2-9B). We noticed that p38 and JNK, but not ERK5, phosphorylate METTL3, although not as strongly as ERK2. Mass spectrometry analysis showed that ERK phosphorylates METTL3 at three highly conserved residues S43, S50, and

S525 (Figure 2-9C, D). Mutational analysis further confirmed these three sites as main ERK phosphorylation sites (Figure 2-9E). There is no available structure for WTAP, and published studies of the METTL3 structure focus on the SAM-binding and methyltransferase domains, which cannot provide information for S43 and S50. However, we noticed that S525 lies on the same face and close to the D Domain of METTL3 (Fig 2-9F). This suggests that the phosphorylation occurs near the ERK binding region.

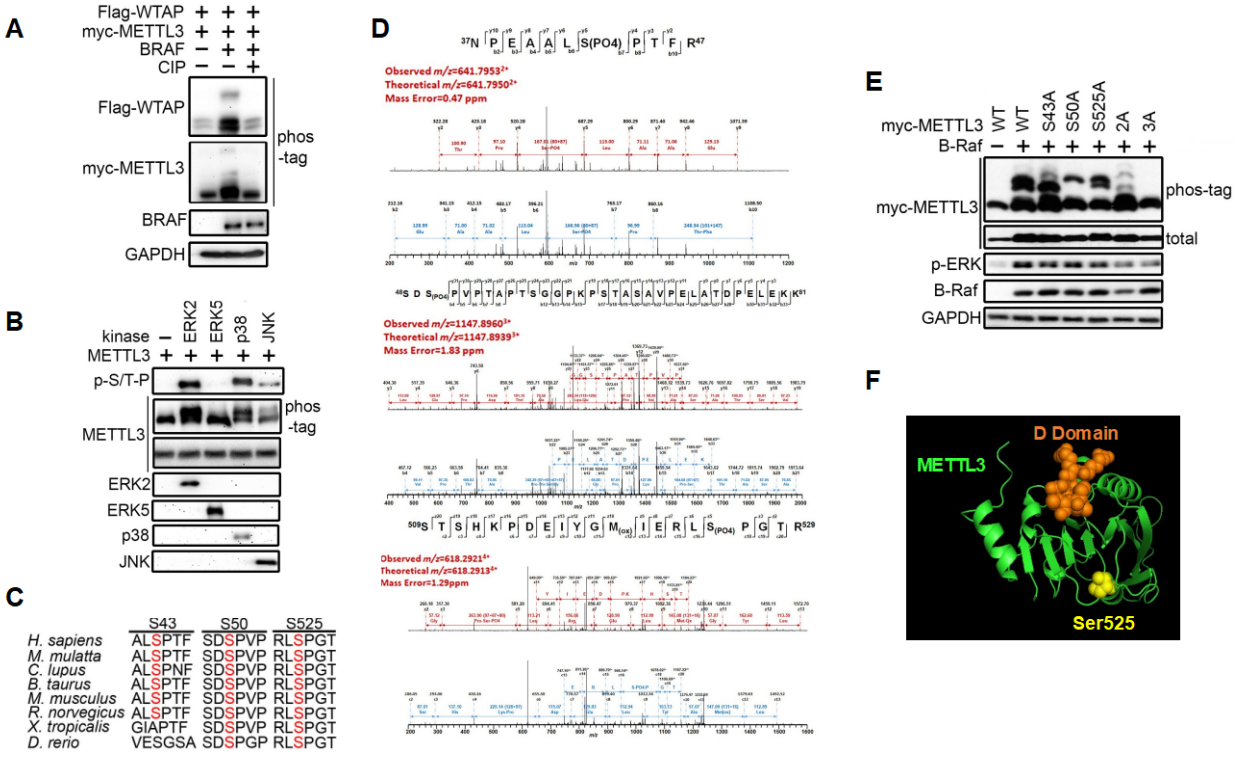

Figure 2-8. ERK phosphorylates METTL3 at Ser43, Ser50, and Ser525.

(A) Lysates from 293T cells transfected as indicated were treated with calf intestine alkaline phosphatase (CIP) then subjected to SDS-PAGE or phos-tag SDS-PAGE. (B) *In vitro* kinase assay was conducted by incubating recombinant activated ERK2, ERK5, p38, JNK with purified METTL3-METTL14. (C) Sequence alignment of the conserved serine residues on METTL3 that are phosphorylated by ERK. (D) Mass spectrometry detected S43, S50 and S525 phosphorylation in METTL3 in 293T cells co-transfected with BRAF V600E. (E) Phos-tag SDS-PAGE showing the phosphorylation status of WT or non-phosphorylatable alanine mutants of METTL3 in 293T cells co-transfected with BRAF. 2A, T43A/S50A; 3A, S43A/S50A/S525A. (F) Relative position of S525 (yellow) and D domain (orange) in the crystal structure of METTL3 (green, PDB: 5IL0)

To investigate METTL3 phosphorylation by ERK inside cells, we raised a polyclonal antibody that targets S43-phosphorylated METTL3. This antibody recognizes S43-phosphorylated METTL3 but not a mutant form of METTL3, 3A METTL3, in which all three phosphorylation serine sites are replaced with alanine (Figure 2-9A). This P-S43 antibody was then used as a tool to monitor METTL3 phosphorylation. The endogenous METTL3 phosphorylation can be detected in A375 (BRAF-V600E mutant) and HCT116 (K-Ras-G12D mutant) and abrogated by MEK inhibitor treatment for 1 hour (PD0325901 or trametinib) (Figure 2-9B, C). Although this antibody is not suitable for immunoprecipitation (data not shown), phos-tag gels suggested about 80% of endogenous METTL3 was phosphorylated in A375 and HCT116 and decreased to 40% upon addition of MEK inhibitors.

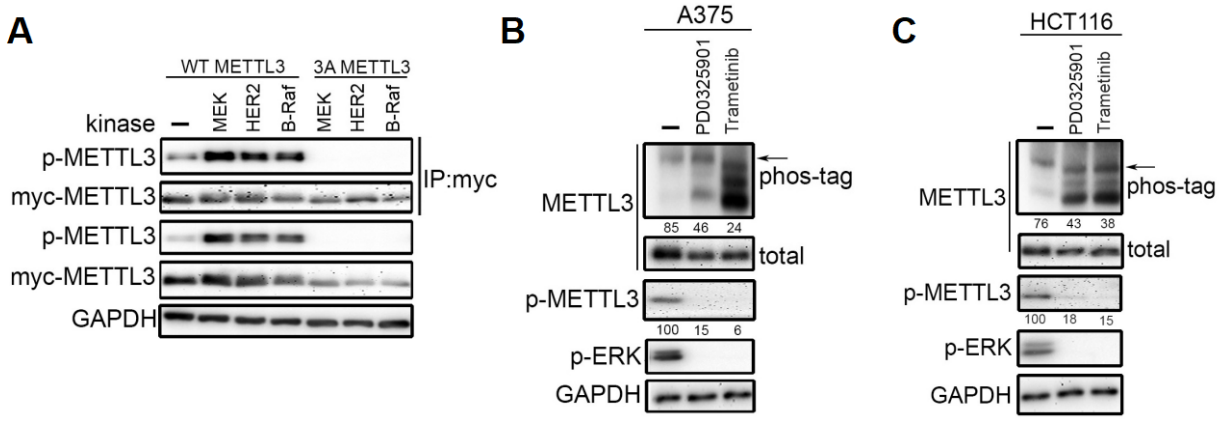

Figure 2-9. Loss of ERK activation abrogates METTL3 phosphorylation.

(A) Characterization of anti-p-METTL3 (S43) antibodies of 293T cells transfected as indicated with MEK S218D/S222D, HER2 V659E, BRAF V600E and WT or non-phosphorylatable alanine mutant (3A) METTL3. (B-C) A375 or HCT116 cells were treated with 10 μM PD0325901or 0.1 μM trametinib for 1 hr. Cell lysates were subjected to SDS-PAGE or phos-tag SDS-PAGE. Arrowheads indicate phosphorylated METTL3. Density of each band was quantified by ImageJ and the relative percentage of phosphorylated to total METTL3 detected by phos-tag or p-S43 METTL3 antibody were indicated below the blots.

To determine the phosphorylation sites of WTAP, we examined whether mutations of the S/T-P motif affect the ERK-induced phosphorylation. Among the three S/T-P motifs in human WTAP (Figure 2-10A), we found that S306 and S341 are the main ERK phosphorylation sites of human WTAP (Figure 2-10B). We noticed that S306 is not conserved in mouse and rat WTAP orthologs; however, there is a unique S/T-P motif at T298 in mouse and rat WTAP, which can also be phosphorylated by ERK (Figure 2-10C). In conclusion, we show that ERK interacts with and phosphorylates METTL3 and WTAP.

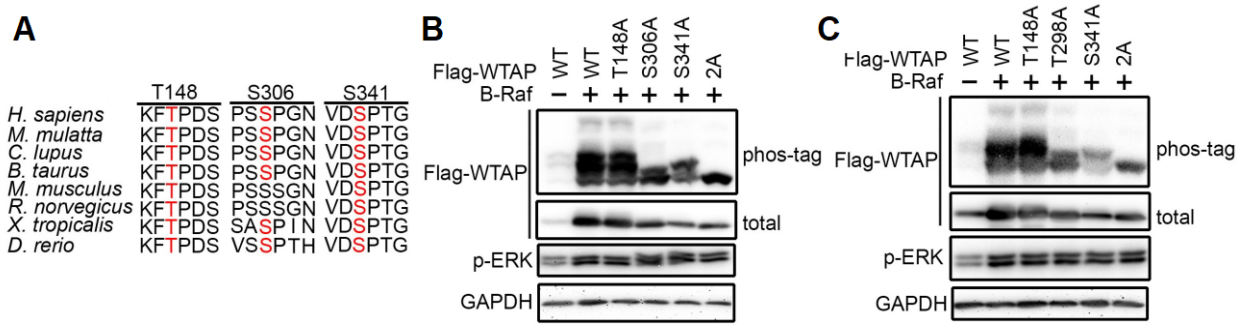

Figure 2-10. WTAP is phosphorylated at Ser306 and Ser341.

(A) Sequence alignment of the serine/threonine-proline (S/T-P) motif on WTAP. (B) Phos-tag SDS-PAGE showing the phosphorylation status of WT or non-phosphorylatable alanine mutants of human WTAP in 293T cells co-transfected with BRAF. 2A, S306A/S341A. (C) Phos-tag SDS-PAGE showing the phosphorylation status of WT or non-phosphorylatable alanine mutants of mice WTAP in 293T cells co-transfected with BRAF. 2A, T298A/S341A.

USP5 is Required for ERK-Mediated METTL3 Stabilization

Next, we investigated how ERK-induced phosphorylation increases RNA m^6A methyltransferase complex activity. We noticed that ERK activation increased wild-type (WT) but not 3A METTL3 expression (Figure 2-8E), and that WT METTL3 stable transfectants maintained consistently higher expression levels than those of 3A METTL3 in both mouse ESCs (mESCs) and human A375 cells. (Figure 2-11A). This observation suggested a model in which METTL3 phosphorylation by ERK stabilizes the protein, which could explain the higher

METTL3 protein level and elevated m^{6}A methylation activity observed with ERK activation. We then investigated whether ERK activation could affect METTL3 stability and found that inhibition of ERK by PD0325901 increased its ubiquitination at 8-hour treatment (Figure 2-11B). Furthermore, the degradation of METTL3 induced by inhibition of ERK activity was restored by addition of a proteasome inhibitor MG132 (Figure 2-11C). The ubiquitination level of 3A METTL3 was also higher than that of WT METTL3 (Figure 2-11D). To assess more directly the effects of ERK on METTL3 stability, cycloheximide was used to suppress protein synthesis and the degradation of METTL3 protein was monitored. As shown in Figure 2-11E, ERK activation increased the stability of WT but not non-phosphorylatable 3A METTL3; meanwhile, phospho-mimetic 3E METTL3 showed an increase in stability compared to WT METTL3.

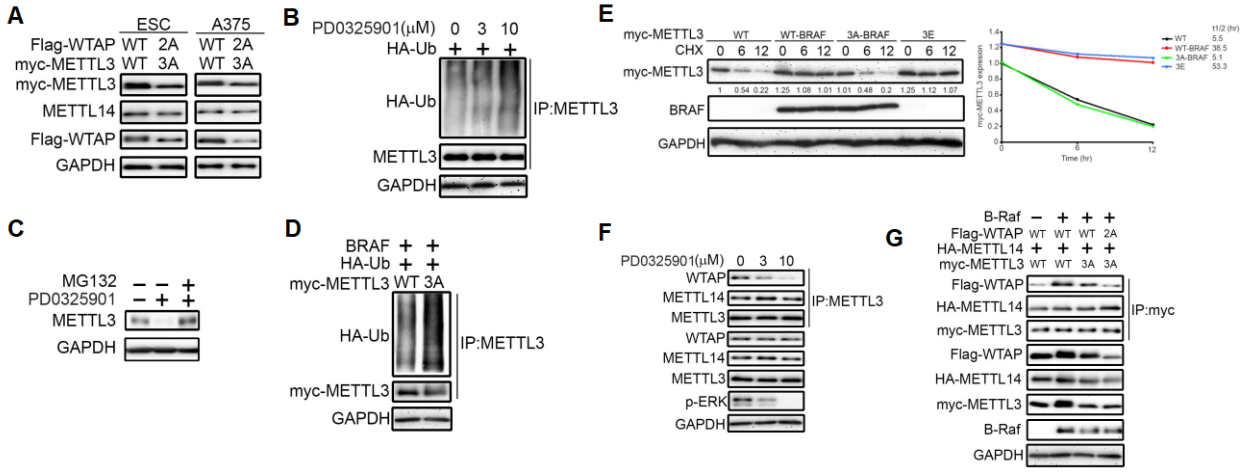

Figure 2-11. Phosphorylation by ERK promotes stabilization of METTL3.

(A) Comparison of METTL3 and WTAP protein levels in mESCs and A375 stable transfectants by immunoblotting (IB). (B) A375 cells transfected with HA-ubiquitin were treated with 10 μM MG-132 and MEK inhibitor PD0325901 for 8 hr. The ubiquitination of METTL3 was detected by IP with anti-METTL3 and IB with anti-HA. (C) After 8 hr treatment with 10 μM PD0325901 with or without 10 μM MG-132, cell lysates from A375 cells were analyzed by IB. (D) 293T cells transfected as indicated were treated with MG-132 (10 μM, 8hr) followed by IP/IB analysis. (E) 293T cells transfected as indicated for 48 hr, followed by cycloheximide (CHX) 10 μg/ml for 0-12 h. Cell lysates were used for IB to measure the protein levels of METTL3.

Figure 2-11, continued. Phosphorylation by ERK promotes stabilization of METTL3. Density of METTL3 expression was quantified by ImageJ and the relative fold compared to the untreated WT was indicated and plotted at the right panel. (F) A375 cells were treated with 3 or 10 μM PD0325901 for 1 hr. Cell lysates were subjected to IP with METTL3 antibody followed by IB. (G) 293T cells transfected as indicated for 48 hr were subjected to IP/IB analysis.

Since METTL14 is known to stabilize METTL3 [52], we investigated whether phosphorylation of METTL3 by ERK affects METTL3-METTL14 complex formation. The interaction between METTL3 and METTL14 was not obviously affected by ERK inhibition treatment for 1 hour (Figure 2-11F). Moreover, 3A METTL3 also interacts with METTL14 normally (Figure 2-11G). Interestingly, we noticed that ERK activation increased the interaction between METTL3 and WTAP, which became weaker with 3A METTL3 and was further attenuated with non-phosphorylatable WTAP S306A/S341A (2A) (Figure 2-11G). It has been shown that WTAP depletion does not affect METTL3 complex stability, but rather reduces nuclear localization of METTL3 [54, 164]. Consistent with previous reports, knockdown of WTAP decreased nuclear METTL3 (Figure 2-12A). Considering the interaction between METTL3 and WTAP was attenuated by non-phosphorylatable mutant forms, cellular fractionation and immunostaining was used to examine METTL3. As shown in Figure 2-12B and 2-12C, nuclear METTL3 was markedly reduced in cells expressing 3A METTL3 and 2A WTAP.

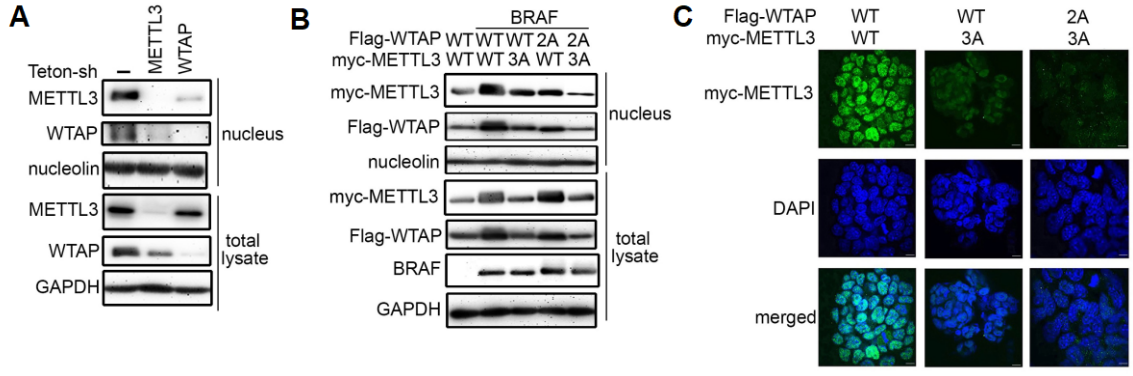

Figure 2-12. Phospho-defective mutants exhibited lower expression and nuclear abundance.

Figure 2-12, continued. Phospho-defective mutants exhibited lower expression and nuclear abundance.
(A) A375 Teton-shMETTL3 or shWTAP stable trasfectants were treated with 2 μg/ml doxycycline for 3 days. Nuclear and total lysates were subjected to IB analysis. (B) IB analysis of nuclear and total lysates of 293T cells transfected as indicated for 48 hr. (C) Immunofluorescence analysis of myc-METTL3 (green) in mESCs stable transfectants. DAPI (blue) was used to mark the nucleus. Scale bars, 10 mm.

To gain further insight into how ERK phosphorylation decreases METTL3 ubiquitination, we examined whether any ubiquitin ligases or deubiquitinases were identified in our CRISPR-based genomic screen. Since the top hits identify regulators of GGACT reporter m^6A methylation rather than just METTL3, not all hits—namely, USP43, USP15, or USP7 (Table S1, top 1000 sgRNAs)—affected METTL3 expression level (Figure 2-13A). However, we found knockdown of USP5 and USP1 (Rank 2845 and 2339) decreased METTL3 in A375 (Figure 2-13B). Commercially available USP1 inhibitor SJB3-019A and USP5 inhibitor EOAI3402143 (EOAI) also decreased METTL3 (Figure 2-13C). Considering USP5 is implicated in a wide range of pathological processes and had the most pronounced effect on METTL3, we chose to further investigate it.

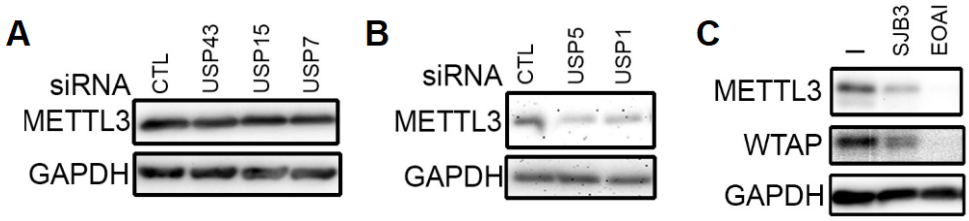

Figure 2-13. USP5 is required for METTL3 stabilization.

(A-B) A375 cells were transfected with siRNA targeting deubiquitinase for 72 hr before IB analysis. (C) A375 cells were treated with 3 μM SJB3-019A (SJB3) or 10 μM USP5 inhibitor EOAI3402143 (EOAI) for 8 hr before IB analysis.

We first investigated whether phosphorylation of METTL3 in the presence of activated BRAF affects the METTL3-USP5 interaction. We noticed that ERK activation increased the

interaction between METTL3 and USP5, which became weaker with phospho-defective mutant S43A, S50A, S525A, and fully attenuated when all three sites were mutated (Figure 2-14A). We also noticed that 3E METTL3 binds to USP5 more strongly. Interestingly, BRAF expression further promoted 3E METTL3-USP5 interaction and increased its expression. This suggests that BRAF may also affect USP5 activity. It has been demonstrated that USP5 activity was increased in cells expressing BRAF V600E [165]. We further found that ERK activation by BRAF promoted USP5 translocation into the nucleus to colocalize with METTL3 (Figure 2-14B). USP5 is a large protein composed of five specific domains, including the cryptic ZnF domain, ZnF domain, C-box domain, UBA1/UBA2 domain, and H-box domain. To define which domain was critical for the action of USP5 on METTL3, constructs of these domains were co-transfected with METTL3. The IP assay suggested that METTL3 binds more strongly to the cryptic ZnF domain compared to the C-box domain and H-box domain (Figure 2-14C). On the other hand, USP5 binds to the methyltransferase domain of METTL3 (Figure 2-14D). Reciprocal IP confirmed the endogenous METTL3-USP5 interaction, which was inhibited by MEK inhibitor (Figure 2-14E). Lastly, ERK-phosphorylated or phosphomimetic 3E METTL3 displayed greater stability upon USP5 inhibitor EOAI treatment (Figure 2-14F). Taken together, these results suggest that ERK activation translocates USP5 to the cell nucleus, which interacts with phosphorylated METTL3 to promote its stability.

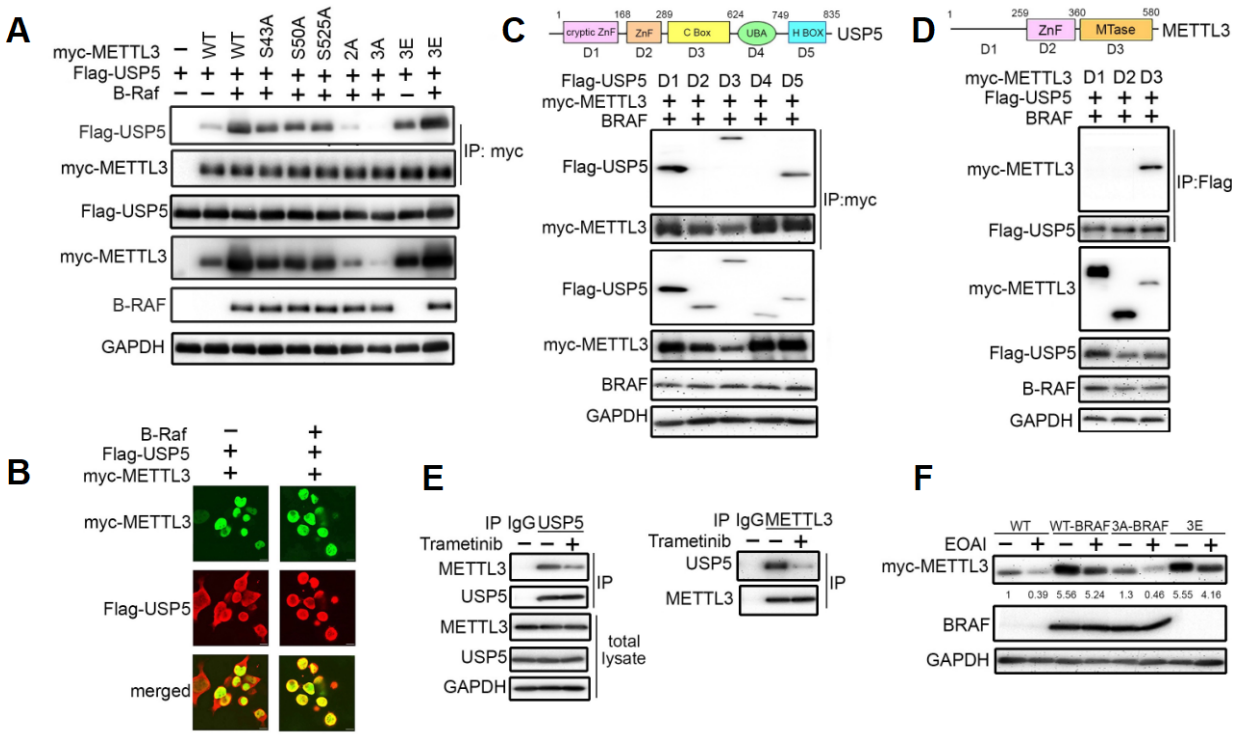

Figure 2-14. USP5 interacts with METTL3 to promote ERK-mediated stabilization.

(A) BRAF expression promotes METTL3-USP5 interaction. Lysates of 293T cells transfected as indicated for 48 hr were subjected to IP with anti-myc antibody followed by IB. (B) Immunofluorescence analysis of 293T cells co-transfected with myc-METTL3 (green), Flag-USP5 with or without constitutively active BRAF. Scale bars, 10 mm. (C) Top: The scheme of USP5 protein domains. Bottom: BRAF, myc-METTL3 and Flag-USP5 domains were co-transfected into 293T cells for 48 hr, followed by IP and IB analysis as indicated. (D) Top: The scheme of METTL3 protein domains. Bottom: BRAF, Flag-USP5, and myc-METTL3 domains were co-transfected into 293T cells for 48 hr, followed by IP and IB analysis as indicated. (E) A375 cells were treated with or without 0.1 μM trametinib for 1 hr. Cell lysates were analyzed by IP and IB as indicated. (F) 293T cells were transfected as indicated for 48 hr before IB analysis. Density of METTL3 expression was quantified by Image J and the relative fold compared to the untreated WT was indicated below the blot.

Because USP5 is an enzyme that could prevent protein ubiquitination, we further examined whether USP5 stabilizes METTL3 through deubiquitination (Figure 2-15A). Overexpression of wild-type but not catalytically dead C335A USP5 decreased ubiquitination and stabilized METTL3. Furthermore, *in vitro* addition of USP5 reduced EOAI-induced METTL3 ubiquitination (Figure 2-15B), suggesting that METTL3 is a direct substrate of USP5.

To identify ubiquitin ligases that contribute to USP5 inhibition-induced degradation of METTL3, we searched consensus motif and physical association databases, as well as our CRISPR-based genomic screen. METTL3 contains an SPOP-binding consensus motif and COP1-binding destruction motif (http://elm.eu.org). It also interacts with TRIM28, HUWE1, and UBR5 (https://thebiogrid.org), and may be ubiquitinated by SMURF1 (http://ubibrowser.ncpsb.org). Finally, we identified FBXW8, FBXW12, SPOPL, TRIM2, and ANAPC1 as negative regulators of m^6A methylation from our CRISPR screen. To find ubiquitin ligases involved in METTL3 degradation, A375 cells with USP5 knockdown were further transfected with siRNA targeting ubiquitin ligases. Knockdown of SPOP, TRIM28, or ANAPC1 partially abolished USP5 inhibition-mediated METTL3 degradation (Figure 2-15C). Because SPOP is a well-known tumor suppressor and localizes to nuclear speckles (where the m^6A methyltransferase localizes), we tested an SPOP inhibitor, SPOP-IN-6b, which was able to partially reverse EOAI-induced ubiquitination and degradation of METTL3 (Figure 2-15D, E). Lastly, we were interested in what type of ubiquitin linkages that the USP5 inhibition induced. USP5 has been shown to cleave multiple types of polyubiquitin linkage, including K6, K11, K29, K48 and K63 [166, 167]. We observed K11, K48 and K63-linked polyubiquitination on METTL3 after USP5 knockdown. Furthermore, knockdown of ANAPC1 and SPOP decreased K11 and K48 ubiquitination, respectively (Figure 2-15F). In summary, these results suggest that USP5 stabilizes METTL3 through deubiquitination.

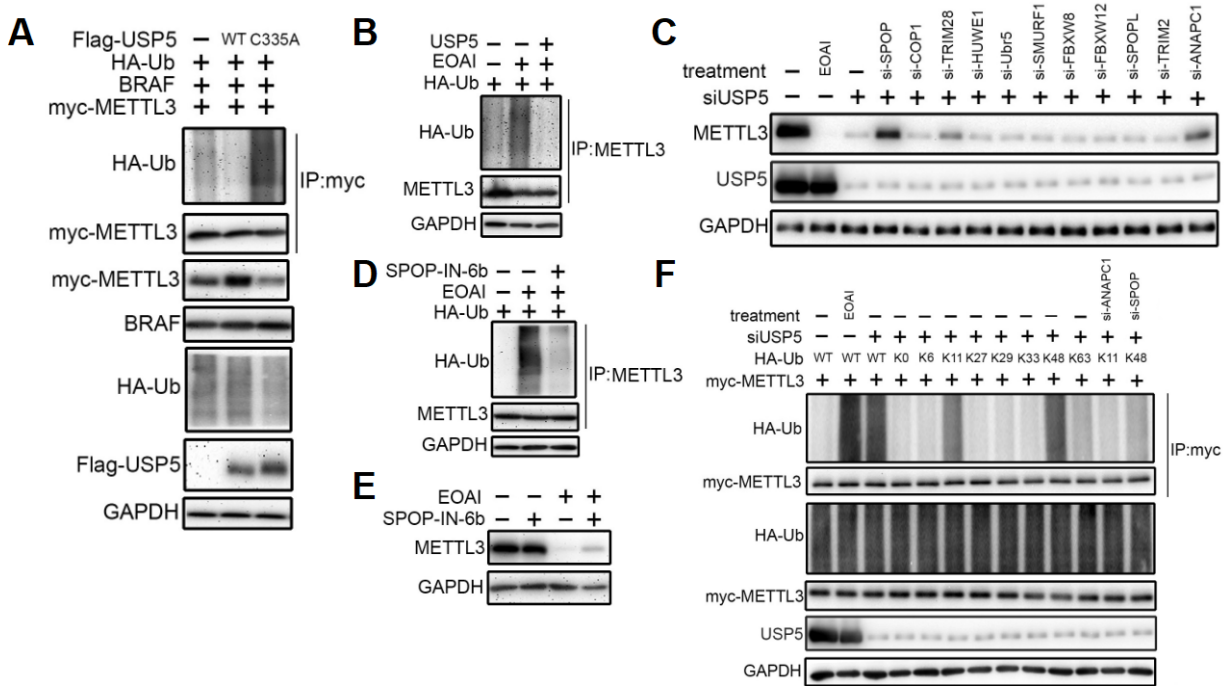

Figure 2-15. USP5 deubiquitinates METTL3.

(A) USP5 decreases ubiquitination of METTL3. Lysates of 293T cells transfected as indicated for 48 hr were subjected to IP with anti-myc antibody followed by IB. (B) 293T cells transfected with HA-ubiquitin were treated with 10 μM MG-132 and 10 μM EOAI3402143 for 8 hr. IP-purified METTL3 were incubated without or with purified USP5 then subjected to IB. (C) Knockdown of SPOP, TRIM28, and ANAPC1 attenuated USP5 inhibition-induced degradation of METTL3. A375 cells were transfected with siRNA for 72 hr or treated with 10 μM EOAI3402143 (EOAI) for 8 hr before IB analysis. (D) A375 cells transfected with HA-ubiquitin were treated with 10 μM MG-132, 10 μM EOAI3402143, and 5μM SPOP-IN-6b for 8 hr. The ubiquitination of METTL3 was detected by IP with anti-METTL3 and IB with anti-HA. (E) After 8 hr treatment with 10 μM EOAI3402143 with or without 5 μM SPOP-IN-6b, cell lysates from A375 cells were analyzed by IB. (F) 293T cells transfected with myc-METTL3, various HA-ubiquitin mutants, and siRNA for USP5, ANAPC1, SPOP for 72hr were treated with 10 μM EOAI3402143 and 10 μM MG-132 for 8 hr. Cell lysates were subjected to IP with anti-myc antibody followed by IB.

Phosphorylation of METTL3/WTAP by ERK Facilitates Resolution of Pluripotency

Autocrine FGF4 is reported to be the major stimulus for ERK signaling in mESCs. Interference with FGFR or ERK activity impeded the ability of mESCs to undergo differentiation and retain expression of pluripotency factors including *Nanog*. We observed that p-43 METTL3 phosphorylation was enhanced by FGF4 and reduced by MEK inhibitor

PD0325901 or FGFR1 inhibitor PD173074 (Figure 2-16A). Because both ERK activation and METTL3 expression have been reported to be required for mESCs to exit the pluripotent state upon differentiation, we further investigated whether phosphorylation of METTL3/WTAP affects mESCs fate. We introduced TetOn-shWTAP into METTL3-KO mESCs to tune endogenous WTAP expression. Cells were then transduced with WT or a phospho-inactive mutant of CuO-METTL3-T2A-WTAP constructs. With 50 µg/ml cumate, the expression level of exogenous R-WT METTL3 is comparable to that of endogenous METTL3 and we noticed that 3A METTL3 expression is consistently lower than that of WT (Figure 2-16B). Quantification of m^6A by LC-MS/MS showed a synergistic reduction of 3A METTL3 and 2A WTAP (Figure 2-16C). We then examined whether pluripotency of mESCs expressing R-3A2A was affected. R-3A2A mESCs exhibited higher stage specific embryonic antigen 1 (SSEA-1) expression (Figure 2-16E) and increased proliferation (Figure 2-16F). These observations support the notion that loss of METTL3 and WTAP phosphorylation trap mESCs in the pluripotent state.

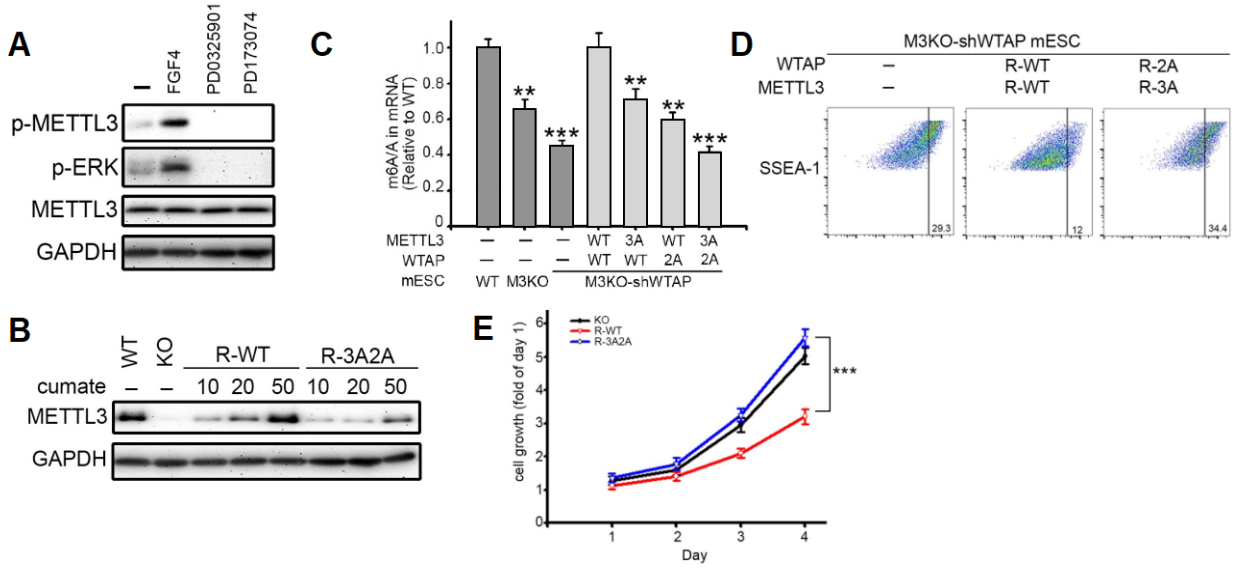

Figure 2-16. Phosphorylation of METTL3/WTAP facilitates resolution of pluripotency.

(A) mESCs were treated with 30 ng/ml FGF4, 10 µM PD0325901or 1 µM PD173074 for 1 hr. Cell lysates were subjected to SDS-PAGE. (B) METTL3 expression in mESCs stable

Figure 2-16, continued. Phosphorylation of METTL3/WTAP facilitates resolution of pluripotency.
transfectants incubated with 2 μg/ml doxycycline and cumate (μg/ml) for three days. KO: METTL3 KO-shWTAP, R-WT: METTL3 KO-shWTAP mESCs with CuO-WT METTL3-T2A-WTAP WT, R-3A2A: METTL3 KO-shWTAP mESCs with CuO-3A METTL3-T2A-2A WTAP. (C) LC-MS/MS quantification of the m^6A/A ratio in mRNA of mESCs stable transfectants. (n = 3 per group, data represent mean ± SEM, p values were calculated by Student's t test). *p < 0.05, **p < 0.01, ***p < 0.001. (D) Representative flow cytometry analysis of stage-specific embryonic antigen-1 (SSEA-1) expression of mESCs stable transfectants. (E) Cell growth of R-WT and R-3A2A mESCs were measured by sulforhodamine B dye (SRB assay). Data are presented as relative to Day 1 (n = 3 per group, data represent mean ± SEM, p values were calculated by Student's t test). ***p < 0.001.

Mettl3-deficient mESCs fail to exit pluripotency despite differentiation cues, likely because loss of m^6A impedes the degradation of pluripotency-promoting transcripts. We subsequently examined reported m^6A-methylated pluripotency factor transcripts, including *Nanog*, *Zfp42*, *Klf2*, *Sox2*, and *Lefty1* [98, 99, 101]. *Pou5f1*, which does not harbor any m^6A modification, was also used as a negative control. m^6A-RIP-qPCR confirmed decreased m^6A (Figure 2-17A) and RT-qPCR indicated upregulation (Figure 2-4D) of these m^6A-labeled pluripotency transcripts in R-3A2A mESCs. Furthermore, after transcription arrest by actinomycin D treatment, these transcripts showed delayed turnover in R-3A2A (Figure 2-17B). These findings suggest that METTL3 phosphorylation controls the level of critical pluripotency regulators. Considering ERK activation is the primary stimulus for mESCs to exit self-renewal and acquire competence of differentiation [168], we then compared the capacity for differentiation by transferring mESCs to differentiation media for embryoid bodies (EBs). R-3A2A mESCs generated smaller EB spheres (Figure 2-17C), failed to repress pluripotent genes, and adequately up-regulated developmental markers (Figure 2-17D). Lastly, because ERK activation controls the transition from the primitive ectoderm-like cell state to a neural progenitor cell state, we tested whether METTL3 phosphorylation could affect differentiation towards a neural lineage. As shown in

Figure 2-17E, even upon induction of differentiation, R-3A2A mESCs continued to express *Nanog* and failed to upregulate primary neural markers *Sox1* and *Nestin*. These results support the notion that ERK-dependent phosphorylation of METTL3 and WTAP promotes mESC differentiation.

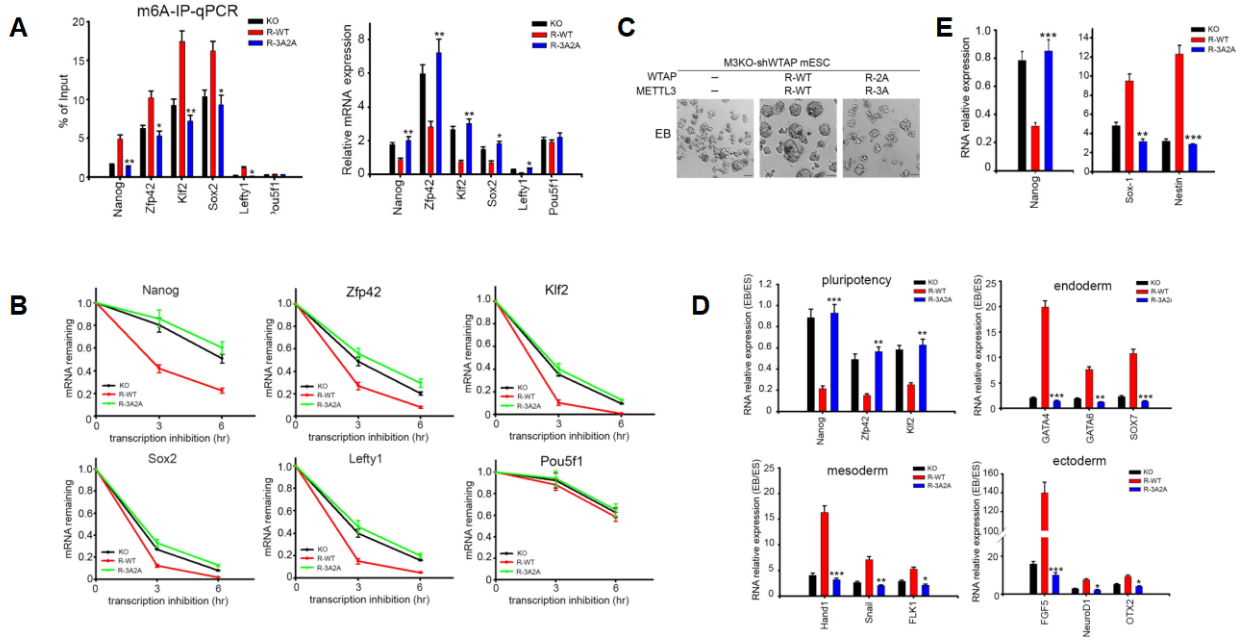

Figure 2-17. Phosphorylation of METT3/WTAP promotes degradation of pluripotency transcripts.

(A) MeRIP-qPCR of pluripotency transcripts in mESCs stable transfectants. (n = 3 per group, data represent mean ± SEM, p values were calculated by Student's t test). *p < 0.05, **p < 0.01. (B) qPCR analysis of pluripotency genes in mESCs stable transfectants. (n = 3 per group, data represent mean ± SEM, p values were calculated by Student's t test). *p < 0.05, **p < 0.01. (C) Relative levels of *Nanog*, *Zfp42*, *Klf2*, *Sox2*, *Lefty1*, and *Pou5f1*, measured by qPCR, at the indicated times after 5 µg/ml actinomycin D treatment. mRNA levels were monitored in METTL3 KO-shWTAP (KO), CuO-WT METTL3-T2A-WTAP WT (R-WT), CuO-3A METTL3-T2A-2A WTAP (R-3A2A) mESCs. (D) Representative phase contrast microscopy showing EB differentiation of mESCs stable transfectants after 8 days. Scale bars, 100 mm. (E) qPCR analysis for pluripotency and differentiation markers expression after 8 days of embryonic body induction. (n = 3 per group, data represent mean ± SEM, p values were calculated by Student's t test). *p < 0.05, **p < 0.01, ***p < 0.001. (F) qPCR analysis for *Nanog, Sox1, Nestin* expression after 4 days of neural differentiation. (n = 3 per group, data represent mean ± SEM, p values were calculated by Student's t test). **p < 0.01, ***p < 0.001.

Transcripts Affected by Phosphorylation of Methyltransferase Complex in mESCs

To gain further insight into how the phosphorylation of the m^{6}A methyltransferase complex affects the m^{6}A-modified transcripts, we mapped the m^{6}A methylome in mESCs. Comparison of the R-WT with R-3A2A mESCs revealed a global loss of methylation sites (Figure 2-18A, B). Consistent with previous m^{6}A-seq results [38, 39], the m^{6}A peaks identified are enriched near the start and stop codons and were characterized by the canonical GGACU motifs (Figure 2-18C, D).

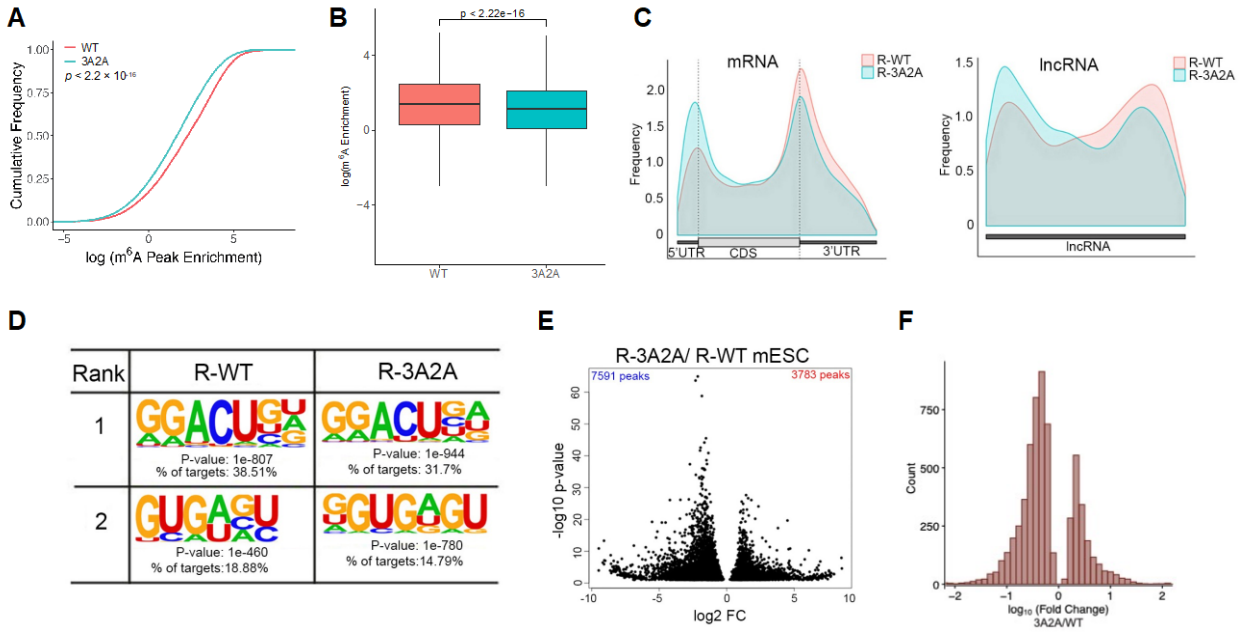

Figure 2-18. m^{6}A-seq reveals transcripts affected by phosphorylation of the m^{6}A methyltransferase complex in mESCs.

(A) Cumulative distribution function of log2 peak intensity of m^{6}A-modified sites in R-WT and R-3A2A mESCs. (B) Metagene plots showing the average distribution of m^{6}A peaks identified across mRNA or lncRNA in the R-WT and R-3A2A mESCs. (C) Consensus sequence motifs among m^{6}A peaks in R-WT and R-3A2A mESCs. (D) Volcano plot for peaks with differential m^{6}A intensity between R-WT and R-3A2A mESCs. Fold change (FC) is the ratio of IP over Input for R-WT and R-3A2A.

Using our in-house R-package "MeRIPtools," which tests for m^{6}A-IP enrichment using a binomial-distribution-based model, we found 7,591 m^{6}A peaks that exhibited a significant decrease in the R-3A2A cells compared to the R-WT cells (Figure 2-18E, F, Table S3), such as modification sites in *Nanog*, *Lefty1*, and *Zfp219* (Figure 2-19A). The genes showing decreased m^{6}A methylation significantly overlap with those in functional gene sets important for pluripotency, including targets of NANOG and MYC (Figure 2-19B). The transcripts exhibiting differential methylation were consistent between replicates (Figure 2-19C).

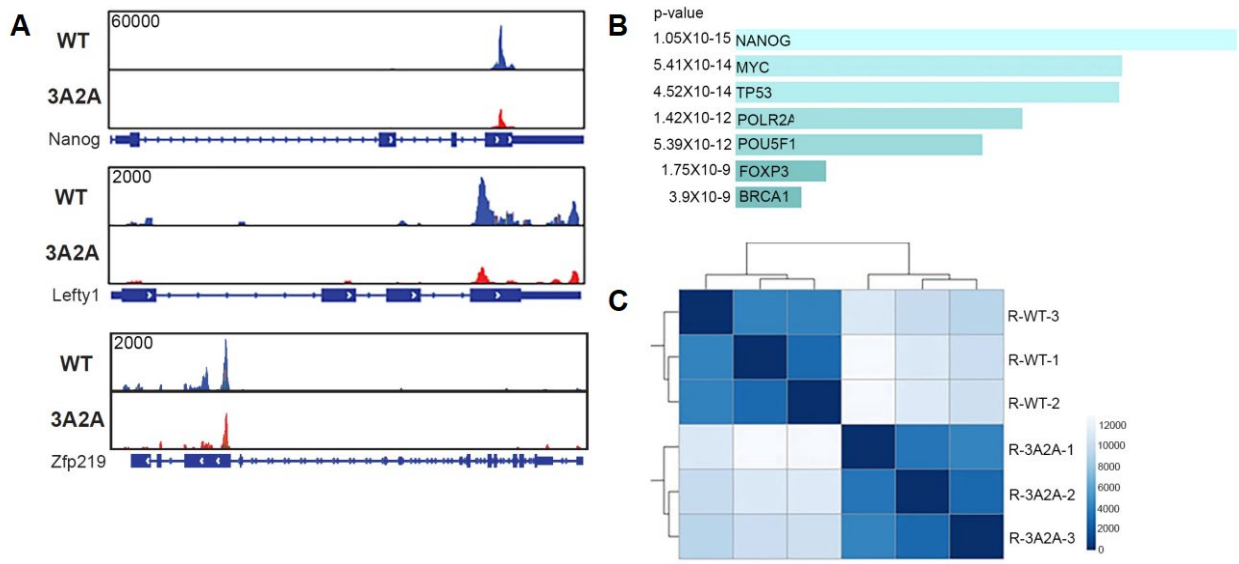

Figure 2-19. Loss of METTL3/WTAP phosphorylation reduces m^{6}A methylation of pluripotency transcripts.

(A) Coverage plots of the m^{6}A peaks of *Nanog*, *Lefty1*, and *Zfp219* comparing R-WT and R-3A2A mESCs. Plotted coverages are the medians of three replicates. (B) Overrepresentation analysis of genes with differential m^{6}A methylation level in R-WT and R-3A2A mESCs that overlapped with targets of transcriptional factors. (C) Distance matrix of the m^{6}A methylation in replicates of R-WT and R-3A2A mESCs.

Furthermore, the transcripts showing decreased m^{6}A methylation (Figure 2-20A) and differential expression (Figure 2-20B were enriched for gene ontology (GO) terms related to pluripotency

and mRNA processing. Importantly, many of the genes involved in pluripotency showed reduced m^{6}A methylation in R-3A2A when compared with R-WT mESCs (Figure 2-20C).

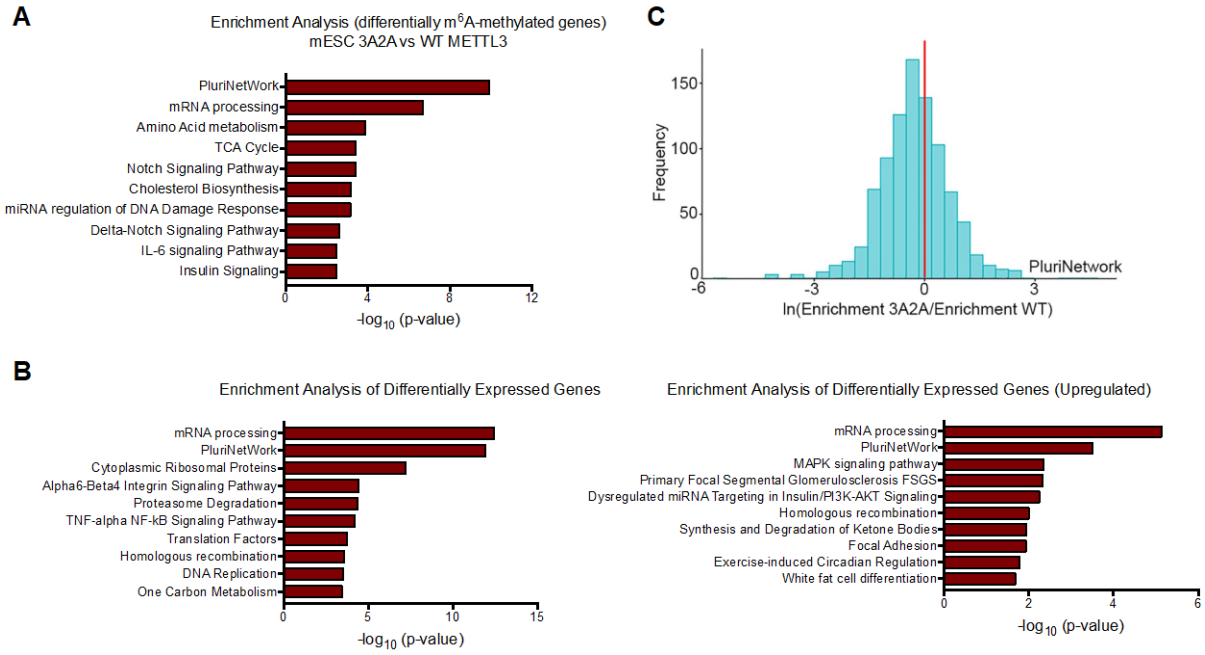

Figure 2-20. Enrichment analysis of differentially methylated and expressed genes.

(A) Gene enrichment analysis with WikiPathway terms of differentially m^{6}A methylated peaks in R-WT and R-3A2A mESCs for molecular functions. (B) Gene enrichment analysis with WikiPathway terms of differentially expressed genes ($p < 0.05$). (C) A histogram showing relative m^{6}A peak enrichment of R-3A2A compared to R-WT mESCs, indicating higher m^{6}A methylation in pluripotency genes (PluriNetwork) for R-WT mESCs.

To expand our observation of pathways that are enriched when comparing R-WT and R-3A2A mESCs, we performed a functional class scoring approach (gene-set enrichment analysis, GSEA) in addition to GO analysis. GSEA showed enrichment of histone binding proteins (Figure 2-21A, Table S4). Considering that it has been reported that m^{6}A regulates histone modifications in part by destabilizing mRNA of histone-modifying enzymes [169], we used an ELISA kit to compare 21 different Histone H3 modifications. H3K27me3 showed the most dramatic changes (Figure 2-21B) and we detected reduced m^{6}A peaks in several components of

the PRC2 complex mRNA (Figure 2-21C). These results suggest phosphorylation of the m^{6}A methyltransferase complex decreases H3K27me3 partially by regulating the PRC2 complex.

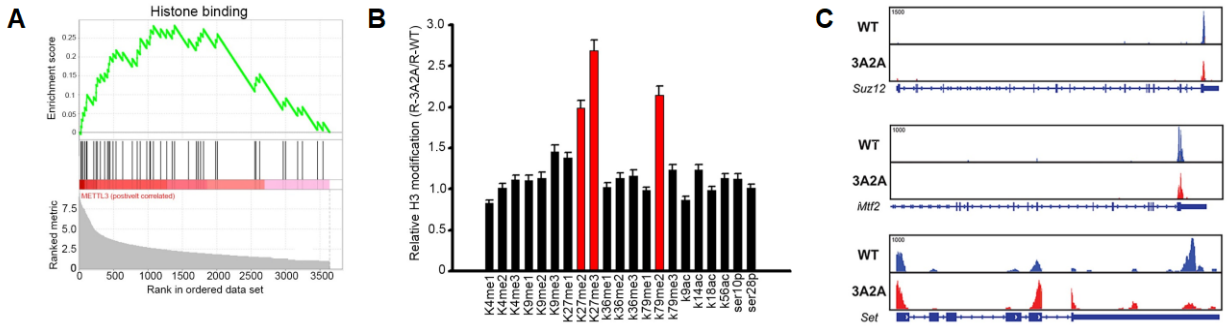

Figure 2-21. METTL3/WTAP phosphorylation may affect histone methylation.

(A) GSEA analysis on enrichment of histone binding protein in R-3A2A versus R-WT mESCs. (B) ELISA analysis for histone H3 post-translational modifications of mESCs. Bars represent the ratio of R-3A2A relative to R-WT mESCs. Red color was used to highlight a ratio greater than 2. (C) Coverage plots of m^{6}A peaks in *Suz12*, *Set*, and *Mtf2* comparing R-WT and R-3A2A mESCs. Plotted coverages are the medians of three replicates.

Phosphorylation of the m^{6}A Methyltransferase Complex May Affect Tumorigenesis

As one of the most frequently mutated signaling pathways in cancer, the RAS/RAF/MEK/ERK signaling cascade has long been viewed as a promising target for cancer therapy [170]. Given that phosphorylation of the m^{6}A methyltransferase complex by ERK facilitates resolution of pluripotency in mESCs, we further investigated whether the m^{6}A methyltransferase complex can be similarly regulated in certain cancer cells. Using CancerMine [171], a literature-mined resource, we summarized that METTL3 could behave as an oncogene in many cancer types (Figure 2-22A).

We first examined melanoma due to the high prevalence of constitutively active *BRAF V600E* mutation (50-60%) and clinical success with BRAF and MEK inhibitors [172]. The m^{6}A levels on mRNA are higher in MEL-624 and A375 cells, which harbor a *BRAF V600E* mutation

(Figure 2-22B). As expected, the stability of the m^{6}A methyltransferase complex was reduced in the R-3A2A A375 cells (Figure 2-22C), which contributed to the overall lower m^{6}A level on mRNA (Figure 2-22D). MEK inhibitors PD0325901 and trametinib were found to reduce the protein levels of the m^{6}A methyltransferase complex at 8 hours (Figure 2-22E) and the overall mRNA m^{6}A levels at 48 hours (Figure 2-22F) in A375 melanoma cells. In addition, these two MEK inhibitors also decreased m^{6}A methyltransferase complex level in HCT-116 cells, which is a colon cancer line that possesses the most common *KRAS* mutation (G12D) (Figure 2-22G).

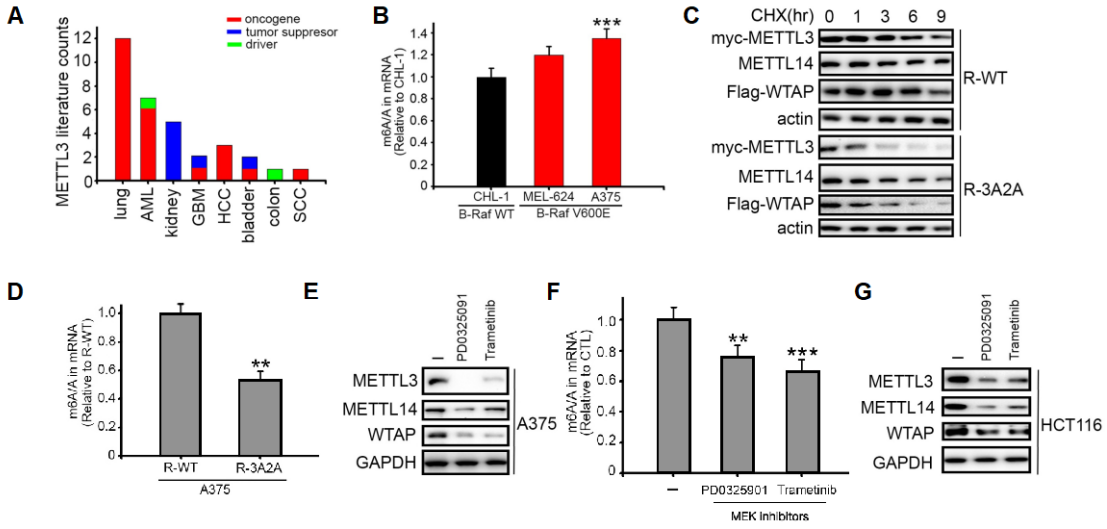

Figure 2-22. Phosphorylation of METTL3 may affect tumorigenesis and m^{6}A methylation.

(A) Oncogenes (promote cancer), tumor suppressors (inhibit carcinogenesis), and drivers (important in cancer development, either oncogene or tumor suppressor) were used as classifiers by the CancerMine database to identify the potential role of METTL3 from the published literature. (B) LC-MS/MS quantification of the m^{6}A/A ratio in mRNA of melanoma cell lines. (n = 3 per group, data represent mean ± SEM, p values were calculated by Student's t test). ***p < 0.001. (C) Lysates of A375 stable transfectants harvested at different time points after treatment with cycloheximide (CHX) 10 µg/ml were analyzed by IB. (D) LC-MS/MS quantification of the m^{6}A/A ratio in mRNA of A375 stable transfectants. (n = 3 per group, data represent mean ± SEM, p values were calculated by Student's t test). **p < 0.01. (E) After 8 hr treatment with 10 µM PD0325901 or 0.1 µM trametinib, cell lysates from A375 cells were analyzed by IB. (F) LC-MS/MS quantification of the m^{6}A/A ratio in mRNA of A375 cells treated with 10 µM PD0325901 or 0.1 µM trametinib for 48 hr. (n = 3 per group, data represent mean ± SEM, p values were calculated by Student's t test). **p < 0.01, ***p < 0.001. (G) After 8 hr treatment with 10 µM PD0325901 or 0.1 µM trametinib, cell lysates from HCT-116 cells were analyzed by IB.

Because knockdown of USP5 increases METTL3 in A375 melanoma cells (Figure 2-13B), we assessed the potential clinical relevance of USP5. Interestingly, melanoma patients with high USP5 had shorter overall survival (Figure 2-23A). Two structurally unrelated USP5 inhibitors, EOAI3402143 and vialinin, were employed to evaluate the effect of USP5 on the METTL3 level in melanoma cells. We found that these two USP5 inhibitors increased ubiquitination of METTL3, resulting in decreased METTL3 protein level (Figure 2-23B-D). Furthermore, MEK inhibition, R-3A2A, or METTL3-WTAP knockdown can sensitize melanoma and colon cancer cells to USP5 inhibition (Figure 2-23E, F), supporting the connection between USP5 and METTL3.

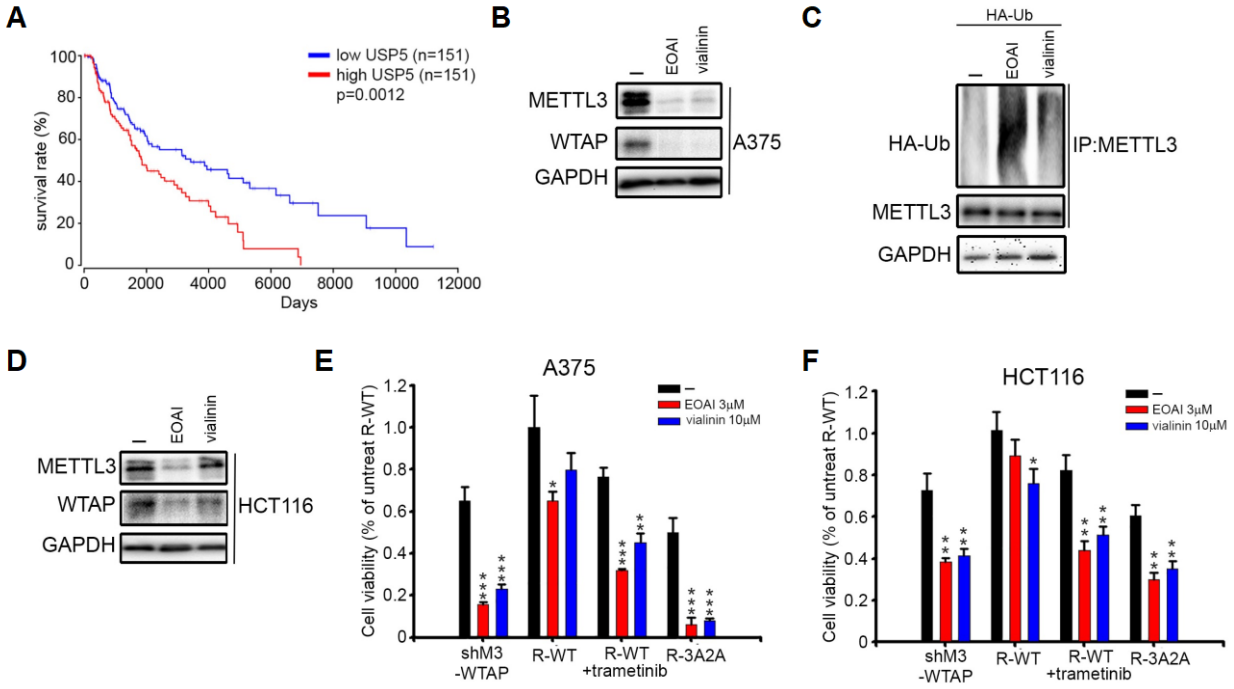

Figure 2-23. USP5 may also modulate METTL3 expression level in cancer cells.

(A) Kaplan-Meier analysis of overall survival time based on METTL3 expression from the skin cutaneous melanoma (SKCM) dataset at The Cancer Genome Atlas (TCGA). (B) After 8 hr treatment with 10 μM EOAI3402143 (EOAI) or 30 μM vialinin A, cell lysates from A375 cells were analyzed by immunoblot. (C) A375 cells transfected with HA-ubiquitin were treated with

Figure 2-23, continued. USP5 may also modulate METTL3 expression level in cancer cells. 10 μM MG-132 and 10 μM EOAI3402143 (EOAI) or 30 μM vialinin A for 8 hr. The ubiquitination of METTL3 was detected by IP with anti-METTL3 and IB with anti-HA. (D) After 8 hr treatment with 10 μM EOAI3402143 (EOAI) or 30 μM vialinin A, cell lysates from HCT-116 cells were analyzed by IB. (E) A375 stable transfectants as indicated were treated with 3 μM EOAI3402143 (EOAI) or 10 μM vialinin A before measuring cell viability by SRB assay. Data are presented as relative to the R-WT cells without drug treatment. (n = 3 per group, data represent mean ± SEM, p values were calculated by Student's t test). *p < 0.05, **p < 0.01, ***p < 0.001. (F) HCT-116 stable transfectants as indicated were treated with 3 μM EOAI3402143 (EOAI) or 10 μM vialinin A for 48 hr before measuring cell viability by SRB assay. Data are presented as relative to the R-WT cells without drug treatment. (n = 3 per group, data represent mean ± SEM, p values were calculated by Student's t test). *p < 0.05, **p < 0.01, ***p < 0.001.

Lastly, considering that HER2 expression phosphorylates METTL3 and WTAP (Figure 2-S1C and S7H) and m^{6}A levels are higher in the HER2-overexpressed SKBR3 and BT474 cells (Figure 2-S7I), we investigated whether inhibition of HER2 could affect m^{6}A methylation. Two HER2 inhibitors, tucatinib and lapatinib, could reduce METTL3 protein level at 8 hours and cellular mRNA m^{6}A methylation at 48 hours in HER2-positive breast cancer (Figure 2-6G and 6H). Overall, our data support that ERK-dependent METTL3 stabilization affects cellular mRNA m^{6}A methylation which could contribute to tumorigenesis. More focused cancer studies are required to assess the effects and scope of such a regulatory mechanism in the future.

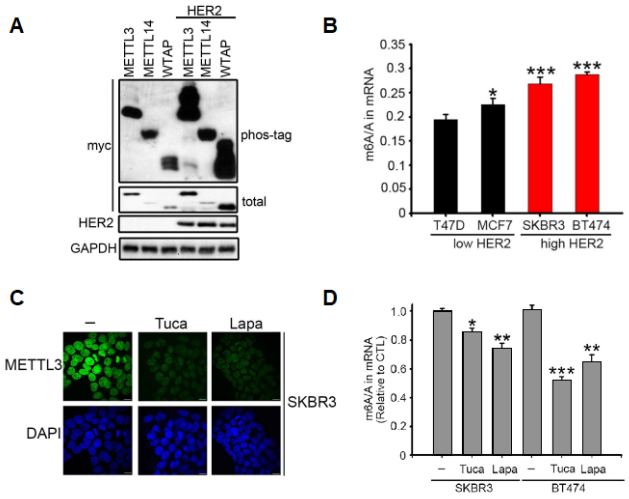

Figure 2-24. HER2 activity phosphorylates METTL3/WTAP and affects m^{6}A levels in breast cancer cells.

Figure 2-24, continued. HER2 activity phosphorylates METTL3/WTAP and affects m^{6}A levels in breast cancer cells.
(A) Phos-tag SDS-PAGE showing the phosphorylation status of METTL3, METTL14, or WTAP in 293T cells co-transfected without or with HER2. (B) LC-MS/MS quantification of the m^{6}A/A ratio in mRNA of breast cancer cell lines. (n = 3 per group, data represent mean ± SEM, p values were calculated by Student's t test). *p < 0.05, ***p < 0.001. (C) Immunofluorescence analysis of METTL3 (green) in SKBR3 cells treated with 1 μM tucatinib and 1 μM lapatinib for 8 hr. DAPI (blue) was used to mark the nucleus. Scale bars, 10 mm. (D) LC-MS/MS quantification of the m^{6}A/A ratio in mRNA of SKBR3 and BT474 cells treated with 1 μM tucatinib and 1 μM lapatinib for 48 hr. (n = 3 per group, data represent mean ± SEM, p values were calculated by Student's t test). *p < 0.05, **p < 0.01, ***p < 0.001.

Discussion

m^{6}A RNA methylation plays crucial roles in regulating RNA metabolism. While many studies have shown the importance of METTL3 [98, 100, 101, 120, 153, 173], few have shown how the methyltransferase complex itself is regulated. Here, we identify an ERK-METTL3/WTAP signaling axis that regulates mESCs differentiation and potentially affects tumorigenesis. Initially, we deployed a genome-wide CRISPR screen using an m^{6}A methylation-dependent GFP reporter. RAS and MAPK pathways were identified as the top pathways in the positive regulation of m^{6}A methylation. Biochemical studies showed that ERK proteins could phosphorylate METTL3 on S43/S50/S525 and WTAP at S306/S341. We also found that phosphorylation of METTL3 decreases METTL3 ubiquitination through interaction with USP5. These findings explain elevated m^{6}A levels on mRNA upon ERK activation. This pathway underlines a previously unrecognized effect of ERK activation through RNA methylation during differentiation of pluripotent mESCs (Figure 2-7).

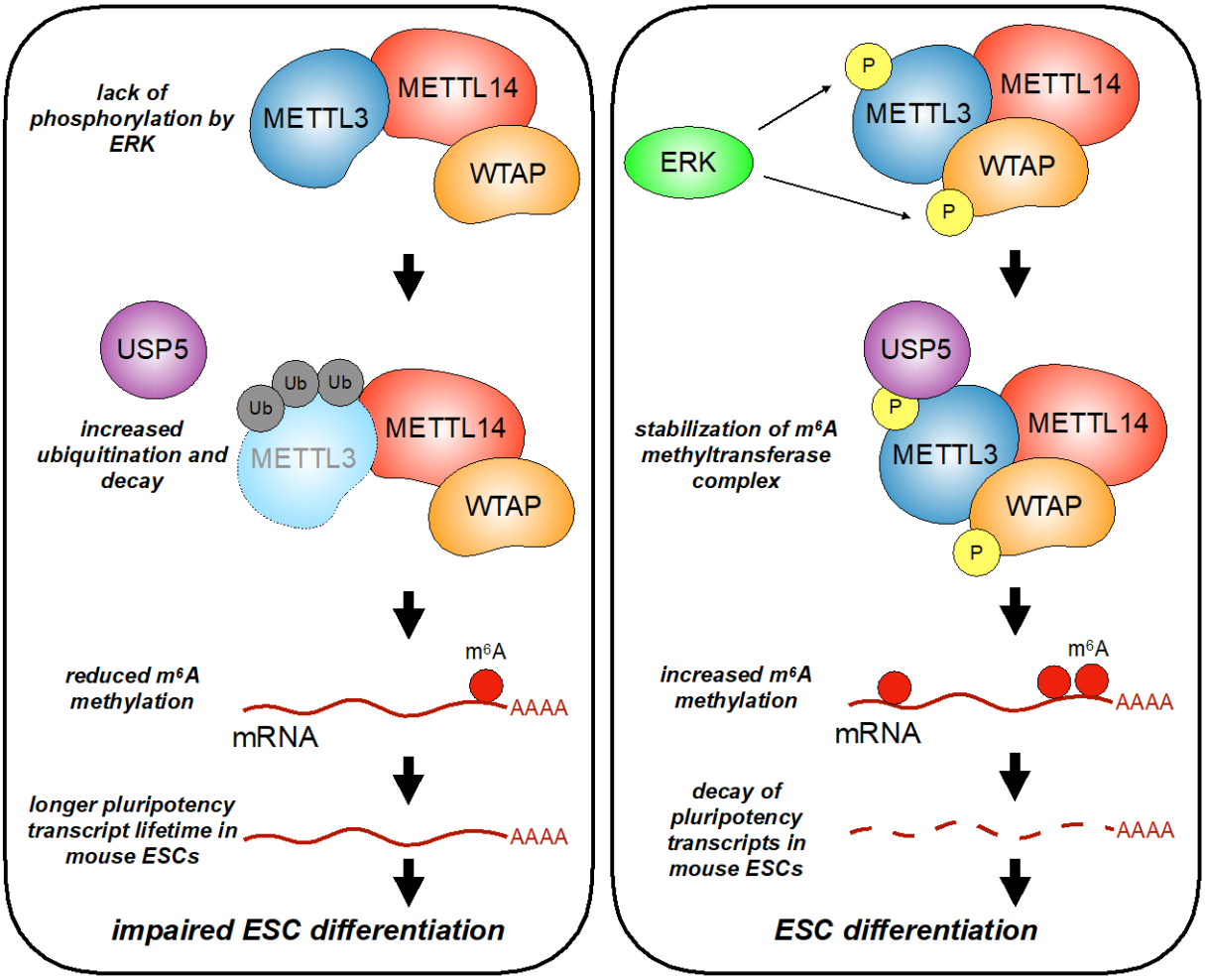

Figure 2-25. A Schematic Model of the Role of the m^{6}A Methyltransferase Phosphorylation by ERK.

Phosphorylation of METTL3 and Potential Effects

Our studies reveal METTL3 phosphorylation by ATM and ATR (Figure 2-S1D). Phosphoproteomic studies of ATM/ATR substrates have previously uncovered that, in response to DNA damage, METTL3 was phosphorylated at residues S350 and T356 in an ATM-dependent manner [162]. Furthermore, phosphorylation of METTL3 was found to be an early responder to DNA damage [174]. Considering that m^{6}A rapidly accumulates at UV-irradiated sites [175] and lack of METTL3 catalytic activity delays DNA repair and Pol κ-mediated response to UV DNA damage, it would be interesting to explore the role of ATM/ATR-induced METTL3

phosphorylation in the future. In addition, *in vitro* kinase assay showed that certain stress-activated MAP kinase, p38 and JNK, can also phosphorylate METTL3. Interestingly, METTL3 has previously been linked to MAPK signaling. In dendritic cells, dental pulp stem cells, or intestinal epithelia, depletion of METTL3 leads to reduced phosphorylation of p38, ERK, and JNK [110, 176, 177]; whereas phosphorylation is increased in osteoblasts and colorectal cancer cells [178, 179]. Although effects of METTL3 on MAPKs may vary based on cell type, taken together, these data suggest potential feedback loop mechanisms between METTL3 and MAPK pathways.

Our phosphorylation studies estimated the relative levels of phosphorylated and non-phosphorylated METTL3. We noticed that trametinib was more effective than PD0325901 in decreasing the mobility shift of METTL3 in A375 cells, although these two MEK inhibitors inhibited ERK activation and METTL3 S43 phosphorylation equally well (Figure 2-S3H). Trametinib is known to inhibit the proliferation of BRAF V600E cells with lower IC50 than PD0325901, even though they had similar potency against MEK1 *in vitro*. Part of the reason is that trametinib inhibits the CRAF-driven signaling more effectively than PD0325901 [180]. We observed that CRAF phosphorylates METTL3 and leads to an additional band in the 3A METTL3 mutant, when comparing to MEK and BRAF expression (data not shown). Therefore, we propose that the more potent effect of trametinib could be partially due to CRAF inhibition. Although the RAF family of enzymes are canonically depicted as activators of MEK, they carry out additional functions as well. BRAF is the most potent MEK activator *in vivo*, whereas ARAF and CRAF interact with several other proteins in a MEK-independent manner [181, 182]. Interestingly, ARAF is also detected in our CRISPR screen (Figure 2-1C). How ARAF and CRAF affect METTL3 through MEK-independent signaling pathway still needs future investigation.

Ubiquitin Ligases and Ubiquitin Linkages of METTL3

To systemically study the regulation of METTL3 ubiquitination, we plan to construct a reporter encoding both DsRed and EGFP-METTL3, which allows us to use EGFP:DsRED ratio as an indicator of the stability of METTL3 in the future [183]. CRISPR activation (CRISPRa) and CRISPR inhibition (CRISPRi) screens, which focus on proteostasis, could be used to identify ubiquitin ligases and deubiquitinases for METTL3. In the current study, we found that SPOP, ANAPC1, and TRIM28 promote degradation of METTL3, while USP5 reverses this process. A previous study showed that TRIM28 immunoprecipitated with METTL3, METTL14, and WTAP (Yue et al., 2018), which raised the possibility that TRIM28 could be a component of the m^6A writer complex. SPOP is known to mediate K48-linked ubiquitination and proteasome degradation of various substrates, such as estrogen receptors, PTEN, BRD4, MyD88, and PD-L1 [184]. Interestingly, when SPOP oligomerizes with increased cellular level, it localizes to nuclear speckles [185], where METTL3-WTAP is located.

We observed K11, K48 and K63-linked polyubiquitination on METTL3 after USP5 knockdown. We also found that K11 ubiquitination of METTL3 can be elevated by USP5 inhibition and attenuated by ANAPC1 (subunit of anaphase-promoting complex, APC) knockdown. APC is the major E3 ligase that assembles K11-linked ubiquitin chain to drive proteasomal degradation and mitotic exit [186]. The abundance of K11 linkage strongly increases when APC is active during mitosis. In accordance with our observation, recently it was found that METTL3 is significantly downregulated during M phase [187]. Elucidation of the post-translational and proteolysis degradation of METTL3 during cell cycle may shed further insights on how METTL3 contributes to normal cell differentiation and tumorigenesis.

METTL3/WTAP Phosphorylation by ERK is Important for mESCs Differentiation

Consistent with previous observations [98, 101], our m^{6}A-seq data revealed extensive mRNA m^{6}A methylation in mESCs. Differentially methylated transcripts upon loss of METTL3/WTAP phosphorylation are enriched for genes involved in pluripotency and RNA processing, like those found in METTL3 KO studies. Our report suggests that ERK activation increases m^{6}A methylation on key pluripotent transcripts, thus contributing to their decay. Tuning the phosphorylation state of METTL3 could be an effective post-translational way to adjust global mRNA m^{6}A methylation.

While we found that phosphorylation of METTL3 affects its interaction with WTAP and USP5, interaction with other binding partners could also be affected. For instance, SMAD2/3 interacts with the METTL3/METT14/WTAP complex to promote m^{6}A binding to particular transcripts in mESCs [99]. ZFP217 has also been found to sequester METTL3, thereby restricting m^{6}A methylation of certain transcripts in ESCs [188]. It would be interesting to determine whether METTL3 phosphorylation affects interaction with SMAD2/3 or ZFP217 in mESCs, which could further explain how phosphorylation of m^{6}A writer proteins can affect methylation of core pluripotency factor transcripts.

Other Pathways that May Regulate RNA m^{6}A Methylation

While our study sheds light on ERK phosphorylation of METTL3, other questions remain. First, what are other pathways that could regulate m^{6}A methylation? Pathways identified from Gene Ontology enrichment analysis for genes that promote m^{6}A include transcriptional regulation by TP53 and HIF-1 signaling. The same analysis for genes that apparently suppress m^{6}A include sphingosine-1-phosphate receptor signaling and protein targeting to mitochondria (data not

shown). Modulation of activity for these pathways may reveal more regulators of m^6A methylation.

Second, how does the interplay between different post-translational modifications of METTL3 affect its activity? METTL3 is not only phosphorylated but also SUMOylated [189]. SUMOylation of METTL3 reduces its methyltransferase activity, thereby lowering m^6A abundance. Intriguingly, MAPK activation can modulate SUMOylation; specifically, ERK activation de-SUMOylates the Elk-1 transcription factor [190, 191]. It would be interesting to further explore whether METTL3 phosphorylation affects SUMOylation level.

Overall, our study sheds light on a signaling relationship between the ERK pathway and m^6A methylation (Figure 2-26). Several challenges remain in understanding how cells regulate m^6A methylation spatiotemporally, as well as which transcripts are methylated. The post-translational regulation of m^6A writers, readers, and erasers may provide insight for these questions and could be an important factor in affecting the m^6A epitranscriptome.

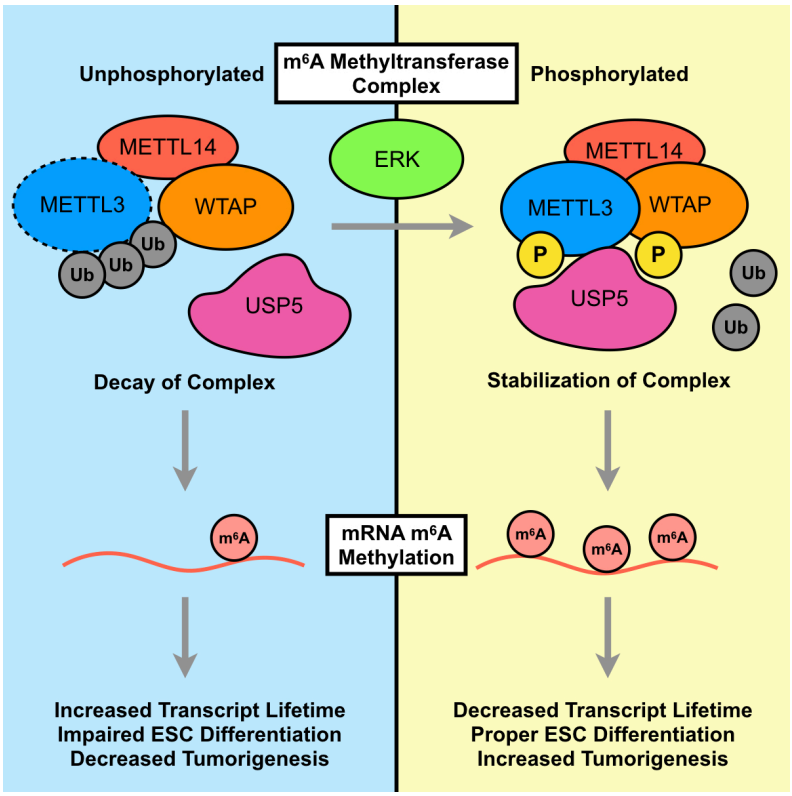

Figure 2-26. Summary diagram demonstrating how ERK phosphorylation of the m^{6}A methyltransferase complex changes methylation and cell biology.

Limitations

While our results support a model in which ERK phosphorylates m^{6}A methyltransferase components METTL3 and WTAP, leading to stabilization by USP5, our study is not without potential caveats. For instance, although we were able to identify ERK as an m^{6}A regulator, we noticed that not all known m^{6}A regulatory proteins were among the top-ranked gene in our genome-wide CRISPR screen. Part of the reason might be due to the use of a circular RNA reporter in our screen. How m^{6}A is installed on circRNA and how it affects translation could be different from mRNA. For example, YTHDF1 is not involved in the translation of circRNA [192]. However, our targeted knockdown of METTL3, METTL14, WTAP, ALKBH5, and FTO did show expected reporter responses (Figure 2-S1A).

We also showed that METTL3 can bind to USP5, and that this binding is promoted by ERK-mediated phosphorylation. This may be an example of how phosphorylation sites act as switches to regulate protein-protein interactions [193]. Based on expression of different USP5 protein domains, METTL3 appears to bind most strongly to the cryptic ZnF domain, which possesses multiple positively charged residues on the domain surface. Our data would be strengthened with structural studies that reveal the nature of the binding site for USP5 on METTL3, as well as the phospho-sites of the METTL/METTL14/WTAP structure. Although there is no structure for WTAP and currently available structural data of METTL3 do not contain S43 and S50, the software xgBoost-based Interface Prediction of Specific Partner Interactions [194] suggests that METTL3 R523 is involved in the interaction with USP5. Its proximity to S525 likely suggests that S525 phosphorylation may increase binding affinity to a positively charged region of USP5, although further studies are needed.

Materials and Methods

Mammalian Cell Culture, and Chemical Treatment of Cells

Human cell lines were obtained from the American Type Culture Collection (ATCC) and cultured under standard conditions. The following cell lines were cultured in DMEM 11965 supplemented with 10% FBS and 1% penicillin-streptomycin: HEK293T (human embryonic kidney), HeLa (cervical carcinoma), A375 (malignant melanoma), CHL-1 (melanoma), and MEL-624 (melanoma). BT474 (HER2+ breast ductal carcinoma) were cultured in RPMI 1640 or ATCC Hybri-Care medium, supplemented with 20% FBS and 1% penicillin-streptomycin. SKBR3 (HER2+ breast adenocarcinoma) was cultured in McCoy's 5A medium or RPMI-1640, supplemented with 10% FBS and 1% penicillin-streptomycin. T47D (breast ductal carcinoma), MCF7 (breast adenocarcinoma)), and HCT116 (colon carcinoma) cells were cultured in RPMI 1640 medium supplemented with 10% FBS and 1% penicillin-streptomycin.

To observe the phenotype of stably transfected cells, doxycycline was added at a concentration of 2 μg/mL to induce knockdown of METTL3 and/or WTAP. Cumate (50 μg/mL) was added to induce CuO-METTL3-T2A-WTAP expression.

In some experiments, cells were cultured with small molecule inhibitors. Inhibitors were dissolved based on manufacturer's recommendations, usually sterile DMSO. To optimize concentration of inhibitor, cells were incubated with various concentration for 24-48 hours, and then harvested for western blot or assayed for proliferation in order to determine the IC50 concentration. Cells were then treated for 6-48 hours depending on the experiment. As a reference, cells were typically treated with 10 μM PD0325901, 0.1 μM trametinib, 10-30 μM vialinin A, 3-10 μM EOAI3402143, 1 μM tucatinib, or 1 μM lapatinib.

Mouse Embryonic Stem Cell Culture and Differentiation

Mouse embryonic stem cells (mESCs) were generated, maintained, and differentiated essentially as previously described [101]. METTL3 knockout mESCs were kindly provided by Dr. Howard Y. Chang (Stanford University) and regularly tested negatively for mycoplasma contamination. Established ESC clones were genotyped by PCR and validated as METTL3-deficient by qPCR and Western blot. mESCs were cultured on mitomycin C-treated mouse embryonic fibroblasts in ES medium containing DMEM supplemented with 15% FBS, 1 mM L-glutamine, 0.1 mM mercaptoethanol, 1% Non-Essential Amino Acid, 1% penicillin-streptomycin, nucleosides 1,000 U /ml leukemia inhibitory factor, 3 μM CHIR99021 and 1 μM PD0325901. To observe the phenotype of METTL3-KO derived stable transfectants, doxycycline was added at a concentration of 2 μg/ml to knock down WTAP in TetOn-shWTAP cells, and cumate at 50 μg/ml was added to induce CuO-METTL3-T2A-WTAP expression. To observe effects of ERK activity, PD0325901 was removed from the medium in order to compare the difference between WT and 3A2A. For embryoid body (EB) differentiation, $5x10^6$ ESC were disaggregated with trypsin and transferred to non-adherent suspension culture dishes and cultured in MEF medium (DMEM supplemented with 1% L-Glutamine, 1% Non-Essential Amino Acid, 1% penicillin-streptomycin and 15% FBS) for 8 days. The serum-free neural induction protocol was applied as previously described [195]. ES cells were plated in 6-well plates at a density of $1.5X10^5$ cells/well in N2B27 medium with LIF (100 units/ml). The next day (day 0), the medium was changed to N2B27 without LIF. The medium was replaced daily thereafter.

Plasmids

The circular RNA reporters containing a split GFP sequence and an m^6A GGACU motif were kindly provided by Zefeng Wang (Chinese Academy of Science, Shanghai, China) and

subcloned into pCDH-CMV-MCS-EF1α-RFP (System Biosciences, CD512B-1). The CRISPR knockout pooled library (#1000000048), METTL3 (#53739), METTL14 (#53740), WTAP (#53741), pKMyc (#19400), Flag-ATM (#31985), Flag-ATR (#31611), Flag-IKKε (#26201), HA-GSK-3β (#14754), ERK1 (#23509), ERK2 (#23498), B-Raf V600E (#17544), HA-Ubiquitin (#17608), Ubiquitin-KO (#17603), Ubiquitin-K6 (#22900), Ubiquitin-K11 (#22901), Ubiquitin-K27 (#22902), Ubiquitin-K29 (#22903), Ubiquitin-K33 (#17603), Ubiquitin-48 (#17605), Ubiquitin-K63 (#17606), pMD2.G (#12259) and psPAX2 (#12260) were ordered from Addgene. Flag-IKKα, Flag-IKKβ, HA-AKT, Flag-mTOR, HA-MEKDD, HA-CDC2, FAK, EGFR, HER2 V659E, pCMV5-HA, and pCMV5-Flag were kindly provided by Mien-Chie Hung (China Medical University, Taichung, Taiwan). pLightSwitch R01_3'UTR and *NANOG* 3'UTR were ordered from Switchgear Genomics. Mouse METTL3 (MR209093), mouse WTAP (MR216877), and human USP5 (RC224191) were purchased from OriGene. METTL3 (human and mice), METTL14, and WTAP were subcloned into pKMyc, METTL14 was subcloned into pCMV5-HA, and WTAP (human and mice), ERK1, ERK2, and USP5 were cloned into pCMV5-Flag. All mutants were generated using the QuikChange Site-Directed Mutagenesis Kit (Stratagene). The annealed shMETTL3 (TRCN0000289742), shWTAP (TRCN0000231424-human, TRCN0000124351-mice) specific targeted sequence was inserted into Tet-pLKO-puro (Addgene, #21915). Myc-METTL3-T2A-Flag-WTAP was cloned into pCDH-CuO-MCS-EF1α-RFP (System Biosciences, QM512B-1). pCDG-EF1α-CymR-T2A-Neo (QM400PA-2) for the cumate suppressor was ordered from System Biosciences. Human METTL3 was subcloned into the pLenti-DsRed_IRES_SNCA:EGFP lentiviral reporter (Addgene, #92195), after removing the SNCA gene from the plasmid in order to form a pLenti-DsRed-IRES-METTL3-EGFP reporter.

Transient Transfection

For transient transfection of plasmids, cells were transfected with Lipofectamine 2000 [196]. Briefly, cells were seeded within 24 hours before transfection. Standard culture medium was then replaced with medium without antibiotics or Opti-MEM medium. The plasmid(s) and Lipofectamine 2000 reagent were each added to Opti-MEM media, combined in Opti-MEM media to form lipid-nucleic acid complexes, and added to the cell culture medium. The medium was then replaced with regular medium without antibiotics 6 hours later. For subsequent experimentation and analysis, cells were harvested 48 hours after the addition of transfection reagents.

For transient transfection of siRNA, cells were transfected with Lipofectamine RNAiMAX following the manufacturer's instructions. The final concentration of siRNA was 50-100 nM. Cells were collected 48 hours after transfection for further experimentation.

Lentivirus Production

For lentivirus production, 5 μg of a lentiviral construct (pCDH-CMV-MCS-EF1α-RFP plasmids for overexpressing circRNA-GFP, Tet-pLKO-puro for inducible knockdown of METTL3 or WTAP, pCDG-EF1α-CymR-T2A-Neo for cumate repressor, pCDH-CuO-MCS-EF1α-RFP for inducible overexpression of METTL3-T2A-WTAP, or pLenti-DsRed-IRES-METTL3-EGFP as METTL3 protein stability reporter), together with 2 μg of pMD2.G and 3 μg psPAX2, were co-transfected into HEK293T or HEK293TN cells (System Biosciences). Cell culture medium supernatant (usually around 6 mL) containing lentivirus particles were collected. To concentrate viruses, PEG-it Virus Precipitation Solution was added. The lentivirus-containing medium was then incubated overnight, centrifuged, re-suspended in 800 μL cell culture medium, and used for

infecting cells with the addition of TransDux (System Biosciences). Pools of stably transduced cells were selected by antibiotics or sorted by flow cytometry. Doxycycline (0.5 μg/mL) was used to induce shRNA while cumate (50 μg/mL) was used to induce shRNA-resistant cDNA expression.

Luciferase Reporter Assay

The luciferase plasmid LightSwitch 3'UTR Reporter, containing the *NANOG* 3'UTR or random negative control R01_3'UTR (Switchgear Genomics) was co-transfected with the m^6A writer complex and ERK-activated kinase into HeLa cells for two days. A *NANOG* wild type RRACT 3'UTR reporter was mutated at 46A, 397A, and 743A (^{44}AAACT^{48}, ^{395}GGACT^{399}, ^{741}AAACT^{745}) to form a mutant RRTCT 3'UTR reporter. Luciferase expression was measured using the Luciferase Assay System according to the commercial protocol (Promega). *NANOG* 3'UTR luciferase activity was normalized to cells transfected with R01_3'UTR.

Flow Cytometry

Flow cytometry analysis was conducted on the BD LSR Fortessa, and cell sorting was conducted on BD FACSAria Fusion. For SSEA-1 expression, cells were disaggregated with trypsin, blocked with TruStain FcX (BioLegend) then incubated with anti-SSEA-1 (BioLegend) in cell staining buffer (BioLegend).

CRISPR Screen

The genome-wide CRISPR-Cas9 gene knockdown screen was accomplished using the GeCKOv2 gene knockout library following a published protocol [159]. Briefly, the GeCKOV2

library was amplified in Endura electrocompetent cells (Lucigen), and then co-transfected with pMD2.G and psPAX2 into HEK293TN cells to produce a lentiviral library. HeLa-circGFP cells were infected at 0.3 MOI for 3 days, then selected with 2 μg/ml puromycin for 1 week before flow cytometry sorting of GFP fluorescence signal. Specifically, to determine the genes with the greatest upregulation and downregulation in GFP signal, the cells in the top and bottom 1% of the GFP signal were sorted and collected for sequencing. Genomes of harvested cells were extracted by Quick-gDNA MidiPrep (Zymo). sgRNA after PCR amplification was sent to the University of Chicago Genomics Facility to be sequenced on Illumina HiSeq 4000 in single-end read mode. To analyze the data and obtain the ranked difference plot, sgRNAs were ranked according to the difference between number of reads in low and high GFP populations. The sgRNAs that ranked with the greatest difference were selected for gene ontology pathway enrichment analysis.

Western Blotting (Protein Immunoblot)

Western blotting was performed first by preparing protein samples. Cells were harvested after culture and/or treatment conditions, and protein samples were isolated from cells either by addition of RIPA lysis buffer (1% Triton X-100, 150 mM NaCl, 20 mM, 20 mM Na_2PO4, pH 7.4) containing Halt Protease and Phosphatase Inhibitor Cocktail (Thermo Scientific), or by direct addition of Laemmli sample buffer (Bio-Rad) containing beta-mercaptoethanol (Bio-Rad). For RIPA buffer-lysed protein samples, a BCA assay (Thermo Scientific) was used to measure the protein concentration.

To perform the immunoblot, equal quantities of protein were loaded onto a polyacrylamide gel and separated by electrophoresis (SDS-PAGE). A wet or dry transfer was then applied to the gel

onto PVDF or nitrocellulose membranes. Membranes were blocked with 5% non-fat milk blocking solution or BSA (for phosphorylation-sensitive applications) for at least 30 minutes, and then incubated with primary antibody at 4ºC overnight. After washing away primary antibody, secondary HRP-conjugated antibody was added, and immunoblot signal was detected with addition of SuperSignal West Pico Plus chemiluminescent substrate and imaged on the FluorChemR system. Densitometry calculations were performed using ImageJ.

Immunoprecipitation

Immunoprecipitation was performed first by obtaining lysate from cells by lysis in RIPA buffer (1% Triton X-100, 150 mM NaCl, 20 mM Na_2PO4, pH 7.4) containing Halt Protease and Phosphatase Inhibitor Cocktail (Thermo Scientific). As a reference, approximately 500 µL of lysis buffer was added to a 10-cm dish of cells. The lysis mixture was incubated on ice for 30 minutes with periodic mixing, and then centrifuged to clear the lysate. Subsequently, a BCA assay (Thermo Scientific) was used to determine the protein concentrations. The appropriate antibody and protein A/G magnetic beads (Thermo Scientific) were incubated with lysate containing equal amounts of protein at 4ºC overnight. Beads were then washed at least three times, and immunoprecipitated protein was eluted with addition of sample buffer (Bio-Rad) heated at 95ºC for 5 minutes. The protein samples were then subjected to a standard western blotting protocol.

Phos-Tag Gels

Phosphate-affinity gel electrophoresis was performed in poured gels containing 60 µM $MnCl_2$, and 30 µM acrylamide-pendant Phos-tag ligand (AAL-107, Wako Chemicals). A standard SDS-

PAGE gel was also performed to serve as a reference for protein separation and immunoblot for equal quantities of protein. Because the Phos-tag ligand traps phosphorylated protein, the samples migrate more slowly, so a lower polyacrylamide concentration than normal (approximately 2%) should be used to run Phos-tag gels. To prevent de-phosphorylation of protein samples, Halt Protease and Phosphatase Inhibitor Cocktail was added, and membranes were blocked with BSA instead of milk.

In Vitro Kinase and Deubiquitination Assays

For in vitro kinase assays, recombinant full-length kinase expressed in E. coli cells with an N-terminal GST tag, and N-terminal GST-tagged human METTL3/METTL14 complex expressed in Sf9 insect cells were purchased from SignalChem. Active kinase was diluted in Kinase Dilution Buffer III (SignalChem) and incubated with METTL3/METTL14 at 30ºC for 15 min. The reaction was stopped by the addition of the sample buffer then analyzed by western blot.
For in vitro deubiquitination, HEK293T cells transfected with HA-ubiquitin were treated with 10 μM MG-132 and 10 μM EOAI3402143 for 8 hr. METTL3 was purified via immunoprecipitation and then incubated without or with purified USP5 (SignalChem) in deubiquitination (DUB) reaction buffer (SignalChem) following the commercial protocol. In brief, 10 μL of the DUB reaction buffer was incubated with 5 μL of the deubiquitinase protein and 5 μL of the substrate protein. The reaction was incubated for 30 min at room temperature and stopped with addition of sample buffer. Samples were then analyzed by western blot.

Cycloheximide Chase Assay

Prior to the cycloheximide chase assay, cells were seeded under standard culture conditions. To measure protein stability and lifetime, cells were treated with 50 μg/mL cycloheximide (CHX) at harvested later at various time points—specifically, at 0, 6, and 12 hours after addition of CHX. Protein was then quantified with western blot, and densitometry calculations were performed using ImageJ.

Immunofluorescence Staining and Confocal Microscopy

To perform immunofluorescent staining for confocal microscopy, cells after treatment were fixed in 4% paraformaldehyde (incubated for 10 min), permeabilized with 0.5% Triton X-100 (incubated for 5-10 min), blocked with 5% bovine serum albumin (incubated for 1 hour), incubated with primary antibodies overnight at 4ºC, and then incubated with the appropriate secondary antibody tagged with Alexa 488 or Alexa 568 (Molecular Probes). Nuclei were stained with 4',6-diamidino-2-phenylindole (DAPI) before mounting. Immunofluorescence images were captured using Olympus FV1000 confocal spectral microscope.

Protein Mass Spectrometry

To identify phosphorylation sites of METTL3, METTL3 precipitated from HEK293T cells co-transfected with myc-METTL3 and B-Raf V600E was analyzed by Coomassie Blue staining. The protein band corresponding to METTL3 was excised and subjected to in-gel digestion with tryspin and chymotrypsin. Samples were analyzed by Ultimate Capillary LC system (Dionex) directly coupled to LTQ Orbitrap Mass Analyzer (Thermo Scientific) using the TopTenTM method. The data were searched on MASCOT (MassMatrix) against the human Swiss-Prot

database. All the identified phospho-peptides were further confirmed by manually checking the results.

RNA Extraction and Real-Time qPCR

Total RNA was isolated using TRIzol (Invitrogen), and 200-1000 ng of RNA was reversed transcribed into cDNA using PrimeScript RT Reagent Kit (Takara). Real-time qPCR was performed using the FastStart Essential DNA Green Master (Roche). HPRT1 or GAPDH was used as an internal control for normalization. For measuring RNA stability, cells were treated with 5 μg/ml actinomycin D and harvested at 0, 6, and 12 hours to determine the half-life of target mRNAs.

LC-MS/MS m^6A quantification of poly(A) RNA.

Total RNA was isolated and purified using TRIzol (Invitrogen). mRNA (poly-A RNA) was extracted from 20 μg of total RNA using 2 rounds of the Dynabeads mRNA DIRECT Purification Kit (Thermo Scientific). 30-50 ng of mRNA was digested by nuclease P1 (1U) in 20 μl of buffer containing 20 mM NH_4OAc (pH = 5.3) at 42°C for 2 hr, followed by dephosphorylation with the addition of FastAP Thermosensitive Alkaline Phosphatase (1U) and FastAP buffer at 37°C for 2-4 hr. The sample was then diluted to 50 μl, and filtered (0.22 μm pore size, 4 mm diameter, Millipore). 5 μl of the solution was separated by reverse phase ultra-performance liquid chromatography on a C18 column, followed by online mass spectrometry detection using an Agilent 6410 QQQ triple-quadrupole LC mass spectrometer in positive electrospray ionization mode. The nucleosides were quantified by using the nucleoside-to-base ion mass transitions of 282 to 150 (m^6A) and 268 to 136 (A). Quantification was carried out by

comparison with a standard curve obtained from pure nucleoside. The ratio of m^6A to A was calculated based on the calibrated concentrations [120].

m^6A-IP and m^6A-seq

100 μg of total RNA was extracted after adding TRIzol to cells and following the manufacturer's protocol. Poly-A mRNA was then enriched using Dynabeads mRNA Direct Kit following the manufacturer's protocol. m^6A-IP was performed using the EpiMark N6-Methyladenosine enrichment kit (NEB), starting with 1 μg mRNA. Full length purified mRNA was used in m^6A-IP-qPCR. For m^6A-seq, prior to m^6A-IP, mRNA was adjusted to 15 ng/μl in 100 μl and fragmented using a BioRuptor Ultrasonicator (Diagenode) with 30 seconds on/off for 30 cycles. Input (5% of total amount) and RNA eluted from m^6A-IP were used to prepare libraries with TruSeq Stranded mRNA Library Prep Kit (Illumina). Sequencing was carried out at the University of Chicago Genomics Facility on Illumina HiSeq 4000 in single-end read mode with 50 bp reads per read.

Cell Proliferation Assay

Cells were seeded in 96-well plates. The cell proliferation was assessed by SRB assay [197] at various time points. Briefly, cells after treatments were fixed with 10% TCA then stained with 0.05% SRB. After washing 3-4 minutes with water, bound SRB was solubilized with 10 mM Trizma base and measured at 515nm.

Quantification of Histone Modifications

Histones were prepared from fresh cell pellets using Total Histone Extraction Kit (Epigentek). The efficiency of histone extraction was controlled by Coomassie Blue staining and IB with anti-H3 antibody. Histone posttranslational modifications were quantified using the Histone H3 Modification Multiplex Assay Kit (Epigentek) following commercial protocol. Each histogram corresponds to the mean of 2 independent experiments and each measure was obtained using a pool of 100 ng of total histones from 2 independent extractions.

Structural Analysis of Protein

The atomic coordinates and structure factors for the reported crystal structures were obtained from the Protein Data Bank (PDB) with the accession code 5IL0 for the ligand-free form of the METTL3-METTL14 complex and 3IHP for the covalent Ubiquitin-USP5 complex. All figures representing structures were prepared with PyMOL. The prediction of partner-specific protein interfaces was performed using the xgBoost based Interface Prediction of Specific Partner Interactions (BIPSPI) web server [194]. Predictions were performed using structural data using PDB atomic coordinates as described in the structural analysis of proteins.

RNA and m^{6}A Sequencing Analysis

RNA-seq and m^{6}A-seq experiments were performed on at least two biological replicates. Total RNA was extracted using TRIzol. mRNA was purified using the Dynabeads mRNA Direct Kit. m^{6}A-IP was performed as previously described. Libraries were prepared using the TruSeq Stranded mRNA Sample Preparation Kit (Illumina), and sequenced on the Illumina HiSeq 4000. Approximately 25-30 million reads were mapped for each sample. Using HISAT2 v2.1.0 (Kim et al., 2015), reads were aligned to the mycoplasma genome to assess contamination and all non-

mycoplasma-aligned reads were retained. The following parameters were used: hisat2 -x $INDEX -k 7 --un-gz $s.IN.noMyco.fastq.gz --summary-file $s.IN.myco_summary -p 4 -U $Data/$s.IN.fastq.gz > $s.myco.input.sam. Depending on the sample type, the reads were subsequently mapped and aligned to either *Mus musculus* genome GRCm10 (mm10) or *Homo sapiens* genome assembly GRCh38 (hg38) with HISAT2 v2.1.0 [198] with parameter –k 1, taking splice sites into account. The following command was used for mapping to the reference genome: hisat2 -x $INDEX --known-splicesite-infile $SPLICE -k 1 --no-unal --summary-file $s.IN.align_summary -p 4 -U $Data/$s.IN.noMyco.fastq.gz | samtools view -bS | samtools sort -o $Output/$s.input.bam.

Input RNA libraries from m^6A-sequencing served as RNA-seq samples to compare gene expression. DESeq2 [199] was applied for differential expression between R-WT and R-3A2A mESCs with a FDR < 0.05 cutoff. Subsequent analyses and figures were generated according to rnaseqGene, an RNA-seq workflow on BioConductor (http://master.bioconductor.org/packages/release/workflows/html/rnaseqGene.html).

m^6A-seq data were analyzed as described before [200]. m^6A peak calling was performed using exomePeak R/Bioconductor package v 3.7 [201]. Significant peaks with FDR < 0.05 were annotated to the RefSeq database (hg38 or mm10). Homer v4.9.1 [202] was used to search for enriched motifs in the m^6A peak regions called, and random peaks of 200 bp were used as background sequences for motif discovery; Homer was also used to generate sequence motif logos. m^6A peak distribution on the metagene was plotted by the R package Guitar [203]. Differential analysis of m^6A methylation was performed using the R package RADAR and MeRIPtools [204]. To summarize and visualize the m^6A methylome data, principal component analysis (PCA) was performed using singular value decomposition approach implemented in R

function (prcomp) on the log-transformed m^6A-IP data. Pathway and gene ontology enrichment analysis were performed using WebGestalt [205] with default settings. Pathway enrichment terms were determined using WikiPathway and KEGG terms.

Data Deposition

The CRISPR screening and m^6A-seq data generated during this study have been deposited to the National Center for Biotechnology Information Gene Expression Omnibus database and are available under accession number GSE138776. The human data for the skin cutaneous melanoma (SKCM) was derived from The Cancer Genome Atlas (TCGA).

Chapter III: METTL3 suppresses double-stranded RNA formation and the RIG-I antiviral innate immune pathway

Note:

The following section (*Chapter III*) is a manuscript in preparation for submission. This project was performed independently and took place during the final phase of my graduate research.

Introduction

The mammalian cell's innate immune system contains signaling pathways that enable it to mount the first response to foreign, invading material. Invading pathogens carry genetic material that are required for their replication but are also detectable by host cell machinery[206] (Figure 3-1A). These invading pathogen nucleic acids are recognized by and trigger cytoplasmic and membrane-bound pattern recognition receptors (PRRs) that can differentiate between host and viral DNA or RNA[207, 208].

The cytoplasmic Retinoic Acid-Induced Gene I (RIG-I) PRR and Melanoma Differentiation-Associated Gene 5 are members of the RIG-I-like Receptor (RLR) family, which detects RNA viruses. These RLRs have similar domain architectures, including tandem N-terminal caspase activation and recruitment domains (CARDs) that partake in signaling cascades, a DExD/H-box helicase domain with RNA binding and hydrolytic activity, and a C-terminal domain (Figure 3-1B). However, RIG-I tends to favor short dsRNAs, whereas MDA5 favors long dsRNAs[209] (Figure 3-1C). The binding of these domains to RNA ligands triggers a

conformation change in RIG-I that allows release of the CARDs and binding to the downstream signaling adaptor MAVS[210, 211].

A

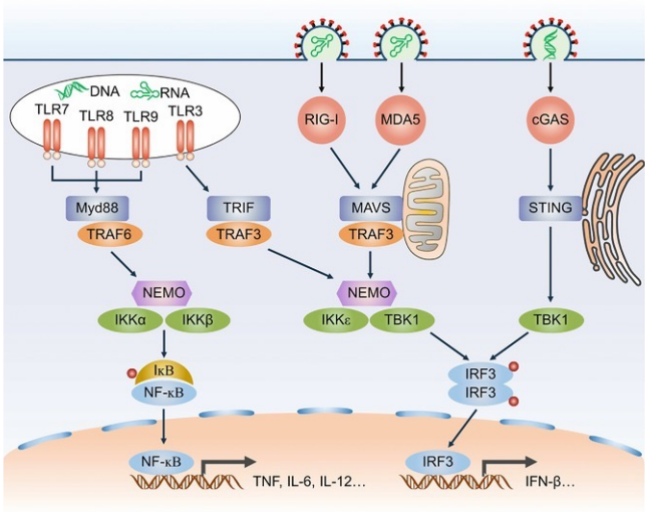

B

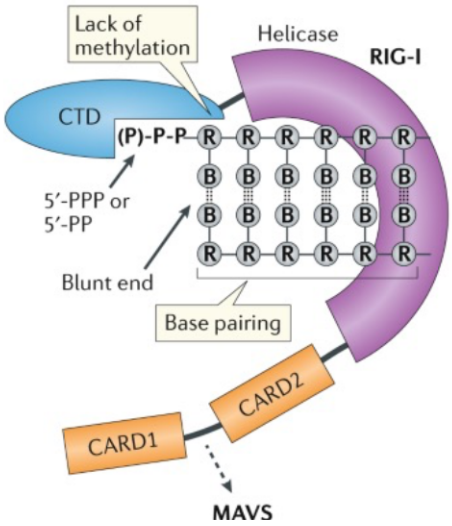

C

Pattern Recognition Receptor (PRR)	Ligand / Structural Pattern	Localization
RIG-I	(usually viral) dsRNA (short; >20 bp) 5'-(P)PP moiety blunt ends unmodified nucleosides	cytosol, nucleus, stress granules
MDA5	dsRNA (long; >1-2 kbp)	cytosol, stress granules
cGAS	dsDNA	cytosol
PKR	dsRNA	cytosol, nucleus
TLRs	dsRNA, RNA degradation products, ssDNA	endolysosomal compartment

Figure 3-1. Pattern recognition receptors (PRRs) have distinct biochemical mechanisms for recognizing foreign nucleic acids.

(A) Antiviral signaling pathways. PRRs (red) are activated by endosomal and cytosolic viral RNA and DNA species. TLR7, TLR8 and TLR9 recruit MyD88 and MyD88 in turn activates TRAF6. TLR3 recruits TRIF and subsequently activates TRAF3. TRAF6 and TRAF3 then induce the formation of NEMO-IKKα/β and NEMO-IKKε/TBK1 complex respectively. IKKα/β activate the transcription factor NF-κB and IKKε/TBK1 phosphorylates the transcription factor IRF3. NF-κB and IRF3 then translocate into the nucleus and drive proinflammatory cytokines and type I IFNs expression. For the RLR pathway, RIG-I and MDA5 activate TRAF3-TBK1 axis through the mitochondria-located adaptor MAVS. For the cGAS pathway, cGAS recognize

Figure 3-1, continued. Pattern recognition receptors (PRRs) have distinct biochemical mechanisms for recognizing foreign nucleic acids.
cytosolic DNA and activate the ER-located adaptor STING, which then translocates to and activates TBK1. Sourced from [206].
(B) RIG-I is shown in its active conformation, bound to an immunostimulatory RNA. The molecular features of RIG-I-stimulatory RNAs are also illustrated; please see text for details. B, nucleobase; IFNα/β, interferon-α/β; LGP2, laboratory of genetics and physiology 2; P, phosphate; PP, diphosphate; PPP, triphosphate; R, ribose. Sourced from [209].
(C) Table of structural patterns recognized by ligands.

Upon activation, RLRs activate signaling cascades to stimulate interferon (IFN) and inflammatory cytokines and chemokines, which form the initial antiviral response. The primary ligand for RIG-I activation is a 5'-tri-phosphorylated or di-phosphorylated single-stranded RNA (ssRNA)[212, 213]. However, it is also capable of detecting double-stranded RNA (dsRNA) as well[214]. This feature is unique to viral RNA, as mammalian RNA contains a 5' cap structure that also contains N^7-methylguanosine (m^7G) and 2'O-methylation, which prevents RIG-I recognition[215, 216]. As part of evolutionary adaptation, many viruses have acquired their own mRNA cap methyltransferases to install 2'-O-methylation in order to avoid detection[20, 217].

Another way that viral RNAs evade innate immune recognition is through post-transcriptional modifications. m^6A has been found on several cytoplasmic viruses since the 1970s, and it plays important roles in viral replication as well, and now know that viruses acquire m^6A to mimic cellular RNA as well[218-220]. The first study showing how these modified nucleosides affected immune activation was done in 2005, when multiple uridine modifications and m^6A could prevent Toll-Like Receptor (TLR) activation[221]. Since then, multiple studies in the last few years have demonstrated that viral RNAs can undergo m^6A methylation to suppress activation of RIG-I or other RLRs and evade immune surveillance[222-224]. For instance, Lu et al. show that human metapneumovirus (HMPV) uses host m^6A methyltransferase complex machinery to install m^6A onto its viral RNA, thereby suppressing the interferon response[225]

(Figure 3-2). m^{6}A methylation has also been reported to negatively regulate the interferon response through gene expression regulation as well[226].

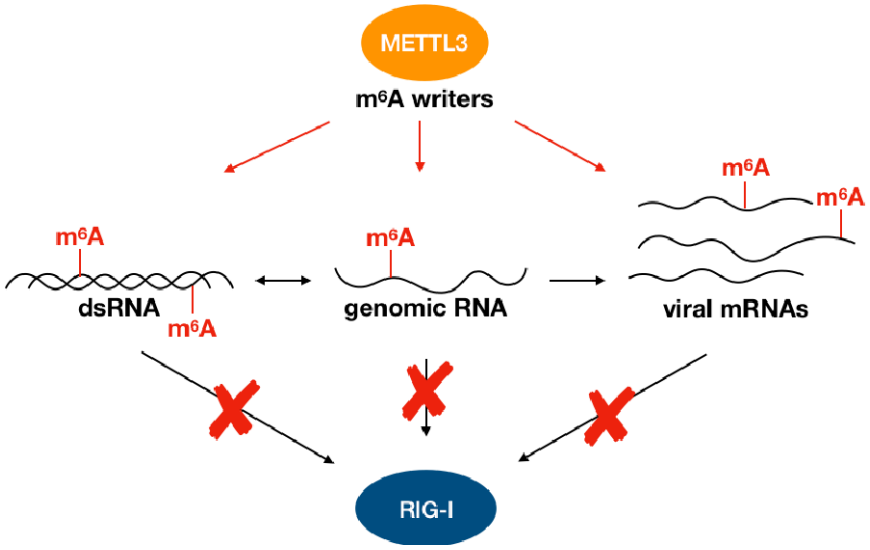

Figure 3-2. Viral RNA co-opts m^{6}A methylation to avoid innate immune system recognition.

m^{6}A serves as a molecular marker for innate immune discrimination of self from non-self RNAs. HMPV RNAs are m^{6}A methylated, and viral m^{6}A methylation promotes HMPV replication and gene expression. Mechanistically, m^{6}A-deficient virion RNA induces higher expression of RIG-I, binds more efficiently to RIG-I and facilitates the conformational change of RIG-I, leading to enhanced interferon expression. Overall, (1) viruses acquire m^{6}A in their RNA as a means of mimicking cellular RNA to avoid detection by innate immunity and (2) viral RNA m^{6}A can serve as a target to attenuate HMPV for vaccine purposes.

Even though RIG-I mainly functions in sensing foreign material, it is also capable of detecting cellular RNA transcripts. Specifically, Chiang et al. found that, upon herpes simplex virus 1 (HSV-1) infection, 5S ribosomal RNA pseudogene 141 (*RNA5SP141*) re-localizes from nucleus to cytoplasm, permitting recognition by RIG-I[227]. Circular RNA is also capable of activating RIG-I as well and requires m^{6}A methylation to suppress innate immunity[228].

m^{6}A has also been found to affect the local structure of mRNA, which, in the case of certain m^{6}A structural switch-based readers HNRNPC or HNRNPG, enhances their RNA-

binding affinity[90, 91]. m^6A has also been found to reshape double-stranded viral RNA to suppress innate sensing pathways[223].

These findings raise some interesting questions that are the focus of this chapter. Do host cellular RNAs use m^6A methylation installed by METTL3 to avoid RIG-I recognition, like viral RNAs? Although methylated 5' cap of host RNAs has canonically been touted to prevent recognition of self RNAs, some find that 5'-capped RNAs without 2'-O-methylation also bind to RIG-I[215]. Given that *RNA5SP141* is recognized by RIG-I, what other cellular RNAs does RIG-I bind to? Since RIG-I also binds to dsRNA, does m^6A methylation alter cellular RNA structure to prevent RIG-I activation? Although innate immunity consists of multiple PRRs aside from RIG-I, we focused on RIG-I to narrow the scope of this project.

Results

To determine whether m^6A methylation could affect RIG-I signaling, we generated HeLa cell lines with heterozygous knockout of *METTL3* or inducible shRNA-mediated knockdown of METTL3. Upon addition of 3p-hpRNA, a specific agonist of RIG-I, we found that the expression of type I interferon *IFNB* mRNA was significantly elevated in METTL3-depleted cells (Figure 3-3A). Across both knockout and knockdown of METTL3, *IFNB* expression was 4- to 5-fold greater in the METTL3 KD or KO cells relative to its negative control or wild-type counterpart (Figure 3-3B).

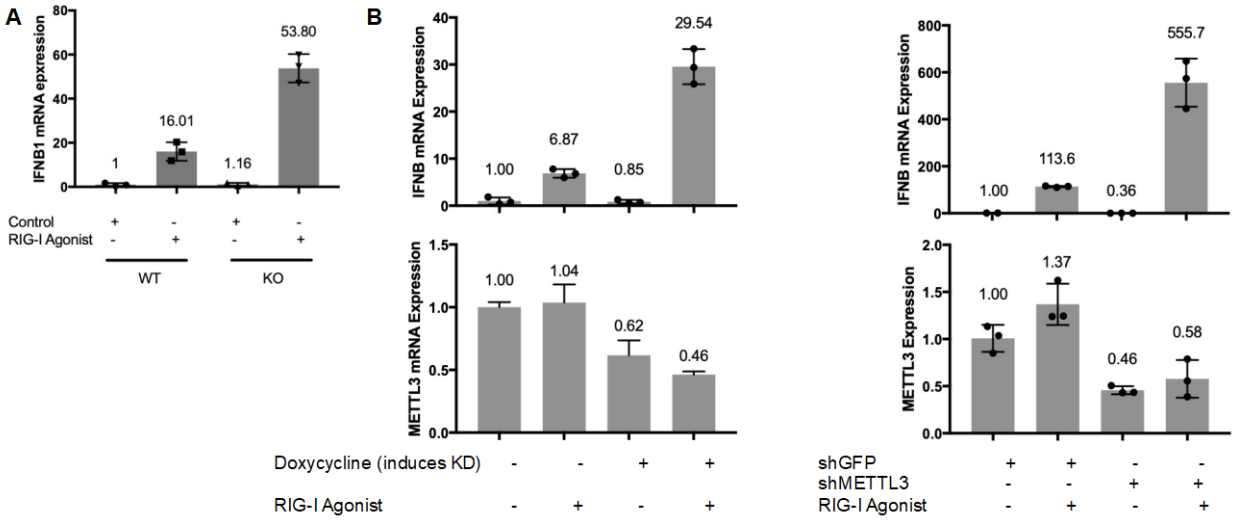

Figure 3-3. Loss of METTL3 leads to a greater RIG-I response.

(A) Measurement of *IFNB1* mRNA as an indicator of RIG-I response upon addition of a RIG-I agonist (3p-hpRNA at 10 ng/mL) for 16-24 hours in METTL3 WT or KO HeLa cells.
(B) qPCR of *IFNB1* and *METTL3* mRNA in inducible knockdown HeLa cells.

To ensure the increased expression of interferon was caused by activation downstream of RIG-I, we knocked down other RIG-I-like receptors and Mitochondrial Anti-Viral Signaling Protein (*MAVS*), a gene that encodes the signaling adaptor protein downstream of RIG-I. Knockdown of *MAVS* attenuated *IFNB*, indicating that the elevated Type I interferon response is due to RLR signaling rather than other PRR pathways (Figure 3-4A).

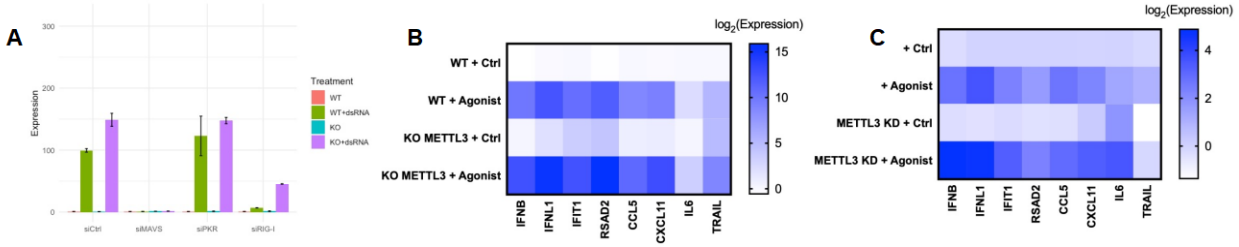

Figure 3-4. Loss METTL3 results in a greater interferon response.

(A) Barplot of RIG-I response measured by *IFNB1* mRNA upon knockdown of various PRRs.
(B) Heatmap of interferon-stimulated genes based on qPCR expression in WT and KO METTL3 HeLa cells, with or without agonist addition.

mRNA levels of other interferon-stimulated genes, such as *IFNL1*, *IFIT*, *RSAD2*, and *CXCL11* were similarly elevated upon RIG-I stimulation in the METTL3-depleted cells, further confirming an increased antiviral response (Figure 3-4B). Moreover, gene set enrichment analysis revealed enrichment in interferon gamma and interferon alpha signaling as well as cytokine signaling (Figure 3-5).

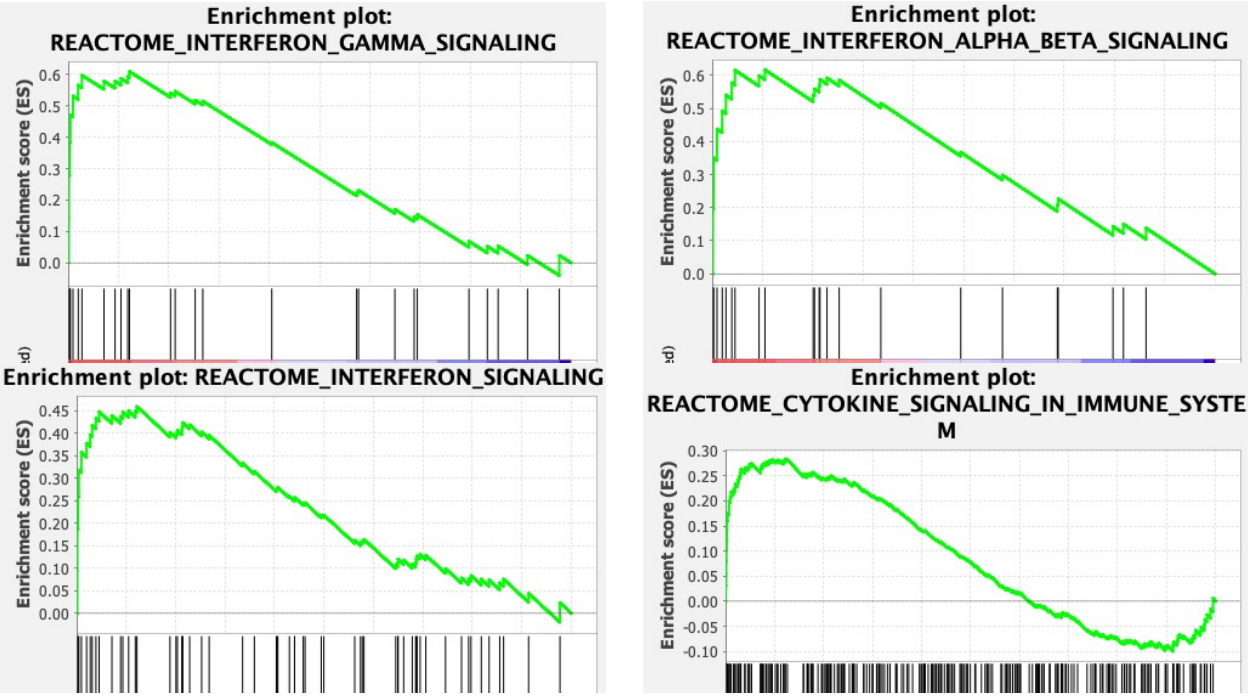

Figure 3-5. Gene set enrichment analysis of interferon signaling pathways.

Gene set enrichment analysis was performed in RNA-seq differential gene expression comparisons between WT and KO METTL3 cells.

To determine how METTL3 affects the RIG-I response, we asked how the presence of m^{6}A on RNA prevents binding to RIG-I. We wondered whether this could be due to recognition by m^{6}A readers, which would bind to m^{6}A-methylated RNAs instead of RIG-I. However, upon knockdown of *YTHDF1* or *YTHDF2*, *IFNB* expression did not significantly change (Figure 3-6).

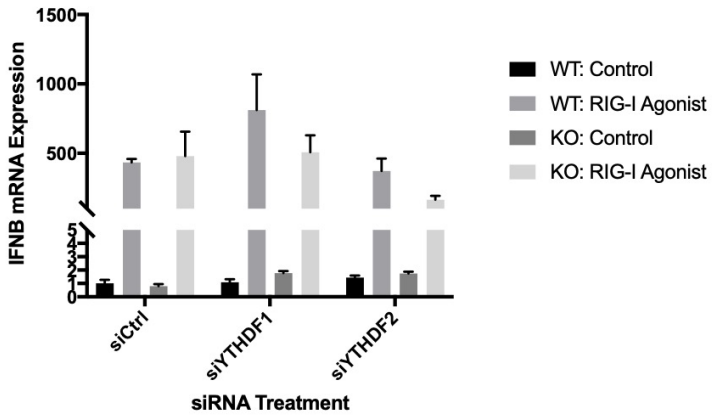

Figure 3-6. RIG-I activation upon knockout of m^{6}A readers.

siRNA for YTHDF1, YTHDF2, or negative control siRNA was transfected into HeLa cells 24 hours prior to addition of the RIG-I agonist and *IFNB1* mRNA expression was quantified by qPCR.

We next asked whether m^{6}A methylation could affect double-stranded RNA formation. Specifically, m^{6}A methylation, which can disrupt local RNA structure, could prevent RNA folding. Using a J2 antibody that specifically targets double-stranded RNA, we performed immunofluorescence staining and found increased dsRNA levels in the METTL3-depleted cells Figure 3-7), suggesting that loss of m^{6}A methylation allows greater abundance of double-stranded RNA.

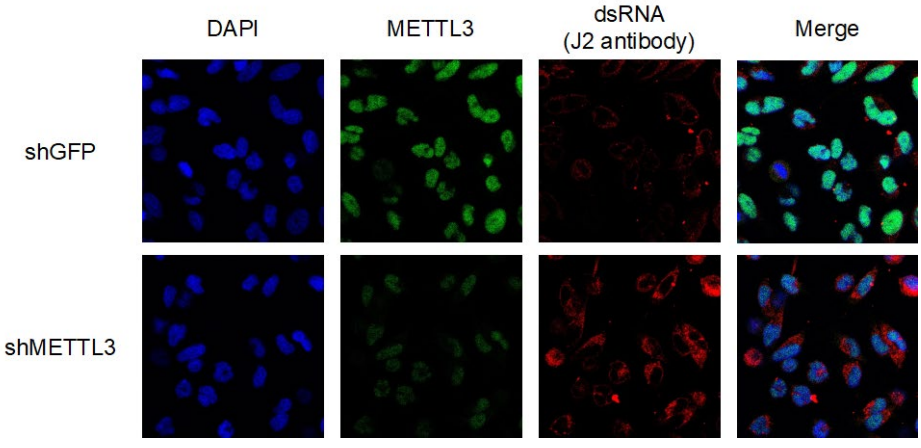

Figure 3-7. Imaging of double-stranded RNA in HeLa cells.

Figure 3-7, continued. Imaging of double-stranded RNA in HeLa cells.
Immunofluorescence images of HeLa cells expressing inducible shRNA targeting either *GFP* or *METTL3*. DAPI (blue) representing nuclei, METTL3 (green), and J2 antibody targeting dsRNA (red) are all shown.

In order to test whether double-stranded RNAs contained less m^{6}A methylation, we performed a J2 RIP and quantified m^{6}A/A ratios in both input and J2 RIP samples. RNA from the J2 RIP was found to have lower m^{6}A abundance, further suggesting that m^{6}A disrupts double-stranded cellular RNA formation (Figure 3-8).

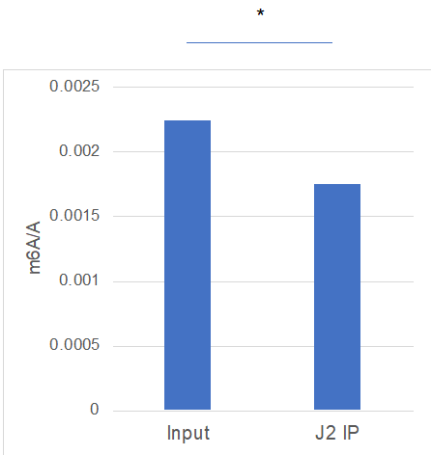

Figure 3-8. m^{6}A quantification in double-stranded RNA.
After a J2 antibody-based RNA immunoprecipitation, input and J2 RIP samples were digested and m^{6}A was quantified with mass spectrometry. Abundances are shown as m^{6}A/A ratios.

To identify which RNAs showed increased double-stranded shape upon METTL3 depletion, we performed high-throughput sequencing of input RNA and J2-immunoprecipitated RNA. Using a likelihood ratio test with a reduced model in DESeq2, we performed differential enrichment analysis comparisons between METTL3 KO cells and WT HeLa cells (Figure 3-9). Testing the differential enrichment of J2-RIP-seq data revealed 752 RNA species enriched in KO cells and 329 RNAs enriched in WT cells, without RIG-I stimulation; likewise, 424 RNAs were enriched in KO cells and 53 RNAs in WT cells, with RIG-I stimulation (Figure 3-9). These

analyses suggest that METTL3 KO cells have a greater abundance of dsRNA species than WT cells. Of note, two of the most J2-enriched RNAs included *CCCDC167*, which is predicted to have sites of secondary structure at the 5' UTR and 3' UTR, and *RN7SL1*, a signal recognition particle RNA that is partially homologous to Alu elements.

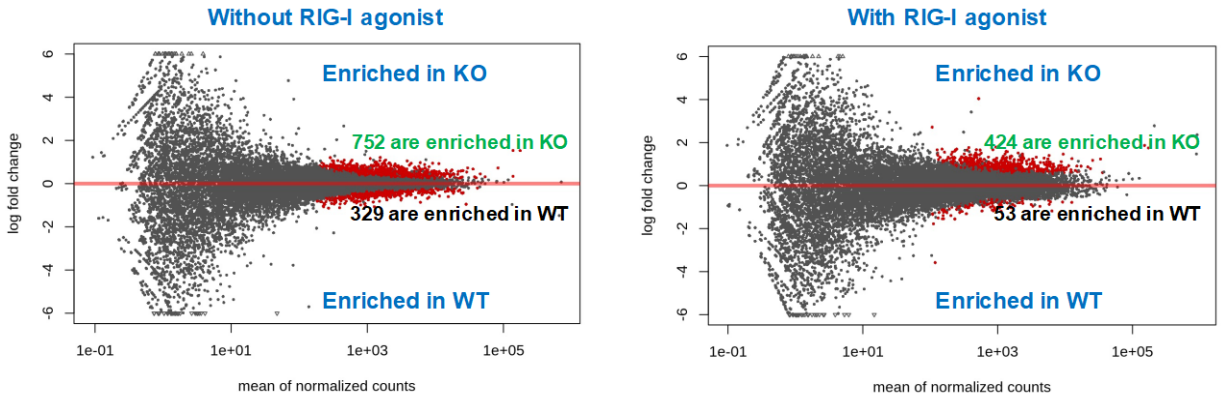

Figure 3-9. Differential enrichment analysis between KO METTL3 and WT HeLa cells in terms of J2 RIP enrichment.

To determine which species were bound to RIG-I, we then performed an RNA immunoprecipitation of stably expressed Flag-tagged RIG-I (Figure 3-10A). Upon RIG-I stimulation, 1241 RNA species were enriched in KO cells relative to WT, of which 367 were repeat RNAs, according to the TEtranscript tool's repeatMasker annotation[229]. Meanwhile, only 657 were enriched in WT cells, of which only 6 were repeats. Long terminal repeats and long interspersed nuclear elements (LINEs) comprised the majority of these enriched repeat RNAs (Figure 3-10B). Similarly, by using a MACS2-based peak calling method, treatment with the RIG-I agonist increased the number of RIG-I-immunoprecipitated RNAs, with a greater number in the *METTL3* KO cells. The RNAs with the greatest differential enrichment consisted mostly of LINE L1 RNAs (Figure 3-11).

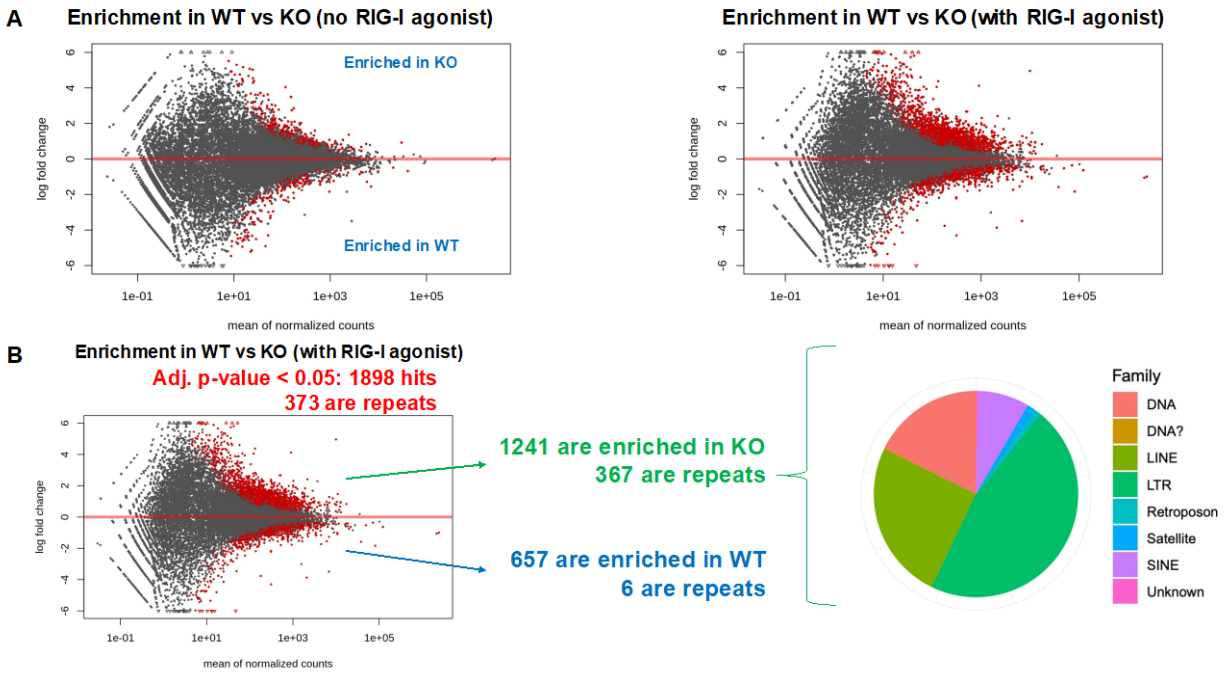

Figure 3-10. Differential enrichment analysis of RIG-I RIP.

(A) Differential enrichment analysis was performed for RNA species, including repeat elements, between KO METTL3 and WT HeLa cells after a RIG-I pulldown.
(B) Differentially enriched RNA species were annotated.

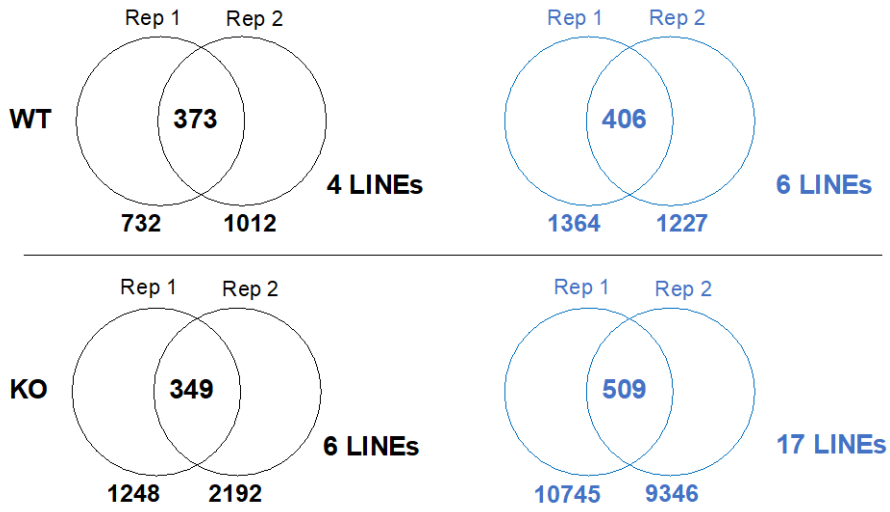

	log2FoldChange	padj
ZC3H12A	***3.663844967***	***3.59E-59***
HAL1ME:L1:LINE	**2.459401115**	**8.72E-15**
L1PA2:L1:LINE	**2.09993426**	**8.72E-15**
ZC2HC1A	8.881713483	2.37E-14
LTR1E:ERV1:LTR	9.272077606	2.45E-13
L1PA5:L1:LINE	**2.213456247**	**6.19E-13**
L1MA4:L1:LINE	**2.183355823**	**8.10E-13**
L1PA7:L1:LINE	**2.271083779**	**8.73E-13**
L1P2:L1:LINE	**2.016987302**	**1.13E-11**
L1M3de:L1:LINE	**4.929109818**	**1.68E-11**
Tigger3b:TcMar-Tigger:DNA	1.898749691	3.17E-11
AluSp:Alu:SINE	1.284897502	8.61E-11

Figure 3-11. Peak calling for RIG-I enriched RNAs.

A MACS2-based peak calling approach to finding enriched RNA species in both the WT and METTL3 KO HeLa cells. The most significantly enriched are shown in the table.

To further confirm that LINE1 elements were enriched in binding to RIG-I, we performed RIG-I RIP-qPCR and found that there was a greater fraction of input RNA in the IP in LINE1 ORF1p and ORF2p RNAs but not in Alu elements (Figure 3-12). We also explored whether *RN7SL1* contributed to RIG-I activation in an m^{6}A-dependent manner. Although *RN7SL1* did not show enrichment of RIG-I IP relative to input, the RNA abundance of *RN7SL1* increased approximately three-fold in *METTL3* KO cells (Figure 3-13).

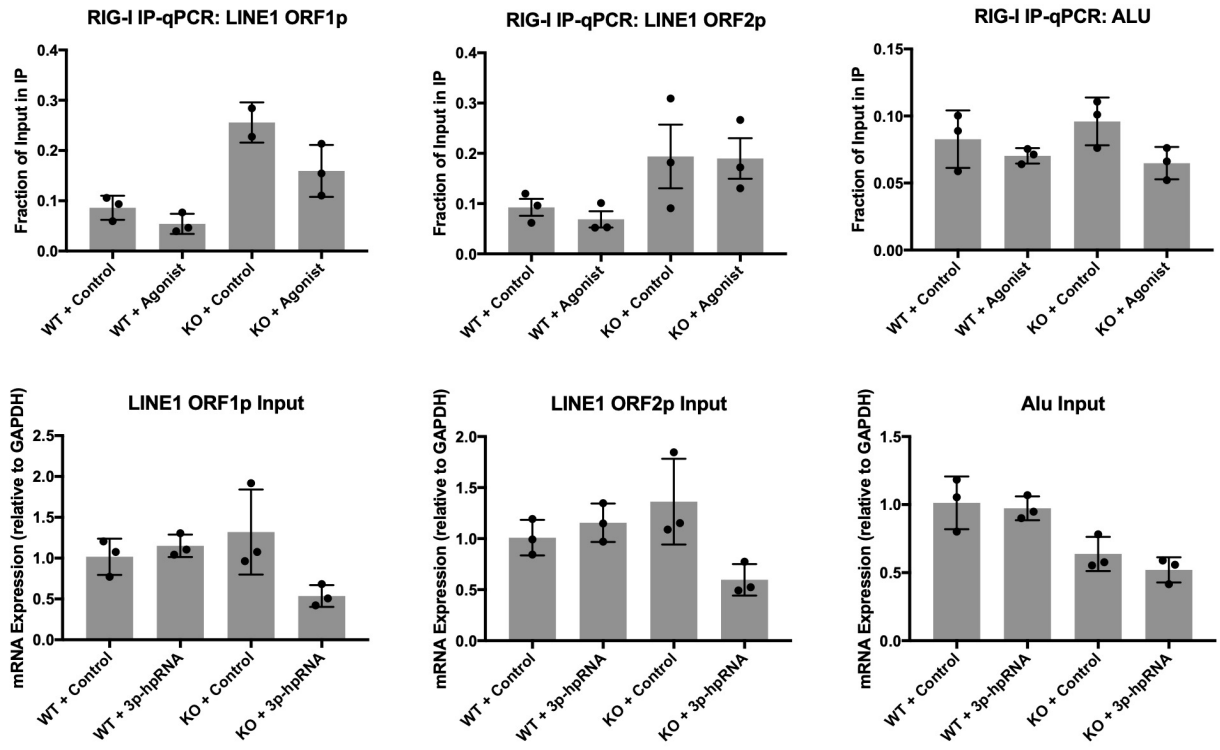

Figure 3-12. RIG-I RIP-qPCR of LINE1 and Alu element RNAs.

Both Input and RIP abundances are shown for LINE1 ORF1p and ORF2p regions, as well as Alu elements. RIP abundances are shown as percentage of input in the IP.

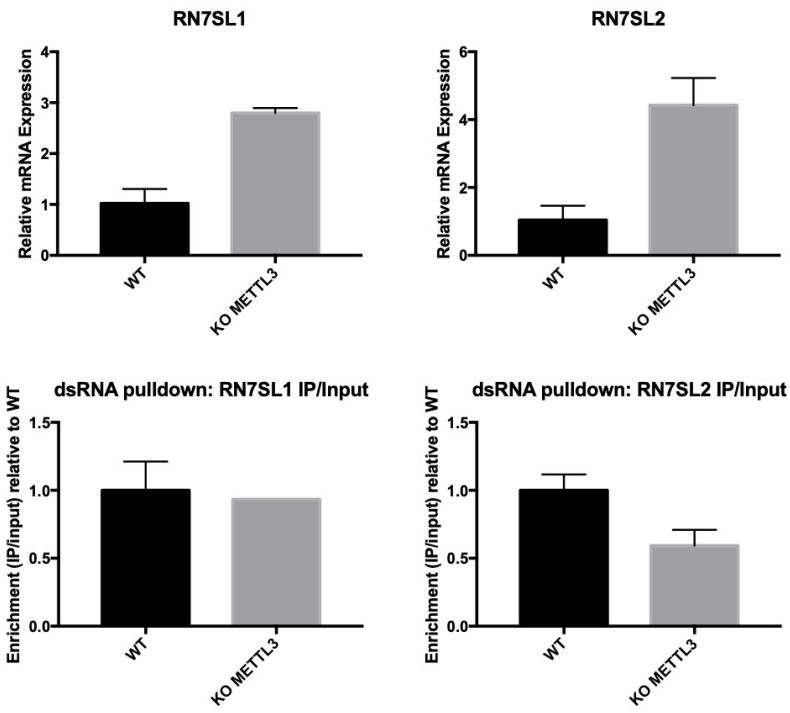

Figure 3-13. RIG-I RIP-qPCR and J2 RIP-qPCR of *RN7SL1* and *RN7SL2* non-coding SRP RNAs.

Discussion

Here we present an investigation of the effects of the m^{6}A methyltransferase METTL3 on the HeLa cell RIG-I-mediated antiviral response We found that m^{6}A depletion resulted in greater RIG-I and downstream pathway cascades. We identified upregulation of type I interferon and cytokine signaling pathways, as well as interferon-stimulated genes. This is likely due to the increased formation of endogenous dsRNAs, which were also upregulated in METTL3-depleted cells. These results suggest that m^{6}A methylation prevents the formation of dsRNAs in cells and prevents aberrant activation of the innate immune response. One of the key mediators of the antiviral response is RIG-I, which binds to viral RNAs but some cellular RNAs as well. We showed that m^{6}A methylation plays a role in the quantity of endogenous RNAs that bind to RIG-I.

Previous work has shown that METTL3 can translocate from nuclear to cytosolic compartments upon viral RNA infection in order to directly install m^6A upon viral RNAs. One limitation of this study then is that it does incorporate the effects of viral infection. As a result, we may exclude other endogenous, reshaped dsRNAs that dwell in the cytoplasm and may also bind to RIG-I. Overall, we uncover another role of m^6A methylation, in which m^6A modifies RNA structure to control the innate immune system.

Methods

Mammalian Cell Culture

Human cell lines were obtained from the American Type Culture Collection (ATCC) or from frozen cell vials and cultured under standard conditions. The cell lines HEK293T (human embryonic kidney) and HeLa (cervical carcinoma), as well as their derived stable cell lines, were cultured in DMEM 11965 or DMEM 11995 supplemented with 10% FBS, with or without 1% (100 U/mL) penicillin-streptomycin.

Plasmid Constructs

Commercial cDNA of DDX58 (NM_014314.4) (RIG-I) cloned into a pcDNA3.1 vector with a C-terminal Flag tag was purchased from GenScript.

Flag-HA tandem-tagged RIG-I was cloned first by PCR amplifying and cloning the cDNA coding sequence of the pcDNA3.1-DDX58-C-Flag vector into an empty modified pPB-CAG vector containing a Flag-HA tandem tag upstream of the restriction enzyme multiple cloning site. The primers of the PCR amplification contained restriction sites for *AgeI* and *XhoI* at the 5' and 3' ends of the coding sequence, respectively. (Forward primer: 5'-GCTAGCTAACCGGTATGACCACCGAGCAGCGA-3'; Reverse primer with stop codon: 5'-AGCTTAGCCTCGAGTTATTTGGACATTTCTGCTGGATCAAATGGT-3'; Reverse primer with Flag tag: 5'-AGCTGACTCTCGAGTCACTTATCGTCGTCATCCTTGTAATCTTTGG-3'). The vector and the PCR insert were digested with *AgeI* and *XhoI* following the manufacturer's instructions, and gel purified or cleaned up using the QIAquick PCR & Gel Cleanup Kit (Qiagen). Vector and insert were ligated with T4 NEB Ligase (NEB, M0202S) following manufacturer's instructions and incubating at 16ºC for at least 6 hours or overnight.

The ligation reaction was transformed into NEB 5-alpha Competent E. coli (High Efficiency) (C2987) cells and plated on LB agar plates with ampicillin. Colonies were Sanger sequenced to confirm successful cloning.

The pEF-BOS-Flag-RIG-I was provided by Jianrong Li (Ohio State University).

The pLKO-puro-tetON-shGFP plasmid was a gift from William Hahn (Addgene plasmid #110939). The shRNA sequence is: CAACAGCCACAACGTCTATAT.

The pLKO-puro-tetON-shMETTL3 plasmid was provided by Dr. Hui-Lung Sun, who cloned the shMETTL3 sequence into the Tet-pLKO-puro, a gift from Dmitri Wiederschain. For METTL3, the clone is TRCN0000289742 and the shRNA sequence is GCCAAGGAACAATCCATTGTT.

Immunofluorescence Staining

Cells were seeded on a Nunc LabTek II Chambered Coverglass (8-well; Thermo Fisher, 155409) at 60-70% confluency. Cells were incubated and treated and then prepared for immunofluorescence staining. Media was removed and cells were washed with 200 µL PBS twice. Cells were then fixed in 4% paraformaldehyde or formaldehyde in PBS for 15 minutes, permeabilized in 0.2% Triton X-100 for 10 minutes and blocked in 3% BSA/PBS for 1 hour. All these steps used a 100 µL volume and occurred at room temperature. Cells were then incubated with primary antibody (usually at a 1:400-1:1000 antibody dilution) at 4ºC overnight or at room temperature for 1 hour and were then incubated with secondary antibody (1:500-1:1000 dilution) at room temperature for 1 hour. Finally, cells were stained with 0.3 µM 4′,6-diamidino-2-phenylindole (DAPI) for 10 minutes at room temperature. All steps had at least two 200-µL PBS washes in between. Cells were then imaged with a Leica SP5 2-Photon Laser Scanning Confocal Microscope.

RIG-I-bound RNA Immunoprecipitation (RIP)

The methods for native RIP in this study followed a previous publication, with modifications (Chiang et al., 2018). HeLa cells were seeded (~50-70% confluency per 15-cm dish) and transfected with constructs coding for Flag-RIG-I or an empty Flag vector (10 or 20 μg plasmid per dish) with Lipofectamine 2000. Cells were later treated with 3p-hpRNA 5' triphosphate hairpin RNA (InvivoGen) 24 hours later. Cells were harvested after 16 hours by washing twice with PBS and then scraping cells into a 15-mL tube. Cells were centrifuged at 500 x g for 5 minutes at 4ºC, and PBS was removed. Cells were lysed in NP-40 Lysis Buffer (50 mM HEPES, pH 7.4, 150 mM KCl, 0.5% (v/v) NP-40, and 0.5 mM Dithiothreitol, supplemented with protease and phosphatase inhibitor). 1 mL NP-40 Lysis Buffer was added per 15-cm dish, and the samples were set on ice for 30 minutes at 4ºC with periodic mixing. Lysates were then cleared by centrifugation at 10k x g for 20 minutes at 4ºC. 5% and 1% of the lysates were saved for input RNA and western blot, respectively. To co-immunoprecipitate RNA-bound FLAG–RIG-I and FLAG-GFP, cleared lysates were mixed with 20 μL anti-FLAG-conjugated M2 magnetic beads that were washed two times with NP-40 Lysis Buffer. The beads and lysate were incubated for 4 hours at 4ºC. Beads were washed three times with NP-40 lysis buffer and two times with High-Salt Wash Buffer (50 mM HEPES, pH 7.5, 300 mM KCl, 0.5% (v/v) NP-40, 0.5 mM DTT, supplemented with protease and phosphatase inhibitor). 5% and 1% of the beads were saved for immunoprecipitated sample RNA and western blot, respectively.500 μL TRIzol was added to the beads and RNA was extracted following the manufacturer's protocol.

Double-stranded RNA Immunoprecipitation (J2 RIP)

The methods for J2 antibody-based dsRNA IP were based on a previous publication, with modifications (Dhri et al., 2019). Protein G Dynabeads were washed and resuspended in 1mL of NET-2 buffer (50 mM Tris-Cl, pH 7.4, 150 mM NaCl, 1 mM $MgCl_2$, 0.5% NP-40). Then, 5 µg of anti-dsRNA mAb (J2) was bound to 100 µl of beads for 1 h at room temperature on a thermal shaker. Conjugated beads were washed three times with 1 mL of NET-2 Buffer. 80–100% confluent HeLa cells from a 10-cm plate were washed with 10 ml of cold PBS. Cells were scraped and transferred to a falcon and spun at 500 x g at 4 °C for 5 minutes. The cell pellet from sample was lysed in 1 mL of NP-40 Lysis Buffer (50 mM Tris-Cl pH 7.4, 150 mM NaCl, 5 mM EDTA, 0.5% NP-40) and transferred to a 1.7 mL microcentrifuge and incubated on ice for 5 minutes. Following centrifugation at 17,000 x g at 4 °C for 5 min, the supernatant was carefully transferred to a new tube. Total RNA was harvested from 10% input lysate using Trizol reagent. For immunoprecipitation, lysate was diluted 1:4 in NET-2 buffer and supplemented with 10 units of RNase free Turbo DNase (Ambion) at 10 mM MgCl2 per 1 mL of mix. 100 µl of J2-Dynabeads was added to 1 ml of above lysate and rotated for 1-2 hours at 4 °C. Following magnetic separation, beads were washed twice with 1 mL of High-Salt Wash Buffer (50 mM Tris-Cl pH 7.4, 1 M NaCl, 1 mM EDTA, 1% NP-40, 0.5% DOC, 0.1% SDS). Beads were transferred to a new tube with NET-2 buffer and washed twice with the same buffer. J2-bound dsRNA was extracted with Trizol reagent according to the manufacturer's instructions.

Ribosomal RNA Depletion

In order to remove ribosomal RNA, two rounds of ribosomal RNA depletion were performed using the RiboMinus Eukaryote Kit v2 (Thermo Fisher), although at half or quarter scale relative

to the manufacturer's instructions. Briefly, 1-1.25 µg total RNA was mixed with pre-heated 2X Hybridization Buffer and 1 µL RiboMinus probe in a total volume of 25 µL, heated at 70ºC for 5 minutes, and then 37ºC for 20-30 minutes. RiboMinus beads were prepared by washing with nuclease-free water twice and re-suspending in 180 µL 1X Hybridization Buffer. One-third was aliquoted for the second round of RiboMinus, whereas two-thirds was aliquoted for the first round and re-suspended in 60 µL Hybridization Buffer; both aliquots of beads were maintained at 37ºC. To remove RNA, the sample mixture was transferred to beads, mixed, and incubated at 37ºC for 15 minutes. The supernatant was then separated from beads and saved, and then added to the second aliquot of beads. Samples were incubated at 37ºC for 15 minutes, and the supernatant was transferred to a new tube. RNA was then concentrated using ethanol precipitation. Specifically, RNA supernatant was mixed with 1 µL of GlycoBlue, 0.1 volumes of 3M sodium acetate, and 2.5 volumes of 100% ethanol, incubated at -80ºC for 30 minutes, centrifuged at 12k x g for 15 minutes at 40C, washed with 500 µL cold 70% ethanol centrifuged at 12k x g for 5 minutes at 4ºC twice, and dried and re-suspended in 10-30 µL nuclease-free water.

RT-qPCR, J2-RIP-qPCR, m^6A-RIP-qPCR

For quantitative PCR, total RNA was isolated using TRIzol, and concentrations were measure with a NanoDrop machine (Thermo Fisher). For total RNA that had not undergone DNase digestion, RNA was incubated with DNase I and purified with RNA Clean and Concentrator-5 (Zymo). 400-1000 ng of RNA was reversed transcribed into cDNA using PrimeScript RT Master Mix (Takara Bio), and then diluted 4- to 8-fold. qPCR was performed using the FastStart Essential DNA Green Master (Roche). 10 µL master mix was mixed with 2 µL of cDNA and 0.4

μL of 10 μM primer mix. GAPDH and HPRT1 (especially in m^6A-dependent assays) was used as an internal control for normalization. Relative gene expression was calculated using the delta-delta Ct ($2^{-\Delta\Delta Ct}$) method.

RNA-seq, RIP-seq Library Preparation and Data Analysis

RNA-seq libraries were prepared from RNA purified from input lysate from Flag-RIG-I RIP-seq or J2 RIP-seq. Flag-RIG-I and J2 RIP-seq libraries were prepared from immunoprecipitated RNA as described in the RIP methods. Libraries were prepared with the SMARTer Stranded Total RNA-Seq Kit v2 at half-scale according to manufacturer's instructions; included in this library preparation is a step that depletes cDNA originating from ribosomal RNA. Contrary to the manufacturer's protocol, library concentration was quantified by qPCR in order to determine an appropriate number of cycles for the final step of library amplification. Libraries were sequenced on a NovaSeq 6000 system (Illumina) with 50-base pair length, paired-end reads. Approximately 20-30 million reads were mapped for each sample.

Fastq files were run through FastQC. Due to the library preparation kit, the first 3 bases of the 3' end for each mate pair was trimmed using trim_galore. Using HISAT2 v2.1.0, reads were aligned to the mycoplasma genome to assess contamination and all non-mycoplasma-aligned reads were retained. The following parameters were used: hisat2 -x $INDEX -k 7 --un-gz $s.IN.noMyco.fastq.gz --summary-file $s.IN.myco_summary -p 24 -U $Data/$s.IN.fastq.gz > $s.myco.input.sam. The reads were subsequently mapped and aligned to the *Homo sapiens* genome assembly GRCh38 (hg38) with HISAT2 v2.1.0 [198] with parameter –k 1, taking splice sites into account. The following command was used for mapping to the reference genome: hisat2 -x $INDEX --known-splicesite-infile $SPLICE -k 1 --no-unal --summary-file

$s.IN.align_summary -p 4 -U $Data/$s.IN.noMyco.fastq.gz | samtools view -bS | samtools sort -o $Output/$s.input.bam.

Input RNA libraries from m^{6}A-sequencing served as RNA-seq samples to compare gene expression. DESeq2 [199] was applied for differential expression analysis, usually with a FDR < 0.05 cutoff. Subsequent analyses and figures were generated according to rnaseqGene, an RNA-seq workflow on BioConductor (http://master.bioconductor.org/packages/release/workflows/html/rnaseqGene.html).

To incorporate transposable or repeat elements as possible double-stranded or RIG-I-binding RNAs, the package TEtranscripts (Yin et al., 2015) was invoked to annotate reads to the UCSC RepeatMasker annotation database. Pre-generated GTF files were also downloaded from the TEtranscripts website (http://hammelllab.labsites.cshl.edu/software/#TEtranscripts). The TEcounts tool was used to generate read count tables that included both transposable and protein-coding RNAs. Subsequent differential expression analysis was performed with DESeq2.

In order to determined enriched RIP targets, count tables were generated and normalized using DESeq2. Enriched targets were then found by determining ratios of IP to Input.

To determine differentially enriched RIP targets between wild-type and *METTL3* knockdown/knockout samples, DESeq2 was used to test a ratio of ratios: (IP for KO / Input for KO) / (IP for WT / Input for WT). A likelihood ratio test was used upon running the DESeq command. The specific parameters are as follows:

```
dds <- DESeqDataSet(se, design= ~ assay + condition + assay:condition)
dds <- DESeq(dds, test="LRT", reduced= ~ assay + condition)
results(dds)
```

Data Deposition

The sequencing data generated in this study will have been deposited to the National Center for Biotechnology Information Gene Expression Omnibus database and are available under accession number GSEXXXXXX (TBD).

Chapter IV: The RNA Demethylase ALKBH5 Selectively Promotes Tumorigenesis and Cancer Stem Cell Self-Renewal in Acute Myeloid Leukemia

Note:

The following section (*Chapter IV*) is reproduced mostly verbatim, with the exception of figure numbering and reference labeling, from my co-first authored reference "RNA Demethylase ALKBH5 Selectively Promotes Tumorigenesis and Cancer Stem Cell Self-Renewal in Acute Myeloid Leukemia." This project was performed in collaboration with Chao Shen and many others from the Jianjun Chen lab and published in *Cell Stem Cell* on July 2, 2020.[2] I performed some mass spectrometry experiments, polysome profiling-related experiments, and library preparation and bioinformatic analysis for the RNA-seq, m^6A-seq, and RIP-seq data.

Authors:

Chao Shen*, Yue Sheng*, Allen C. Zhu*, Sean Robinson*, Xi Jiang*, Lei Dong*, Huiying Chen*, Rui Su, Zhe Yin, Wei Li, Xiaolan Deng, Yinhuai Chen, Yueh-Chiang Hu, Hengyou Weng, Huilin Huang, Emily Prince, Christopher R. Cogle, Miao Sun, Bin Zhang, Chun-Wei Chen, Guido Marcucci, Chuan He, Zhijian Qian, Jianjun Chen

[2] Shen, C., Sheng, Y., Zhu, A. C., Robinson, S., Jiang, X., Dong, L., Chen, H., Su, R., Yin, Z., Li, W., Deng, X., Chen, Y., Hu, Y. C., Weng, H., Huang, H., Prince, E., Cogle, C. R., Sun, M., Zhang, B., Chen, C. W., … Chen, J. (2020). RNA Demethylase ALKBH5 Selectively Promotes Tumorigenesis and Cancer Stem Cell Self-Renewal in Acute Myeloid Leukemia. *Cell Stem Cell*, 27(1), 64–80.e9. Used with permission from Elsevier.

*These authors contributed equally to this work.

Abstract

N^6-methyladenosine (m^{6}A), the most abundant internal modification in mRNA, has been implicated in tumorigenesis. As an m^{6}A demethylase, ALKBH5 has been shown to promote the development of breast cancer and brain tumors. However, in acute myeloid leukemia (AML), ALKBH5 was reported to be frequently deleted, implying a tumor-suppressor role. Here, we show that ALKBH5 deletion is rare in human AML; instead, ALKBH5 is aberrantly overexpressed in AML. Moreover, its increased expression correlates with poor prognosis in AML patients. We demonstrate that ALKBH5 is required for the development and maintenance of AML and self-renewal of leukemia stem/initiating cells (LSCs/LICs) but not essential for normal hematopoiesis. Mechanistically, ALKBH5 exerts tumor-promoting effects in AML by post-transcriptional regulation of its critical targets such as TACC3, a prognosis-associated oncogene in various cancers. Collectively, our findings reveal crucial functions of ALKBH5 in leukemogenesis and LSC/LIC self-renewal/maintenance and highlight the therapeutic potential of targeting the ALKBH5/m^{6}A axis.

Introduction

Acute myeloid leukemia (AML) is a fatal form of hematopoietic malignancy, characterized with the clonal expansion and differentiation block of myeloid progenitor cells [230, 231]. Leukemia stem/initiating cells (LSCs/LICs), characterized by their unlimited self-renewal/repopulating potential, are considered to be the root cause for the initiation and

progression of the disease, as well as for treatment failure and relapse of AML [231-233]. With currently available therapeutics, over 70% of AML patients cannot survive more than 5 years, [230]. Thus, there is still an unmet and urgent medical need to develop more effective novel therapeutic approaches to eliminate LSCs/LICs and cure AML.

FTO, the first identified m^6A demethylase [234], is overexpressed and plays a critical oncogenic role in AML pathogenesis and drug response by post-transcriptionally regulating expression of a set of important targets (e.g., *ASB2*, *RARA*, *MYC* and *CEBPA*) [123, 235], and is a druggable target in AML [236]. ALKBH5 was identified as the second RNA m^6A demethylase [70], which, similar to FTO, is also an Fe(II)/2OG-dependent dioxygenase [237]. Complete deletion of *Alkbh5* in mice led to impaired spermatogenesis and male infertility [70]. However, the function and underlying mechanism of ALKBH5 in leukemogenesis, LSC/LIC self-renewal and normal hematopoiesis have yet to be investigated.

A previous study [238] reported that *ALKBH5* is frequently deleted in AML patients, especially in TP53-mutant cases, based on the analysis of The Cancer Genome Atlas (TCGA) AML cohort dataset [239], which implies that ALKBH5 may play a tumor-suppressor role in AML [240]. Surprisingly, however, here we show that *ALKBH5* is actually overexpressed in human AML and that its increased expression is associated with poor prognosis in AML. We reanalyzed the TCGA AML dataset [239], along with several other independent AML cohort datasets, and found that *ALKBH5* deletion is very rare in AML, and that its expression level is not correlated with TP53 mutations in cancer. We next conducted a series of functional and mechanistic studies, which revealed that ALKBH5 plays an important role in promoting leukemogenesis and LSC/LIC self-renewal/maintenance as an m^6A demethylase by post-transcriptional regulation of its critical

target transcripts (e.g., *TACC3*), but exhibits little effect on normal hematopoiesis. These data highlight that ALKBH5 is a promising therapeutic target in AML.

Results

Identification of Potential Targets of ALKBH5 in AML

To understand the molecular mechanisms underlying the role of ALKBH5 in AML, we conducted transcriptome-wide RNA-sequencing (RNA-seq), RNA Immunoprecipitation-sequencing (RIP-seq) and m^6A-sequencing (m^6A-seq) in human AML cells. RNA-seq revealed that 623 and 1,237 genes were significantly up- and down-regulated (fold change>1.5), respectively, upon *ALKBH5* knockdown in both MOLM13 and NOMO1 cells (Figures 4-1A-D).

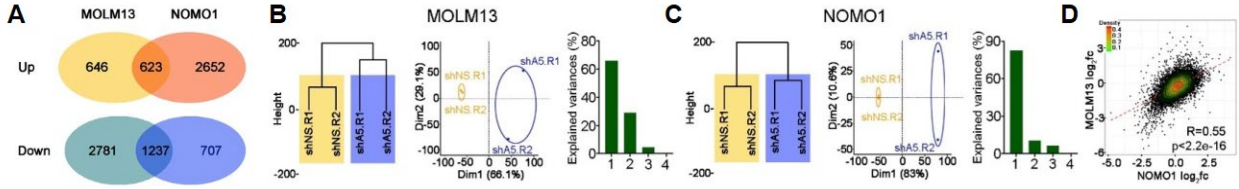

Figure 4-1. Transcriptome-wide identification of ALKBH5 potential targets in AML cells.

RNA-seq analysis of gene expression profiles in *ALKBH5* knockdown AML cells and control AML cells.
(A) Venn diagram shows numbers of genes with significant changes in expression (RPKM>1, fold change>1.5) upon *ALKBH5* knockdown.
(B-C) Hierarchical clustering and principal component analysis (PCA) of control (shNS.R1 and shNS.R2) and *ALKBH5* knockdown (shA5.R1 and shA5.R2) MOLM13 (B) and NOMO1 (C) AML cells based on the RNA-seq data.
(D) Scatterplots of expression fold changes of genes upon *ALKBH5* knockdown in MOLM13 and NOMO1 cells based on the RNA-seq data.

Using the Molecular Signature Database (MSigDB) of Gene Set Enrichment Analysis (GSEA) [241], we identified the top 10 pathways in which those up-regulated and down-regulated genes were enriched (Figure 4-2A). Notably, *ALKBH5* knockdown activated apoptosis

and p53 pathways, while causing significant suppression of E2F targets, G2M checkpoints, MYC targets and mitotic spindle pathways (Figures 4-2B-D), which was consistent with our findings that *ALKBH5* knockdown increased apoptosis and inhibited cell growth/proliferation in AML cells.

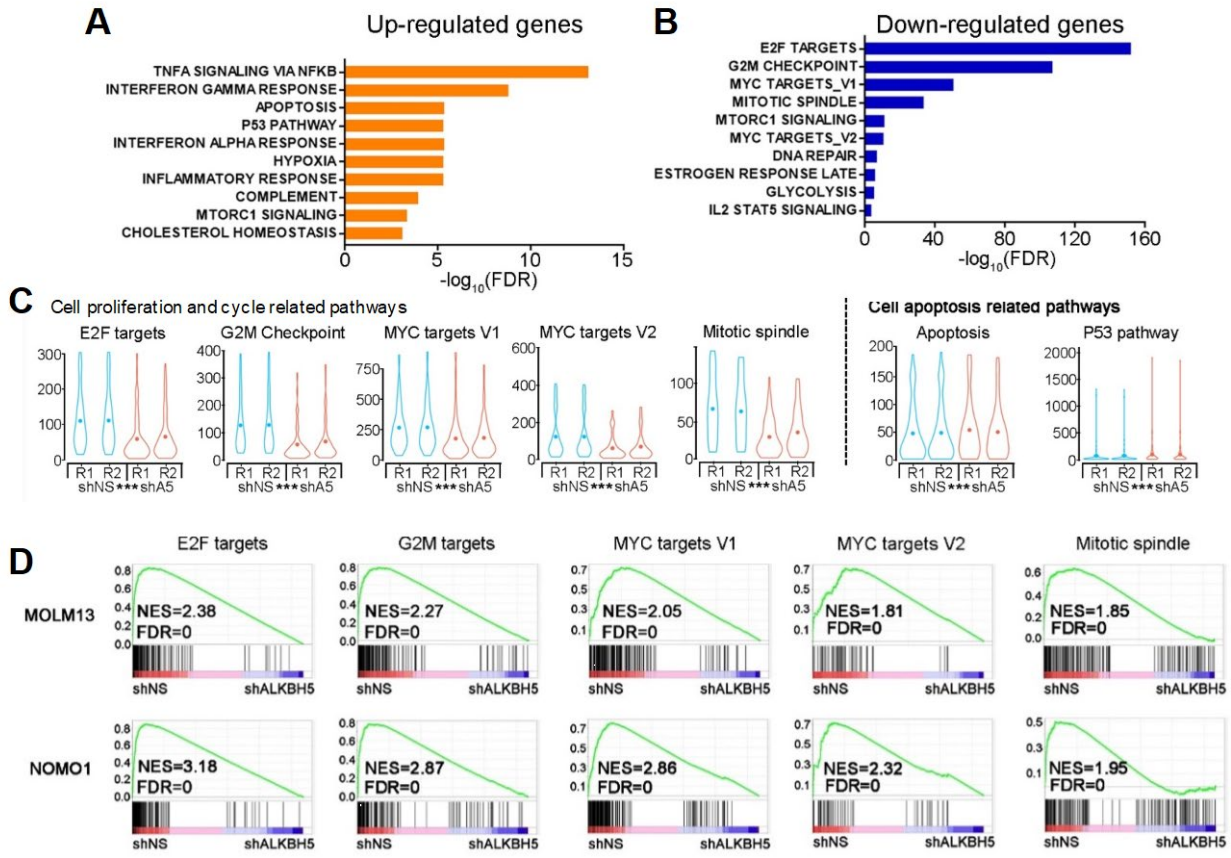

Figure 4-2. Gene set enrichment analysis of ALKBH5 targets in AML cells.

(A) GSEA of up- and down-regulated genes. (B) Violin plots showing the relative abundance of genes involved in the indicated pathways in *ALKBH5* knockdown or control NOMO1 cells. (C) Gene set enrichment analysis (GSEA) in MOLM13 and NOMO1 cells. Representative gene sets (pathways) that are significantly enriched (FDR<0.001) with genes downregulated in AML cells upon *ALKBH5* knockdown were shown. NES, normalized enrichment score; FDR, false discovery rate.

To identify direct targets and pathways regulated by ALKBH5, we also performed RIP-seq and m^{6}A-seq in *ALKBH5* overexpressing and knockdown NOMO1 cells, respectively. In

RIP-seq (Figures 4-3A, B), we found that the vast majority of ALKBH5 binding sites are located in protein coding transcripts (Figure 4-3C). The genes whose mRNA transcripts were strongly bound by ALKBH5 are enriched in cell cycle- and proliferation-related pathways (Figure 4-3D).

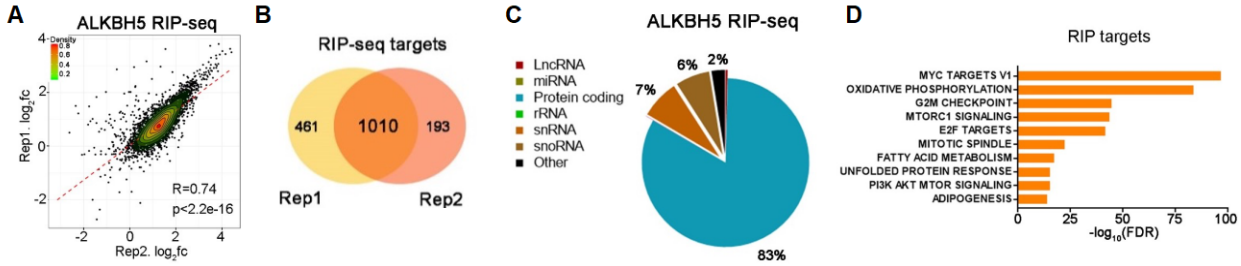

Figure 4-3. RIP-seq analysis of *ALKBH5* overexpressing NOMO1 cells.

(A) Scatter plots of ALKBH5 RIP-seq replicates showing the correlation of enriched genes. (B) Venn diagram of ALKBH5-RIP targets in two RIP-seq replicates (target gene: RPKM>1, immunoprecipitation/input>2).
(C) Pie charts showing the distribution of RIP-seq reads in RNA classes. (D) GSEA of significantly enriched genes in RIP samples (RPKM>1, immunoprecipitation/input>2).

Our m^{6}A-seq data showed that the vast majority of m^{6}A peaks are distributed in the protein-coding region (CDS) and 3' untranslated region (3'UTR) of mRNA transcripts in AML cells (Figures 4-4A, B).

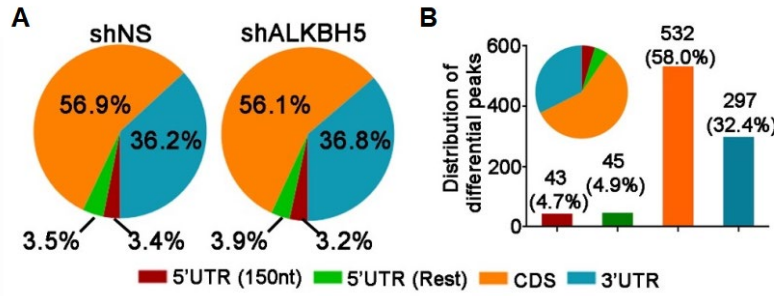

Figure 4-4. m^{6}A-seq analysis of *ALKBH5* knockdown NOMO1 cells.

(A) The distribution of total m^{6}A peaks in the indicated regions of mRNA transcripts in the control and *ALKBH5*-knockdown cells. (B) The distribution of differential m^{6}A peaks (i.e., those with significant changes upon *ALKBH5* manipulation). 5'UTR (150 nt) represents the first 150 nt of 5' end of 5'UTR, while 5'UTR (Rest) represents the remaining regions of 5'UTR.

The major signaling pathways enriched with the genes whose transcripts are associated with significantly increased m^{6}A methylation peaks (Hyper) upon *ALKBH5* knockdown were shown in Figure 4-5A. Notably, many pathways are commonly detected by RNA-seq, RIP-seq and m^{6}A-seq (Figures 4-5B-D), suggesting that they are the main pathways that are enriched with potential direct targets of ALKBH5 that would be most significantly affected by ALKBH5 expression changes.

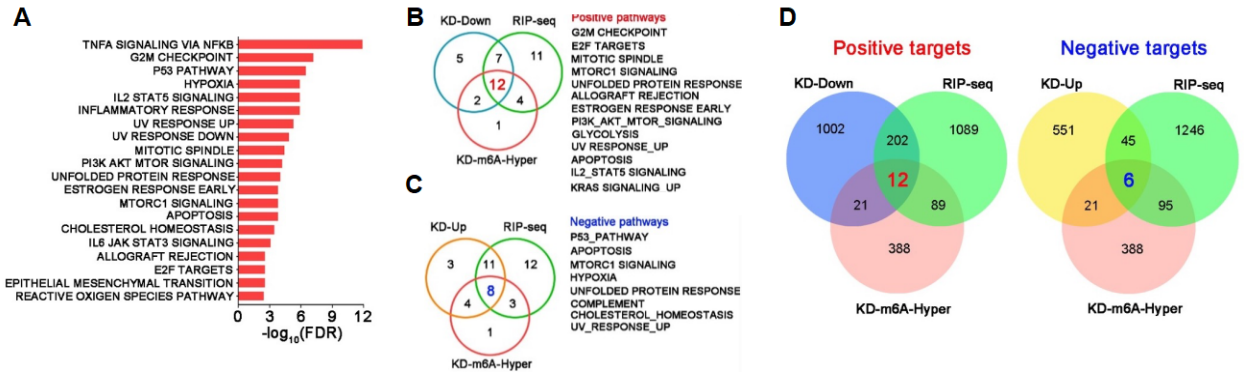

Figure 4-5. Integrative analysis of RNA-seq, ALKBH5 RIP-seq, and m^{6}A-seq data.

(A) GSEA of the genes with significantly increased m^{6}A abundance in *ALKBH5* knockdown cells ($p<0.05$).
(B-C) Venn diagram of pathways that were positively (B) or negatively (C) regulated by ALKBH5 in human AML cells. KD-Down: down-regulated pathways in *ALKBH5* knockdown RNA-seq samples. RIP-seq, pathways significantly enriched in Flag-IP samples. KD-m^{6}A-Hyper: pathways with higher m^{6}A abundance in *ALKBH5* knockdown m^{6}A-seq samples. Only pathways with FDR<0.01 are used for the overlapping.
(D) Integrative analysis to identify transcriptome-wide potential targets of ALKBH5 in AML. Left: potential positive targets of ALKBH5. Right: potential negative targets of ALKBH5. KD-Down and KD-Up: genes with significantly decreased and increased expression, respectively, upon *ALKBH5* knockdown in both NOMO1 and MOLM13 cells as detected by RNA-seq (RPKM>1, fold change >1.5). RIP-seq: genes with significant enrichment in RIP samples (RPKM>1, immunoprecipitation/input>2). KD-m^{6}A-Hyper: genes with significantly higher m^{6}A abundance in *ALKBH5* knockdown cells ($p<0.05$).

Through integrative analysis of the RNA-seq, RIP-seq and m^{6}A-seq data, we identified 12 and 6 genes being significantly positively and negatively regulated by ALKBH5, respectively, and they are also strongly bound by ALKBH5 and are associated with increased m^{6}A abundance in

their transcripts upon *ALKBH5* knockdown (Figure 4-5C and Table S1). As they were detected by all the three methods, these 18 genes are highly confident potential targets of ALKBH5 in AML. Indeed, our ALKBH5-RIP-qPCR, gene-specific m^{6}A-RIP-qPCR, and qPCR results confirmed that most of these transcripts were strongly bound by ALKBH5 and were associated with significantly increased m^{6}A abundance and also associated with significant and expected expression level changes in AML cells upon *ALKBH5* knockdown (Figures 4-6A-C).

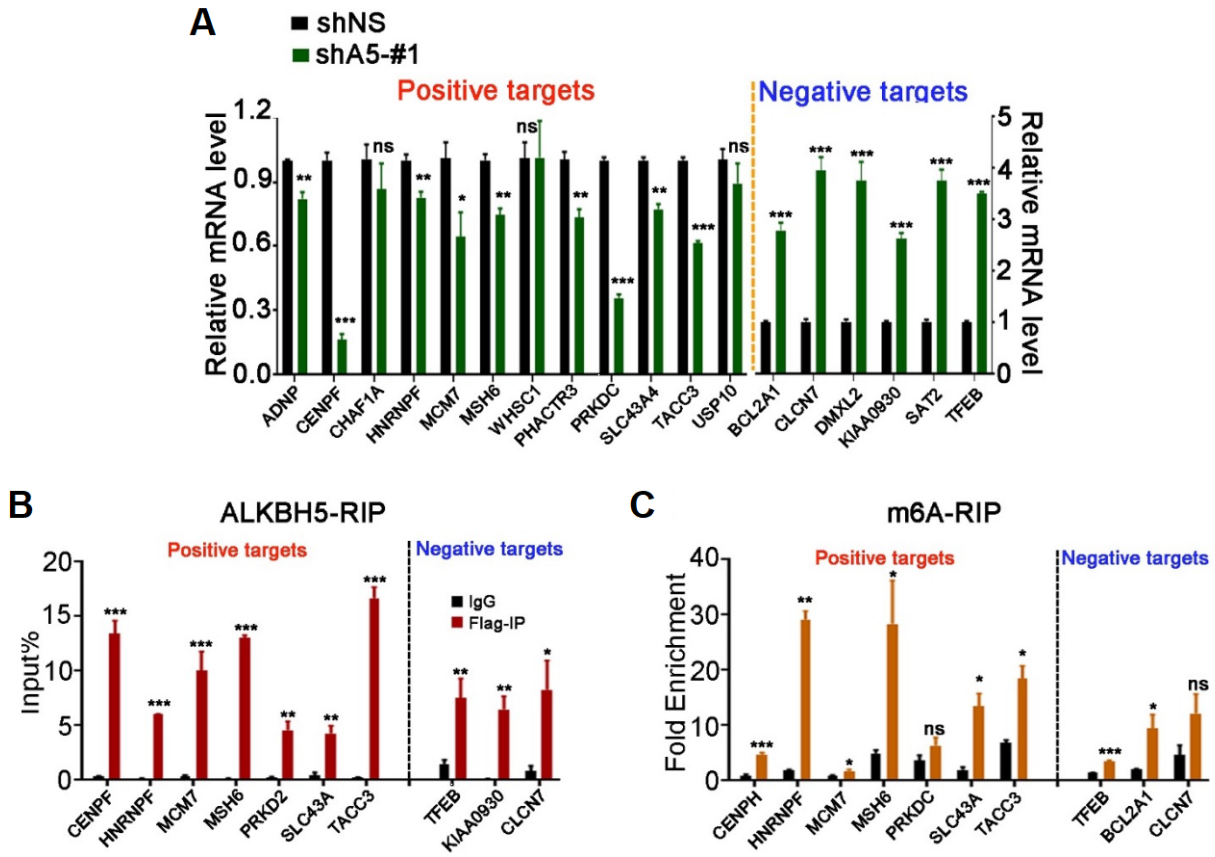

Figure 4-6. Validation of ALKBH5 RIP targets.

(A) Expression change validation of potential positive and negative targets of ALKBH5 by qPCR.
(B) ALKBH5-RIP qPCR validation of ALKBH5 binding of representative positive and negative targets.
(C) Gene-specific m^{6}A-RIP qPCR validation of m^{6}A level changes of representative positive targets and negative targets.

As our previous studies showed that FTO, another m^6A eraser, also plays an important oncogenic role in AML [123, 235], it would be interesting to compare the targets and pathways affected by the two m^6A erasers in AML. By comparing the RNA-seq data, we found *ALKBH5* knockdown (A5-KD) caused more genes to be down-regulated (Down vs. Up: 1,237 vs. 623) while *FTO* knockdown (FTO-KD) led to more genes to be up-regulated (Down vs. Up: 888 vs. 2,279). Among those down-regulated genes, 119 genes were shared by ALKBH5 and FTO which account for 9.6% of A5-KD-down genes and 13.4% of FTO-KD-Down genes. Among the up-regulated genes, 251 genes were shared, which accounts for 40.2% of A5-KD-up genes and 11% of FTO-KD-up genes (Figure 4-7A, top panel). Although FTO and ALKBH5 shared a relatively small fraction of potential targets, the pathways affected by the two m^6A erasers substantially overlapped (Figure 4-7A, bottom panel), suggesting that knockdown of either m^6A eraser affects multiple similar biological processes/pathways in AML. Similar findings were also observed in analysis of the m^6A-seq data of the two m^6A erasers (Figure 4-7B). Notably, among the 18 highly confident potential targets of ALKBH5 (Table S1), only *MCM7* and *TFEB* are also potential targets of FTO based on the above data analysis. Overall, it appears that ALKBH5 and FTO target more distinct transcripts than shared ones, although they target many shared pathways.

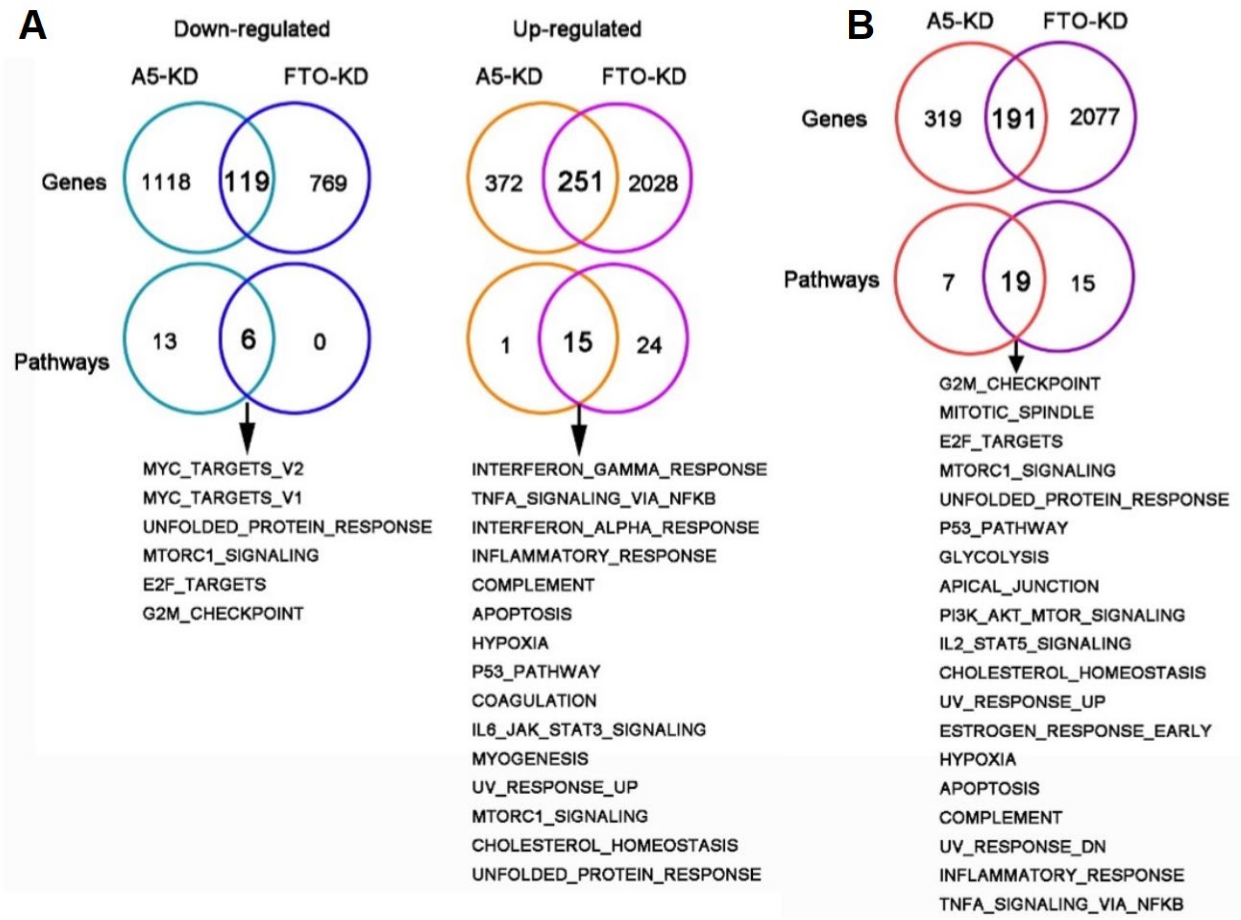

Figure 4-7. Pathway analysis of up- and down-regulated genes.

(A) Comparison of down- or up-regulated genes (RPKM>1, fold change>1.5) and pathways (FDR<0.01) caused by *FTO* knockdown (based on the RNA-seq data from [236]) with those caused by *ALKBH5* knockdown (based on the RNA-seq data herein).
(B) Comparison of m^6A hypermethylated genes ($p<0.05$) and pathways (FDR<0.01) caused by *FTO* knockdown (based on the m^6A-seq data from [123]) with those caused by *ALKBH5* knockdown (based on the m^6A-seq data herein).

TACC3 Is a Direct and Functionally Important Target of ALKBH5 in AML

Since ALKBH5 expression has an adverse prognostic impact in AML patients (Figure 4-1C), we checked the prognostic impacts of the 18 highly confident potential targets of ALKBH5 in AML patients, and found that three genes showed significant prognostic impacts in AML patients (see Table S1). However, only *TACC3* displayed an expected adverse prognostic impact in the TCGA AML cohort, which is consistent with the positive regulation of ALKBH5 on its

expression (Figure 4-8A and Table S1). *TACC3* exhibited a significantly ($p<0.05$) positive correlation in expression with *ALKBH5* across primary AML samples in the TCGA AML dataset (Figure 4-8B). In fact, among all the candidate targets tested, *TACC3* transcripts are associated with the greatest enrichment of ALKBH5 (Figure 4-6B). Consistent with RNA-seq and m^{6}A-seq data (Figure 4-8C), our qPCR validations confirmed that *TACC3* transcripts are associated with significantly decreased expression level and increased m^{6}A abundance upon *ALKBH5* knockdown (Figures 4-6A, B). Moreover, TACC3 has been reported to be overexpressed in various types of cancers (e.g., breast cancer, brain tumor, prostate cancer, liver cancer, gastric cancer, lung cancer, pancreatic cancer, myeloma, lymphoma, cholangiocarcinoma, and osteosarcoma); play a critical role in regulation of cell cycle and apoptosis; promote tumor initiation, progression and metastasis; facilitate/enhance CSC maintenance/self-renewal; and exhibit an adverse prognostic impact on patients carrying breast cancer, brain tumor, prostate cancer, liver cancer, gastric cancer, lung cancer, pancreatic cancer, or cholangiocarcinoma [242-253]. Such functional characteristics of TACC3 are largely similar to those of ALKBH5 (see Refs. [126, 254-258] and data shown herein). Therefore, we decided to focus on TACC3 for further studies.

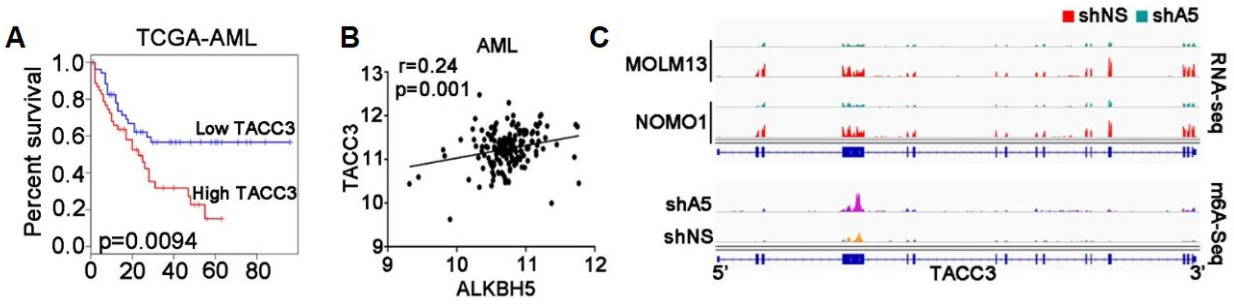

Figure 4-8. ALKBH5 regulates *TACC3* m^{6}A methylation.

(A) Kaplan-Meier survival analysis of *TACC3* in the TCGA AML dataset. The p value was detected by the log-rank test.
(B) The correlation of *TACC3* with *ALKBH5* in expression across human AML samples in the TCGA-AML dataset (n=177). Pearson correlation analysis was conducted. r, correlation coefficient.

Figure 4-8, continued. ALKBH5 regulates *TACC3* m^{6}A methylation.
(C) The RNA (top) and m^{6}A (bottom) abundance in *TACC3* mRNA transcripts in *ALKBH5* knockdown and control AML cells as detected by RNA-seq and m^{6}A-seq.

We first confirmed that both constitutive and inducible *ALKBH5* knockdown caused significant decrease in the TACC3 protein level in human AML cell lines and primary AML cells (Figures 4-9). Conversely, forced expression of wild-type ALKBH5 (A5-WT) but not mutant ALKBH5 (A5-Mut) increased TACC3 expression at both the mRNA and protein levels (Figures 4-10A, B). Consistently, *Alkbh5* knockout or knockdown also caused a significant decrease in the *Tacc3* mRNA level in primary mouse BM cells (Figure 4-10C) and mouse MA9 AML cells (Figure 4-10D). Furthermore, through analyzing the RNA-seq data of AML cells with or without *FTO* knockdown [236] and our qPCR data, we demonstrated that *TACC3* expression level is not significantly suppressed by *FTO* knockdown in AML cells (Figure 4-10E). Thus, our data indicate that *TACC3* is a specific target of ALKBH5 in AML.

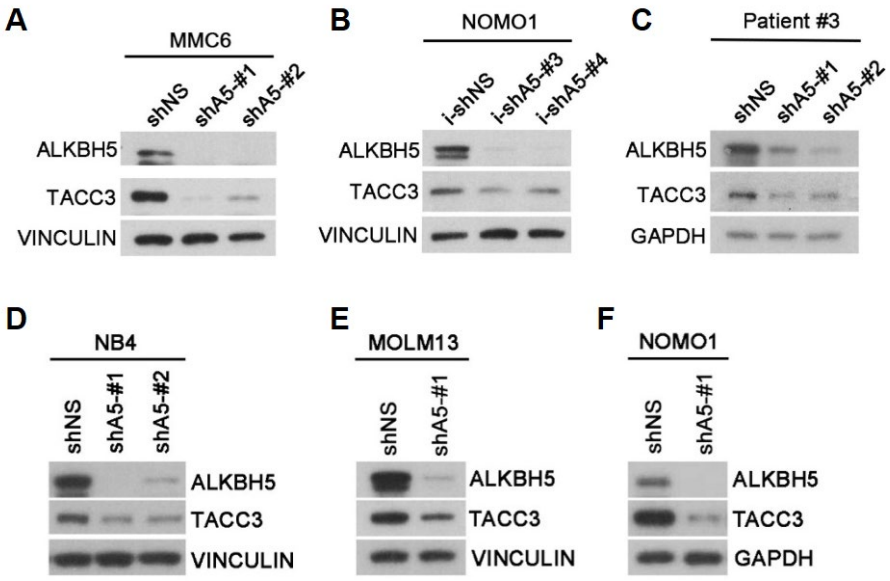

Figure 4-9. ALKBH5 regulates *TACC3* expression (continued).

(A-C) Western blots of ALKBH5 and TACC3 in *ALKBH5* stable knockdown MMC6 cells (A), *ALKBH5* inducible knockdown NOMO1 cells (Dox induction for 4 days) (B) and *ALKBH5* stable knockdown primary AML cells (C). VINCULIN or GAPDH was used as a loading control.

Figure 4-9, continued. ALKBH5 regulates *TACC3* expression (continued).
(D-F) Western blots of ALKBH5 and TACC3 in NB4 (D), MOLM13 (E) and NOMO1 (F) cells transduced with shNS or *ALKBH5* shRNAs. VINCULIN or GAPDH was used as a loading control.

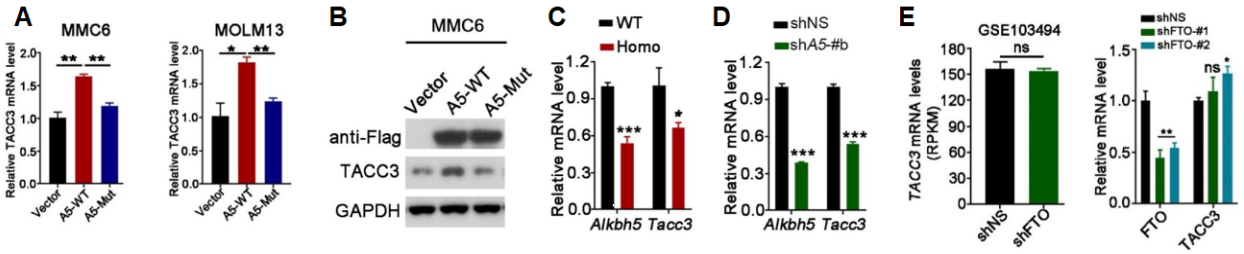

Figure 4-10. ALKBH5 regulates *TACC3* expression via mRNA stability.

(A) qPCR detection of *TACC3* expression changes in ALKBH5 wild-type (A5-WT)- or ALKBH5-mutant (A5-Mut)-overexpressing AML cells, relative to their controls.
(B) Western blots of ALKBH5 and TACC3 in MMC6 cells transduced with lentiviruses expressing empty vector (Vector) or wild-type ALKBH5 protein (A5-WT) or m^{6}A demethylase-inactive mutant (A5-Mut). GAPDH was used as a loading control.
(C-D) qPCR detection of *Tacc3* expression in *Alkbh5* wild-type (WT) or homozygous knockout (Homo) mouse BM cells (C) and in primary mouse MA9 AML cells transduced with lentiviruses expressing scrambled shRNA (shNS) or *Alkbh5* shRNA (shA5-#b) (D).
(E) Effect of *FTO* knockdown on *TACC3* RNA level in AML cells. (Left panel) *TACC3* mRNA level in the control (shNS) or *FTO* knockdown (shFTO) NB4 cells based on the RNA-seq dataset (GSE103494). (Right panel) qPCR detection of *FTO* and *TACC3* mRNA levels in MMC6 cells transduced with shNS or FTO shRNAs (shFTO-#1 and shFTO-#2).

The RNA m^{6}A modification has been reported to affect mRNA stability and translation [79, 88, 240, 259]. To investigate whether ALKBH5, as an m^{6}A demethylase, affects its targets mRNA stability, we treated *ALKBH5* knockdown or control AML cells with transcription inhibitor actinomycin D (Act D) and then harvested the cells for mRNA stability profiling. Strikingly, we found that *ALKBH5* knockdown caused globally reduced shorter half-lives of mRNA transcripts in AML cells (Figures 4-11A, B), with the trend being even more evident among transcripts of the potential targets of ALKBH5 (i.e., those detected by RIP-seq) (Figure 4-11C). Notably, around 600 hundred transcripts (including *TACC3*) showed a significantly decreased half-life, whereas only a few transcripts had increased half-lives (Figure 4-11B). GSEA showed that pathways

related with cell cycle and cell growth/proliferation were also significantly enriched with these genes (Figure 4-11D).

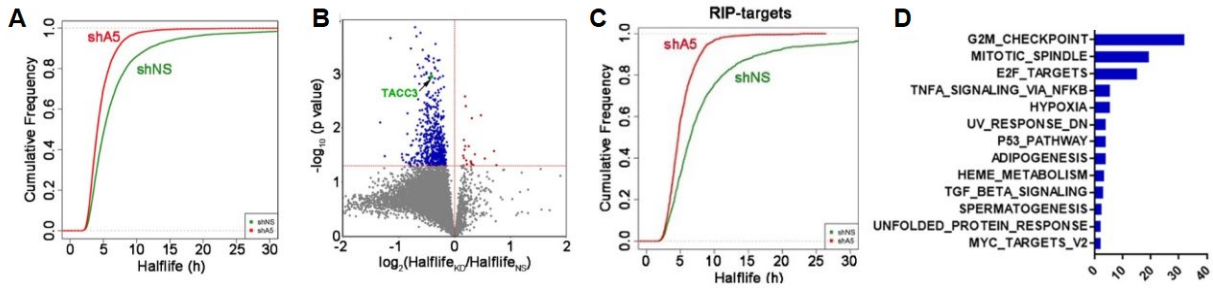

Figure 4-11. mRNA stability profiling upon ALKBH5 knockdown.

(A-B, D) mRNA stability profiling. (A) Cumulative distribution of global transcript stability changes in shNS or shA5-#1 transduced NOMO1 cells. (B) Distribution of genes with significant half-life change in *ALKBH5* knockdown cells compared to control cells.
(C) Cumulative distribution of RNA transcript stability changes of ALKBH5 RIP targets between shNS- and shA5-#1-transduced NOMO1 cells.
(D) Pathway analysis by GSEA showing the major pathways in which the genes with significantly shortened half-lives upon *ALKBH5* knockdown are enriched.

To validate these results, we detected the half-life changes of *TACC3* mRNA transcripts in AML cells upon *ALKBH5* knockdown or overexpression. As expected, knockdown of *ALKBH5* led to a significant decrease in the half-life of *TACC3* transcripts in both MOLM13 cells (2.35 to 1.56 h) and NOMO1 cells (3.40 to 1.55 h) (Figures 4-12A, B), while overexpression of the wild-type, but not mutant, ALKBH5 significantly increased the half-life of *TACC3* transcripts in NOMO1 cells (Figure 4-12C). To investigate whether ALKBH5 affects the translation of its targets, we performed polysome profiling and showed that *ALKBH5* knockdown caused a slight drop in transcript levels in polysome fractions (Figure 4-12D), which may be due to the overall decrease of mRNA level as we observed in the RNA-seq and mRNA stability profiling results (Figures 4-1 and 4-11A, B). Moreover, we did not observe a significant difference in *TACC3* mRNA level in the translating pool between the control and *ALKBH5* knockdown AML cells

(Figure 4-12E). Thus, our data suggest that ALKBH5 regulates its targets' expression level more likely by affecting mRNA stability rather than translation.

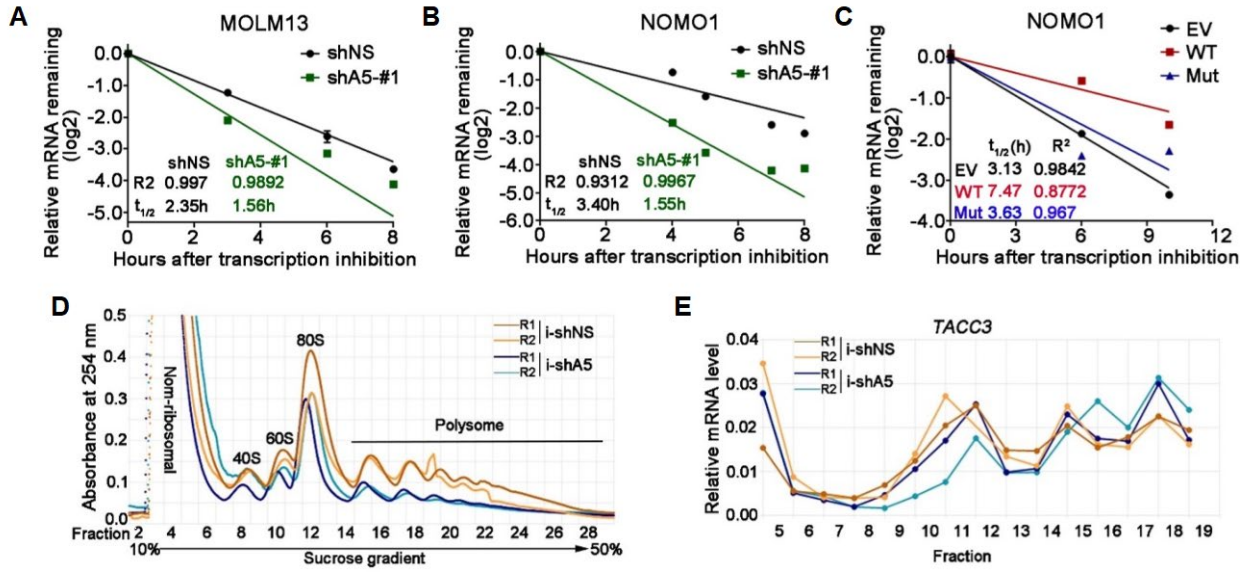

Figure 4-12. Half-life analysis and polysome profiling upon ALKBH5 knockdown.

(A-C) The mRNA half-life ($t_{1/2}$) of *TACC3* in MOLM13 cells (A) and NOMO1 cells (B) transduced with shNS or *ALKBH5* shRNA (shA5-#1), and in NOMO1 cells transduced with empty vector (EV) or wild-type *ALKBH5* (A5-WT) or *ALKBH5* mutant (A5-Mut) (C).
(D-E) Polysome profiling assays. (D) Absorbance of different fractions of NOMO1 cell lysates. (E) Total RNAs in different fractions of ribosomes were extracted and subjected to qPCR analysis, *TACC3* mRNA level was normalized to *GAPDH* and input.

TACC3 has been reported previously to regulate MYC and P21 levels in normal or cancer cells [247, 260-262] (Figure 4-13A). Consistently, we found that the *ALKBH5* knockdown not only led to TACC3 suppression but also concordant changes in MYC (decrease) and P21 (increase) levels in AML cells (Figures 4-13B-D). These data could indicate the ALKBH5/m^{6}A/TACC3 axis also regulates P21 and MYC pathways in AML cells.

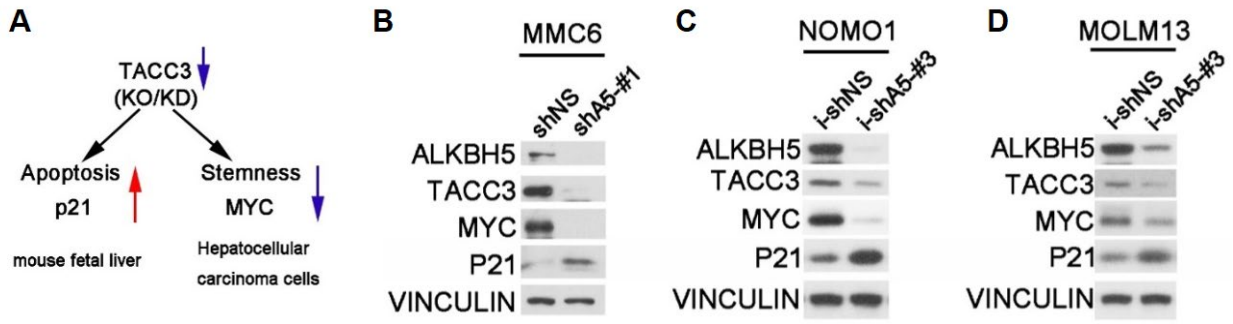

Figure 4-13. Summary of how ALKBH5 regulating *TACC3* expression affects subsequent downstream pathways.

(A) Summary of previous reports about the effects of TACC3 on expression of p21 and MYC. *Tacc3* knockout caused apoptosis in mouse fetal liver with increased p21 expression [260-262]. *TACC3* knockdown suppressed cell proliferation and stem-like phenotype of hepatocellular carcinoma cells *in vitro* with decreased MYC expression [247].
(B-D) Western blots of ALKBH5, TACC3, MYC and P21 in AML cells transduced with shNS or shALKBH5 (shA5-#1) (B) or with inducible shNS (i-shNS) or shALKBH5 (i-shA5-#3) (C and D). VINCULIN was used as a loading control.

Discussion

Through transcriptome-wide RNA-seq, RIP-seq and m^{6}A-seq, we identified a set of potential target transcripts of ALKBH5, which could be directly bound by ALKBH5 and significantly responded to *ALKBH5* knockdown in mRNA levels and m^{6}A abundance in AML cells. We also identified pathways which could be positively or negatively regulated by ALKBH5. Interestingly, among those pathways, cell cycle- and cell growth/proliferation-related pathways such as E2F targets, G2/M checkpoints and apoptosis pathways are commonly detected by different sequencing analyses, which likely contribute to the phenomenon that *ALKBH5* depletion signficantly inhibits AML cell growth/proliferation and promotes apoptosis. By comparing the sequencing data of ALKBH5 and FTO, we found that ALKBH5 and FTO have more distinct than shared targets. Next, we identified *TACC3* as a direct target of ALKBH5 in AML cells. We showed that ALKBH5 positively regulates the mRNA stability but not translation efficiency of *TACC3*

transcripts, which leads to increased *TACC3* expression through an m^6A-dependent mechanism. In general, *ALKBH5* knockdown significantly shortened the half-lives of the vast majority of its potential targets. Importantly, similar to ALKBH5, TACC3 has also been reported to be aberrantly overexpressed in various cancer types and play a critical oncogenic role in promoting tumorigenesis and CSC self-renewal/mainteance; moreover, its increased expression levels also indicate poor prognosis in patients with various types of cancers [242-253].

Our functional studies indicate that *TACC3* knockdown could mimic the effects of *ALKBH5* knockdown on cell growth/proliferation, apoptosis, colony forming/replating ability and LSC/LIC frequency in human AML cells or primary mouse MA9 cells. Moreover, its forced expression could at least partially reverse the effect of *ALKBH5* knockdown on AML cell growth/proliferation. These results suggest that *TACC3* is a functionally important target of ALKBH5. As critical downstream targets of TACC3, MYC and P21 levels can also be indirectly regulated by ALKBH5 in AML. Through this axis, increased expression of ALKBH5 and TACC3 in cancer patients promoted LSC/LIC self-renewal and confers drug resistance and/or relapse, leading to poor prognosis (Figure 4-14). Of course, besides *TACC3*, some other potential targets of ALKBH5 identified herein might also be important downstream targets of ALKBH5 and may partially mediate the overall function/effects of ALBKH5 in AML (and other cancer types), which warrants further systematic investigation.

In conclusion, our studies demonstrate that ALKBH5 plays critical roles in leukemic cell transformation, AML initiation/development and maintenance, and LSC/LIC self-renewal through post-transcriptional regulation of critical targets (e.g., *TACC3*) via m^6A-dependent mechanism(s), but minimally affects normal hematopoiesis (Figure 4-14). Mechnistially, we found ALKBH5 knockdown could globally shorten mRNA stability of its potential targets in AML cells. Our work

also revealed a previously unrecognized signaling axis involving ALKBH5/m^{6}A/TACC3 /MYC-p21 in AML pathogenesis and LSC/LIC biology, highlighting the functional importance of ALKBH5-mediated modulation of mRNA m^{6}A methylation in leukemogenesis and LSC/LIC self-renewal. Notably, although several other m^{6}A regulatory genes (e.g., *METTL3*, *METTL14*, *WTAP*, *FTO*, and *YTHDF2*) have also been reported to play oncogenic roles in AML, *ALKBH5* is the only gene whose increased expression level is signficantly associated with a poor prognosis in AML patients. Given the essential roles of ALKBH5 in AML pathogenesis and LSC/LIC maintenance, with little effect on normal hematopoiesis, targeting ALKBH5 signaling represents an effective and novel therapeutic strategy for the treatment of AML patients (especially those who are resistant to currently available therapeutics) by eliminating LSCs/LICs and overcoming drug resistance, while sparing normal hematopoietic system. In particular, given the broad adverse prognostic imapcts of high ALKBH5 and TACC3 expression levels in patients with various types of cancers, targeting ALKBH5 and/or TACC3 by effective small-molecule compound inhibitors or agents that specifically degrade their proteins (e.g., proteolysis-targeting chimeras (PROTACs) [263, 264]), alone or in combination with other therapeutic agents, holds potent therapeutic potential in treating a wide variety of cancers in the clinic in the near future.

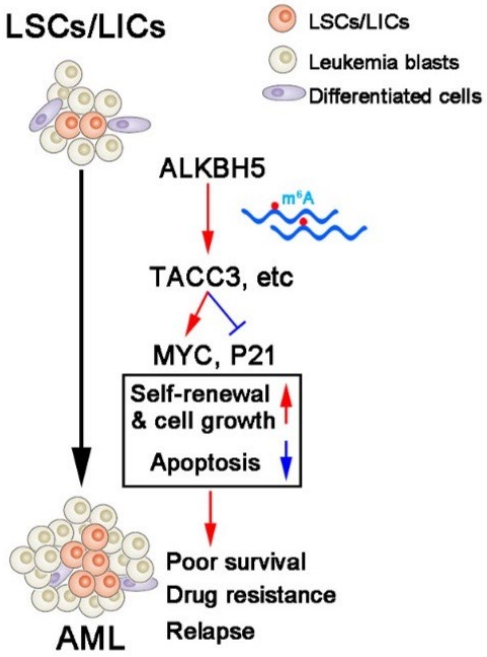

Figure 4-14. Proposed model demonstrating the role and underlying mechanism(s) of ALKBH5 in AML pathogenesis and LSC/LIC self-renewal.

Note: The following results are from a co-first authored collaboration with Fang Yu, although this manuscript has yet to be published.

RBM33 acts as a new m^{6}A reader essential for ALKBH5-mediated m^{6}A demethylation

Because RBM33 strongly interacts with ALKBH5, we then wondered whether RBM33 was also involved in m^{6}A demethylation. Overexpression of strep-tagged ALKBH5 or RBM33 (Figure 4-15A) resulted in substantially increased demethylation of m^{6}A (Figure 4-15B). Concordantly, stable knockdown of RBM33 led to globally increased mRNA m^{6}A methylation in both HEK (Figure 4-15C) and HeLa cells (Figure 4-16), which was demonstrated by both dot blot and mass spectrometry quantification. Since RBM33 interacts with ALKBH5 and affects m^{6}A levels, we next asked to what extent the effect of RBM33 on m^{6}A levels depends on ALKBH5. After generating a CRISPR knockout of ALKBH5 (Figure 4-15D), we overexpressed strep-tagged RBM33 (Figure 4-15E) and found negligible change in m^{6}A methylation, according to dot blot (Figure 4-15F). This suggests that RBM33 mediates m^{6}A demethylation through interaction with ALKBH5. This then raised the question of whether activity of ALKBH5 occurs in an RBM33-dependent manner. To test this, we overexpressed strep-tagged ALKBH5 with or without stable knockdown of RBM33 (Figure 4-15G). Intriguingly, a substantial decrease in m^{6}A occurred only in cells without RBM33 knockdown (Figure 4-15H). Overall, we found that ALKBH5 and RBM33 form a complex to mediate m^{6}A demethylation.

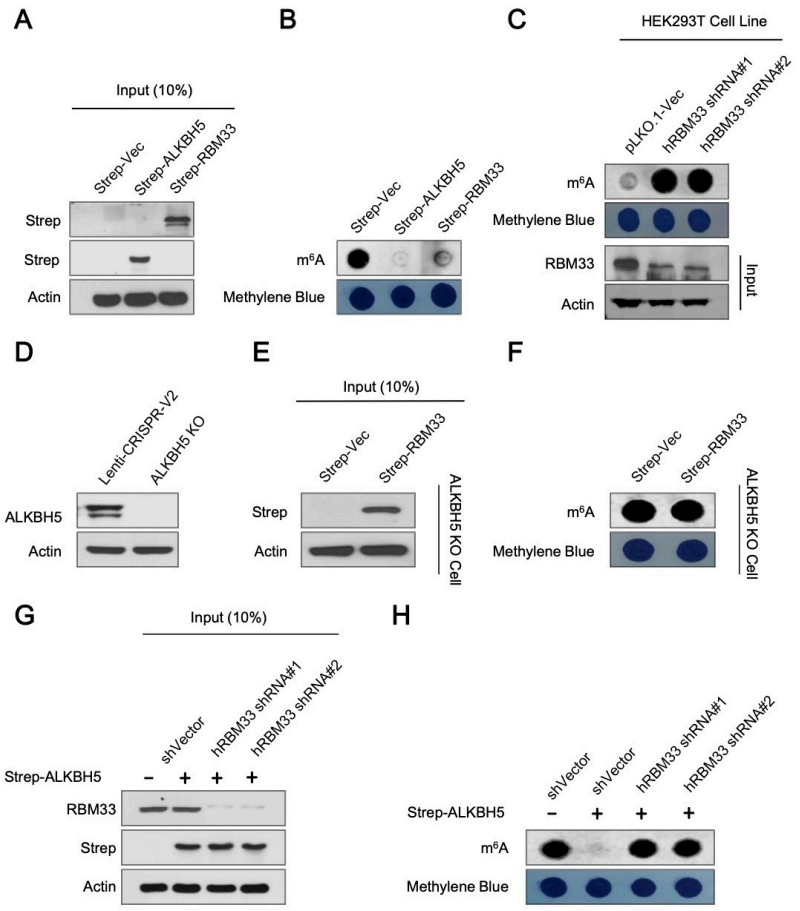

Figure 4-15. The RBM33/ALKBH5 complex mediates mRNA m^{6}A demethylation.

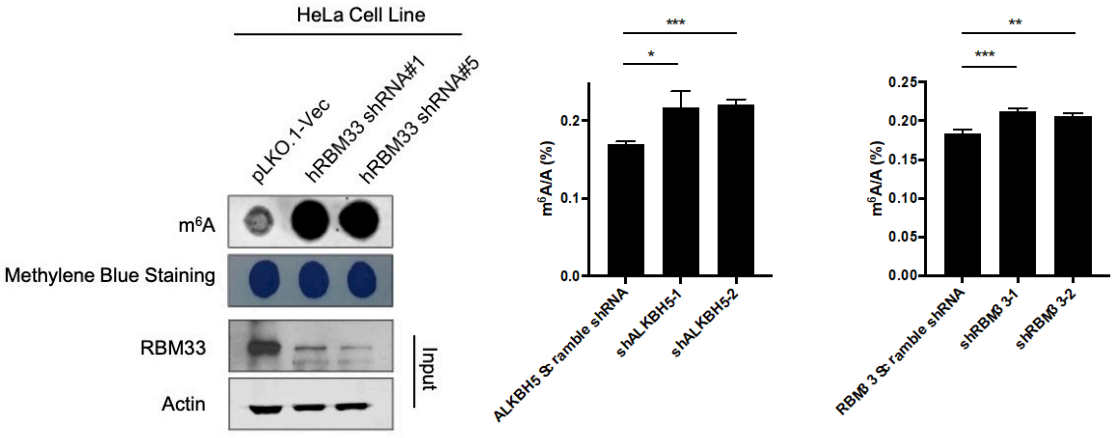

Figure 4-16. Knockdown of RBM33 globally increases m^{6}A methylation.

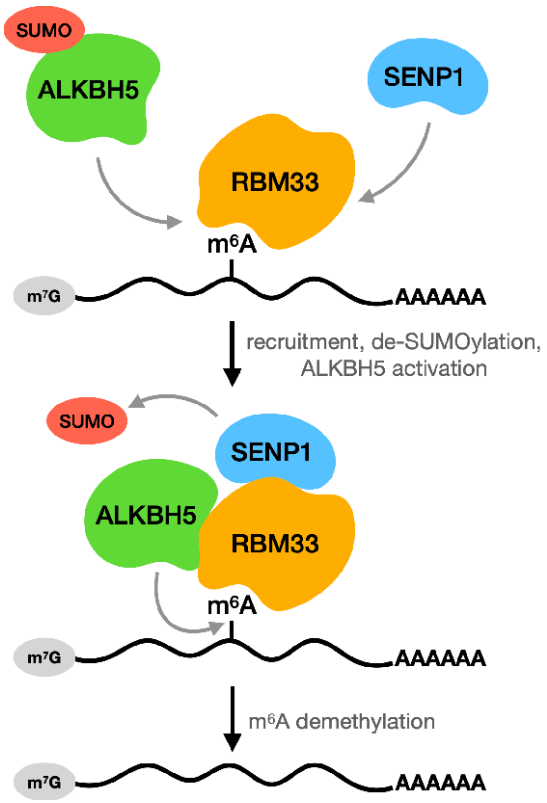

Figure 4-17. Overall model for mechanism of RBM33/ALKBH5 complex-mediated m^6A demethylation.

Methods

Plasmid Construction

The wild type *ALKBH5*-CDS and mutant *ALKBH5*-CDS were PCR-amplified from pFRT/TO/HIS/FLAG/HA-ALKBH5 plasmid (#38073, addgene) and pFLAG CMV5.1-ABH5-H204A (kindly provided by Dr. Chuan He), and then cloned into the pCDH lentiviral vector (CD513B-1, SBI, Mountain View, CA) using XbaI and BamHI enzyme sites. The TRC shRNAs targeting human *ALKBH5* (shA5-#1: TRCN0000291838; shA5-#2: TRCN0000291769), mouse *Alkbh5* (sh*A5*-#a: TRCN0000201776; sh*A5*-#b: TRCN0000192524), the inducible shRNA plasmids (TRIPZ-shA5-#3: V2THS_173653; TRIPZ-shA5-#4: V2THS_173654), as well as the non-targeting control shRNA, were all purchased from GE Dharmacon. The Lenti-iCas9-neo (doxycycline-inducible Cas9-EGFP vector) and lenti-guide (gRNA expression vector) were purchased from Addgene. Lenti-sgALKBH5 was constructed as previously described.

LC-MS/MS Quantification of m^6A/A

Total RNA was subjected to two rounds of polyadenylated (poly-A) mRNA purification, using the Dynabeads mRNA DIRECT kit (Thermo Fisher). The mRNA was digested by nuclease P1 (1U, Sigma-Aldrich, St. Louis, MO) in 20 μL of buffer containing 20 mM NH_4OAc (pH = 5.3) at 42°C for 2 hours. After digestion, the nucleosides were dephosphorylated by adding FastAP Buffer (Thermo Fisher) and FastAP Thermosensitive Alkaline Phosphatase (1 U, Thermo Fisher) and incubating at 37°C for 4 hours. The samples were then diluted to 50 μL and filtered (0.22 μm pore size, 4 mm diameter, Millipore), and 5 μL of the solution was injected into LC-MS/MS (three injections were performed per sample to serve as technical replicates). Nucleosides were separated by reverse phase ultra-performance liquid chromatography on a C18 column, followed

by online mass spectrometry detection using an Agilent 6410 QQQ triple-quadrupole LC mass spectrometer in positive electrospray ionization mode. The nucleosides were quantified by using retention time and the nucleoside-to-base ion mass transitions of 282.1 to 150.1 (m^6A), and 268 to 136 (A). The nucleosides of each sample were quantified by comparing the standard curve obtained from pure nucleoside standards that were run with the same batch of samples. The m^6A level was calculated as the ratio of the calibrated concentrations of m^6A to A (Jia et al., 2011a).

m^6A-seq and Data Analysis

For m^6A-seq, total RNA was isolated from NOMO1 cells with or without *ALKBH5* knockdown using QIAzol Lysis Reagent. Polyadenylated RNA was further enriched from total RNA using the Dynabeads mRNA DIRECT kit (Thermo Fisher). RNA fragmentation was performed by sonicating 1 µg mRNA in 100 µl RNase-free water using the Bioruptor Pico (Diagenode) with 30s on/30s off for 30 cycles at 4ºC. m^6A-IP and library preparation were performed per the reported protocol (Dominissini et al., 2012) with some modified instructions based on the EpiMark N6-Methyladenosine Enrichment Kit. Briefly, 25 µL Pierce Protein A/G Magnetic Beads (Thermo Fisher) were washed twice with 1x IP buffer and mixed with 2 µL m^6A antibody from the EpiMark N6-Methyladenosine Enrichment Kit (New England Biolabs, E1610S) and incubated with orbital rotation at 4°C for 30 min. The beads were washed twice with 1x IP buffer, and immunoprecipitation was performed by adding 1 µg sonicated RNA and mixing with orbital rotation for 3 hours at 4ºC. The beads were then separated and washed twice with 1x IP buffer, twice with low salt reaction buffer (50 mM NaCl, 0.1% NP-40, 10 mM Tris-HCl, pH 7.4), and twice with high salt reaction buffer (500 mM NaCl, 0.1% NP-40, 10 mM Tris-HCl, pH 7.4) before elution with Buffer RLT (Qiagen). The eluate was purified with the RNA Clean and

Concentrator-5 kit (Zymo, Orange, CA). The purified mRNA fragments were then used to construct libraries with the TruSeq Stranded mRNA Library Prep Kit (Illumina, San Diego, CA). Sequencing was carried out on Illumina HiSeq 4000 according to the manufacturer's instructions with single-end 50-bp read length. Reads were aligned to the mycoplasma genome to assess contamination, followed by alignment to human genome version 38 (GRCh38) with HISAT2. The longest isoform was retained if a gene has more than one isoform. Differential m^6A modified peaks between IP and input samples were identified using exomePeak ($p < 0.05$).

RNA immunoprecipitation (RIP) and RIP-seq

RNA immunoprecipitation was performed as previously described [265] with some modifications. Briefly, after UV-crosslinking, 60 million cells per sample were harvested and washed with PBS. Cells were lysed with two volumes of lysis buffer consisting of 10 mM HEPES pH 7.6, 150 mM KCl, 2 mM EDTA, 0.5% NP-40, 0.5 mM DTT, 1X cOmplete Protease Inhibitor (Roche), and 400 U/mL SUPERase-In RNase Inhibitor (Thermo). Cell lysate was cleared through a 0.22 μm filter. Input sample for RNA sequencing was prepared by saving 5% of lysate and adding 1 mL TRIzol reagent. Samples were subjected to immunoprecipitation using anti-Flag M2 magnetic beads. Beads were washed 4 times and re-suspended with cold NT2 buffer (50 mM HEPES pH 7.6, 200 mM NaCl, 2 mM EDTA, 0.05% NP-40, 0.5 mM DTT, and 200 U/mL RNase inhibitor). Sample lysates were immunoprecipitated with orbital rotation at 4ºC for 4 hours. Afterwards, beads were washed 8 times with cold NT2 buffer. Immunoprecipitated samples were subjected to Proteinase K digestion in NT2 buffer supplemented with 1% SDS and 1.2 mg/mL Proteinase K (ThermoFisher) incubated with shaking at 1200 rpm at 55ºC for 1 hour. Total RNA was extracted from both input and immunoprecipitated RNA by adding 5 volumes of TRIzol reagent, followed

by Direct-zol RNA Miniprep (Zymo) and used for qPCR analysis or RNA-seq. For RIP-seq, RNA was then fragmented with an average length of 150 nucleotides using the Bioruptor Pico sonication device. Libraries for high-throughput sequencing were constructed using the TruSeq Stranded v2 mRNA Sample Prep Kit (Illumina), and were quantified by BioAnalyzer High Sensitivity DNA chip. RIP-seq libraries were sequenced on Illumina HiSeq 4000 according to the manufacturer's instructions with single-end 50-bp read length.

Polysome Profiling

We followed the reported protocols [79, 266] with the following modifications. NOMO1 cells were transduced with ishNS or ishA5-#3 lentivirus and selected with puromycin (1 μg/mL). Doxycycline was added into the culture to induce *ALKBH5* knockdown and refreshed every 2 days for 6 days. Before collection, cycloheximide (CHX) was added to the culture media at 100 μg/mL for 7 min. Approximately 60-70 million AML cells from each group were harvested, rinsed in cold PBS with 100 μg/mL CHX and quickly frozen in liquid nitrogen before lysis. The lysis buffer was formulated as 20 mM HEPES (pH7.6), 100 mM KCl, 5 mM MgCl2, 100 μg/ml CHX, 1% Triton-X-100, with freshly added 1X cOmplete Protease Inhibitor (Roche) and 20 U/ml of SUPERase-In RNase inhibitor (ThermoFisher Scientific). The cell lysate was then layered on top of a 5%-to-50% sucrose gradient containing 20 mM HEPES pH 7.6, 100 mM KCl, 5 mM MgCl2, 100 μg/mL cycloheximide, 1X protease inhibitor (Roche), and 20 U/mL RNase inhibitor (ThermoFisher Scientific). The sucrose gradient was formed in an open-top polyclear tube (Seton) by the Gradient Maker on a Master unit from BioComp Instruments. The lysate and gradient were then centrifuged on an Optima L-100 XP Ultracentrifuge at 28,000 rpm for 3 hours at 4ºC in order to separate components of the lysate. The sample was then

fractionated into 30 fractions (0.5 mL per fraction) and analyzed by Gradient Station (BioComp Instruments) equipped with an ECONO UV monitor (BioRad, Hercules, CA) and Gilson FC203B fraction collector (Mandel Scientific, Guelph, Canada). RNA was purified from fractions 5-20 and subjected to RT-qPCR analysis. Expression of *TACC3* in each fraction was normalized to *GAPDH* as well as Input.

Sequencing Data Analysis.

(1) RNA-seq data.

Samples were sequenced by Illumina HiSeq 2500 with a single-end 50-base pair (bp) read length. Reads were mapped to human genome version GRCh38 by STAR. Gene expression (RPKM) was calculated by RSEM. The average gene expressions of two biological replicates were used for the following analysis.

(2) RIP-seq data.

Samples were sequenced on Illumina HiSeq 4000 according to the manufacturer's instructions with single-end 50-bp read length. Reads were mapped to human genome version GRCh38 by STAR. Gene expression (RPKM) was calculated by RSEM. The RIP targets were defined as genes with reads per kilobase, per million reads (RPKM) ≥1, immunoprecipitation/input ≥2.

(3) mRNA lifetime (stability) profiling data.

Samples were sequenced by Illumina HiSeq 2500 with a single-end 50-base pair (bp) read length. Reads were mapped to human genome version GRCh38 by STAR. Gene expression (RPKM) was calculated by RSEM. RPKM was converted to attomoles by linear fitting of the RNA spike-in. The degradation rate of RNA and the mRNA half-life were calculated according to the aforementioned formula. The final half-life was calculated by using the average value of 0 h, 8 h and 12 h.

(4) m^6A-seq data.

Sequencing was carried out on Illumina HiSeq 4000 according to the manufacturer's instructions with single-end 50-bp read length. Reads were mapped to human genome version GRCh38 by STAR. The longest isoform was retained if a gene has more than one isoforms. Differential m6A modified peaks between IP and input samples were identified using exomePeak ($p < 0.05$).

Data Deposition

Data of m^6A-seq obtained in this study have been deposited in the NCBI Gene Expression Omnibus (GEO) repository and made accessible under accession number GSE144984.

Methods for the RBM33 Study

Photoactivatable Ribonucleoside Cross-Linking and RNA Immunoprecipitation (PAR-CLIP)

PAR-CLIP for sequencing: Our protocol was similar to previous reports[55]. Starting material consisted of 100 million streptavidin-tagged ALKBH5 or RBM33 stably overexpressing cells. 12-16 hours prior to harvest, 4-thiouridine (4SU) was added to cell culture medium to a final concentration of 200 μM and incubated at 37ºC. Cells were then washed with ice-cold PBS twice, UV-crosslinked at 365 nm (1500*100 $\mu J/cm^2$) twice and collected in a cell pellet. Lysis buffer at 2-3 times the volume of the pellet was added on ice to lyse cells, followed by centrifugation and filtering to clear lysate. RNase T1 (1000 U/μL, Thermo) was added to a final concentration of 0.2 U/μL, incubated at 15 minutes for 22ºC, and quenched on ice for 5 minutes. 5% of lysate was saved as input for sequencing, and 1% saved for western blot. Anti-streptavidin

magnetic beads were then added to lysate, and rotated for 2-4 hours at 4ºC, followed by three washes. Beads were subjected to RNase T1 digestion (10 U/μL) for 8-10 minutes at 22ºC and washed three times with high salt wash buffer. Following dephosphorylation with Antarctic Phosphatase (M0289S) at 0.5 U/μL for 20 minutes at 37ºC, and end repair with ATP (1 mM) and T4 PNK (1 U/μL) for 30 minutes at 37ºC, the streptavidin-tagged protein-RNA complex was subject to protein size selection. The complex was SDS-PAGE purified with a size selection ranging from 45-80 kDa for ALKBH5 and 120-160 kDa for RBM33.The RNA fragments were extracted via ethanol precipitation after Proteinase K digestion of the excised gel slices. The purified RNA pellet was dissolved in 12 μL of RNase-free water, of which 6 μL was subjected to small RNA library preparation with NEBNext® Multiplex Small RNA Library Prep Set for Illumina (E7300S, NEB).

PAR-CLIP for quantification of protein-bound RNAs: 20 million streptavidin-tagged stably expressing cells were subjected to the same PAR-CLIP procedure while using γ-^{32}P-ATP in T4 PNK 5' end- repairing. After stringent washing following radioactive-labeling, the samples were subjected to SDS-PAGE and the gel was exposed to a blanked phosphor imager screen overnight. The screen was then imaged with the Molecular Imager FXTM (Bio-Rad).

m^{6}A-seq

For m^{6}A-seq, total RNA was isolated from UM-SCC-1 cells with or without *ALKBH5* or RBM33 knockdown using TRIzol. Polyadenylated RNA was further enriched from total RNA using the Dynabeads mRNA DIRECT kit (Thermo Fisher). RNA fragmentation was performed by sonicating 1 μg mRNA in 100 μl RNase-free water using the Bioruptor Pico (Diagenode) with 30s on/30s off for 30 cycles at 4ºC. m^{6}A-IP and library preparation were performed as

previously described. Briefly, 25 µL Pierce Protein A/G Magnetic Beads (Thermo Fisher) were washed twice with 1x IP buffer and mixed with 2 µL m^6A antibody from the EpiMark N6-Methyladenosine Enrichment Kit (New England Biolabs, E1610S) and incubated with orbital rotation at 4°C for 30 min. The beads were washed twice with 1x IP buffer, and immunoprecipitation was performed by adding 1 µg sonicated RNA and mixing with orbital rotation for 3 hours at 4ºC. The beads were then separated and washed before elution with Buffer RLT (Qiagen). The eluate was purified with the RNA Clean and Concentrator-5 kit (Zymo, Orange, CA). The purified mRNA fragments were then used to construct libraries with the TruSeq Stranded mRNA Library Prep Kit (Illumina, San Diego, CA). Sequencing was carried out on Illumina HiSeq 4000 according to the manufacturer's instructions with single-end 50-bp read length. Reads were aligned to the mycoplasma genome to assess contamination, followed by alignment to human genome version 38 (GRCh38) with HISAT2.

Chapter V: Discussion and Future Perspectives

Introduction

The combined work in this dissertation demonstrates the profound effects that m^6A methylation can have on the transcriptome. By modulating the phosphorylation of the m^6A methyltransferase complex with ERK pathway kinases or inhibitors, we can identify biochemical effects of phosphorylation upon the m^6A methylation process. We determined that phosphorylation increases the interaction between METTL3/METTL14 and WTAP and stabilizes the complex. This results in increased m^6A methylation, which promotes differentiation in embryonic stem cells. We also found that m^6A methylation installed by METTL3 affects antiviral immune activation by disrupting the structure of RNA in the host cell. Finally, we found that ALKBH5 contributes to demethylation of transcripts that maintain acute myeloid leukemia.

METTL3 Phosphorylation as an Extrinsic Factor of m^6A Specificity

The effects of phosphorylation upon m^6A methylation comprise one part of another question open for exploration in the m^6A field: what factors determine where and when m^6A is deposited within the transcriptome? Sequence specificity is certainly important, given that m^6A prefers the DRACH consensus sequence motif. However, the majority of these DRACH motifs do not all contain m^6A. Furthermore, m^6A resides in specific regions of the transcript, namely long internal exon and the stop codon. In other words, RNA sequence as an intrinsic determinant is not sufficient to determine where m^6A is written. Other phosphorylation sites by different kinases may affect m^6A writer complex interactions or localizations. Thus, it will be interesting to find the extent to which phosphorylation acts as a determinant of m^6A methylation, relative to other extrinsic factors.

These extrinsic factors include transcription factors, RNA-binding proteins, other interactors, such as CEBPZ or SMAD2/3, which aid in recruiting the m^6A methyltransferase complex to specific RNA loci[99, 119]. Another factor includes the histone modification H3K36me3, which has been shown to recruit the m^6A methyltransferase complex for co-transcriptional deposition upon the nascent RNA substrate[267]. Aside from these extrinsic interactors with the m^6A writer complex, another facet that has emerged from our work is the post-translational regulation of the m^6A methyltransferase complex. Although we focused on phosphorylation by the ERK2 kinase, multiple post-translation modifications of METTL3 have been identified[268]. However, the functional outcomes of each modification have yet to be fully unraveled.

Phosphoproteomics studies of ATM/ATR substrates have previously uncovered that, in response to DNA damage, METTL3 is phosphorylated at residues S350 and T356 in an ATM-dependent manner[162]. Furthermore, phosphorylation of METTL3 has been found to be an early responder to DNA damage[174]. Considering that m^6A rapidly accumulates at UV-irradiated sites[175] and that lack of METTL3 catalytic activity delays DNA repair and Pol κ-mediated response to UV DNA damage, it would be interesting to explore the role of ATM/ATR-induced METTL3 phosphorylation.

Later, it was found that, in response to double-stranded breaks (DSBs) of DNA, METTL3 is activated by ATM-mediated phosphorylation at S43, one of the sites that we found to be phosphorylated by ERK2[269]. S43-phosphorylated METTL3 is then recruited to DSBs, resulting in m^6A methylation of nascent RNAs that are recognized and protected by YTHDC1. These RNAs then hybridize with DNA at DSB sites to promote homologous recombination DSB repair. Intriguingly, because mutation of the METTL3 S43 residue hinders interaction with RNA Pol II,

this phosphorylation may serve multiple purposes—recruitment of the m^6A writer complex to areas of DNA damage and deubiquitination.

Potential Regulatory Roles of METTL3 Phosphorylation

Another post-translational modification we observed on METTL3 was polyubiquitin, specifically K11, K48 and K63 polyubiquitin chains. It remains unclear which other deubiquitinase enzymes remove each of the linkages, although USP5 appears to affect K11 polyubiquitin chains. SUMOylation of METTL3 has also been identified and it is found to methyltransferase activity, thereby lowering m^6A abundance[189]. The authors found that SUMOylation of METTL3 does not alter stability, localization, or interaction with other complex components or translation initiation factors. SUMOylation of METTL3 increases upon chemotherapy-induced stress and is removed by SUMO1-specific protease SENP1. Intriguingly, MAPK activation can modulate SUMOylation of METTL3[270]; specifically, ERK activation de-SUMOylates the Elk-1 transcription factor[190, 191]. It would be interesting to explore whether METTL3 phosphorylation affects SUMOylation level as well.

Currently, in the field, how phosphorylation affects the m^6A writer complex is up for debate. At first, one study concluded that phosphorylation of METTL3 does not affect interaction with WTAP, subcellular localization, or catalytic activity[271]. Our work reports that ERK2 phosphorylation increases the interaction between METTL3 and WTAP. A key discrepancy, however, is that both METTL3 and WTAP are phosphorylated by ERK2, so phosphorylated WTAP may enhance the METTL3-WTAP interaction. Structural studies are needed to further shed light on this phenomenon. We did not study catalytic activity of METTL3 in our own work, but

we did find greater m^6A methylation overall, although we attribute this to a USP5-mediated increase in METTL3 stability.

Based on phosphorylation studies on METTL3 so far, it appears that phosphorylation may fine-tune certain functions of METTL3. Slobodin et al. previously reported that METTL3 is recruited to the genome by interacting with RNA polymerase II[272]. With ATM-mediated phosphorylation, METTL3 interaction with RNA Pol II and subsequent m^6A deposition onto nascent RNA are enhanced. With ERK2-mediated phosphorylation, METTL3 interaction with USP5, enforcing stabilization of METTL3. Overall, phosphorylation seems to impart the m^6A writer complex with a more acute response to certain extracellular stimuli or environmental stress. The half-life of mRNA is relatively short, with a median of 10 hours in human cells. Even though it is constantly being degraded, biological processes that demand an even more rapid response and faster turnover of the transcriptome may depend on post-translational regulation of m^6A in order to finely adjust the cell's ability to adapt.

Phosphorylation does not appear to affect catalytic activity or m^6A complex interactions of core components to a dramatic extent. It does, however, appear to affect the interactome of METTL3. It stands to reason that perhaps m^6A methylation sites that occur more so because of extrinsic determinants may be more affected by METTL3 phosphorylation and exhibit differential methylation upon differentiation or signals from stress or stimulation.

We also found that METTL3 can suppress antiviral signaling through m^6A-dependent suppression of RIG-I activation in Chapter 3. Bridging the phosphorylation and innate immune studies of METTL3, one should consider the effects of various kinase activities under environmental stimuli or stress. TBK1, a key kinase of antiviral pathways, may phosphorylate

METTL3 or other m^{6}A-related proteins, and mediate a different pattern of m^{6}A methylation. How METTL3 PTMs vary under different biological conditions is also an interesting question.

Roles for Other Post-Translational Modifications of the m^{6}A Writer Complex

It is important to note that other m^{6}A writer complex components are also post-translationally modified and affect m^{6}A methylation. Our work showed that WTAP is also phosphorylated by ERK2 and is also stabilized as a result. However, other m^{6}A writer components are also modified. METTL14 has been found to undergo methylation at Arg255 by PRMT1[273, 274]. Abrogation of this arginine methylation decreases m^{6}A by approximately three-fold in mESCs and diminishes the interaction between METTL3/METTL14 and WTAP. This loss of methylation also disrupts normal mESC endoderm differentiation, similar to how phosphorylation affects mESCs. In sum, these studies have begun to highlight and establish a potentially new layer of regulation that ought to be considered when studying RNA methylation. Protein methylation and phosphorylation have been shown to be involved in all sorts of biological processes, including, but not limited to, gene transcription, cell signaling, RNA splicing, cell fate, and oncogenic activity. Now it has been established that they modulate RNA methylation too[275-277]. These different PTM pathways affect m^{6}A deposition, which, in turn, also affects the expression of many pathways, including PTM regulators themselves. This feedback loop presents a complex regulatory network that enables cells to carefully govern gene expression levels and activities of mRNA.

It seems that PTMs could be a useful way for the cell to control the epitranscriptome both locally and globally. Locally, they can recruit the m^{6}A writer complex to certain loci, such as how H3K36me3 recruits METTL14 to gene bodies or how METTL3 S43 phosphorylation promotes binding at RNA Pol II sites. Globally, removal of PTMs from the writer complex can result in

hypo-methylation. With differential levels of signaling pathways active across different cell types, one can begin to comprehend why the m^6A methylome varies greatly across different tissues in the same organism.

We studied the effects of ERK signaling on METTL3, but our focus was isolated on the m^6A writer complex alone and did not take into regard other m^6A effectors. EGFR/SRC/ERK signaling also phosphorylates Ser39 and Thr381 of YTHDF2, resulting in its stabilization[278]. Because kinase signaling occurs on the scale of minutes, coupling phosphorylation with YTHDF2 function enables a rapid response in m^6A-dependent gene repression. It may be worth investigating whether other m^6A readers also undergo methylation, phosphorylation, or other PTMs, and whether those PTMs result in different subcellular localization, m^6A binding affinities, or protein-protein interactions. This, in addition to different relative levels of m^6A reader expression, could lead to very different outcomes in gene expression. Understanding these models may further describe the mechanisms that govern m^6A-mediated gene regulation.

Given that YTH proteins contain a low-complexity, intrinsically disordered N-terminal region, it is possible that phosphorylation affects their localization. Previously, a study on RNA polymerase II, which also contains a disordered C-terminal region, found that hypophosphorylation of the C-terminal domain results in preferential incorporation into mediator condensates[279]. Upon phosphorylation by cyclin-dependent kinases, the C-terminal domain is found in condensates formed by splicing factors. This exchange suggests phosphorylation-dependent phase separation as a mechanism to shuttle the RNA polymerase from transcription to RNA processing. In a similar fashion, YTHDF proteins have been found to also undergo liquid-liquid phase separation, often in response to stress such as the heat shock response[280]. It may be

worth investigating whether phosphorylation or other PTMs act as a means of controlling the localization of the disordered regions of m^6A readers.

To truly understand how phosphorylation or other PTMs affect protein interactions or activity, structures of these proteins should be solved, as has been down for other proteins[281]. In the case of ERK-phosphorylated METTL3, a crystal structure would elucidate how the interaction between METTL3 and WTAP is affected and where the PTM resides on the surface of the target protein. It would also show how USP5 displays increased binding affinity towards METTL3, as it is not clear whether the nature of the METTL3-USP5 interaction is more transient or stable.

Many other questions are open for future exploration. For example, how are other m^6A writer complex sites affected by PTMs such as phosphorylation? Some PTMs can cross talk with one another, in which the deposition of one PTM antagonize the other—could a similar phenomenon occur with METTL3? Can we sequence the m^6A methylome and the phosphoproteome in multiple tissue types and observe correlation? Can post-translational modifications explain which m^6A sites are recognized by certain readers or erasers of m^6A? How do various kinases differ in their effects on METTL3 upon phosphorylation? What other mRNAs and pathways are targets of METTL3 phosphorylation? How does dysregulation of ERK signaling or deleterious mutations in various types of cancers affect activity of m^6A writers?

Post-Translational Modifications ALKBH5: Crosstalk between ERK and SUMOylation?

Our work in Chapter 4 also discussed how ALKBH5 undergoes removal post-translational modifications. Previous work from the same collaborators showed that reactive oxygen species activate ERK/JNK signaling to SUMOylate ALKBH5[282]. The SUMOylation of ALKBH5 then

leads to inhibited m^{6}A demethylase activity because substrate accessibility is blocked, resulting in globally greater m^{6}A methylation. This change in methylation results in delayed DNA repair and increased apoptosis. Interestingly, MAPK signaling, which includes ERK, JNK, and p38 regulatory pathways has been known to be activated by reactive oxygen species-induced stress[283, 284]. This suggests that modulation of m^{6}A levels by SUMOylation is simply one arm of the set of pathway axes activated by these MAPKs. It may also lead one to wonder the relative contribution of m^{6}A-dependent regulation on ROS stress response within ERK/JNK signaling.

It is interesting that SUMOylated ALKBH5 inhibition increases *METTL3* and *METTL14* in response ROS and that this phenomenon does not occur upon ALKBH5 depletion, suggesting a unique role for PTMs of ALKBH5. The fact that METTL3 is also and phosphorylated by ERK signaling to respond to DNA damage suggests that these downstream targets of ERK are coordinated to respond to environmental stress in a rapid and efficient manner. This raises an interesting perspective when studying effects of PTMs on m^{6}A methylation. Although a single m^{6}A-related protein is usually the focus, other m^{6}A regulatory proteins may also be affected by the same enzyme, suggesting multiple pathways working in tandem or a positive feedback loop.

How exactly does RBM33 assist ALKBH5 in m^{6}A demethylation?

From our work in the second part of Chapter 4, we now also know that RBM33 serves at least roles; it acts as an m^{6}A reader to aid in substrate recognition and m^{6}A demethylation for ALKBH5, and it promotes SENP1-mediated SUMO deconjugation from ALKBH5. In other words, RBM33 is necessary and sufficient for ALKBH5 m^{6}A eraser activity. One question, however, is how crucial RBM33 is for ALKBH5 activity. Is it analogous to the role of METTL14 towards METTL3 activity? METTL14 stabilizes METTL3 and also contains RGG repeats that enable it to recognize

m^6A-methylated RNA. In the original publications displaying the solved crystal structure of ALKBH5, the authors found a conserved double-stranded beta helix fold (amino acids 66 to 292) that serves as the catalytic core[285]. On the other hand, they only identified putative residues involved in m^6A recognition, and mutagenesis still resulted in some, albeit lower, demethylase activity. Although the m^6A base is predicted to pack against His204 in a pocket composed of Arg130 and Tyr139, only structural modeling has been done; moreover, attempts to crystallize an m^6A-methylated single-stranded nucleic acid were unsuccessful. Modeling showed a positively charged groove in the Flip3 region of ALKBH5 but does not directly prove m^6A binding modes of ALKBH5. Perhaps crystallization of ALKBH5 and RBM33 would be more successful and provide more insight into the binding affinity of ALKBH5 and RBM33. If future studies suggest that RBM33 is dispensable for ALKBH5-mediated demethylation, then, at the very least, it would play a similar role as RBM15 or WTAP does for METTL3—as an accessory subunit of an m^6A eraser complex. Either way, it is very possible that ALKBH5 should not be thought of as an individual demethylase protein.

Although we focused on ALKBH5 in this dissertation, both FTO and ALKBH5 are known m^6A erasers. However, their structures and mechanisms of action differ remarkably. Whereas FTO contains a unique loop (residues 210-223), ALKBH5 replaces it with a short alpha-helix that prevents binding with dsRNA. FTO contains a Glu234 residue that contributes to substrate recognition, and the analogous residue in ALKBH5 is abolished, as it is a Pro207. Enzymatically, ALKBH5 directly demethylates m^6A to A, whereas FTO gives hm^6A as a major product, followed by conversion to adenosine over a longer timescale. FTO also has a broader substrate preference than ALKBH5. ALKBH5 specifically binds m^6A, whereas FTO exhibits demethylation of mRNA m^6A, cap m^6A_m, and m^1A. The two proteins also have distinct substrate preferences, with different

sites on mRNAs, tRNAs, and snRNAs. Biologically, this results in completely different phenotypes. *FTO*-deficient mice have lean body mass and growth retardation, whereas *ALKBH5*-deficient mice exhibit impaired fertility. This is apparently the result of different mRNA targets. It would be interesting to determine how ALKBH5 PTMs and interactions with RBM33 affect its mRNA substrate preferences and whether other processes besides demethylation are also affected. Whether RBM33 is directly responsible for certain ALKBH5-related phenotypes or cancers, aside from head and neck cancer as we showed in our work, has yet to be discovered.

In the first part of Chapter 4, we discovered the substantial role of ALKBH5 in promoting acute myeloid leukemia. ALKBH5 is also involved in several other cancers. Zhang et al. found that ALKBH5 expression is heightened in GSCs, and that it predicts poorer prognosis[125]. Knocking down *ALKBH5* hindered GSC self-renewal, proliferation, and tumorigenesis because ALKBH5 demethylates and reduces expression of *FOXM1*. In breast cancer cells, hypoxia induces expression of ALKBH5, which then demethylates *NANOG* mRNA, resulting in enrichment of cancer stem cells[126]. As part of the host cell's innate immune response, ALKBH5 m^6A eraser activity is impaired upon viral infection[286]. This increases methylation and reduces stability of *ODGH* mRNA, which subsequently reduces production of the metabolite itaconate required for viral replication. The critical role ALKBH5 has in promoting cancer or diminishing an antiviral response raises the demand for ALKBH5 inhibitors. However, few compounds with clinical success have been reported. Although drug development is ongoing, work cited in this thesis suggests that inhibitors of SENPs or RBM33 may have some efficacy in restraining ALKBH5 activity.

Concluding Remarks

The functional studies of mRNA modifications have vastly expanded in the last decade. We have gained a much better understanding of how perturbations in m^6A methylation can severely affect biological processes and systems. The latest progress in the field has been on understanding other molecular functions of m^6A methylation, such as its role in regulating transcription and chromatin. In this dissertation, we emphasized the study of how the cell regulates m^6A methylation with cell signaling pathways for proper gene expression regulation under certain stimuli. The vast interconnectedness between transcription, translation, and post-translational regulation is a salient feature of the central dogma, and further research in the area will only continue to unveil this complex regulatory network within the cell.

Appendix: Targeting RNA m^{6}A Methylation for Cancer Therapies

Note:

The following text is originally from a manuscript of a review on using small molecule inhibitors to target RNA m^{6}A methylation for cancer therapy. Because much of the material is redundant with material in the introduction, only excerpts are included, with minor adjustments. The discussion consists mostly of a literature review of small molecules developed to inhibit effectors and regulators of m^{6}A methylation, their efficacies, and their caveats. Discussion on how these m^{6}A effectors have been studied in a disease context is also included.

Introduction

The understanding of both normal and pathological processes in multicellular organisms, as well as the development of treatments for such diseases, requires comprehending the mechanisms that regulate the expression of genes. Multiple processes—including transcription, messenger RNA (mRNA) processing, export of mRNA from the nucleus, mRNA decay, and protein translation—must be dynamically regulated for proper cellular homeostasis[13]. One crucial mechanism of the regulation of gene expression is the post-transcriptional chemical modification of RNA.

The burgeoning field of m^{6}A methylation is still growing, with new roles of m^{6}A and its regulatory proteins being uncovered. In this review, we discuss the disease relevance of m^{6}A methylation by describing biological processes that key m^{6}A regulatory proteins are involved in.

This review also maintains a chemical perspective focused on potential therapies, as we also describe the successes and challenges of developing small molecules that modulate the activity of these proteins. Reviewing these findings will present the diverse and critical roles that m^6A methylation plays upon the transcriptome and provide a snapshot of the current state of small molecule inhibitor developments for clinical treatment.

METTL3/METTL14

Small Molecule Inhibitors

With the widespread effects of METTL3 in multiple cancers, it is imperative that researchers develop tools that can inhibit METTL3 activity or expression. Researchers have sought to identify and characterize small molecules that target m^6A methylation proteins. METTL3 is an optimal target for multiple reasons—it is an enzyme, dynamically regulated post-translationally, and contains a SAM-binding pocket found to be targetable in protein methyltransferase enzymes[287]. No specific inhibitors of the METTL3 had been found, until Moroz-Omori et al. reported on UZH1a[288]. Using MOLM-13 leukemia cells, they found that UZH1a is a potent, selective METTL3 inhibitor that could dose-dependently reduce m^6A mRNA methylation and cell viability. Interestingly, they found METTL3 inhibition had less effect on other cell lines, suggesting different dependencies on cellular m^6A.

Most recently, Yankova et al. characterized another small molecule inhibitor of METTL3, named STM2457 (Figure A1-A), as a therapeutic strategy against acute myeloid leukemia[289]. STM2457 is not only a very potent inhibitor of METTL3-METTL14 catalytic activity, but also over a thousand-fold selective for METTL3 relative to other methyltransferases. Crystal structures reveal that this strong selectivity is due to structural dissimilarity from SAM, avoidance of the

SAM homocysteine binding pocket (Figure A1-B, C), and reorganization of K513 upon STM2457 binding (Figure A1-D). STM2457 was able to reduce growth in multiple human AML cell lines without affecting normal human blood cells, and it prevented AML expansion in leukemic stem cell subpopulations. After STM2457 treatment, almost half of the m^6A peaks were reduced, especially on core leukemogenic transcripts, and with reduced mRNA translational efficiency of METTL3-dependent substrates. This work is the first to provide proof of concept on how a bioavailable inhibitor of METTL3 has therapeutic efficacy against cancer, motivating new avenues for treating cancer.

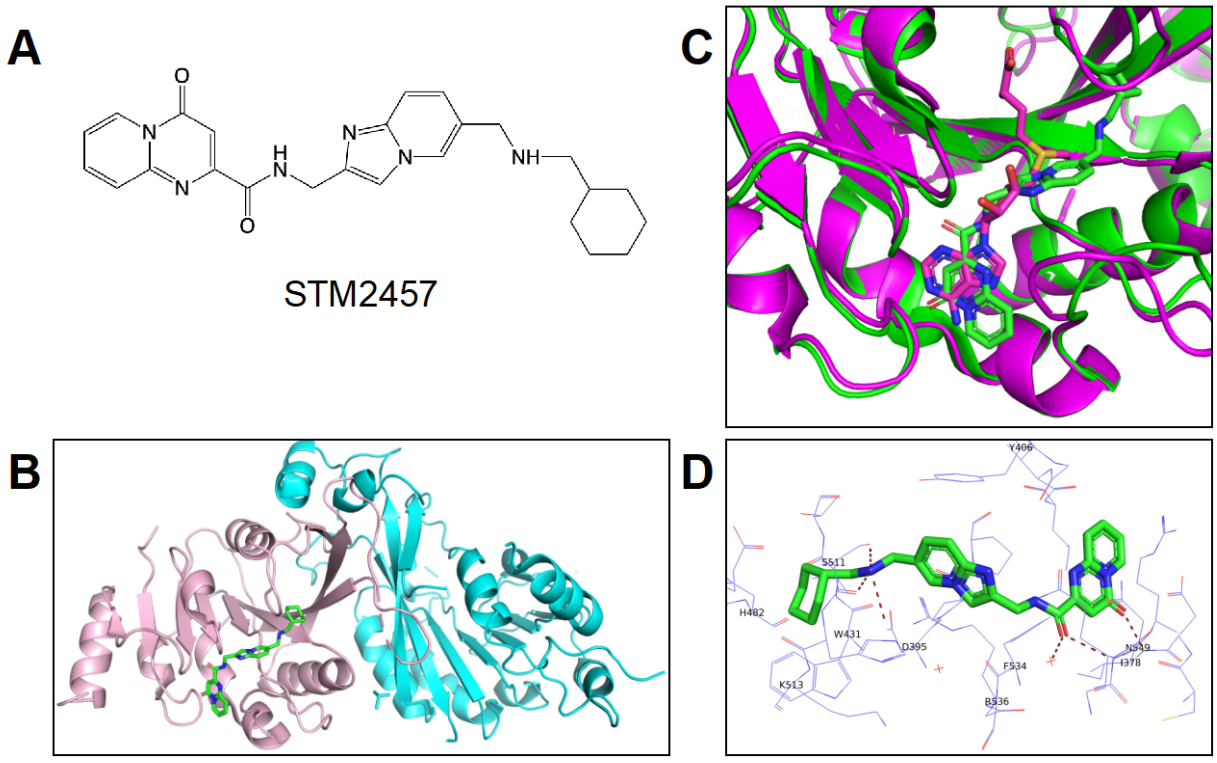

Figure A1: STM2457 is an active inhibitor of METTL3/METTL14 in AML

(A) Chemical structure of the STM2457 molecule. (B) Crystal structure of STM2457 within METTL3/METTL14. (C) Structural comparison of SAM (magenta) or STM2457 (green) bound to METTL3/METTL14. (D) Intermolecular bonds between STM2457 and multiple residues of METTL3.

Notwithstanding these promising results, targeting methyltransferases with small molecules presents multiple caveats and challenges. Many inhibitors against DNA, RNA, or protein methyltransferases act as SAM-competitive inhibitors[290, 291]. Within cells, these molecules face competition against high intracellular concentrations (~20-40 μM) of SAM[291]. As a result, even if a SAM-competitive inhibitor is efficacious in vitro, its potency may severely decrease intracellularly. Another obstacle is the structural similarity of the SAM-binding pocket among methyltransferases, which may prevent selectivity for a particular methyltransferase. For instance, although the SAM analog sinefungin inhibits METTL3, it targets most SAM-dependent methyltransferases[292]. Moreover, other m^6A methyltransferases, such as METTL5, METTL16, and ZCCHC4, not to mention other RNA methyltransferases of the same family, which structurally contain similar catalytic active sites and may present further challenges in selectivity[293, 294].

Genetic silencing and pharmacological inhibition may exhibit substantial discrepancies. For instance, inhibition of METTL3 appears to have a milder effect compared to knockout of METTL3. Whereas addition of METTL3 inhibitor STM2457 affected leukemic but not normal hematopoietic stem cells, knockout of METTL3 affected both groups[289]. This difference may be due to dosage, as the small molecule may not deplete as much enzymatic activity as a genetic knockout, in which one of two copies is ablated. One should also note that inhibiting catalytic activity may not necessarily affect catalytic activity-independent role a protein may play as a scaffold. To illustrate, METTL3 can tether eukaryotic translation initiation factors without catalytic activity or in an m^6A-independent manner[153, 173]. Similarly, METTL3 and METTL14 are bound to promoters and enhancers to express genes that drive a senescence-associated secretory phenotype[295].

In any case, the contrast in the suppression of proliferation between leukemia cells and normal cells is crucial for therapeutic applications. If patients are treated with METTL3 inhibitor, it is important that the immune system is not concomitantly suppressed. Since inhibition of normal hematopoiesis would stifle anti-tumor immunity, any therapies that inhibit METTL3 need to specifically affect their targeted cells.

m^6A Demethylases

FTO

Although FTO was originally named after its initially discovery in obesity and metabolic disease[296], its role as an m^6A demethylase was shown to be oncogenic. In AML, FTO promotes leukemic transformation through demethylation of target genes such as *ASB2* and *RARA*, which promote all-*trans*-retinoic acid (ATRA)-induced differentiation in normal hematopoietic stem cells[122]. Intriguingly, some AML cells naturally inhibit FTO through production of R-2-hydroxyglutarate (R-2HG), thereby elevating global m^6A levels[123]. R-2HG is produced by a mutant form of isocitrate dehydrogenase 1/2 (IDH1/2) often found in AML. Because R-2HG is structurally very similar to α-KG, it acts as a natural small molecule inhibitor of Fe^{2+}/α-KG-dependent dioxygenases[124] (Figure A2-A). In R-2HG-sensitive leukemia cells, R-2HG enzymatically inhibits FTO, resulting in accumulation of m^6A on transcripts, leading to destabilization of targets such as *MYC* and *CEBPA*[123] (Figure A2-B). Additionally, R-2HG can attenuate glycolysis by disrupting FTO-mediated upregulation of glycolytic genes *PFKP* and *LDHB*[297].

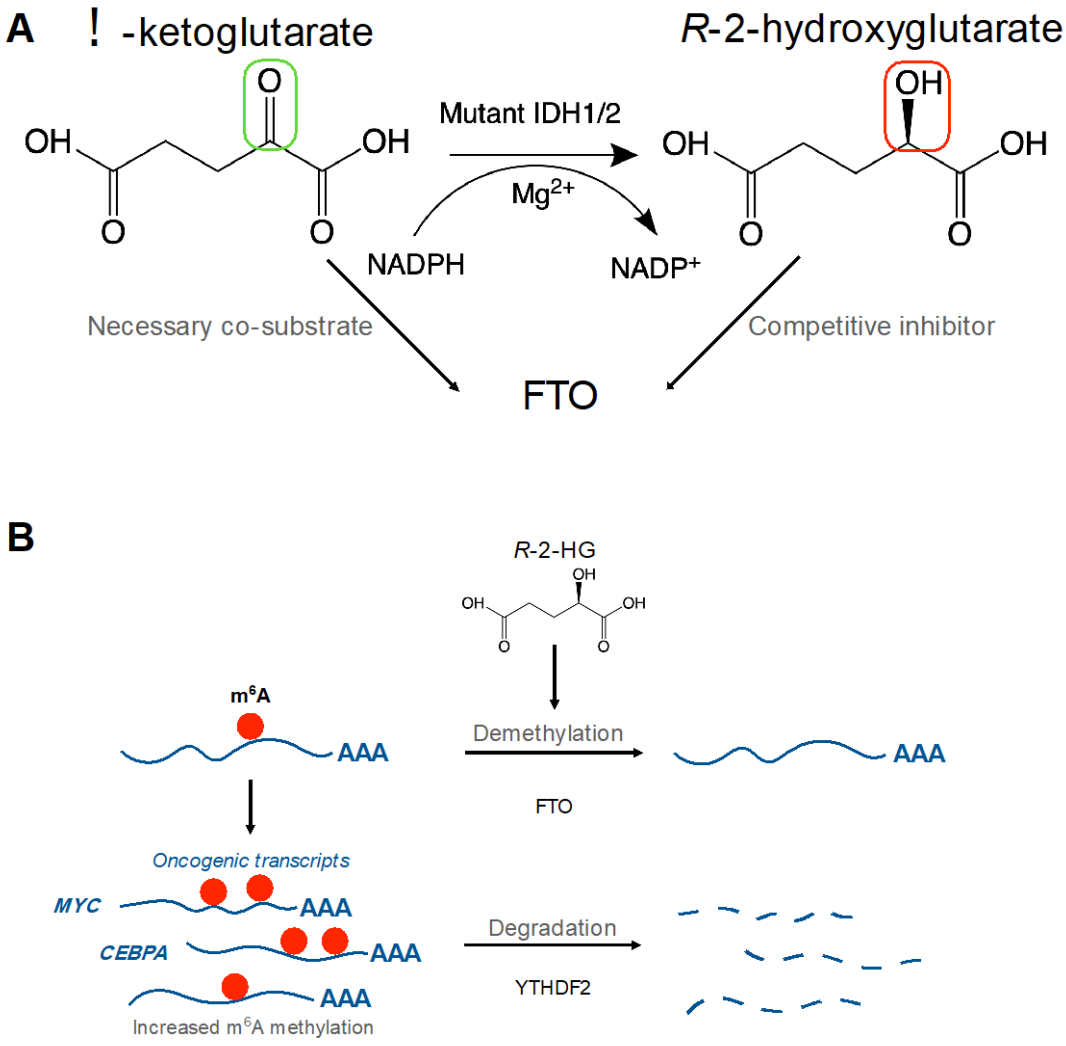

Figure A2: *R*-2HG targets FTO to increase m^{6}A methylation and suppress tumor growth

(A) Mutant IDH1/2 turns α-ketoglutarate into *R*-2-hydroxyglutarate, which can then competitively inhibit FTO. (B) Thought to be an oncometabolite, *R*-2-HG in tumor cells exhibits antitumor activity by promoting degradation of oncogenic transcripts via reduced FTO demethylation.

FTO not only promotes cancer initiation and progression, but also influences the efficacy of cancer treatment. In cervical cancer, FTO is elevated, especially in poorly differentiated, stem cell-like cancers[298]. Overexpression of FTO reduces m^{6}A methylation on β-catenin, an effector of the epithelial-to-mesenchymal transition, resulting in cisplatin resistance. In addition, FTO enhances stability of cell proliferation and survival transcripts that enable resistance to tyrosine

kinase inhibitor therapies[299]. It also promotes resistance to anti-PD-1 checkpoint blockade immunotherapy by increasing expression of *PD-1*, *CXCR4*, and *SOX10*[300].

Small molecule inhibitors have also been developed to target FTO and its oncogenic activity. Since m^6A erasers are AlkB enzymes, α-KG derivatives have been designed as inhibitors. A major concern, however, is that they would have to compete with internal α-KG. Shortly after the publication of FTO as an m^6A eraser and its crystal structure[36, 301], the natural product rhein was the first discovered FTO inhibitor[302]. However, structural studies showed that rhein could bind to AlkB domains in other enzymes as well, raising the issue of selectivity[303]. Later, meclofenamic acid (MA) was identified as a highly selective inhibitor of FTO over ALKBH5[304]. Both MA and rhein competitively inhibit the interaction between FTO and the m^6A-containing nucleic acid. The key difference is that MA also binds to the nucleotide recognition lid of FTO, which ALKBH5 lacks. Other inhibitors have also been synthesized or discovered, such as dihydroxyfuran sulfonamides with anticonvulsant activity[305], fluorescein which can both inhibit and label FTO[306], or multiple small molecules that target other novel binding sites on FTO have also been found[307].

Given that dysregulation of FTO has been associated with diseases such as cancer, it is crucial to develop inhibitors with potent and selective therapeutic efficacy. MA2, an ethyl esterified form of meclofenamic acid, was shown to inhibit GSC self-renewal and tumor growth, and more inhibitors been developed to inhibit glioblastoma neurosphere formation[308]. Another recent small molecule is FB23-2, a highly selective FTO inhibitor that inhibits AML proliferation, and promotes myeloid differentiation and apoptosis[309].

FB23-2 was further optimized into a more potent inhibitor named Dac51 by Liu et al[115]. They found that FTO inhibition in tumor cells resulted in greater m^6A methylation and YTHDF2-

mediated decay of mRNAs that drive glycolysis. Dampening glycolysis in tumor cells permits greater metabolic activity and an enhanced anti-tumor response by surrounding cytotoxic T cells. Thus, FTO inhibition is a potential immunogenic therapeutic strategy.

ALKBH5

ALKBH5 was discovered soon after FTO as another m^6A eraser[70]. Although the two m^6A erasers are in the same AlkB family, ALKBH5 is smaller in size and has different structural properties, with a much smaller active site cavity which may explain its more potent binding preference to smaller-sized molecule inhibitors[70]. In its initial publication, ALKBH5 was shown to demethylate m^6A, and ALKBH5 deficiency in mice impaired spermatogenesis and fertility[70]. Interestingly, ALKBH5 activity also affects multiple aspects of mRNA metabolism, such as mRNA export and processing within nuclear speckles. Another study found that removal of m^6A by ALKBH5 in germ cells ensures proper splicing and degradation of the 3' UTR during spermiogenesis[74].

Since then, multiple studies have continued to expand the biological importance of ALKBH5. For example, host cells impair ALKBH5 m^6A eraser activity as a response to viral infection[286]. This increases methylation and reduces stability of *ODGH* mRNA, which subsequently reduces production of the metabolite itaconate required for viral replication. ALKBH5 is also involved in other processes such as cardiomyocyte differentiation, autophagy and apoptosis, trophoblast invasion, post-ischemic angiogenesis, and liver disease[256, 310-313]. Furthermore, ALKBH5 SUMOylation regulates ROS-induced DNA damage response[282].

Two recent studies, one of which is forms a part of this dissertation, also reported the role ALKBH5 plays in AML[314-316]. In the first study, ALKBH5 was found to promote growth,

leukemogenesis, and leukemic stem cell (LSC) self-renewal. This occurs because ALKBH5 demethylates *TACC3*, thereby modulating MYC and P21 pathways[315]. In the other study, the histone demethylase KDM4C opens chromatin to promote ALKBH5 expression, which stabilizes oncogene *AXL* in an m^{6}A-dependent manner[316]. Notably, both studies found that ALKBH5 was required for LSC maintenance but were dispensable for normal hematopoietic stem cells, which offers a potential therapeutic strategy. Other cancer-related studies show that ALKBH5 can suppress anti-PD-1 immunotherapy in melanoma, promote lung cancer via FOXM1 or TIMP3 signaling, suppress hepatocellular carcinoma through *LYPD1* demethylation, promote gastric cancer, or suppress osteosarcoma[317-320].

All these findings demand effective small molecule inhibitor strategies against ALKBH5. At first, structural studies revealed that the TCA cycle intermediate citrate is a natural yet weak inhibitor[321]. Though it binds to ALKBH5, citrate also inhibits FTO (and other ALKBH enzymes), albeit in a different binding mode (which may allow for design of ALKBH5-specific inhibitors, although few inhibitors have been reported). Malacrida et al. found that the compound MV1035 could inhibit ALKBH5 within the U87 glioblastoma cell line and reduce cell migration and invasiveness, showing promise for treating ALKBH5-dependent neoplasia[322]. Selberg et al. also identify two new ALKBH5 inhibitors that show efficacy in a few AML cell lines[323]. Though more research is needed, development of ALKBH5 inhibitory compounds shows exciting promise.

m^{6}A Readers

Although earlier studies focused on the balance between m^{6}A writer and eraser activity, studies now show that change in m^{6}A reader function can be just as crucial, given their role in

mediating the metabolism and fate of RNAs. We will now discuss the disease relevance of m^6A readers and some of their underlying mechanisms, mostly focusing on the YTH domain-containing protein family, which possess a pocket specific for recognizing m^6A.

YTHDF1 promotes translation of methylated transcripts in cancer cells and is cell context-dependent[79]. It is also involved in tumorigenesis. In NSCLC, YTHDF1 upregulates translation of cell cycle regulators[324]. Moreover, in hypoxic conditions, YTHDF1 expression falls, permitting NRF2 upregulation and resistance to cisplatin. In colorectal and intestinal cancer stem cells, as well as in gastric cancer, YTHDF1 upregulates translation of m^6A-methylated genes in the WNT signaling pathway, thereby promoting stemness[325-327]. In ovarian cancer, YTHDF1 increases translation of *EIF3C* and *TRIM29* in an m^6A-dependent manner to increase metastasis and cancer stem cells, respectively[328, 329].

YTHDF3 has been reported to promote the translational efficiency or decay of its targets[80, 81]; this includes facilitating translation of m^6A-methylated circular RNAs and during a heat shock response[158, 330]. Elsewhere, YTHDF3 was shown to suppress antiviral Type I interferon signaling by promoting the translation of *FOXO3* mRNA[129]. In CRC, YTHDF3 binds and degrades m^6A-modified lncRNA *GAS5*, which stabilizes YAP, thereby permitting CRC tumor progression.

Small molecule inhibitors specific for each m^6A reader are needed. The YTH domains all have highly conserved aromatic residues that form a hydrophobic core critical for discriminative recognition and binding of m^6A-modified RNA[331, 332]. These pockets of the three YTHDF proteins are quite similar, which may complicate development of specific inhibitors to each member of YTHDF proteins. Thus far, Bedi et al. have identified 30 small molecules that can disrupt the m^6A-YTHDC1 interaction, which holds promise for future development[333].

Concluding Remarks

Throughout the past decade, our understanding of how m^6A methylation impacts gene expression has rapidly transformed. After the identification of m^6A regulatory proteins, their pivotal role in development and disease processes has also been established, and, subsequently, researchers have sought ways to chemically modulate their activity. Combing pharmacological inhibition of m^6A proteins with other established cancer therapies may prove to enhance efficacy from a clinical standpoint. Of course, challenges remain in developing molecules with high selectivity and potency in vivo, but as our understanding of RNA modifications matures, so will our ability to target mRNA modifications as a means of treating pathophysiological processes.

References

1. Andersson, R. and A. Sandelin, *Determinants of enhancer and promoter activities of regulatory elements.* Nat Rev Genet, 2020. **21**(2): p. 71-87.

2. Holliday, R., *Epigenetics: a historical overview.* Epigenetics, 2006. **1**(2): p. 76-80.

3. Avery, O.T., C.M. Macleod, and M. McCarty, *Studies on the Chemical Nature of the Substance Inducing Transformation of Pneumococcal Types : Induction of Transformation by a Desoxyribonucleic Acid Fraction Isolated from Pneumococcus Type Iii.* J Exp Med, 1944. **79**(2): p. 137-58.

4. Waddington, C.H., *The epigenotype. 1942.* Int J Epidemiol, 2012. **41**(1): p. 10-3.

5. Deichmann, U., *Epigenetics: The origins and evolution of a fashionable topic.* Dev Biol, 2016. **416**(1): p. 249-254.

6. Bannister, A.J. and T. Kouzarides, *Regulation of chromatin by histone modifications.* Cell Res, 2011. **21**(3): p. 381-95.

7. Holliday, R. and J.E. Pugh, *DNA modification mechanisms and gene activity during development.* Science, 1975. **187**(4173): p. 226-32.

8. Jones, P.A., *Functions of DNA methylation: islands, start sites, gene bodies and beyond.* Nat Rev Genet, 2012. **13**(7): p. 484-92.

9. Breiling, A. and F. Lyko, *Epigenetic regulatory functions of DNA modifications: 5-methylcytosine and beyond.* Epigenetics Chromatin, 2015. **8**: p. 24.

10. Panning, B. and R. Jaenisch, *DNA hypomethylation can activate Xist expression and silence X-linked genes.* Genes Dev, 1996. **10**(16): p. 1991-2002.

11. Pfeifer, G.P., S. Kadam, and S.G. Jin, *5-hydroxymethylcytosine and its potential roles in development and cancer.* Epigenetics Chromatin, 2013. **6**(1): p. 10.

12. Chen, J., Y.C. Zhang, C. Huang, H. Shen, B. Sun, X. Cheng, Y.J. Zhang, Y.G. Yang, Q. Shu, Y. Yang, and X. Li, *m(6)A Regulates Neurogenesis and Neuronal Development by Modulating Histone Methyltransferase Ezh2.* Genomics Proteomics Bioinformatics, 2019. **17**(2): p. 154-168.

13. Haimovich, G., M. Choder, R.H. Singer, and T. Trcek, *The fate of the messenger is pre-determined: a new model for regulation of gene expression.* Biochim Biophys Acta, 2013. **1829**(6-7): p. 643-53.

14. Boccaletto, P., M.A. Machnicka, E. Purta, P. Piatkowski, B. Baginski, T.K. Wirecki, V. de Crecy-Lagard, R. Ross, P.A. Limbach, A. Kotter, M. Helm, and J.M. Bujnicki,

MODOMICS: a database of RNA modification pathways. 2017 update. Nucleic Acids Res, 2018. **46**(D1): p. D303-D307.

15. Grosjean, H., *RNA modification: the Golden Period 1995-2015.* RNA, 2015. **21**(4): p. 625-6.

16. Suzuki, T., *The expanding world of tRNA modifications and their disease relevance.* Nat Rev Mol Cell Biol, 2021. **22**(6): p. 375-392.

17. Jackman, J.E. and J.D. Alfonzo, *Transfer RNA modifications: nature's combinatorial chemistry playground.* Wiley Interdiscip Rev RNA, 2013. **4**(1): p. 35-48.

18. Cowling, V.H., *Regulation of mRNA cap methylation.* Biochem J, 2009. **425**(2): p. 295-302.

19. Wei, C.M., A. Gershowitz, and B. Moss, *Methylated nucleotides block 5' terminus of HeLa cell messenger RNA.* Cell, 1975. **4**(4): p. 379-86.

20. Daffis, S., K.J. Szretter, J. Schriewer, J. Li, S. Youn, J. Errett, T.Y. Lin, S. Schneller, R. Zust, H. Dong, V. Thiel, G.C. Sen, V. Fensterl, W.B. Klimstra, T.C. Pierson, R.M. Buller, M. Gale, Jr., P.Y. Shi, and M.S. Diamond, *2'-O methylation of the viral mRNA cap evades host restriction by IFIT family members.* Nature, 2010. **468**(7322): p. 452-6.

21. Zust, R., L. Cervantes-Barragan, M. Habjan, R. Maier, B.W. Neuman, J. Ziebuhr, K.J. Szretter, S.C. Baker, W. Barchet, M.S. Diamond, S.G. Siddell, B. Ludewig, and V. Thiel, *Ribose 2'-O-methylation provides a molecular signature for the distinction of self and non-self mRNA dependent on the RNA sensor Mda5.* Nat Immunol, 2011. **12**(2): p. 137-43.

22. Dominissini, D., S. Nachtergaele, S. Moshitch-Moshkovitz, E. Peer, N. Kol, M.S. Ben-Haim, Q. Dai, A. Di Segni, M. Salmon-Divon, W.C. Clark, G. Zheng, T. Pan, O. Solomon, E. Eyal, V. Hershkovitz, D. Han, L.C. Dore, N. Amariglio, G. Rechavi, and C. He, *The dynamic N(1)-methyladenosine methylome in eukaryotic messenger RNA.* Nature, 2016. **530**(7591): p. 441-6.

23. Li, X., X. Xiong, K. Wang, L. Wang, X. Shu, S. Ma, and C. Yi, *Transcriptome-wide mapping reveals reversible and dynamic N(1)-methyladenosine methylome.* Nat Chem Biol, 2016. **12**(5): p. 311-6.

24. Li, X., X. Xiong, M. Zhang, K. Wang, Y. Chen, J. Zhou, Y. Mao, J. Lv, D. Yi, X.W. Chen, C. Wang, S.B. Qian, and C. Yi, *Base-Resolution Mapping Reveals Distinct m(1)A Methylome in Nuclear- and Mitochondrial-Encoded Transcripts.* Mol Cell, 2017. **68**(5): p. 993-1005 e9.

25. Safra, M., A. Sas-Chen, R. Nir, R. Winkler, A. Nachshon, D. Bar-Yaacov, M. Erlacher, W. Rossmanith, N. Stern-Ginossar, and S. Schwartz, *The m1A landscape on cytosolic and mitochondrial mRNA at single-base resolution.* Nature, 2017. **551**(7679): p. 251-255.

26. Carlile, T.M., M.F. Rojas-Duran, B. Zinshteyn, H. Shin, K.M. Bartoli, and W.V. Gilbert, *Pseudouridine profiling reveals regulated mRNA pseudouridylation in yeast and human cells.* Nature, 2014. **515**(7525): p. 143-6.

27. Schwartz, S., D.A. Bernstein, M.R. Mumbach, M. Jovanovic, R.H. Herbst, B.X. Leon-Ricardo, J.M. Engreitz, M. Guttman, R. Satija, E.S. Lander, G. Fink, and A. Regev, *Transcriptome-wide mapping reveals widespread dynamic-regulated pseudouridylation of ncRNA and mRNA.* Cell, 2014. **159**(1): p. 148-162.

28. Linder, B., A.V. Grozhik, A.O. Olarerin-George, C. Meydan, C.E. Mason, and S.R. Jaffrey, *Single-nucleotide-resolution mapping of m6A and m6Am throughout the transcriptome.* Nat Methods, 2015. **12**(8): p. 767-72.

29. Squires, J.E., H.R. Patel, M. Nousch, T. Sibbritt, D.T. Humphreys, B.J. Parker, C.M. Suter, and T. Preiss, *Widespread occurrence of 5-methylcytosine in human coding and non-coding RNA.* Nucleic Acids Res, 2012. **40**(11): p. 5023-33.

30. Arango, D., D. Sturgill, N. Alhusaini, A.A. Dillman, T.J. Sweet, G. Hanson, M. Hosogane, W.R. Sinclair, K.K. Nanan, M.D. Mandler, S.D. Fox, T.T. Zengeya, T. Andresson, J.L. Meier, J. Coller, and S. Oberdoerffer, *Acetylation of Cytidine in mRNA Promotes Translation Efficiency.* Cell, 2018. **175**(7): p. 1872-1886 e24.

31. Enroth, C., L.D. Poulsen, S. Iversen, F. Kirpekar, A. Albrechtsen, and J. Vinther, *Detection of internal N7-methylguanosine (m7G) RNA modifications by mutational profiling sequencing.* Nucleic Acids Res, 2019. **47**(20): p. e126.

32. Zhang, L.S., C. Liu, H. Ma, Q. Dai, H.L. Sun, G. Luo, Z. Zhang, L. Zhang, L. Hu, X. Dong, and C. He, *Transcriptome-wide Mapping of Internal N(7)-Methylguanosine Methylome in Mammalian mRNA.* Mol Cell, 2019. **74**(6): p. 1304-1316 e8.

33. Schaefer, M., U. Kapoor, and M.F. Jantsch, *Understanding RNA modifications: the promises and technological bottlenecks of the 'epitranscriptome'.* Open Biol, 2017. **7**(5).

34. Desrosiers, R., K. Friderici, and F. Rottman, *Identification of methylated nucleosides in messenger RNA from Novikoff hepatoma cells.* Proc Natl Acad Sci U S A, 1974. **71**(10): p. 3971-5.

35. He, C., *Grand challenge commentary: RNA epigenetics?* Nat Chem Biol, 2010. **6**(12): p. 863-5.

36. Jia, G., Y. Fu, X. Zhao, Q. Dai, G. Zheng, Y. Yang, C. Yi, T. Lindahl, T. Pan, Y.G. Yang, and C. He, *N6-methyladenosine in nuclear RNA is a major substrate of the obesity-associated FTO.* Nat Chem Biol, 2011. **7**(12): p. 885-7.

37. Frye, M., B.T. Harada, M. Behm, and C. He, *RNA modifications modulate gene expression during development.* Science, 2018. **361**(6409): p. 1346-1349.

38. Dominissini, D., S. Moshitch-Moshkovitz, S. Schwartz, M. Salmon-Divon, L. Ungar, S. Osenberg, K. Cesarkas, J. Jacob-Hirsch, N. Amariglio, M. Kupiec, R. Sorek, and G. Rechavi, *Topology of the human and mouse m6A RNA methylomes revealed by m6A-seq.* Nature, 2012. **485**(7397): p. 201-6.

39. Meyer, K.D., Y. Saletore, P. Zumbo, O. Elemento, C.E. Mason, and S.R. Jaffrey, *Comprehensive analysis of mRNA methylation reveals enrichment in 3' UTRs and near stop codons.* Cell, 2012. **149**(7): p. 1635-46.

40. Zhu, A.C. and C. He, *Global Detection of RNA Methylation by Click Degradation.* ACS Cent Sci, 2020. **6**(12): p. 2126-2129.

41. Garcia-Campos, M.A., S. Edelheit, U. Toth, M. Safra, R. Shachar, S. Viukov, R. Winkler, R. Nir, L. Lasman, A. Brandis, J.H. Hanna, W. Rossmanith, and S. Schwartz, *Deciphering the "m(6)A Code" via Antibody-Independent Quantitative Profiling.* Cell, 2019. **178**(3): p. 731-747 e16.

42. Meyer, K.D., *DART-seq: an antibody-free method for global m(6)A detection.* Nat Methods, 2019. **16**(12): p. 1275-1280.

43. Wang, Y., Y. Xiao, S. Dong, Q. Yu, and G. Jia, *Antibody-free enzyme-assisted chemical approach for detection of N(6)-methyladenosine.* Nat Chem Biol, 2020. **16**(8): p. 896-903.

44. Zhang, Z., L.Q. Chen, Y.L. Zhao, C.G. Yang, I.A. Roundtree, Z. Zhang, J. Ren, W. Xie, C. He, and G.Z. Luo, *Single-base mapping of m(6)A by an antibody-independent method.* Sci Adv, 2019. **5**(7): p. eaax0250.

45. Li, X., X. Xiong, and C. Yi, *Epitranscriptome sequencing technologies: decoding RNA modifications.* Nat Methods, 2016. **14**(1): p. 23-31.

46. Grozhik, A.V., A.O. Olarerin-George, M. Sindelar, X. Li, S.S. Gross, and S.R. Jaffrey, *Antibody cross-reactivity accounts for widespread appearance of m(1)A in 5'UTRs.* Nat Commun, 2019. **10**(1): p. 5126.

47. Akichika, S., S. Hirano, Y. Shichino, T. Suzuki, H. Nishimasu, R. Ishitani, A. Sugita, Y. Hirose, S. Iwasaki, O. Nureki, and T. Suzuki, *Cap-specific terminal N (6)-methylation of RNA by an RNA polymerase II-associated methyltransferase.* Science, 2019. **363**(6423).

48. Zhang, L.S., Q.P. Xiong, S. Pena Perez, C. Liu, J. Wei, C. Le, L. Zhang, B.T. Harada, Q. Dai, X. Feng, Z. Hao, Y. Wang, X. Dong, L. Hu, E.D. Wang, T. Pan, A. Klungland, R.J. Liu, and C. He, *ALKBH7-mediated demethylation regulates mitochondrial polycistronic RNA processing.* Nat Cell Biol, 2021. **23**(7): p. 684-691.

49. Roundtree, I.A., M.E. Evans, T. Pan, and C. He, *Dynamic RNA Modifications in Gene Expression Regulation.* Cell, 2017. **169**(7): p. 1187-1200.

50. Liu, J., Y. Yue, D. Han, X. Wang, Y. Fu, L. Zhang, G. Jia, M. Yu, Z. Lu, X. Deng, Q. Dai, W. Chen, and C. He, *A METTL3-METTL14 complex mediates mammalian nuclear RNA N6-adenosine methylation.* Nat Chem Biol, 2014. **10**(2): p. 93-5.

51. Wang, X., J. Huang, T. Zou, and P. Yin, *Human m(6)A writers: Two subunits, 2 roles.* RNA Biol, 2017. **14**(3): p. 300-304.

52. Wang, P., K.A. Doxtader, and Y. Nam, *Structural Basis for Cooperative Function of Mettl3 and Mettl14 Methyltransferases.* Mol Cell, 2016. **63**(2): p. 306-317.

53. Wang, X., J. Feng, Y. Xue, Z. Guan, D. Zhang, Z. Liu, Z. Gong, Q. Wang, J. Huang, C. Tang, T. Zou, and P. Yin, *Structural basis of N(6)-adenosine methylation by the METTL3-METTL14 complex.* Nature, 2016. **534**(7608): p. 575-8.

54. Ping, X.L., B.F. Sun, L. Wang, W. Xiao, X. Yang, W.J. Wang, S. Adhikari, Y. Shi, Y. Lv, Y.S. Chen, X. Zhao, A. Li, Y. Yang, U. Dahal, X.M. Lou, X. Liu, J. Huang, W.P. Yuan, X.F. Zhu, T. Cheng, Y.L. Zhao, X. Wang, J.M. Rendtlew Danielsen, F. Liu, and Y.G. Yang, *Mammalian WTAP is a regulatory subunit of the RNA N6-methyladenosine methyltransferase.* Cell Res, 2014. **24**(2): p. 177-89.

55. Zhong, S., H. Li, Z. Bodi, J. Button, L. Vespa, M. Herzog, and R.G. Fray, *MTA is an Arabidopsis messenger RNA adenosine methylase and interacts with a homolog of a sex-specific splicing factor.* Plant Cell, 2008. **20**(5): p. 1278-88.

56. Meyer, K.D. and S.R. Jaffrey, *Rethinking m(6)A Readers, Writers, and Erasers.* Annu Rev Cell Dev Biol, 2017. **33**: p. 319-342.

57. Wen, J., R. Lv, H. Ma, H. Shen, C. He, J. Wang, F. Jiao, H. Liu, P. Yang, L. Tan, F. Lan, Y.G. Shi, C. He, Y. Shi, and J. Diao, *Zc3h13 Regulates Nuclear RNA m(6)A Methylation and Mouse Embryonic Stem Cell Self-Renewal.* Mol Cell, 2018. **69**(6): p. 1028-1038 e6.

58. Knuckles, P., T. Lence, I.U. Haussmann, D. Jacob, N. Kreim, S.H. Carl, I. Masiello, T. Hares, R. Villasenor, D. Hess, M.A. Andrade-Navarro, M. Biggiogera, M. Helm, M. Soller, M. Buhler, and J.Y. Roignant, *Zc3h13/Flacc is required for adenosine methylation by bridging the mRNA-binding factor Rbm15/Spenito to the m(6)A machinery component Wtap/Fl(2)d.* Genes Dev, 2018. **32**(5-6): p. 415-429.

59. Yue, Y., J. Liu, X. Cui, J. Cao, G. Luo, Z. Zhang, T. Cheng, M. Gao, X. Shu, H. Ma, F. Wang, X. Wang, B. Shen, Y. Wang, X. Feng, C. He, and J. Liu, *VIRMA mediates preferential m(6)A mRNA methylation in 3'UTR and near stop codon and associates with alternative polyadenylation.* Cell Discov, 2018. **4**: p. 10.

60. Schwartz, S., M.R. Mumbach, M. Jovanovic, T. Wang, K. Maciag, G.G. Bushkin, P. Mertins, D. Ter-Ovanesyan, N. Habib, D. Cacchiarelli, N.E. Sanjana, E. Freinkman, M.E. Pacold, R. Satija, T.S. Mikkelsen, N. Hacohen, F. Zhang, S.A. Carr, E.S. Lander, and A. Regev, *Perturbation of m6A writers reveals two distinct classes of mRNA methylation at internal and 5' sites.* Cell Rep, 2014. **8**(1): p. 284-96.

61. Horiuchi, K., T. Kawamura, H. Iwanari, R. Ohashi, M. Naito, T. Kodama, and T. Hamakubo, *Identification of Wilms' tumor 1-associating protein complex and its role in alternative splicing and the cell cycle.* J Biol Chem, 2013. **288**(46): p. 33292-302.

62. Lence, T., J. Akhtar, M. Bayer, K. Schmid, L. Spindler, C.H. Ho, N. Kreim, M.A. Andrade-Navarro, B. Poeck, M. Helm, and J.Y. Roignant, *m(6)A modulates neuronal functions and sex determination in Drosophila.* Nature, 2016. **540**(7632): p. 242-247.

63. Patil, D.P., C.K. Chen, B.F. Pickering, A. Chow, C. Jackson, M. Guttman, and S.R. Jaffrey, *m(6)A RNA methylation promotes XIST-mediated transcriptional repression.* Nature, 2016. **537**(7620): p. 369-373.

64. Pendleton, K.E., B. Chen, K. Liu, O.V. Hunter, Y. Xie, B.P. Tu, and N.K. Conrad, *The U6 snRNA m(6)A Methyltransferase METTL16 Regulates SAM Synthetase Intron Retention.* Cell, 2017. **169**(5): p. 824-835 e14.

65. van Tran, N., F.G.M. Ernst, B.R. Hawley, C. Zorbas, N. Ulryck, P. Hackert, K.E. Bohnsack, M.T. Bohnsack, S.R. Jaffrey, M. Graille, and D.L.J. Lafontaine, *The human 18S rRNA m6A methyltransferase METTL5 is stabilized by TRMT112.* Nucleic Acids Res, 2019. **47**(15): p. 7719-7733.

66. Ma, H., X. Wang, J. Cai, Q. Dai, S.K. Natchiar, R. Lv, K. Chen, Z. Lu, H. Chen, Y.G. Shi, F. Lan, J. Fan, B.P. Klaholz, T. Pan, Y. Shi, and C. He, *N(6-)Methyladenosine methyltransferase ZCCHC4 mediates ribosomal RNA methylation.* Nat Chem Biol, 2019. **15**(1): p. 88-94.

67. Xing, M., Q. Liu, C. Mao, H. Zeng, X. Zhang, S. Zhao, L. Chen, M. Liu, B. Shen, X. Guo, H. Ma, H. Chen, and J. Zhang, *The 18S rRNA m(6) A methyltransferase METTL5 promotes mouse embryonic stem cell differentiation.* EMBO Rep, 2020. **21**(10): p. e49863.

68. Ren, W., J. Lu, M. Huang, L. Gao, D. Li, G.G. Wang, and J. Song, *Structure and regulation of ZCCHC4 in m(6)A-methylation of 28S rRNA.* Nat Commun, 2019. **10**(1): p. 5042.

69. Pinto, R., C.B. Vagbo, M.E. Jakobsson, Y. Kim, M.P. Baltissen, M.F. O'Donohue, U.H. Guzman, J.M. Malecki, J. Wu, F. Kirpekar, J.V. Olsen, P.E. Gleizes, M. Vermeulen, S.A. Leidel, G. Slupphaug, and P.O. Falnes, *The human methyltransferase ZCCHC4 catalyses N6-methyladenosine modification of 28S ribosomal RNA.* Nucleic Acids Res, 2020. **48**(2): p. 830-846.

70. Zheng, G., J.A. Dahl, Y. Niu, P. Fedorcsak, C.M. Huang, C.J. Li, C.B. Vagbo, Y. Shi, W.L. Wang, S.H. Song, Z. Lu, R.P. Bosmans, Q. Dai, Y.J. Hao, X. Yang, W.M. Zhao, W.M. Tong, X.J. Wang, F. Bogdan, K. Furu, Y. Fu, G. Jia, X. Zhao, J. Liu, H.E. Krokan, A. Klungland, Y.G. Yang, and C. He, *ALKBH5 is a mammalian RNA demethylase that impacts RNA metabolism and mouse fertility.* Mol Cell, 2013. **49**(1): p. 18-29.

71. Gerken, T., C.A. Girard, Y.C. Tung, C.J. Webby, V. Saudek, K.S. Hewitson, G.S. Yeo, M.A. McDonough, S. Cunliffe, L.A. McNeill, J. Galvanovskis, P. Rorsman, P. Robins, X. Prieur, A.P. Coll, M. Ma, Z. Jovanovic, I.S. Farooqi, B. Sedgwick, I. Barroso, T. Lindahl, C.P. Ponting, F.M. Ashcroft, S. O'Rahilly, and C.J. Schofield, *The obesity-associated FTO gene encodes a 2-oxoglutarate-dependent nucleic acid demethylase.* Science, 2007. **318**(5855): p. 1469-72.

72. Fu, Y., G. Jia, X. Pang, R.N. Wang, X. Wang, C.J. Li, S. Smemo, Q. Dai, K.A. Bailey, M.A. Nobrega, K.L. Han, Q. Cui, and C. He, *FTO-mediated formation of N6-hydroxymethyladenosine and N6-formyladenosine in mammalian RNA.* Nat Commun, 2013. **4**: p. 1798.

73. Wei, J., F. Liu, Z. Lu, Q. Fei, Y. Ai, P.C. He, H. Shi, X. Cui, R. Su, A. Klungland, G. Jia, J. Chen, and C. He, *Differential m(6)A, m(6)Am, and m(1)A Demethylation Mediated by FTO in the Cell Nucleus and Cytoplasm.* Mol Cell, 2018. **71**(6): p. 973-985 e5.

74. Tang, C., R. Klukovich, H. Peng, Z. Wang, T. Yu, Y. Zhang, H. Zheng, A. Klungland, and W. Yan, *ALKBH5-dependent m6A demethylation controls splicing and stability of long 3′-UTR mRNAs in male germ cells.* Proc Natl Acad Sci U S A, 2018. **115**(2): p. E325-E333.

75. Li, F., D. Zhao, J. Wu, and Y. Shi, *Structure of the YTH domain of human YTHDF2 in complex with an m(6)A mononucleotide reveals an aromatic cage for m(6)A recognition.* Cell Res, 2014. **24**(12): p. 1490-2.

76. Zhu, T., I.A. Roundtree, P. Wang, X. Wang, L. Wang, C. Sun, Y. Tian, J. Li, C. He, and Y. Xu, *Crystal structure of the YTH domain of YTHDF2 reveals mechanism for recognition of N6-methyladenosine.* Cell Res, 2014. **24**(12): p. 1493-6.

77. Xu, C., X. Wang, K. Liu, I.A. Roundtree, W. Tempel, Y. Li, Z. Lu, C. He, and J. Min, *Structural basis for selective binding of m6A RNA by the YTHDC1 YTH domain.* Nat Chem Biol, 2014. **10**(11): p. 927-9.

78. Wang, X., Z. Lu, A. Gomez, G.C. Hon, Y. Yue, D. Han, Y. Fu, M. Parisien, Q. Dai, G. Jia, B. Ren, T. Pan, and C. He, *N6-methyladenosine-dependent regulation of messenger RNA stability.* Nature, 2014. **505**(7481): p. 117-20.

79. Wang, X., B.S. Zhao, I.A. Roundtree, Z. Lu, D. Han, H. Ma, X. Weng, K. Chen, H. Shi, and C. He, *N(6)-methyladenosine Modulates Messenger RNA Translation Efficiency.* Cell, 2015. **161**(6): p. 1388-99.

80. Shi, H., X. Wang, Z. Lu, B.S. Zhao, H. Ma, P.J. Hsu, C. Liu, and C. He, *YTHDF3 facilitates translation and decay of N(6)-methyladenosine-modified RNA.* Cell Res, 2017. **27**(3): p. 315-328.

81. Li, A., Y.S. Chen, X.L. Ping, X. Yang, W. Xiao, Y. Yang, H.Y. Sun, Q. Zhu, P. Baidya, X. Wang, D.P. Bhattarai, Y.L. Zhao, B.F. Sun, and Y.G. Yang, *Cytoplasmic m(6)A reader YTHDF3 promotes mRNA translation.* Cell Res, 2017. **27**(3): p. 444-447.

82. Xiao, W., S. Adhikari, U. Dahal, Y.S. Chen, Y.J. Hao, B.F. Sun, H.Y. Sun, A. Li, X.L. Ping, W.Y. Lai, X. Wang, H.L. Ma, C.M. Huang, Y. Yang, N. Huang, G.B. Jiang, H.L. Wang, Q. Zhou, X.J. Wang, Y.L. Zhao, and Y.G. Yang, *Nuclear m(6)A Reader YTHDC1 Regulates mRNA Splicing.* Mol Cell, 2016. **61**(4): p. 507-519.

83. Roundtree, I.A., G.Z. Luo, Z. Zhang, X. Wang, T. Zhou, Y. Cui, J. Sha, X. Huang, L. Guerrero, P. Xie, E. He, B. Shen, and C. He, *YTHDC1 mediates nuclear export of N(6)-methyladenosine methylated mRNAs.* Elife, 2017. **6**.

84. Liu, J., X. Dou, C. Chen, C. Chen, C. Liu, M.M. Xu, S. Zhao, B. Shen, Y. Gao, D. Han, and C. He, *N (6)-methyladenosine of chromosome-associated regulatory RNA regulates chromatin state and transcription.* Science, 2020. **367**(6477): p. 580-586.

85. Hsu, P.J., Y. Zhu, H. Ma, Y. Guo, X. Shi, Y. Liu, M. Qi, Z. Lu, H. Shi, J. Wang, Y. Cheng, G. Luo, Q. Dai, M. Liu, X. Guo, J. Sha, B. Shen, and C. He, *Ythdc2 is an N(6)-methyladenosine binding protein that regulates mammalian spermatogenesis.* Cell Res, 2017. **27**(9): p. 1115-1127.

86. Wojtas, M.N., R.R. Pandey, M. Mendel, D. Homolka, R. Sachidanandam, and R.S. Pillai, *Regulation of m(6)A Transcripts by the 3'-->5' RNA Helicase YTHDC2 Is Essential for a Successful Meiotic Program in the Mammalian Germline.* Mol Cell, 2017. **68**(2): p. 374-387 e12.

87. Mao, Y., L. Dong, X.M. Liu, J. Guo, H. Ma, B. Shen, and S.B. Qian, *m(6)A in mRNA coding regions promotes translation via the RNA helicase-containing YTHDC2.* Nat Commun, 2019. **10**(1): p. 5332.

88. Huang, H., H. Weng, W. Sun, X. Qin, H. Shi, H. Wu, B.S. Zhao, A. Mesquita, C. Liu, C.L. Yuan, Y.C. Hu, S. Huttelmaier, J.R. Skibbe, R. Su, X. Deng, L. Dong, M. Sun, C. Li, S. Nachtergaele, Y. Wang, C. Hu, K. Ferchen, K.D. Greis, X. Jiang, M. Wei, L. Qu, J.L. Guan, C. He, J. Yang, and J. Chen, *Recognition of RNA N(6)-methyladenosine by IGF2BP proteins enhances mRNA stability and translation.* Nat Cell Biol, 2018. **20**(3): p. 285-295.

89. Zhou, K.I., H. Shi, R. Lyu, A.C. Wylder, Z. Matuszek, J.N. Pan, C. He, M. Parisien, and T. Pan, *Regulation of Co-transcriptional Pre-mRNA Splicing by m(6)A through the Low-Complexity Protein hnRNPG.* Mol Cell, 2019. **76**(1): p. 70-81 e9.

90. Liu, N., K.I. Zhou, M. Parisien, Q. Dai, L. Diatchenko, and T. Pan, *N6-methyladenosine alters RNA structure to regulate binding of a low-complexity protein.* Nucleic Acids Res, 2017. **45**(10): p. 6051-6063.

91. Alarcon, C.R., H. Goodarzi, H. Lee, X. Liu, S. Tavazoie, and S.F. Tavazoie, *HNRNPA2B1 Is a Mediator of m(6)A-Dependent Nuclear RNA Processing Events.* Cell, 2015. **162**(6): p. 1299-308.

92. Liu, N., Q. Dai, G. Zheng, C. He, M. Parisien, and T. Pan, *N(6)-methyladenosine-dependent RNA structural switches regulate RNA-protein interactions.* Nature, 2015. **518**(7540): p. 560-4.

93. Hsu, P.J., H. Shi, A.C. Zhu, Z. Lu, N. Miller, B.M. Edens, Y.C. Ma, and C. He, *The RNA-binding protein FMRP facilitates the nuclear export of N (6)-methyladenosine-containing mRNAs.* J Biol Chem, 2019. **294**(52): p. 19889-19895.

94. Liu, J., M. Gao, S. Xu, Y. Chen, K. Wu, H. Liu, J. Wang, X. Yang, J. Wang, W. Liu, X. Bao, and J. Chen, *YTHDF2/3 Are Required for Somatic Reprogramming through Different RNA Deadenylation Pathways.* Cell Rep, 2020. **32**(10): p. 108120.

95. Zaccara, S. and S.R. Jaffrey, *A Unified Model for the Function of YTHDF Proteins in Regulating m(6)A-Modified mRNA.* Cell, 2020. **181**(7): p. 1582-1595 e18.

96. Li, Y., R.K. Bedi, E.V. Moroz-Omori, and A. Caflisch, *Structural and Dynamic Insights into Redundant Function of YTHDF Proteins.* J Chem Inf Model, 2020. **60**(12): p. 5932-5935.

97. Lasman, L., V. Krupalnik, S. Viukov, N. Mor, A. Aguilera-Castrejon, D. Schneir, J. Bayerl, O. Mizrahi, S. Peles, S. Tawil, S. Sathe, A. Nachshon, T. Shani, M. Zerbib, I. Kilimnik, S. Aigner, A. Shankar, J.R. Mueller, S. Schwartz, N. Stern-Ginossar, G.W. Yeo, S. Geula, N. Novershtern, and J.H. Hanna, *Context-dependent functional compensation between Ythdf m(6)A reader proteins.* Genes Dev, 2020. **34**(19-20): p. 1373-1391.

98. Batista, P.J., B. Molinie, J. Wang, K. Qu, J. Zhang, L. Li, D.M. Bouley, E. Lujan, B. Haddad, K. Daneshvar, A.C. Carter, R.A. Flynn, C. Zhou, K.S. Lim, P. Dedon, M. Wernig, A.C. Mullen, Y. Xing, C.C. Giallourakis, and H.Y. Chang, *m(6)A RNA modification controls cell fate transition in mammalian embryonic stem cells.* Cell Stem Cell, 2014. **15**(6): p. 707-19.

99. Bertero, A., S. Brown, P. Madrigal, A. Osnato, D. Ortmann, L. Yiangou, J. Kadiwala, N.C. Hubner, I.R. de Los Mozos, C. Sadee, A.S. Lenaerts, S. Nakanoh, R. Grandy, E. Farnell, J. Ule, H.G. Stunnenberg, S. Mendjan, and L. Vallier, *The SMAD2/3 interactome reveals that TGFbeta controls m(6)A mRNA methylation in pluripotency.* Nature, 2018. **555**(7695): p. 256-259.

100. Wang, Y., Y. Li, J.I. Toth, M.D. Petroski, Z. Zhang, and J.C. Zhao, *N6-methyladenosine modification destabilizes developmental regulators in embryonic stem cells.* Nat Cell Biol, 2014. **16**(2): p. 191-8.

101. Geula, S., S. Moshitch-Moshkovitz, D. Dominissini, A.A. Mansour, N. Kol, M. Salmon-Divon, V. Hershkovitz, E. Peer, N. Mor, Y.S. Manor, M.S. Ben-Haim, E. Eyal, S. Yunger, Y. Pinto, D.A. Jaitin, S. Viukov, Y. Rais, V. Krupalnik, E. Chomsky, M. Zerbib, I. Maza, Y. Rechavi, R. Massarwa, S. Hanna, I. Amit, E.Y. Levanon, N. Amariglio, N. Stern-Ginossar, N. Novershtern, G. Rechavi, and J.H. Hanna, *Stem cells. m6A mRNA*

methylation facilitates resolution of naive pluripotency toward differentiation. Science, 2015. **347**(6225): p. 1002-6.

102. Cheng, Y., H. Luo, F. Izzo, B.F. Pickering, D. Nguyen, R. Myers, A. Schurer, S. Gourkanti, J.C. Bruning, L.P. Vu, S.R. Jaffrey, D.A. Landau, and M.G. Kharas, *m(6)A RNA Methylation Maintains Hematopoietic Stem Cell Identity and Symmetric Commitment.* Cell Rep, 2019. **28**(7): p. 1703-1716 e6.

103. Lee, H., S. Bao, Y. Qian, S. Geula, J. Leslie, C. Zhang, J.H. Hanna, and L. Ding, *Stage-specific requirement for Mettl3-dependent m(6)A mRNA methylation during haematopoietic stem cell differentiation.* Nat Cell Biol, 2019. **21**(6): p. 700-709.

104. Yoon, K.J., F.R. Ringeling, C. Vissers, F. Jacob, M. Pokrass, D. Jimenez-Cyrus, Y. Su, N.S. Kim, Y. Zhu, L. Zheng, S. Kim, X. Wang, L.C. Dore, P. Jin, S. Regot, X. Zhuang, S. Canzar, C. He, G.L. Ming, and H. Song, *Temporal Control of Mammalian Cortical Neurogenesis by m(6)A Methylation.* Cell, 2017. **171**(4): p. 877-889 e17.

105. Zhang, Z., M. Wang, D. Xie, Z. Huang, L. Zhang, Y. Yang, D. Ma, W. Li, Q. Zhou, Y.G. Yang, and X.J. Wang, *METTL3-mediated N(6)-methyladenosine mRNA modification enhances long-term memory consolidation.* Cell Res, 2018. **28**(11): p. 1050-1061.

106. Li, Z., P. Qian, W. Shao, H. Shi, X.C. He, M. Gogol, Z. Yu, Y. Wang, M. Qi, Y. Zhu, J.M. Perry, K. Zhang, F. Tao, K. Zhou, D. Hu, Y. Han, C. Zhao, R. Alexander, H. Xu, S. Chen, A. Peak, K. Hall, M. Peterson, A. Perera, J.S. Haug, T. Parmely, H. Li, B. Shen, J. Zeitlinger, C. He, and L. Li, *Suppression of m(6)A reader Ythdf2 promotes hematopoietic stem cell expansion.* Cell Res, 2018. **28**(9): p. 904-917.

107. Wang, H., H. Zuo, J. Liu, F. Wen, Y. Gao, X. Zhu, B. Liu, F. Xiao, W. Wang, G. Huang, B. Shen, and Z. Ju, *Loss of YTHDF2-mediated m(6)A-dependent mRNA clearance facilitates hematopoietic stem cell regeneration.* Cell Res, 2018. **28**(10): p. 1035-1038.

108. Li, H.B., J. Tong, S. Zhu, P.J. Batista, E.E. Duffy, J. Zhao, W. Bailis, G. Cao, L. Kroehling, Y. Chen, G. Wang, J.P. Broughton, Y.G. Chen, Y. Kluger, M.D. Simon, H.Y. Chang, Z. Yin, and R.A. Flavell, *m(6)A mRNA methylation controls T cell homeostasis by targeting the IL-7/STAT5/SOCS pathways.* Nature, 2017. **548**(7667): p. 338-342.

109. Yao, Y., Y. Yang, W. Guo, L. Xu, M. You, Y.C. Zhang, Z. Sun, X. Cui, G. Yu, Z. Qi, J. Liu, F. Wang, J. Liu, T. Zhao, L. Ye, Y.G. Yang, and S. Yu, *METTL3-dependent m(6)A modification programs T follicular helper cell differentiation.* Nat Commun, 2021. **12**(1): p. 1333.

110. Wang, H., X. Hu, M. Huang, J. Liu, Y. Gu, L. Ma, Q. Zhou, and X. Cao, *Mettl3-mediated mRNA m(6)A methylation promotes dendritic cell activation.* Nat Commun, 2019. **10**(1): p. 1898.

111. Zheng, Z., L. Zhang, X.L. Cui, X. Yu, P.J. Hsu, R. Lyu, H. Tan, M. Mandal, M. Zhang, H.L. Sun, A. Sanchez Castillo, J. Peng, M.R. Clark, C. He, and H. Huang, *Control of*

Early B Cell Development by the RNA N(6)-Methyladenosine Methylation. Cell Rep, 2020. **31**(13): p. 107819.

112. Grenov, A.C., L. Moss, S. Edelheit, R. Cordiner, D. Schmiedel, A. Biram, J.H. Hanna, T.H. Jensen, S. Schwartz, and Z. Shulman, *B Cell Division Capacity in Germinal Centers Depends on Myc Transcript Stabilization Through m⁶A mRNA Methylation and IGF2BP3 Functions.* bioRxiv, 2020: p. 2020.09.08.287433.

113. Han, D., J. Liu, C. Chen, L. Dong, Y. Liu, R. Chang, X. Huang, Y. Liu, J. Wang, U. Dougherty, M.B. Bissonnette, B. Shen, R.R. Weichselbaum, M.M. Xu, and C. He, *Anti-tumour immunity controlled through mRNA m(6)A methylation and YTHDF1 in dendritic cells.* Nature, 2019. **566**(7743): p. 270-274.

114. Kim, D.J. and A. Iwasaki, *YTHDF1 Control of Dendritic Cell Cross-Priming as a Possible Target of Cancer Immunotherapy.* Biochemistry, 2019. **58**(15): p. 1945-1946.

115. Liu, Y., G. Liang, H. Xu, W. Dong, Z. Dong, Z. Qiu, Z. Zhang, F. Li, Y. Huang, Y. Li, J. Wu, S. Yin, Y. Zhang, P. Guo, J. Liu, J.J. Xi, P. Jiang, D. Han, C.G. Yang, and M.M. Xu, *Tumors exploit FTO-mediated regulation of glycolytic metabolism to evade immune surveillance.* Cell Metab, 2021. **33**(6): p. 1221-1233 e11.

116. Baghban, R., L. Roshangar, R. Jahanban-Esfahlan, K. Seidi, A. Ebrahimi-Kalan, M. Jaymand, S. Kolahian, T. Javaheri, and P. Zare, *Tumor microenvironment complexity and therapeutic implications at a glance.* Cell Commun Signal, 2020. **18**(1): p. 59.

117. Dong, L., C. Chen, Y. Zhang, P. Guo, Z. Wang, J. Li, Y. Liu, J. Liu, R. Chang, Y. Li, G. Liang, W. Lai, M. Sun, U. Dougherty, M.B. Bissonnette, H. Wang, L. Shen, M.M. Xu, and D. Han, *The loss of RNA N(6)-adenosine methyltransferase Mettl14 in tumor-associated macrophages promotes CD8(+) T cell dysfunction and tumor growth.* Cancer Cell, 2021.

118. Vu, L.P., B.F. Pickering, Y. Cheng, S. Zaccara, D. Nguyen, G. Minuesa, T. Chou, A. Chow, Y. Saletore, M. MacKay, J. Schulman, C. Famulare, M. Patel, V.M. Klimek, F.E. Garrett-Bakelman, A. Melnick, M. Carroll, C.E. Mason, S.R. Jaffrey, and M.G. Kharas, *The N(6)-methyladenosine (m(6)A)-forming enzyme METTL3 controls myeloid differentiation of normal hematopoietic and leukemia cells.* Nat Med, 2017. **23**(11): p. 1369-1376.

119. Barbieri, I., K. Tzelepis, L. Pandolfini, J. Shi, G. Millan-Zambrano, S.C. Robson, D. Aspris, V. Migliori, A.J. Bannister, N. Han, E. De Braekeleer, H. Ponstingl, A. Hendrick, C.R. Vakoc, G.S. Vassiliou, and T. Kouzarides, *Promoter-bound METTL3 maintains myeloid leukaemia by m(6)A-dependent translation control.* Nature, 2017. **552**(7683): p. 126-131.

120. Liu, J., M.A. Eckert, B.T. Harada, S.M. Liu, Z. Lu, K. Yu, S.M. Tienda, A. Chryplewicz, A.C. Zhu, Y. Yang, J.T. Huang, S.M. Chen, Z.G. Xu, X.H. Leng, X.C. Yu, J. Cao, Z. Zhang, J. Liu, E. Lengyel, and C. He, *m(6)A mRNA methylation regulates AKT activity to*

promote the proliferation and tumorigenicity of endometrial cancer. Nat Cell Biol, 2018. **20**(9): p. 1074-1083.

121. Cancer Genome Atlas Research, N., C. Kandoth, N. Schultz, A.D. Cherniack, R. Akbani, Y. Liu, H. Shen, A.G. Robertson, I. Pashtan, R. Shen, C.C. Benz, C. Yau, P.W. Laird, L. Ding, W. Zhang, G.B. Mills, R. Kucherlapati, E.R. Mardis, and D.A. Levine, *Integrated genomic characterization of endometrial carcinoma.* Nature, 2013. **497**(7447): p. 67-73.

122. Li, Z., H. Weng, R. Su, X. Weng, Z. Zuo, C. Li, H. Huang, S. Nachtergaele, L. Dong, C. Hu, X. Qin, L. Tang, Y. Wang, G.M. Hong, H. Huang, X. Wang, P. Chen, S. Gurbuxani, S. Arnovitz, Y. Li, S. Li, J. Strong, M.B. Neilly, R.A. Larson, X. Jiang, P. Zhang, J. Jin, C. He, and J. Chen, *FTO Plays an Oncogenic Role in Acute Myeloid Leukemia as a N(6)-Methyladenosine RNA Demethylase.* Cancer Cell, 2017. **31**(1): p. 127-141.

123. Su, R., L. Dong, C. Li, S. Nachtergaele, M. Wunderlich, Y. Qing, X. Deng, Y. Wang, X. Weng, C. Hu, M. Yu, J. Skibbe, Q. Dai, D. Zou, T. Wu, K. Yu, H. Weng, H. Huang, K. Ferchen, X. Qin, B. Zhang, J. Qi, A.T. Sasaki, D.R. Plas, J.E. Bradner, M. Wei, G. Marcucci, X. Jiang, J.C. Mulloy, J. Jin, C. He, and J. Chen, *R-2HG Exhibits Anti-tumor Activity by Targeting FTO/m(6)A/MYC/CEBPA Signaling.* Cell, 2018. **172**(1-2): p. 90-105 e23.

124. Xu, W., H. Yang, Y. Liu, Y. Yang, P. Wang, S.H. Kim, S. Ito, C. Yang, P. Wang, M.T. Xiao, L.X. Liu, W.Q. Jiang, J. Liu, J.Y. Zhang, B. Wang, S. Frye, Y. Zhang, Y.H. Xu, Q.Y. Lei, K.L. Guan, S.M. Zhao, and Y. Xiong, *Oncometabolite 2-hydroxyglutarate is a competitive inhibitor of alpha-ketoglutarate-dependent dioxygenases.* Cancer Cell, 2011. **19**(1): p. 17-30.

125. Zhang, S., B.S. Zhao, A. Zhou, K. Lin, S. Zheng, Z. Lu, Y. Chen, E.P. Sulman, K. Xie, O. Bogler, S. Majumder, C. He, and S. Huang, *m(6)A Demethylase ALKBH5 Maintains Tumorigenicity of Glioblastoma Stem-like Cells by Sustaining FOXM1 Expression and Cell Proliferation Program.* Cancer Cell, 2017. **31**(4): p. 591-606 e6.

126. Zhang, C., D. Samanta, H. Lu, J.W. Bullen, H. Zhang, I. Chen, X. He, and G.L. Semenza, *Hypoxia induces the breast cancer stem cell phenotype by HIF-dependent and ALKBH5-mediated m(6)A-demethylation of NANOG mRNA.* Proc Natl Acad Sci U S A, 2016. **113**(14): p. E2047-56.

127. Chen, M., L. Wei, C.T. Law, F.H. Tsang, J. Shen, C.L. Cheng, L.H. Tsang, D.W. Ho, D.K. Chiu, J.M. Lee, C.C. Wong, I.O. Ng, and C.M. Wong, *RNA N6-methyladenosine methyltransferase-like 3 promotes liver cancer progression through YTHDF2-dependent posttranscriptional silencing of SOCS2.* Hepatology, 2018. **67**(6): p. 2254-2270.

128. Chang, G., L. Shi, Y. Ye, H. Shi, L. Zeng, S. Tiwary, J.T. Huse, L. Huo, L. Ma, Y. Ma, S. Zhang, J. Zhu, V. Xie, P. Li, L. Han, C. He, and S. Huang, *YTHDF3 Induces the Translation of m(6)A-Enriched Gene Transcripts to Promote Breast Cancer Brain Metastasis.* Cancer Cell, 2020. **38**(6): p. 857-871 e7.

129. Zhang, Y., X. Wang, X. Zhang, J. Wang, Y. Ma, L. Zhang, and X. Cao, *RNA-binding protein YTHDF3 suppresses interferon-dependent antiviral responses by promoting FOXO3 translation.* Proc Natl Acad Sci U S A, 2019. **116**(3): p. 976-981.

130. Wei, J. and C. He, *Chromatin and transcriptional regulation by reversible RNA methylation.* Curr Opin Cell Biol, 2021. **70**: p. 109-115.

131. Chelmicki, T., E. Roger, A. Teissandier, M. Dura, L. Bonneville, S. Rucli, F. Dossin, C. Fouassier, S. Lameiras, and D. Bourc'his, *m(6)A RNA methylation regulates the fate of endogenous retroviruses.* Nature, 2021. **591**(7849): p. 312-316.

132. Liu, J., M. Gao, J. He, K. Wu, S. Lin, L. Jin, Y. Chen, H. Liu, J. Shi, X. Wang, L. Chang, Y. Lin, Y.L. Zhao, X. Zhang, M. Zhang, G.Z. Luo, G. Wu, D. Pei, J. Wang, X. Bao, and J. Chen, *The RNA m(6)A reader YTHDC1 silences retrotransposons and guards ES cell identity.* Nature, 2021. **591**(7849): p. 322-326.

133. Xu, W., J. Li, C. He, J. Wen, H. Ma, B. Rong, J. Diao, L. Wang, J. Wang, F. Wu, L. Tan, Y.G. Shi, Y. Shi, and H. Shen, *METTL3 regulates heterochromatin in mouse embryonic stem cells.* Nature, 2021. **591**(7849): p. 317-321.

134. Chen, C., W. Liu, J. Guo, Y. Liu, X. Liu, J. Liu, X. Dou, R. Le, Y. Huang, C. Li, L. Yang, X. Kou, Y. Zhao, Y. Wu, J. Chen, H. Wang, B. Shen, Y. Gao, and S. Gao, *Nuclear m(6)A reader YTHDC1 regulates the scaffold function of LINE1 RNA in mouse ESCs and early embryos.* Protein Cell, 2021. **12**(6): p. 455-474.

135. Prabakaran, S., G. Lippens, H. Steen, and J. Gunawardena, *Post-translational modification: nature's escape from genetic imprisonment and the basis for dynamic information encoding.* Wiley Interdiscip Rev Syst Biol Med, 2012. **4**(6): p. 565-83.

136. Barber, K.W. and J. Rinehart, *The ABCs of PTMs.* Nat Chem Biol, 2018. **14**(3): p. 188-192.

137. Muller, M.M., *Post-Translational Modifications of Protein Backbones: Unique Functions, Mechanisms, and Challenges.* Biochemistry, 2018. **57**(2): p. 177-185.

138. Lothrop, A.P., M.P. Torres, and S.M. Fuchs, *Deciphering post-translational modification codes.* FEBS Lett, 2013. **587**(8): p. 1247-57.

139. Ramazi, S. and J. Zahiri, *Posttranslational modifications in proteins: resources, tools and prediction methods.* Database (Oxford), 2021. **2021**.

140. Levene, P.A. and C.L. Alsberg, *The Cleavage Products of Vitellin.* Journal of Biological Chemistry, 1906. **2**(1): p. 127-133.

141. Pawson, T. and J.D. Scott, *Protein phosphorylation in signaling--50 years and counting.* Trends Biochem Sci, 2005. **30**(6): p. 286-90.

142. Pearson, G., F. Robinson, T. Beers Gibson, B.E. Xu, M. Karandikar, K. Berman, and M.H. Cobb, *Mitogen-activated protein (MAP) kinase pathways: regulation and physiological functions.* Endocr Rev, 2001. **22**(2): p. 153-83.

143. Scheffner, M., U. Nuber, and J.M. Huibregtse, *Protein ubiquitination involving an E1-E2-E3 enzyme ubiquitin thioester cascade.* Nature, 1995. **373**(6509): p. 81-3.

144. Swatek, K.N. and D. Komander, *Ubiquitin modifications.* Cell Res, 2016. **26**(4): p. 399-422.

145. Pickart, C.M. and M.J. Eddins, *Ubiquitin: structures, functions, mechanisms.* Biochim Biophys Acta, 2004. **1695**(1-3): p. 55-72.

146. Tracz, M. and W. Bialek, *Beyond K48 and K63: non-canonical protein ubiquitination.* Cell Mol Biol Lett, 2021. **26**(1): p. 1.

147. Geiss-Friedlander, R. and F. Melchior, *Concepts in sumoylation: a decade on.* Nat Rev Mol Cell Biol, 2007. **8**(12): p. 947-56.

148. Yang, Y., Y. He, X. Wang, Z. Liang, G. He, P. Zhang, H. Zhu, N. Xu, and S. Liang, *Protein SUMOylation modification and its associations with disease.* Open Biol, 2017. **7**(10).

149. Cheng, M., L. Sheng, Q. Gao, Q. Xiong, H. Zhang, M. Wu, Y. Liang, F. Zhu, Y. Zhang, X. Zhang, Q. Yuan, and Y. Li, *The m(6)A methyltransferase METTL3 promotes bladder cancer progression via AFF4/NF-kappaB/MYC signaling network.* Oncogene, 2019. **38**(19): p. 3667-3680.

150. Dahal, U., K. Le, and M. Gupta, *RNA m6A methyltransferase METTL3 regulates invasiveness of melanoma cells by matrix metallopeptidase 2.* Melanoma Res, 2019. **29**(4): p. 382-389.

151. Hua, W., Y. Zhao, X. Jin, D. Yu, J. He, D. Xie, and P. Duan, *METTL3 promotes ovarian carcinoma growth and invasion through the regulation of AXL translation and epithelial to mesenchymal transition.* Gynecol Oncol, 2018. **151**(2): p. 356-365.

152. Li, T., P.S. Hu, Z. Zuo, J.F. Lin, X. Li, Q.N. Wu, Z.H. Chen, Z.L. Zeng, F. Wang, J. Zheng, D. Chen, B. Li, T.B. Kang, D. Xie, D. Lin, H.Q. Ju, and R.H. Xu, *METTL3 facilitates tumor progression via an m(6)A-IGF2BP2-dependent mechanism in colorectal carcinoma.* Mol Cancer, 2019. **18**(1): p. 112.

153. Lin, S., J. Choe, P. Du, R. Triboulet, and R.I. Gregory, *The m(6)A Methyltransferase METTL3 Promotes Translation in Human Cancer Cells.* Mol Cell, 2016. **62**(3): p. 335-345.

154. Liu, T., S. Yang, J. Sui, S.Y. Xu, Y.P. Cheng, B. Shen, Y. Zhang, X.M. Zhang, L.H. Yin, Y.P. Pu, and G.Y. Liang, *Dysregulated N6-methyladenosine methylation writer METTL3*

contributes to the proliferation and migration of gastric cancer. J Cell Physiol, 2020. **235**(1): p. 548-562.

155. Miao, W., J. Chen, L. Jia, J. Ma, and D. Song, *The m6A methyltransferase METTL3 promotes osteosarcoma progression by regulating the m6A level of LEF1.* Biochem Biophys Res Commun, 2019. **516**(3): p. 719-725.

156. Taketo, K., M. Konno, A. Asai, J. Koseki, M. Toratani, T. Satoh, Y. Doki, M. Mori, H. Ishii, and K. Ogawa, *The epitranscriptome m6A writer METTL3 promotes chemo- and radioresistance in pancreatic cancer cells.* Int J Oncol, 2018. **52**(2): p. 621-629.

157. Visvanathan, A., V. Patil, A. Arora, A.S. Hegde, A. Arivazhagan, V. Santosh, and K. Somasundaram, *Essential role of METTL3-mediated m(6)A modification in glioma stem-like cells maintenance and radioresistance.* Oncogene, 2018. **37**(4): p. 522-533.

158. Yang, Y., X. Fan, M. Mao, X. Song, P. Wu, Y. Zhang, Y. Jin, Y. Yang, L.L. Chen, Y. Wang, C.C. Wong, X. Xiao, and Z. Wang, *Extensive translation of circular RNAs driven by N(6)-methyladenosine.* Cell Res, 2017. **27**(5): p. 626-641.

159. Joung, J., S. Konermann, J.S. Gootenberg, O.O. Abudayyeh, R.J. Platt, M.D. Brigham, N.E. Sanjana, and F. Zhang, *Genome-scale CRISPR-Cas9 knockout and transcriptional activation screening.* Nat Protoc, 2017. **12**(4): p. 828-863.

160. Kinoshita, E., E. Kinoshita-Kikuta, K. Takiyama, and T. Koike, *Phosphate-binding tag, a new tool to visualize phosphorylated proteins.* Mol Cell Proteomics, 2006. **5**(4): p. 749-57.

161. Casar, B., A. Pinto, and P. Crespo, *ERK dimers and scaffold proteins: unexpected partners for a forgotten (cytoplasmic) task.* Cell Cycle, 2009. **8**(7): p. 1007-13.

162. Matsuoka, S., B.A. Ballif, A. Smogorzewska, E.R. McDonald, 3rd, K.E. Hurov, J. Luo, C.E. Bakalarski, Z. Zhao, N. Solimini, Y. Lerenthal, Y. Shiloh, S.P. Gygi, and S.J. Elledge, *ATM and ATR substrate analysis reveals extensive protein networks responsive to DNA damage.* Science, 2007. **316**(5828): p. 1160-6.

163. Roskoski, R., Jr., *ERK1/2 MAP kinases: structure, function, and regulation.* Pharmacol Res, 2012. **66**(2): p. 105-43.

164. Kobayashi, M., M. Ohsugi, T. Sasako, M. Awazawa, T. Umehara, A. Iwane, N. Kobayashi, Y. Okazaki, N. Kubota, R. Suzuki, H. Waki, K. Horiuchi, T. Hamakubo, T. Kodama, S. Aoe, K. Tobe, T. Kadowaki, and K. Ueki, *The RNA Methyltransferase Complex of WTAP, METTL3, and METTL14 Regulates Mitotic Clonal Expansion in Adipogenesis.* Mol Cell Biol, 2018. **38**(16).

165. Potu, H., L.F. Peterson, A. Pal, M. Verhaegen, J. Cao, M. Talpaz, and N.J. Donato, *Usp5 links suppression of p53 and FAS levels in melanoma to the BRAF pathway.* Oncotarget, 2014. **5**(14): p. 5559-69.

166. Raasi, S., R. Varadan, D. Fushman, and C.M. Pickart, *Diverse polyubiquitin interaction properties of ubiquitin-associated domains.* Nat Struct Mol Biol, 2005. **12**(8): p. 708-14.

167. Avvakumov, G.V., J.R. Walker, S. Xue, A. Allali-Hassani, A. Asinas, U.B. Nair, X. Fang, X. Zuo, Y.X. Wang, K.D. Wilkinson, and S. Dhe-Paganon, *Two ZnF-UBP domains in isopeptidase T (USP5).* Biochemistry, 2012. **51**(6): p. 1188-98.

168. Kunath, T., M.K. Saba-El-Leil, M. Almousailleakh, J. Wray, S. Meloche, and A. Smith, *FGF stimulation of the Erk1/2 signalling cascade triggers transition of pluripotent embryonic stem cells from self-renewal to lineage commitment.* Development, 2007. **134**(16): p. 2895-902.

169. Wang, Y., Y. Li, M. Yue, J. Wang, S. Kumar, R.J. Wechsler-Reya, Z. Zhang, Y. Ogawa, M. Kellis, G. Duester, and J.C. Zhao, *N(6)-methyladenosine RNA modification regulates embryonic neural stem cell self-renewal through histone modifications.* Nat Neurosci, 2018. **21**(2): p. 195-206.

170. Liu, F., X. Yang, M. Geng, and M. Huang, *Targeting ERK, an Achilles' Heel of the MAPK pathway, in cancer therapy.* Acta Pharm Sin B, 2018. **8**(4): p. 552-562.

171. Lever, J., E.Y. Zhao, J. Grewal, M.R. Jones, and S.J.M. Jones, *CancerMine: a literature-mined resource for drivers, oncogenes and tumor suppressors in cancer.* Nat Methods, 2019. **16**(6): p. 505-507.

172. Schadendorf, D., A.C.J. van Akkooi, C. Berking, K.G. Griewank, R. Gutzmer, A. Hauschild, A. Stang, A. Roesch, and S. Ugurel, *Melanoma.* Lancet, 2018. **392**(10151): p. 971-984.

173. Choe, J., S. Lin, W. Zhang, Q. Liu, L. Wang, J. Ramirez-Moya, P. Du, W. Kim, S. Tang, P. Sliz, P. Santisteban, R.E. George, W.G. Richards, K.K. Wong, N. Locker, F.J. Slack, and R.I. Gregory, *mRNA circularization by METTL3-eIF3h enhances translation and promotes oncogenesis.* Nature, 2018. **561**(7724): p. 556-560.

174. Bennetzen, M.V., D.H. Larsen, J. Bunkenborg, J. Bartek, J. Lukas, and J.S. Andersen, *Site-specific phosphorylation dynamics of the nuclear proteome during the DNA damage response.* Mol Cell Proteomics, 2010. **9**(6): p. 1314-23.

175. Xiang, Y., B. Laurent, C.H. Hsu, S. Nachtergaele, Z. Lu, W. Sheng, C. Xu, H. Chen, J. Ouyang, S. Wang, D. Ling, P.H. Hsu, L. Zou, A. Jambhekar, C. He, and Y. Shi, *RNA m(6)A methylation regulates the ultraviolet-induced DNA damage response.* Nature, 2017. **543**(7646): p. 573-576.

176. Feng, Z., Q. Li, R. Meng, B. Yi, and Q. Xu, *METTL3 regulates alternative splicing of MyD88 upon the lipopolysaccharide-induced inflammatory response in human dental pulp cells.* J Cell Mol Med, 2018. **22**(5): p. 2558-2568.

177. Zong, X., J. Zhao, H. Wang, Z. Lu, F. Wang, H. Du, and Y. Wang, *Mettl3 Deficiency Sustains Long-Chain Fatty Acid Absorption through Suppressing Traf6-Dependent Inflammation Response.* J Immunol, 2019. **202**(2): p. 567-578.

178. Deng, R., Y. Cheng, S. Ye, J. Zhang, R. Huang, P. Li, H. Liu, Q. Deng, X. Wu, P. Lan, and Y. Deng, *m(6)A methyltransferase METTL3 suppresses colorectal cancer proliferation and migration through p38/ERK pathways.* Onco Targets Ther, 2019. **12**: p. 4391-4402.

179. Zhang, Y., X. Gu, D. Li, L. Cai, and Q. Xu, *METTL3 Regulates Osteoblast Differentiation and Inflammatory Response via Smad Signaling and MAPK Signaling.* Int J Mol Sci, 2019. **21**(1).

180. Lito, P., A. Saborowski, J. Yue, M. Solomon, E. Joseph, S. Gadal, M. Saborowski, E. Kastenhuber, C. Fellmann, K. Ohara, K. Morikami, T. Miura, C. Lukacs, N. Ishii, S. Lowe, and N. Rosen, *Disruption of CRAF-mediated MEK activation is required for effective MEK inhibition in KRAS mutant tumors.* Cancer Cell, 2014. **25**(5): p. 697-710.

181. Desideri, E., A.L. Cavallo, and M. Baccarini, *Alike but Different: RAF Paralogs and Their Signaling Outputs.* Cell, 2015. **161**(5): p. 967-970.

182. Leicht, D.T., V. Balan, A. Kaplun, V. Singh-Gupta, L. Kaplun, M. Dobson, and G. Tzivion, *Raf kinases: function, regulation and role in human cancer.* Biochim Biophys Acta, 2007. **1773**(8): p. 1196-212.

183. Yen, H.C., Q. Xu, D.M. Chou, Z. Zhao, and S.J. Elledge, *Global protein stability profiling in mammalian cells.* Science, 2008. **322**(5903): p. 918-23.

184. Wei, X., J. Fried, Y. Li, L. Hu, M. Gao, S. Zhang, and B. Xu, *Functional roles of Speckle-Type Poz (SPOP) Protein in Genomic stability.* J Cancer, 2018. **9**(18): p. 3257-3262.

185. Marzahn, M.R., S. Marada, J. Lee, A. Nourse, S. Kenrick, H. Zhao, G. Ben-Nissan, R.M. Kolaitis, J.L. Peters, S. Pounds, W.J. Errington, G.G. Prive, J.P. Taylor, M. Sharon, P. Schuck, S.K. Ogden, and T. Mittag, *Higher-order oligomerization promotes localization of SPOP to liquid nuclear speckles.* EMBO J, 2016. **35**(12): p. 1254-75.

186. Wickliffe, K.E., A. Williamson, H.J. Meyer, A. Kelly, and M. Rape, *K11-linked ubiquitin chains as novel regulators of cell division.* Trends Cell Biol, 2011. **21**(11): p. 656-63.

187. Fei, Q., Z. Zou, I.A. Roundtree, H.L. Sun, and C. He, *YTHDF2 promotes mitotic entry and is regulated by cell cycle mediators.* PLoS Biol, 2020. **18**(4): p. e3000664.

188. Aguilo, F., F. Zhang, A. Sancho, M. Fidalgo, S. Di Cecilia, A. Vashisht, D.F. Lee, C.H. Chen, M. Rengasamy, B. Andino, F. Jahouh, A. Roman, S.R. Krig, R. Wang, W. Zhang, J.A. Wohlschlegel, J. Wang, and M.J. Walsh, *Coordination of m(6)A mRNA Methylation and Gene Transcription by ZFP217 Regulates Pluripotency and Reprogramming.* Cell Stem Cell, 2015. **17**(6): p. 689-704.

189. Du, Y., G. Hou, H. Zhang, J. Dou, J. He, Y. Guo, L. Li, R. Chen, Y. Wang, R. Deng, J. Huang, B. Jiang, M. Xu, J. Cheng, G.Q. Chen, X. Zhao, and J. Yu, *SUMOylation of the m6A-RNA methyltransferase METTL3 modulates its function.* Nucleic Acids Res, 2018. **46**(10): p. 5195-5208.

190. Yang, S.H. and A.D. Sharrocks, *MAP Kinase: SUMO pathway interactions.* Methods Mol Biol, 2010. **661**: p. 343-67.

191. Yang, S.H., E. Jaffray, R.T. Hay, and A.D. Sharrocks, *Dynamic interplay of the SUMO and ERK pathways in regulating Elk-1 transcriptional activity.* Mol Cell, 2003. **12**(1): p. 63-74.

192. Di Timoteo, G., D. Dattilo, A. Centron-Broco, A. Colantoni, M. Guarnacci, F. Rossi, D. Incarnato, S. Oliviero, A. Fatica, M. Morlando, and I. Bozzoni, *Modulation of circRNA Metabolism by m(6)A Modification.* Cell Rep, 2020. **31**(6): p. 107641.

193. Jin, J. and T. Pawson, *Modular evolution of phosphorylation-based signalling systems.* Philos Trans R Soc Lond B Biol Sci, 2012. **367**(1602): p. 2540-55.

194. Sanchez-Garcia, R., C.O.S. Sorzano, J.M. Carazo, and J. Segura, *BIPSPI: a method for the prediction of partner-specific protein-protein interfaces.* Bioinformatics, 2019. **35**(3): p. 470-477.

195. Ying, Q.L., M. Stavridis, D. Griffiths, M. Li, and A. Smith, *Conversion of embryonic stem cells into neuroectodermal precursors in adherent monoculture.* Nat Biotechnol, 2003. **21**(2): p. 183-6.

196. Lee, D.F., H.P. Kuo, C.T. Chen, J.M. Hsu, C.K. Chou, Y. Wei, H.L. Sun, L.Y. Li, B. Ping, W.C. Huang, X. He, J.Y. Hung, C.C. Lai, Q. Ding, J.L. Su, J.Y. Yang, A.A. Sahin, G.N. Hortobagyi, F.J. Tsai, C.H. Tsai, and M.C. Hung, *IKK beta suppression of TSC1 links inflammation and tumor angiogenesis via the mTOR pathway.* Cell, 2007. **130**(3): p. 440-55.

197. Vichai, V. and K. Kirtikara, *Sulforhodamine B colorimetric assay for cytotoxicity screening.* Nat Protoc, 2006. **1**(3): p. 1112-6.

198. Kim, D., B. Langmead, and S.L. Salzberg, *HISAT: a fast spliced aligner with low memory requirements.* Nat Methods, 2015. **12**(4): p. 357-60.

199. Love, M.I., W. Huber, and S. Anders, *Moderated estimation of fold change and dispersion for RNA-seq data with DESeq2.* Genome Biol, 2014. **15**(12): p. 550.

200. De Jesus, D.F., Z. Zhang, S. Kahraman, N.K. Brown, M. Chen, J. Hu, M.K. Gupta, C. He, and R.N. Kulkarni, *m6A mRNA methylation regulates human β-cell biology in physiological states and in type 2 diabetes.* Nature Metabolism, 2019. **1**(8): p. 765-774.

201. Meng, J., X. Cui, M.K. Rao, Y. Chen, and Y. Huang, *Exome-based analysis for RNA epigenome sequencing data.* Bioinformatics, 2013. **29**(12): p. 1565-7.

202. Heinz, S., C. Benner, N. Spann, E. Bertolino, Y.C. Lin, P. Laslo, J.X. Cheng, C. Murre, H. Singh, and C.K. Glass, *Simple combinations of lineage-determining transcription factors prime cis-regulatory elements required for macrophage and B cell identities.* Mol Cell, 2010. **38**(4): p. 576-89.

203. Cui, X., Z. Wei, L. Zhang, H. Liu, L. Sun, S.W. Zhang, Y. Huang, and J. Meng, *Guitar: An R/Bioconductor Package for Gene Annotation Guided Transcriptomic Analysis of RNA-Related Genomic Features.* Biomed Res Int, 2016. **2016**: p. 8367534.

204. Zhang, Z., Q. Zhan, M. Eckert, A. Zhu, A. Chryplewicz, D.F. De Jesus, D. Ren, R.N. Kulkarni, E. Lengyel, C. He, and M. Chen, *RADAR: differential analysis of MeRIP-seq data with a random effect model.* Genome Biol, 2019. **20**(1): p. 294.

205. Liao, Y., J. Wang, E.J. Jaehnig, Z. Shi, and B. Zhang, *WebGestalt 2019: gene set analysis toolkit with revamped UIs and APIs.* Nucleic Acids Res, 2019. **47**(W1): p. W199-W205.

206. Zhou, Y., C. He, L. Wang, and B. Ge, *Post-translational regulation of antiviral innate signaling.* Eur J Immunol, 2017. **47**(9): p. 1414-1426.

207. Goubau, D., S. Deddouche, and C. Reis e Sousa, *Cytosolic sensing of viruses.* Immunity, 2013. **38**(5): p. 855-69.

208. Takeuchi, O. and S. Akira, *Pattern recognition receptors and inflammation.* Cell, 2010. **140**(6): p. 805-20.

209. Rehwinkel, J. and M.U. Gack, *RIG-I-like receptors: their regulation and roles in RNA sensing.* Nat Rev Immunol, 2020. **20**(9): p. 537-551.

210. Loo, Y.M. and M. Gale, Jr., *Immune signaling by RIG-I-like receptors.* Immunity, 2011. **34**(5): p. 680-92.

211. Wu, J. and Z.J. Chen, *Innate immune sensing and signaling of cytosolic nucleic acids.* Annu Rev Immunol, 2014. **32**: p. 461-88.

212. Hornung, V., J. Ellegast, S. Kim, K. Brzozka, A. Jung, H. Kato, H. Poeck, S. Akira, K.K. Conzelmann, M. Schlee, S. Endres, and G. Hartmann, *5'-Triphosphate RNA is the ligand for RIG-I.* Science, 2006. **314**(5801): p. 994-7.

213. Pichlmair, A., O. Schulz, C.P. Tan, T.I. Naslund, P. Liljestrom, F. Weber, and C. Reis e Sousa, *RIG-I-mediated antiviral responses to single-stranded RNA bearing 5'-phosphates.* Science, 2006. **314**(5801): p. 997-1001.

214. Schlee, M., A. Roth, V. Hornung, C.A. Hagmann, V. Wimmenauer, W. Barchet, C. Coch, M. Janke, A. Mihailovic, G. Wardle, S. Juranek, H. Kato, T. Kawai, H. Poeck, K.A. Fitzgerald, O. Takeuchi, S. Akira, T. Tuschl, E. Latz, J. Ludwig, and G. Hartmann, *Recognition of 5' triphosphate by RIG-I helicase requires short blunt double-stranded*

RNA as contained in panhandle of negative-strand virus. Immunity, 2009. **31**(1): p. 25-34.

215. Devarkar, S.C., C. Wang, M.T. Miller, A. Ramanathan, F. Jiang, A.G. Khan, S.S. Patel, and J. Marcotrigiano, *Structural basis for m7G recognition and 2'-O-methyl discrimination in capped RNAs by the innate immune receptor RIG-I.* Proc Natl Acad Sci U S A, 2016. **113**(3): p. 596-601.

216. Schuberth-Wagner, C., J. Ludwig, A.K. Bruder, A.M. Herzner, T. Zillinger, M. Goldeck, T. Schmidt, J.L. Schmid-Burgk, R. Kerber, S. Wolter, J.P. Stumpel, A. Roth, E. Bartok, C. Drosten, C. Coch, V. Hornung, W. Barchet, B.M. Kummerer, G. Hartmann, and M. Schlee, *A Conserved Histidine in the RNA Sensor RIG-I Controls Immune Tolerance to N1-2'O-Methylated Self RNA.* Immunity, 2015. **43**(1): p. 41-51.

217. Decroly, E., F. Ferron, J. Lescar, and B. Canard, *Conventional and unconventional mechanisms for capping viral mRNA.* Nat Rev Microbiol, 2011. **10**(1): p. 51-65.

218. Kane, S.E. and K. Beemon, *Precise localization of m6A in Rous sarcoma virus RNA reveals clustering of methylation sites: implications for RNA processing.* Mol Cell Biol, 1985. **5**(9): p. 2298-306.

219. Krug, R.M., M.A. Morgan, and A.J. Shatkin, *Influenza viral mRNA contains internal N6-methyladenosine and 5'-terminal 7-methylguanosine in cap structures.* J Virol, 1976. **20**(1): p. 45-53.

220. Thomason, A.R., D.A. Brian, L.F. Velicer, and F.M. Rottman, *Methylation of high-molecular-weight subunit RNA of feline leukemia virus.* J Virol, 1976. **20**(1): p. 123-32.

221. Kariko, K., M. Buckstein, H. Ni, and D. Weissman, *Suppression of RNA recognition by Toll-like receptors: the impact of nucleoside modification and the evolutionary origin of RNA.* Immunity, 2005. **23**(2): p. 165-75.

222. Durbin, A.F., C. Wang, J. Marcotrigiano, and L. Gehrke, *RNAs Containing Modified Nucleotides Fail To Trigger RIG-I Conformational Changes for Innate Immune Signaling.* mBio, 2016. **7**(5).

223. Gao, Y., R. Vasic, Y. Song, R. Teng, C. Liu, R. Gbyli, G. Biancon, R. Nelakanti, K. Lobben, E. Kudo, W. Liu, A. Ardasheva, X. Fu, X. Wang, P. Joshi, V. Lee, B. Dura, G. Viero, A. Iwasaki, R. Fan, A. Xiao, R.A. Flavell, H.B. Li, T. Tebaldi, and S. Halene, *m(6)A Modification Prevents Formation of Endogenous Double-Stranded RNAs and Deleterious Innate Immune Responses during Hematopoietic Development.* Immunity, 2020. **52**(6): p. 1007-1021 e8.

224. Qiu, W., Q. Zhang, R. Zhang, Y. Lu, X. Wang, H. Tian, Y. Yang, Z. Gu, Y. Gao, X. Yang, G. Cui, B. Sun, Y. Peng, H. Deng, H. Peng, A. Yang, Y.G. Yang, and P. Yang, *N(6)-methyladenosine RNA modification suppresses antiviral innate sensing pathways via reshaping double-stranded RNA.* Nat Commun, 2021. **12**(1): p. 1582.

225. Lu, M., Z. Zhang, M. Xue, B.S. Zhao, O. Harder, A. Li, X. Liang, T.Z. Gao, Y. Xu, J. Zhou, Z. Feng, S. Niewiesk, M.E. Peeples, C. He, and J. Li, *N(6)-methyladenosine modification enables viral RNA to escape recognition by RNA sensor RIG-I.* Nat Microbiol, 2020. **5**(4): p. 584-598.

226. Winkler, R., E. Gillis, L. Lasman, M. Safra, S. Geula, C. Soyris, A. Nachshon, J. Tai-Schmiedel, N. Friedman, V.T.K. Le-Trilling, M. Trilling, M. Mandelboim, J.H. Hanna, S. Schwartz, and N. Stern-Ginossar, *m(6)A modification controls the innate immune response to infection by targeting type I interferons.* Nat Immunol, 2019. **20**(2): p. 173-182.

227. Chiang, J.J., K.M.J. Sparrer, M. van Gent, C. Lassig, T. Huang, N. Osterrieder, K.P. Hopfner, and M.U. Gack, *Viral unmasking of cellular 5S rRNA pseudogene transcripts induces RIG-I-mediated immunity.* Nat Immunol, 2018. **19**(1): p. 53-62.

228. Chen, Y.G., R. Chen, S. Ahmad, R. Verma, S.P. Kasturi, L. Amaya, J.P. Broughton, J. Kim, C. Cadena, B. Pulendran, S. Hur, and H.Y. Chang, *N6-Methyladenosine Modification Controls Circular RNA Immunity.* Mol Cell, 2019. **76**(1): p. 96-109 e9.

229. Jin, Y., O.H. Tam, E. Paniagua, and M. Hammell, *TEtranscripts: a package for including transposable elements in differential expression analysis of RNA-seq datasets.* Bioinformatics, 2015. **31**(22): p. 3593-9.

230. Döhner, H., E. Estey, D. Grimwade, S. Amadori, F.R. Appelbaum, T. Büchner, H. Dombret, B.L. Ebert, P. Fenaux, R.A. Larson, R.L. Levine, F. Lo-Coco, T. Naoe, D. Niederwieser, G.J. Ossenkoppele, M. Sanz, J. Sierra, M.S. Tallman, H.-F. Tien, A.H. Wei, B. Löwenberg, and C.D. Bloomfield, *Diagnosis and management of AML in adults: 2017 ELN recommendations from an international expert panel.* Blood, 2017. **129**(4): p. 424-447.

231. Thomas, D. and R. Majeti, *Biology and relevance of human acute myeloid leukemia stem cells.* Blood, 2017. **129**(12): p. 1577-1585.

232. Pollyea, D.A. and C.T. Jordan, *Therapeutic targeting of acute myeloid leukemia stem cells.* Blood, 2017. **129**(12): p. 1627-1635.

233. Krause, D.S. and R.A. Van Etten, *Right on target: eradicating leukemic stem cells.* Trends Mol Med, 2007. **13**(11): p. 470-81.

234. Jia, G.F., Y. Fu, X. Zhao, Q. Dai, G.Q. Zheng, Y. Yang, C.Q. Yi, T. Lindahl, T. Pan, Y.G. Yang, and C. He, *N6-Methyladenosine in nuclear RNA is a major substrate of the obesity-associated FTO (vol 7, pg 885, 2011).* Nature Chemical Biology, 2012. **8**(12): p. 1008-1008.

235. Li, Z., H. Weng, R. Su, X. Weng, Z. Zuo, C. Li, H. Huang, S. Nachtergaele, L. Dong, C. Hu, X. Qin, L. Tang, Y. Wang, G.M. Hong, H. Huang, X. Wang, P. Chen, S. Gurbuxani, S. Arnovitz, Y. Li, S. Li, J. Strong, M.B. Neilly, R.A. Larson, X. Jiang, P. Zhang, J. Jin,

C. He, and J. Chen, *FTO Plays an Oncogenic Role in Acute Myeloid Leukemia as a N6-Methyladenosine RNA Demethylase.* Cancer Cell, 2017. **31**(1): p. 127-141.

236. Huang, Y., R. Su, Y. Sheng, L. Dong, Z. Dong, H. Xu, T. Ni, Z.S. Zhang, T. Zhang, C. Li, L. Han, Z. Zhu, F. Lian, J. Wei, Q. Deng, Y. Wang, M. Wunderlich, Z. Gao, G. Pan, D. Zhong, H. Zhou, N. Zhang, J. Gan, H. Jiang, J.C. Mulloy, Z. Qian, J. Chen, and C.G. Yang, *Small-molecule targeting of oncogenic FTO demethylase in acute myeloid leukemia.* Cancer Cell, 2019. **35**: p. 677-691.

237. Thalhammer, A., Z. Bencokova, R. Poole, C. Loenarz, J. Adam, L. O'Flaherty, J. Schodel, D. Mole, K. Giaslakiotis, C.J. Schofield, E.M. Hammond, P.J. Ratcliffe, and P.J. Pollard, *Human AlkB homologue 5 is a nuclear 2-oxoglutarate dependent oxygenase and a direct target of hypoxia-inducible factor 1alpha (HIF-1alpha).* PLoS One, 2011. **6**(1): p. e16210.

238. Kwok, C.T., A.D. Marshall, J.E. Rasko, and J.J. Wong, *Genetic alterations of m(6)A regulators predict poorer survival in acute myeloid leukemia.* J Hematol Oncol, 2017. **10**(1): p. 39.

239. Ley, T.J., C. Miller, L. Ding, B.J. Raphael, A.J. Mungall, A. Robertson, K. Hoadley, T.J. Triche, P.W. Laird, J.D. Baty, L.L. Fulton, R. Fulton, S.E. Heath, J. Kalicki-Veizer, C. Kandoth, J.M. Klco, D.C. Koboldt, K.L. Kanchi, S. Kulkarni, and E. al., *Genomic and epigenomic landscapes of adult de novo acute myeloid leukemia.* N Engl J Med, 2013. **368**(22): p. 2059-74.

240. Deng, X., R. Su, H. Weng, H. Huang, Z. Li, and J. Chen, *RNA N(6)-methyladenosine modification in cancers: current status and perspectives.* Cell Res, 2018. **28**(5): p. 507-517.

241. Subramanian, A., P. Tamayo, V.K. Mootha, S. Mukherjee, B.L. Ebert, M.A. Gillette, A. Paulovich, S.L. Pomeroy, T.R. Golub, E.S. Lander, and J.P. Mesirov, *Gene set enrichment analysis: a knowledge-based approach for interpreting genome-wide expression profiles.* Proc Natl Acad Sci USA, 2005. **102**(43): p. 15545-50.

242. Yun, M., J. Rong, Z.R. Lin, Y.L. He, J.X. Zhang, Z.W. Peng, L.Q. Tang, M.S. Zeng, Q. Zhong, and S. Ye, *High expression of transforming acidic coiled coil-containing protein 3 strongly correlates with aggressive characteristics and poor prognosis of gastric cancer.* Oncol Rep, 2015. **34**(3): p. 1397-405.

243. Song, H., C. Liu, N. Shen, P. Yi, F. Dong, X. Li, N. Zhang, and T. Huang, *Overexpression of TACC3 in Breast Cancer Associates With Poor Prognosis.* Appl Immunohistochem Mol Morphol, 2018. **26**(2): p. 113-119.

244. Sun, Y., Y. Tian, G.Z. Wang, S.H. Zhao, B. Han, Y.L. Li, and C.L. Jiang, *Overexpression of Transforming Acidic Coiled CoilContaining Protein 3 Reflects Malignant Characteristics and Poor Prognosis of Glioma.* Int J Mol Sci, 2017. **18**(3).

245. Li, Q., L. Ye, W. Guo, M. Wang, S. Huang, and X. Peng, *Overexpression of TACC3 is correlated with tumor aggressiveness and poor prognosis in prostate cancer.* Biochem Biophys Res Commun, 2017. **486**(4): p. 872-878.

246. Nahm, J.H., H. Kim, H. Lee, J.Y. Cho, Y.R. Choi, Y.S. Yoon, H.S. Han, and Y.N. Park, *Transforming acidic coiled-coil-containing protein 3 (TACC3) overexpression in hepatocellular carcinomas is associated with "stemness" and epithelial-mesenchymal transition-related marker expression and a poor prognosis.* Tumour Biol, 2016. **37**(1): p. 393-403.

247. Zhou, D.S., H.B. Wang, Z.G. Zhou, Y.J. Zhang, Q. Zhong, L. Xu, Y.H. Huang, S.C. Yeung, M.S. Chen, and M.S. Zeng, *TACC3 promotes stemness and is a potential therapeutic target in hepatocellular carcinoma.* Oncotarget, 2015. **6**(27): p. 24163-77.

248. Jung, C.K., J.H. Jung, G.S. Park, A. Lee, C.S. Kang, and K.Y. Lee, *Expression of transforming acidic coiled-coil containing protein 3 is a novel independent prognostic marker in non-small cell lung cancer.* Pathol Int, 2006. **56**(9): p. 503-9.

249. Wang, Y., X. Ding, H. Hu, Y. He, Z. Lu, P. Wu, L. Tian, T. Xia, J. Yin, H. Yuan, G. Shi, D. Liu, K. Jiang, and Y. Miao, *Long non-coding RNA lnc-PCTST predicts prognosis through inhibiting progression of pancreatic cancer by downregulation of TACC-3.* Int J Cancer, 2018. **143**(12): p. 3143-3154.

250. Zhao, C., X. He, H. Li, J. Zhou, X. Han, D. Wang, G. Tian, and F. Sui, *Downregulation of TACC3 inhibits tumor growth and migration in osteosarcoma cells through regulation of the NF-kappaB signaling pathway.* Oncol Lett, 2018. **15**(5): p. 6881-6886.

251. He, J.C., W. Yao, J.M. Wang, P. Schemmer, Y. Yang, Y. Liu, Y.W. Qian, W.P. Qi, J. Zhang, Q. Shen, and T. Yang, *TACC3 overexpression in cholangiocarcinoma correlates with poor prognosis and is a potential anti-cancer molecular drug target for HDAC inhibitors.* Oncotarget, 2016. **7**(46): p. 75441-75456.

252. Ha, G.H., J.L. Kim, and E.K. Breuer, *TACC3 is essential for EGF-mediated EMT in cervical cancer.* PLoS One, 2013. **8**(8): p. e70353.

253. Yao, R., Y. Natsume, Y. Saiki, H. Shioya, K. Takeuchi, T. Yamori, H. Toki, I. Aoki, T. Saga, and T. Noda, *Disruption of Tacc3 function leads to in vivo tumor regression.* Oncogene, 2012. **31**(2): p. 135-48.

254. Zhang, S., B.S. Zhao, A. Zhou, K. Lin, S. Zheng, Z. Lu, Y. Chen, E.P. Sulman, K. Xie, O. Bogler, S. Majumder, C. He, and S. Huang, *m(6)A Demethylase ALKBH5 Maintains Tumorigenicity of Glioblastoma Stem-like Cells by Sustaining FOXM1 Expression and Cell Proliferation Program.* Cancer Cell, 2017. **31**(4): p. 591-606.e6.

255. Zhang, J., S. Guo, H.Y. Piao, Y. Wang, Y. Wu, X.Y. Meng, D. Yang, Z.C. Zheng, and Y. Zhao, *ALKBH5 promotes invasion and metastasis of gastric cancer by decreasing methylation of the lncRNA NEAT1.* J Physiol Biochem, 2019.

256. Zhu, H., X. Gan, X. Jiang, S. Diao, H. Wu, and J. Hu, *ALKBH5 inhibited autophagy of epithelial ovarian cancer through miR-7 and BCL-2.* J Exp Clin Cancer Res, 2019. **38**(1): p. 163.

257. Cho, S.H., M. Ha, Y.H. Cho, J.H. Ryu, K. Yang, K.H. Lee, M.E. Han, S.O. Oh, and Y.H. Kim, *ALKBH5 gene is a novel biomarker that predicts the prognosis of pancreatic cancer: A retrospective multicohort study.* Ann Hepatobiliary Pancreat Surg, 2018. **22**(4): p. 305-309.

258. Zhang, C., W.I. Zhi, H. Lu, D. Samanta, I. Chen, E. Gabrielson, and G.L. Semenza, *Hypoxia-inducible factors regulate pluripotency factor expression by ZNF217- and ALKBH5-mediated modulation of RNA methylation in breast cancer cells.* Oncotarget, 2016. **7**(40): p. 64527-64542.

259. Wang, X., Z.K. Lu, A. Gomez, G.C. Hon, Y.N. Yue, D.L. Han, Y. Fu, M. Parisien, Q. Dai, G.F. Jia, B. Ren, T. Pan, and C. He, *N-6-methyladenosine-dependent regulation of messenger RNA stability.* Nature, 2014. **505**(7481): p. 117-+.

260. Piekorz, R.P., A. Hoffmeyer, C.D. Duntsch, C. McKay, H. Nakajima, V. Sexl, L. Snyder, J. Rehg, and J.N. Ihle, *The centrosomal protein TACC3 is essential for hematopoietic stem cell function and genetically interfaces with p53-regulated apoptosis.* Embo Journal, 2002. **21**(4): p. 653-664.

261. Schneider, L., F. Essmann, A. Kletke, P. Rio, H. Hanenberg, K. Schulze-Osthoff, B. Nurnberg, and R.P. Piekorz, *TACC3 depletion sensitizes to paclitaxel-induced cell death and overrides p21WAF-mediated cell cycle arrest.* Oncogene, 2008. **27**(1): p. 116-25.

262. Suhail, T.V., P. Singh, and T.K. Manna, *Suppression of centrosome protein TACC3 induces G1 arrest and cell death through activation of p38-p53-p21 stress signaling pathway.* Eur J Cell Biol, 2015. **94**(2): p. 90-100.

263. Sakamoto, K.M., K.B. Kim, A. Kumagai, F. Mercurio, C.M. Crews, and R.J. Deshaies, *Protacs: chimeric molecules that target proteins to the Skp1-Cullin-F box complex for ubiquitination and degradation.* Proc Natl Acad Sci U S A, 2001. **98**(15): p. 8554-9.

264. Chi, K.R., *Drug developers delve into the cell's trash-disposal machinery.* Nat Rev Drug Discov, 2016. **15**(5): p. 295-7.

265. Rinn, J.L., M. Kertesz, J.K. Wang, S.L. Squazzo, X. Xu, S.A. Brugmann, L.H. Goodnough, J.A. Helms, P.J. Farnham, E. Segal, and H.Y. Chang, *Functional demarcation of active and silent chromatin domains in human HOX loci by Noncoding RNAs.* Cell, 2007. **129**(7): p. 1311-1323.

266. Gandin, V., K. Sikstrom, T. Alain, M. Morita, S. McLaughlan, O. Larsson, and I. Topisirovic, *Polysome fractionation and analysis of mammalian translatomes on a genome-wide scale.* J Vis Exp, 2014(87).

267. Huang, H., H. Weng, K. Zhou, T. Wu, B.S. Zhao, M. Sun, Z. Chen, X. Deng, G. Xiao, F. Auer, L. Klemm, H. Wu, Z. Zuo, X. Qin, Y. Dong, Y. Zhou, H. Qin, S. Tao, J. Du, J. Liu, Z. Lu, H. Yin, A. Mesquita, C.L. Yuan, Y.C. Hu, W. Sun, R. Su, L. Dong, C. Shen, C. Li, Y. Qing, X. Jiang, X. Wu, M. Sun, J.L. Guan, L. Qu, M. Wei, M. Muschen, G. Huang, C. He, J. Yang, and J. Chen, *Histone H3 trimethylation at lysine 36 guides m(6)A RNA modification co-transcriptionally.* Nature, 2019. **567**(7748): p. 414-419.

268. Lence, T., C. Paolantoni, L. Worpenberg, and J.Y. Roignant, *Mechanistic insights into m(6)A RNA enzymes.* Biochim Biophys Acta Gene Regul Mech, 2019. **1862**(3): p. 222-229.

269. Zhang, C., L. Chen, D. Peng, A. Jiang, Y. He, Y. Zeng, C. Xie, H. Zhou, X. Luo, H. Liu, L. Chen, J. Ren, W. Wang, and Y. Zhao, *METTL3 and N6-Methyladenosine Promote Homologous Recombination-Mediated Repair of DSBs by Modulating DNA-RNA Hybrid Accumulation.* Mol Cell, 2020. **79**(3): p. 425-442 e7.

270. Xu, H., H. Wang, W. Zhao, S. Fu, Y. Li, W. Ni, Y. Xin, W. Li, C. Yang, Y. Bai, M. Zhan, and L. Lu, *SUMO1 modification of methyltransferase-like 3 promotes tumor progression via regulating Snail mRNA homeostasis in hepatocellular carcinoma.* Theranostics, 2020. **10**(13): p. 5671-5686.

271. Scholler, E., F. Weichmann, T. Treiber, S. Ringle, N. Treiber, A. Flatley, R. Feederle, A. Bruckmann, and G. Meister, *Interactions, localization, and phosphorylation of the m(6)A generating METTL3-METTL14-WTAP complex.* RNA, 2018. **24**(4): p. 499-512.

272. Slobodin, B., R. Han, V. Calderone, J. Vrielink, F. Loayza-Puch, R. Elkon, and R. Agami, *Transcription Impacts the Efficiency of mRNA Translation via Co-transcriptional N6-adenosine Methylation.* Cell, 2017. **169**(2): p. 326-337 e12.

273. Liu, X., H. Wang, X. Zhao, Q. Luo, Q. Wang, K. Tan, Z. Wang, J. Jiang, J. Cui, E. Du, L. Xia, W. Du, D. Chen, L. Xia, and S. Xiao, *Arginine methylation of METTL14 promotes RNA N(6)-methyladenosine modification and endoderm differentiation of mouse embryonic stem cells.* Nat Commun, 2021. **12**(1): p. 3780.

274. Wang, Z., Z. Pan, S. Adhikari, B.T. Harada, L. Shen, W. Yuan, T. Abeywardana, Q. Al-Hadid, J.M. Stark, C. He, L. Lin, and Y. Yang, *m(6) A deposition is regulated by PRMT1-mediated arginine methylation of METTL14 in its disordered C-terminal region.* EMBO J, 2021. **40**(5): p. e106309.

275. Lee, D.Y., C. Teyssier, B.D. Strahl, and M.R. Stallcup, *Role of protein methylation in regulation of transcription.* Endocr Rev, 2005. **26**(2): p. 147-70.

276. Paik, W.K., D.C. Paik, and S. Kim, *Historical review: the field of protein methylation.* Trends Biochem Sci, 2007. **32**(3): p. 146-52.

277. Humphrey, S.J., D.E. James, and M. Mann, *Protein Phosphorylation: A Major Switch Mechanism for Metabolic Regulation.* Trends Endocrinol Metab, 2015. **26**(12): p. 676-687.

278. Fang, R., X. Chen, S. Zhang, H. Shi, Y. Ye, H. Shi, Z. Zou, P. Li, Q. Guo, L. Ma, C. He, and S. Huang, *EGFR/SRC/ERK-stabilized YTHDF2 promotes cholesterol dysregulation and invasive growth of glioblastoma.* Nat Commun, 2021. **12**(1): p. 177.

279. Guo, Y.E., J.C. Manteiga, J.E. Henninger, B.R. Sabari, A. Dall'Agnese, N.M. Hannett, J.H. Spille, L.K. Afeyan, A.V. Zamudio, K. Shrinivas, B.J. Abraham, A. Boija, T.M. Decker, J.K. Rimel, C.B. Fant, T.I. Lee, Cisse, II, P.A. Sharp, D.J. Taatjes, and R.A. Young, *Pol II phosphorylation regulates a switch between transcriptional and splicing condensates.* Nature, 2019. **572**(7770): p. 543-548.

280. Ries, R.J., S. Zaccara, P. Klein, A. Olarerin-George, S. Namkoong, B.F. Pickering, D.P. Patil, H. Kwak, J.H. Lee, and S.R. Jaffrey, *m(6)A enhances the phase separation potential of mRNA.* Nature, 2019. **571**(7765): p. 424-428.

281. Tsai, K.L., Y.J. Sun, C.Y. Huang, J.Y. Yang, M.C. Hung, and C.D. Hsiao, *Crystal structure of the human FOXO3a-DBD/DNA complex suggests the effects of post-translational modification.* Nucleic Acids Res, 2007. **35**(20): p. 6984-94.

282. Yu, F., J. Wei, X. Cui, C. Yu, W. Ni, J. Bungert, L. Wu, C. He, and Z. Qian, *Post-translational modification of RNA m6A demethylase ALKBH5 regulates ROS-induced DNA damage response.* Nucleic Acids Res, 2021. **49**(10): p. 5779-5797.

283. Son, Y., S. Kim, H.T. Chung, and H.O. Pae, *Reactive oxygen species in the activation of MAP kinases.* Methods Enzymol, 2013. **528**: p. 27-48.

284. Zhang, J., X. Wang, V. Vikash, Q. Ye, D. Wu, Y. Liu, and W. Dong, *ROS and ROS-Mediated Cellular Signaling.* Oxid Med Cell Longev, 2016. **2016**: p. 4350965.

285. Feng, C., Y. Liu, G. Wang, Z. Deng, Q. Zhang, W. Wu, Y. Tong, C. Cheng, and Z. Chen, *Crystal structures of the human RNA demethylase Alkbh5 reveal basis for substrate recognition.* J Biol Chem, 2014. **289**(17): p. 11571-11583.

286. Liu, Y., Y. You, Z. Lu, J. Yang, P. Li, L. Liu, H. Xu, Y. Niu, and X. Cao, *N (6)-methyladenosine RNA modification-mediated cellular metabolism rewiring inhibits viral replication.* Science, 2019. **365**(6458): p. 1171-1176.

287. Cully, M., *Chemical inhibitors make their RNA epigenetic mark.* Nat Rev Drug Discov, 2019. **18**(12): p. 892-894.

288. Moroz-Omori, E.V., D. Huang, R.K. Bedi, S.J. Cheriyamkunnel, E. Bochenkova, A. Dolbois, M.D. Rzeczkowski, L. Wiedmer, and A. Caflisch, *METTL3 inhibitors for epitranscriptomic modulation of cellular processes.* bioRxiv, 2020: p. 2020.09.25.311803.

289. Yankova, E., W. Blackaby, M. Albertella, J. Rak, E. De Braekeleer, G. Tsagkogeorga, E.S. Pilka, D. Aspris, D. Leggate, A.G. Hendrick, N.A. Webster, B. Andrews, R. Fosbeary, P. Guest, N. Irigoyen, M. Eleftheriou, M. Gozdecka, J.M.L. Dias, A.J. Bannister, B. Vick, I. Jeremias, G.S. Vassiliou, O. Rausch, K. Tzelepis, and T.

Kouzarides, *Small-molecule inhibition of METTL3 as a strategy against myeloid leukaemia.* Nature, 2021. **593**(7860): p. 597-601.

290. Kaniskan, H.U., K.D. Konze, and J. Jin, *Selective inhibitors of protein methyltransferases.* J Med Chem, 2015. **58**(4): p. 1596-629.

291. Copeland, R.A., *Protein methyltransferase inhibitors as precision cancer therapeutics: a decade of discovery.* Philos Trans R Soc Lond B Biol Sci, 2018. **373**(1748).

292. Aktas, M., J. Gleichenhagen, R. Stoll, and F. Narberhaus, *S-adenosylmethionine-binding properties of a bacterial phospholipid N-methyltransferase.* J Bacteriol, 2011. **193**(14): p. 3473-81.

293. Oerum, S., V. Meynier, M. Catala, and C. Tisne, *A comprehensive review of m6A/m6Am RNA methyltransferase structures.* Nucleic Acids Res, 2021.

294. Ruszkowska, A., *METTL16, Methyltransferase-Like Protein 16: Current Insights into Structure and Function.* Int J Mol Sci, 2021. **22**(4).

295. Liu, P., F. Li, J. Lin, T. Fukumoto, T. Nacarelli, X. Hao, A.V. Kossenkov, M.C. Simon, and R. Zhang, *m(6)A-independent genome-wide METTL3 and METTL14 redistribution drives the senescence-associated secretory phenotype.* Nat Cell Biol, 2021. **23**(4): p. 355-365.

296. Frayling, T.M., N.J. Timpson, M.N. Weedon, E. Zeggini, R.M. Freathy, C.M. Lindgren, J.R. Perry, K.S. Elliott, H. Lango, N.W. Rayner, B. Shields, L.W. Harries, J.C. Barrett, S. Ellard, C.J. Groves, B. Knight, A.M. Patch, A.R. Ness, S. Ebrahim, D.A. Lawlor, S.M. Ring, Y. Ben-Shlomo, M.R. Jarvelin, U. Sovio, A.J. Bennett, D. Melzer, L. Ferrucci, R.J. Loos, I. Barroso, N.J. Wareham, F. Karpe, K.R. Owen, L.R. Cardon, M. Walker, G.A. Hitman, C.N. Palmer, A.S. Doney, A.D. Morris, G.D. Smith, A.T. Hattersley, and M.I. McCarthy, *A common variant in the FTO gene is associated with body mass index and predisposes to childhood and adult obesity.* Science, 2007. **316**(5826): p. 889-94.

297. Qing, Y., L. Dong, L. Gao, C. Li, Y. Li, L. Han, E. Prince, B. Tan, X. Deng, C. Wetzel, C. Shen, M. Gao, Z. Chen, W. Li, B. Zhang, D. Braas, J. Ten Hoeve, G.J. Sanchez, H. Chen, L.N. Chan, C.W. Chen, D. Ann, L. Jiang, M. Muschen, G. Marcucci, D.R. Plas, Z. Li, R. Su, and J. Chen, *R-2-hydroxyglutarate attenuates aerobic glycolysis in leukemia by targeting the FTO/m(6)A/PFKP/LDHB axis.* Mol Cell, 2021. **81**(5): p. 922-939 e9.

298. Zhou, S., Z.L. Bai, D. Xia, Z.J. Zhao, R. Zhao, Y.Y. Wang, and H. Zhe, *FTO regulates the chemo-radiotherapy resistance of cervical squamous cell carcinoma (CSCC) by targeting beta-catenin through mRNA demethylation.* Mol Carcinog, 2018. **57**(5): p. 590-597.

299. Yan, F., A. Al-Kali, Z. Zhang, J. Liu, J. Pang, N. Zhao, C. He, M.R. Litzow, and S. Liu, *A dynamic N(6)-methyladenosine methylome regulates intrinsic and acquired resistance to tyrosine kinase inhibitors.* Cell Res, 2018. **28**(11): p. 1062-1076.

300. Yang, S., J. Wei, Y.H. Cui, G. Park, P. Shah, Y. Deng, A.E. Aplin, Z. Lu, S. Hwang, C. He, and Y.Y. He, *m(6)A mRNA demethylase FTO regulates melanoma tumorigenicity and response to anti-PD-1 blockade.* Nat Commun, 2019. **10**(1): p. 2782.

301. Han, Z., T. Niu, J. Chang, X. Lei, M. Zhao, Q. Wang, W. Cheng, J. Wang, Y. Feng, and J. Chai, *Crystal structure of the FTO protein reveals basis for its substrate specificity.* Nature, 2010. **464**(7292): p. 1205-9.

302. Chen, B., F. Ye, L. Yu, G. Jia, X. Huang, X. Zhang, S. Peng, K. Chen, M. Wang, S. Gong, R. Zhang, J. Yin, H. Li, Y. Yang, H. Liu, J. Zhang, H. Zhang, A. Zhang, H. Jiang, C. Luo, and C.G. Yang, *Development of cell-active N6-methyladenosine RNA demethylase FTO inhibitor.* J Am Chem Soc, 2012. **134**(43): p. 17963-71.

303. Li, Q., Y. Huang, X. Liu, J. Gan, H. Chen, and C.G. Yang, *Rhein Inhibits AlkB Repair Enzymes and Sensitizes Cells to Methylated DNA Damage.* J Biol Chem, 2016. **291**(21): p. 11083-93.

304. Huang, Y., J. Yan, Q. Li, J. Li, S. Gong, H. Zhou, J. Gan, H. Jiang, G.F. Jia, C. Luo, and C.G. Yang, *Meclofenamic acid selectively inhibits FTO demethylation of m6A over ALKBH5.* Nucleic Acids Res, 2015. **43**(1): p. 373-84.

305. Zheng, G., T. Cox, L. Tribbey, G.Z. Wang, P. Iacoban, M.E. Booher, G.J. Gabriel, L. Zhou, N. Bae, J. Rowles, C. He, and M.J. Olsen, *Synthesis of a FTO inhibitor with anticonvulsant activity.* ACS Chem Neurosci, 2014. **5**(8): p. 658-65.

306. Wang, T., T. Hong, Y. Huang, H. Su, F. Wu, Y. Chen, L. Wei, W. Huang, X. Hua, Y. Xia, J. Xu, J. Gan, B. Yuan, Y. Feng, X. Zhang, C.G. Yang, and X. Zhou, *Fluorescein Derivatives as Bifunctional Molecules for the Simultaneous Inhibiting and Labeling of FTO Protein.* J Am Chem Soc, 2015. **137**(43): p. 13736-9.

307. Selberg, S., L.-Y. Yu, O. Bondarenko, E. Kankuri, N. Seli, V. Kovaleva, K. Herodes, M. Saarma, and M. Karelson, *Small-molecule inhibitors of the RNA m⁶A demethylase FTO potently support the survival of dopamine neurons.* bioRxiv, 2021: p. 2021.02.23.432419.

308. Cui, Q., H. Shi, P. Ye, L. Li, Q. Qu, G. Sun, G. Sun, Z. Lu, Y. Huang, C.G. Yang, A.D. Riggs, C. He, and Y. Shi, *m(6)A RNA Methylation Regulates the Self-Renewal and Tumorigenesis of Glioblastoma Stem Cells.* Cell Rep, 2017. **18**(11): p. 2622-2634.

309. Huang, Y., R. Su, Y. Sheng, L. Dong, Z. Dong, H. Xu, T. Ni, Z.S. Zhang, T. Zhang, C. Li, L. Han, Z. Zhu, F. Lian, J. Wei, Q. Deng, Y. Wang, M. Wunderlich, Z. Gao, G. Pan, D. Zhong, H. Zhou, N. Zhang, J. Gan, H. Jiang, J.C. Mulloy, Z. Qian, J. Chen, and C.G. Yang, *Small-Molecule Targeting of Oncogenic FTO Demethylase in Acute Myeloid Leukemia.* Cancer Cell, 2019. **35**(4): p. 677-691 e10.

310. Chen, G., Q. Zhao, B. Yuan, B. Wang, Y. Zhang, Z. Li, S. Du, and Z. Zeng, *ALKBH5-modified HMGB1-STING Activation Contributes to Radiation Induced Liver Disease Via Innate Immune Response.* Int J Radiat Oncol Biol Phys, 2021.

311. Han, Z., X. Wang, Z. Xu, Y. Cao, R. Gong, Y. Yu, Y. Yu, X. Guo, S. Liu, M. Yu, W. Ma, Y. Zhao, J. Xu, X. Li, S. Li, Y. Xu, R. Song, B. Xu, F. Yang, D. Bamba, N. Sukhareva, H. Lei, M. Gao, W. Zhang, N. Zagidullin, Y. Zhang, B. Yang, Z. Pan, and B. Cai, *ALKBH5 regulates cardiomyocyte proliferation and heart regeneration by demethylating the mRNA of YTHDF1.* Theranostics, 2021. **11**(6): p. 3000-3016.

312. Li, X.C., F. Jin, B.Y. Wang, X.J. Yin, W. Hong, and F.J. Tian, *The m6A demethylase ALKBH5 controls trophoblast invasion at the maternal-fetal interface by regulating the stability of CYR61 mRNA.* Theranostics, 2019. **9**(13): p. 3853-3865.

313. Zhao, Y., J. Hu, X. Sun, K. Yang, L. Yang, L. Kong, B. Zhang, F. Li, C. Li, B. Shi, K. Hu, A. Sun, and J. Ge, *Loss of m6A demethylase ALKBH5 promotes post-ischemic angiogenesis via post-transcriptional stabilization of WNT5A.* Clin Transl Med, 2021. **11**(5): p. e402.

314. Cheng, Y., H. Luo, and M.G. Kharas, *Rubbing Out Leukemia Stem Cells by Erasing the Eraser.* Cell Stem Cell, 2020. **27**(1): p. 3-5.

315. Shen, C., Y. Sheng, A.C. Zhu, S. Robinson, X. Jiang, L. Dong, H. Chen, R. Su, Z. Yin, W. Li, X. Deng, Y. Chen, Y.C. Hu, H. Weng, H. Huang, E. Prince, C.R. Cogle, M. Sun, B. Zhang, C.W. Chen, G. Marcucci, C. He, Z. Qian, and J. Chen, *RNA Demethylase ALKBH5 Selectively Promotes Tumorigenesis and Cancer Stem Cell Self-Renewal in Acute Myeloid Leukemia.* Cell Stem Cell, 2020. **27**(1): p. 64-80 e9.

316. Wang, J., Y. Li, P. Wang, G. Han, T. Zhang, J. Chang, R. Yin, Y. Shan, J. Wen, X. Xie, M. Feng, Q. Wang, J. Hu, Y. Cheng, T. Zhang, Y. Li, Z. Gao, C. Guo, J. Wang, J. Liang, M. Cui, K. Gao, J. Chai, W. Liu, H. Cheng, L. Li, F. Zhou, L. Liu, Y. Luo, S. Li, and H. Zhang, *Leukemogenic Chromatin Alterations Promote AML Leukemia Stem Cells via a KDM4C-ALKBH5-AXL Signaling Axis.* Cell Stem Cell, 2020. **27**(1): p. 81-97 e8.

317. Chen, Y., Y. Zhao, J. Chen, C. Peng, Y. Zhang, R. Tong, Q. Cheng, B. Yang, X. Feng, Y. Lu, H. Xie, L. Zhou, J. Wu, and S. Zheng, *ALKBH5 suppresses malignancy of hepatocellular carcinoma via m(6)A-guided epigenetic inhibition of LYPD1.* Mol Cancer, 2020. **19**(1): p. 123.

318. Li, N., Y. Kang, L. Wang, S. Huff, R. Tang, H. Hui, K. Agrawal, G.M. Gonzalez, Y. Wang, S.P. Patel, and T.M. Rana, *ALKBH5 regulates anti-PD-1 therapy response by modulating lactate and suppressive immune cell accumulation in tumor microenvironment.* Proc Natl Acad Sci U S A, 2020. **117**(33): p. 20159-20170.

319. Yuan, Y., G. Yan, M. He, H. Lei, L. Li, Y. Wang, X. He, G. Li, Q. Wang, Y. Gao, Z. Qu, Z. Mei, Z. Shen, J. Pu, A. Wang, W. Zhao, H. Jiang, W. Du, and L. Yang, *ALKBH5 suppresses tumor progression via an m(6)A-dependent epigenetic silencing of pre-miR-181b-1/YAP signaling axis in osteosarcoma.* Cell Death Dis, 2021. **12**(1): p. 60.

320. Zhang, J., S. Guo, H.Y. Piao, Y. Wang, Y. Wu, X.Y. Meng, D. Yang, Z.C. Zheng, and Y. Zhao, *ALKBH5 promotes invasion and metastasis of gastric cancer by decreasing methylation of the lncRNA NEAT1.* J Physiol Biochem, 2019. **75**(3): p. 379-389.

321. Xu, C., K. Liu, W. Tempel, M. Demetriades, W. Aik, C.J. Schofield, and J. Min, *Structures of human ALKBH5 demethylase reveal a unique binding mode for specific single-stranded N6-methyladenosine RNA demethylation.* J Biol Chem, 2014. **289**(25): p. 17299-311.

322. Malacrida, A., M. Rivara, A. Di Domizio, G. Cislaghi, M. Miloso, V. Zuliani, and G. Nicolini, *3D proteome-wide scale screening and activity evaluation of a new ALKBH5 inhibitor in U87 glioblastoma cell line.* Bioorg Med Chem, 2020. **28**(4): p. 115300.

323. Selberg, S., N. Seli, E. Kankuri, and M. Karelson, *Rational Design of Novel Anticancer Small-Molecule RNA m6A Demethylase ALKBH5 Inhibitors.* ACS Omega, 2021. **6**(20): p. 13310-13320.

324. Shi, Y., S. Fan, M. Wu, Z. Zuo, X. Li, L. Jiang, Q. Shen, P. Xu, L. Zeng, Y. Zhou, Y. Huang, Z. Yang, J. Zhou, J. Gao, H. Zhou, S. Xu, H. Ji, P. Shi, D.D. Wu, C. Yang, and Y. Chen, *YTHDF1 links hypoxia adaptation and non-small cell lung cancer progression.* Nat Commun, 2019. **10**(1): p. 4892.

325. Bai, Y., C. Yang, R. Wu, L. Huang, S. Song, W. Li, P. Yan, C. Lin, D. Li, and Y. Zhang, *YTHDF1 Regulates Tumorigenicity and Cancer Stem Cell-Like Activity in Human Colorectal Carcinoma.* Front Oncol, 2019. **9**: p. 332.

326. Han, B., S. Yan, S. Wei, J. Xiang, K. Liu, Z. Chen, R. Bai, J. Sheng, Z. Xu, and X. Gao, *YTHDF1-mediated translation amplifies Wnt-driven intestinal stemness.* EMBO Rep, 2020. **21**(4): p. e49229.

327. Pi, J., W. Wang, M. Ji, X. Wang, X. Wei, J. Jin, T. Liu, J. Qiang, Z. Qi, F. Li, Y. Liu, Y. Ma, Y. Si, Y. Huo, Y. Gao, Y. Chen, L. Dong, R. Su, J. Chen, S. Rao, P. Yi, S. Yu, F. Wang, and J. Yu, *YTHDF1 Promotes Gastric Carcinogenesis by Controlling Translation of FZD7.* Cancer Res, 2021. **81**(10): p. 2651-2665.

328. Liu, T., Q. Wei, J. Jin, Q. Luo, Y. Liu, Y. Yang, C. Cheng, L. Li, J. Pi, Y. Si, H. Xiao, L. Li, S. Rao, F. Wang, J. Yu, J. Yu, D. Zou, and P. Yi, *The m6A reader YTHDF1 promotes ovarian cancer progression via augmenting EIF3C translation.* Nucleic Acids Res, 2020. **48**(7): p. 3816-3831.

329. Hao, L., J.M. Wang, B.Q. Liu, J. Yan, C. Li, J.Y. Jiang, F.Y. Zhao, H.Y. Qiao, and H.Q. Wang, *m6A-YTHDF1-mediated TRIM29 upregulation facilitates the stem cell-like phenotype of cisplatin-resistant ovarian cancer cells.* Biochim Biophys Acta Mol Cell Res, 2021. **1868**(1): p. 118878.

330. Coots, R.A., X.M. Liu, Y. Mao, L. Dong, J. Zhou, J. Wan, X. Zhang, and S.B. Qian, *m(6)A Facilitates eIF4F-Independent mRNA Translation.* Mol Cell, 2017. **68**(3): p. 504-514 e7.

331. Shi, R., S. Ying, Y. Li, L. Zhu, X. Wang, and H. Jin, *Linking the YTH domain to cancer: the importance of YTH family proteins in epigenetics.* Cell Death Dis, 2021. **12**(4): p. 346.

332. Dai, X.Y., L. Shi, Z. Li, H.Y. Yang, J.F. Wei, and Q. Ding, *Main N6-Methyladenosine Readers: YTH Family Proteins in Cancers.* Front Oncol, 2021. **11**: p. 635329.

333. Bedi, R.K., D. Huang, L. Wiedmer, Y. Li, A. Dolbois, J.A. Wojdyla, M.E. Sharpe, A. Caflisch, and P. Sledz, *Selectively Disrupting m(6)A-Dependent Protein-RNA Interactions with Fragments.* ACS Chem Biol, 2020. **15**(3): p. 618-625.